NASA-CR-191193

N-27-CR
30748
p. 164

Contract NAS3-25269
CR No. 191193

Design and Fabrication of Forward-Swept Counterrotation Blade Configuration for Wind Tunnel Testing

Final Report
March 1, 1994

Prepared by
G. H. Nichols
GE Aircraft Engines
Advanced Technology Operations
Cincinnati, Ohio 45215

Prepared for

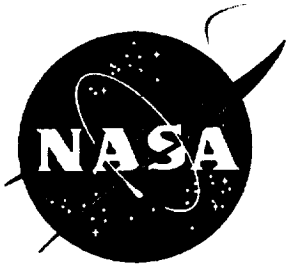

National Aeronautics and Space Administration
Lewis Research Center
21000 Brookpark Road

Contract NAS3-25269
CR No. 191193

Design and Fabrication of Forward-Swept Counterrotation Blade Configuration for Wind Tunnel Testing

Final Report
March 1, 1994

Table of Contents

Table of Contents

List of Illustrations

List of Illustrations

List of Illustrations

List of Tables

1.0 Summary

This report describes the work performed by GE Aircraft Engines under NASA Contract NAS3-25269 (Investigation of Advanced Counterrotation Blade Configuration Concepts for High Speed Turboprop System). Primary emphasis was placed on theoretically and experimentally evaluating the aerodynamic, aeromechanical, and acoustic performance of GE-defined counter-rotating blade concepts.

Several blade design concepts were considered. Feasibility studies were conducted to evaluate a forward-swept versus an aft-swept blade application and how the given blade design would affect interaction between rotors. Two blade designs were initially selected. Both designs involved in-depth aerodynamic, aeromechanical, mechanical, and acoustic analyses followed by the fabrication of forward-swept, forward rotor blade sets to be wind tunnel tested with an aft-swept, aft rotor blade set.

A third blade set was later produced from a NASA design that was based on wind tunnel test results from the first two blade sets. This blade set had a stiffer outer ply material added to the original blade design, in order to reach the design point operating line (that neither blade set had achieved).

Detailed analyses, feasibility studies, and fabrication procedures for all blade sets are presented in this report. Contributors to this report included:

T.J. Sullivan	–	Aerodynamic Design
A. Breeze-Stringfellow	–	Aerodynamic Design
E.H. Ducharme	–	Aeromechanical Design
P.A. Battle	–	Mechanical Design
C.E. Whitfield	–	Acoustic Analysis
B.J. Fuhrmann	–	Manufacturing

Scale-model propulsor testing was later performed at NASA Lewis Research Center in Cleveland, Ohio. Since this effort was not part of GEAE's defined program scope, test results and subsequent comparisons to analytical predictions are not presented in this report.

2.0 Introduction

2.1 Background

Over the past several years, GEAE has been engaged in internal, as well as Government-sponsored, studies to evaluate advanced technology, energy-efficient propulsion systems for potential use in both commercial and military subsonic aircraft. These studies have covered a wide spectrum of engines from pure turbojets to helicopters, in terms of size and performance as a function of effective bypass ratio. These studies have included modern turbofans, such as the direct-drive NASA/GE Energy Efficient Engine (E^3) and the geared fan for very high bypass ratio, such as the NASA/GE Quiet, Clean, Short-haul Experimental Engine (QCSEE), conventional turboprops, and the more modern, NASA single-rotation propfans.

Figure 1 illustrates the spectrum of bypass ratios considered. Between the bypass ratio spectrum bounded by the turbofan and turboprop engines lies a region of higher bypass fans, unique cycle engines, and counterrotation propulsor systems. This region is identified as the "unused range" of engines. It is within this range of engines that the advantages of turbofans and turboprops can be combined.

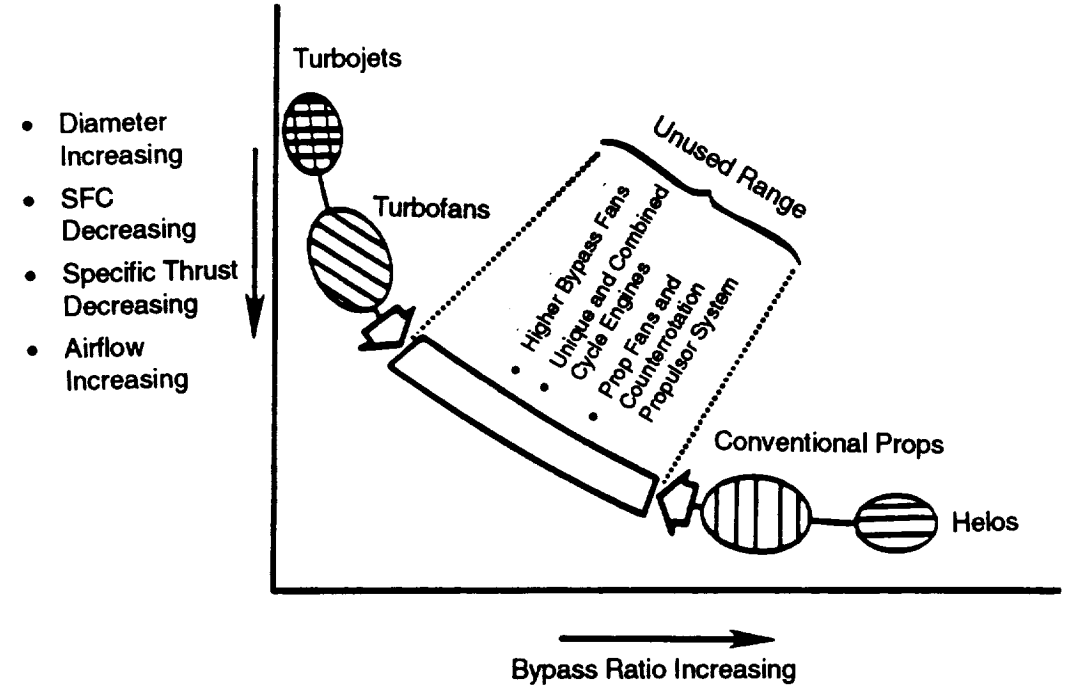

Figure 1. GEAE Study of Bypass Ratio Spectrum.

The GE studies identified particular aerodynamic and acoustic configurations for unconventional propulsors that used a modern, counterrotation blading system, particularly for "pusher-type" propulsor designs. This blading system incorporated a concept of high hub-to-tip radius ratio and

high disk loading (that is, an shp/D^2 of approximately 60). By using a higher hub-to-tip ratio, the conventional airfoil designs more closely resembled fan-type blading designs, resulting in both higher flow rates and thinner airfoil cross sections at the hub region. In addition, higher radius ratios significantly lessened blade retention stresses and allowed for more aeromechanically and aeroacoustically favorable blade sweep designs. The work described in this report involved an investigation of these modern, GE-conceived, counterrotation blade concepts, as were used on the GE Unducted Fan (UDF®) engine.

GE's in-house, full-scale UDF® development program began in 1983.

At the outset, it was recognized that an adequate base for counterrotating blade concepts was needed, and that counterrotating propulsor test rigs would be a cost-effective means of generating the data. In another program during that time, three Model Propulsion Simulator (MPS) test rigs were designed and fabricated. In compliance with the terms and conditions of the program, one of the test rigs was provided to NASA Lewis by GE for use in their wind tunnel facilities in Cleveland, Ohio. This was the MPS test rig used for testing the blades designed and fabricated under this contract.

2.2 Objective

The overall objective of the program associated with this document was to theoretically and experimentally investigate additional unique counterrotating blade concepts. Aerodynamic, acoustic, and aeromechanical performance of these concepts were defined, evaluated, and documented for future application. In order to accomplish this, the work was segmented into several tasks:

- Conduct a feasibility study of a forward-swept, forward blade and an aft-swept, aft blade.
- Conduct a feasibility study to determine the performance of a forward-swept, forward blade when operating with an existing aft-swept, aft blade. Conduct a feasibility study to determine the performance of a forward-swept, aft blade.
- Conduct the final design and analysis of the forward-swept forward blade for the counterrotating blade design.
- Fabricate, bench test, and instrument as required, 16 forward-swept, forward propeller blades in accordance with the final design results of the above tasks.
- Design and fabricate an aeroelastically divergent build of the forward-swept, forward propeller blades through the application of a different ply material and schedule to the cold shape of the original blade design.
- Fabricate and instrument a modified set of 15 forward-swept, forward propeller blades having a geometry identical to the original set of procured blades, but with a different blade material and ply lay-up orientation for the outermost six layers.

To develop airfoil designs for the program, internal funding and NASA Contract NAS3-25269 (Investigation of Advanced Counterrotation Blade Configuration Concepts for High Speed Turboprop Systems) funding supported the scale-model blade design and fabrication. Scale-model

propulsor testing for aerodynamic and acoustic performance, aeroelastic stability, and aeromechanical integrity was performed at NASA Lewis Research Center in Cleveland, Ohio. Since this effort was not a part of GE's defined program scope, only blade designs and fabrication processes are presented in this report.

3.0 Forward-Swept F39 Final Design and Analysis

3.1 Aerodynamic Design

The aerodynamic design approach adopted for the forward-swept, unducted fan blade (F39) was the same quasi-three-dimensional approach used for conventional ducted fans. Much of the technology developed from engines with high bypass ratio transonic fans was used in the design of these highly loaded, counterrotating blade rows. The F39 blade had a forward-swept planform with other geometric parameters patterned after a previous GE unducted fan (UDF®), F31. Aerodynamic design point parameters for the F39 blade are listed in ***Table 1***.

Table 1. Aero Design Point Parameters.

Flight Mach Number	0.80
Altitude, feet	35,000
Ambient Temperature Delta, °F	+18
Tip Speed, ft/sec	758
Design Loading	
• SHP/D^2, HP/ft^2	65.6
• SHP/A_{ANN}, HP/ft^2	100
Number of Blades (F39-A39)	12 + 10
Blade Angle, degrees	56.8
Full-Scale Diameter, inches	128.0
Chord Distribution, Airfoil Thicknesses, Flowpath Shape	Same as F31-A31

The aerodynamic design was done in full scale and was carried out using the general method described in *Reference 1*. The design procedure is shown in flowchart format in ***Figure 2***. The circumferential-average flow solution was calculated for the UDF® configuration, with the forward rotor designated F39 and aft rotor A31, using the optimum loading distribution developed in *Reference 2* for counterrotating propellers. The analytical results are shown in ***Figure 3***. When executing the aero design, primary attention was focused on the top-of-climb design point (Mach = 0.80, 35,000 feet). This was where the blading Mach numbers would be the highest and, therefore, where the need for airfoil design precision would be the greatest. The vector diagrams calculated from this circumferential-average flow solution were used for setting the blade meanline angles. The F39 airfoil shapes were selected using the standard blade generator code, making allowances for the sweep-end effects and secondary flow vorticity as described in *Reference 1*.

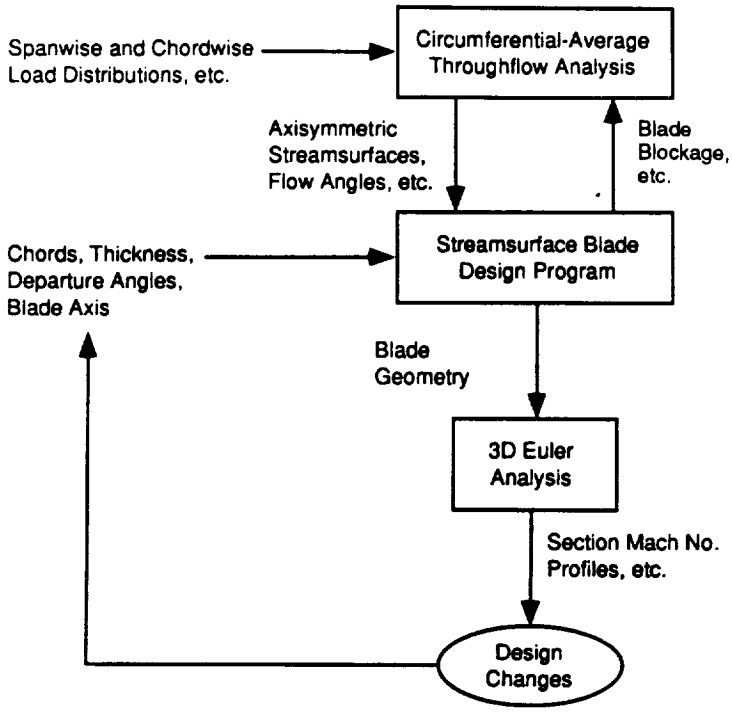

Figure 2. Aerodynamic Design Procedure.

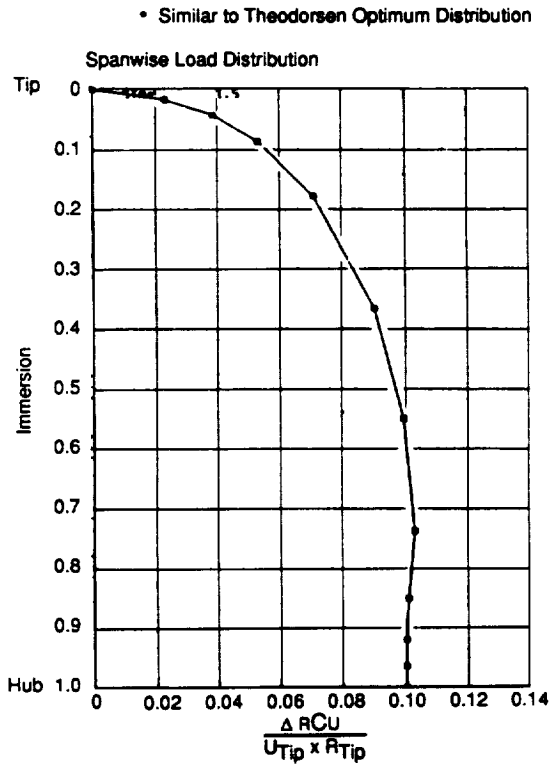

Figure 3. Circumferential-Average Throughflow Analysis Results.

The airfoils were designed on stream surfaces using blade-to-blade analyses or cascade concepts. The F39 blade planform shape was chosen as a mirror-image of the aft-swept F31 blade. The blade axis, located at 40% chord, was defined by the radial distributions of sweep and lean. Shown in ***Figure 4a*** is the radial distribution of sweep and lean for the F39 blade compared to the aft-swept F31. The chord, thickness, and twist distributions of the F39 blade were specified to be the same as those for the F31 blade and are shown in Figures ***4b***, ***4c***, and ***4d***, respectively.

The fully three-dimensional blade (F39) was then analyzed using the GE Euler Code to determine the surface velocity distributions. The presence of the aft rotor was represented in the calculation by circumferentially constant source terms. Several iterations on blade meanline angle were made to improve the velocity distributions and reduce the passage shock strengths. The airfoil coordinates were defined at the hot running condition (aero design point), and the appropriate deflections, calculated from the air loads and centrifugal loads, were applied to define the cold, manufacturing airfoil shape. An indication of the amount of deflection from static to design point running condition is shown in ***Figure 5***. The F39 blade tended to straighten up from the cold to the hot running condition, deflecting about 15% of the chord length opposite the direction of rotation.

The F39A31 configuration was designed at the Mach 0.80, max-climb condition with 12 forward rotor blades and 10 aft rotor blades. The hub flowpath shape was similar to the F31A31 configuration to maintain commonality of the hardware necessary for scale-model testing. The meridional view of the UDF® configuration is shown in ***Figure 6*** with the streamlines, calculation stations, and meridional Mach number contours superimposed. The meridional Mach number contours indicate the regions of the flow field where the highest throughflow velocities occurred, generally inside the blade rows where the thickness blockage reduced the effective flow area. The F39A31 case had local regions inside both rotors and downstream of the aft rotor where the flow was at, or very near, choked conditions. Some area-ruling of the hub flowpath in the region of the blades was employed in the design of the F39A31 to alleviate the choked conditions as much as possible. Upstream of the blades, the nacelle was shaped to provide a gentle diffusion ahead of the forward rotor leading edge. Downstream of the rotors, the hub contour was designed to follow the direction of the exhaust plume of the engine.

The blade planform shapes were defined early in the design phase to allow time for the detailed aerodynamic cascade flow analysis. The planform was shaped by stacking custom-tailored airfoil sections along the swept and leaned blade axis. The airfoil meanline shapes were then finely tuned at all streamlines with several iterations using the GE 3D-Euler code. The meridional view of the F39 Euler grid is shown in ***Figure 7***, and the velocity distributions for tip, near-tip, pitch, and near-hub sections are shown in ***Figures 8*** through ***12***. The Mach number shown is the surface relative Mach number and is calculated from the relative total pressure and local surface static pressure. The Euler analysis of the F39 blade showed an absence of suction surface shocks on the outer half of the blade, largely due to the high degree of trailing edge sweep. This was the largest difference between the forward-swept and aft-swept blades. The reduced shock losses in the tip were determined to improve overall aero performance relative to the aft-swept rotor.

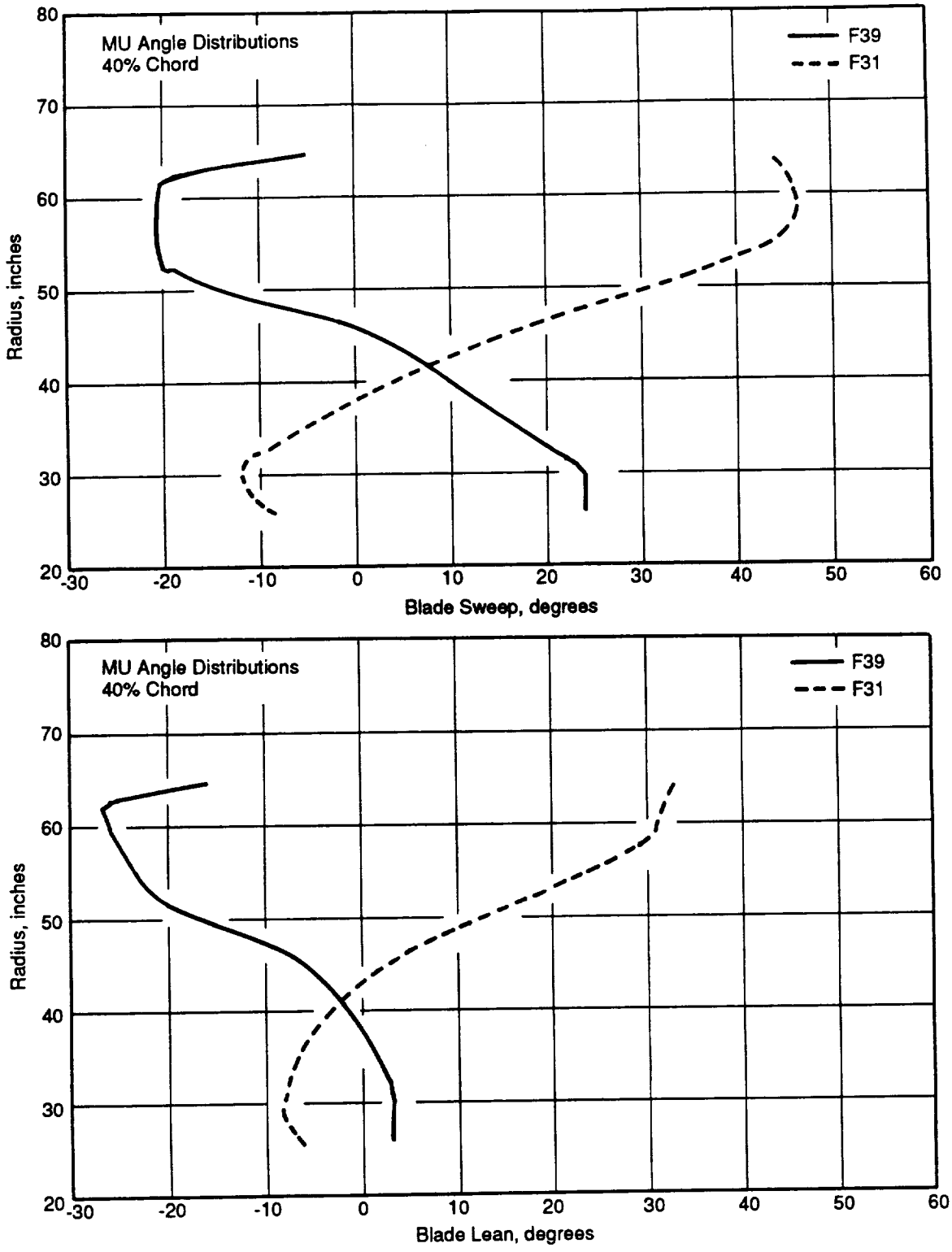

Figure 4a. Blade Sweep Angle and Lean Angle Distributions of F39 and F31 at the Blade Axis.

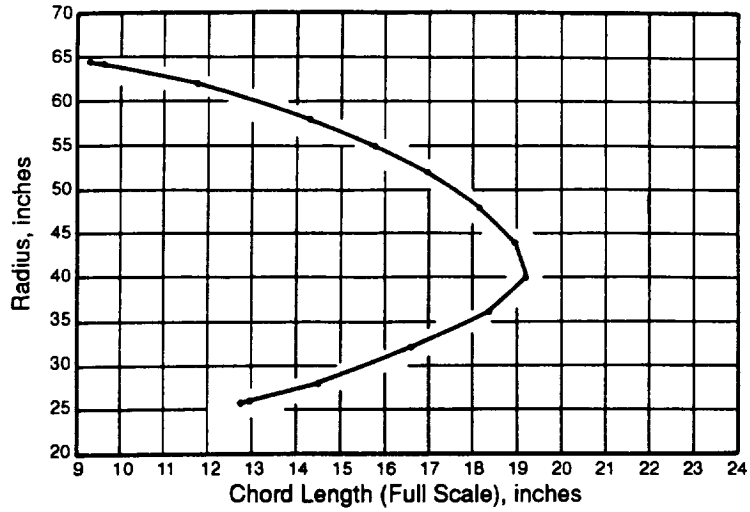

Figure 4b. Chord Distribution for the F39 Blade.

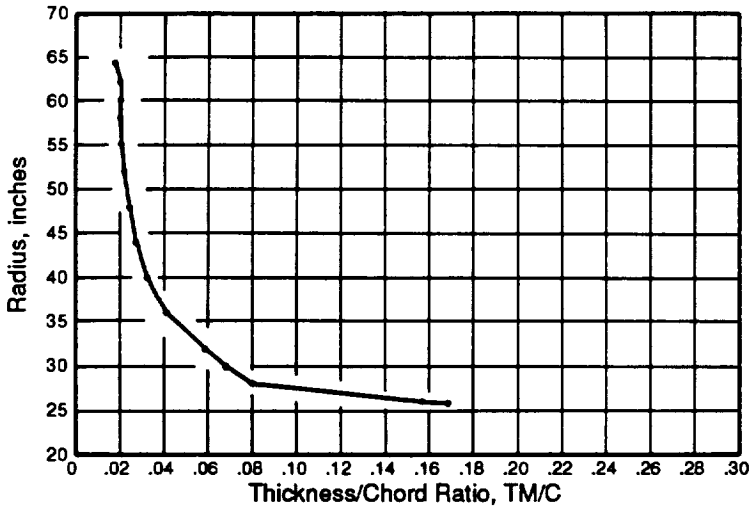

Figure 4c. Thickness Distribution for the F39 Blade.

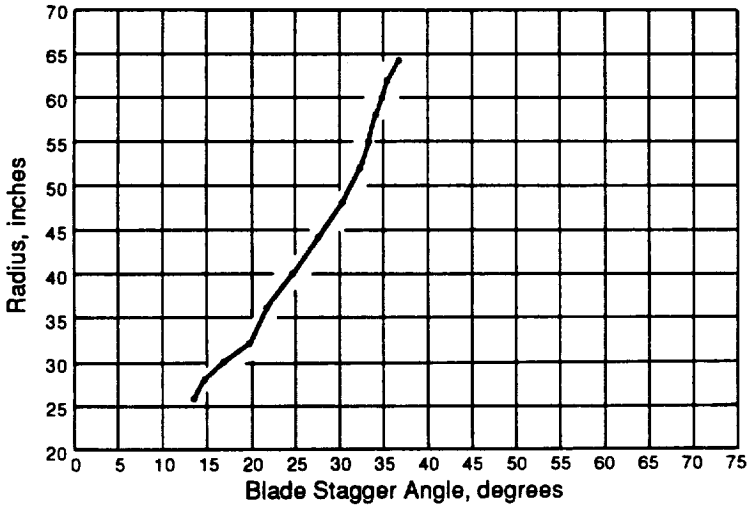

Figure 4d. Twist Distribution for the F39 Blade.

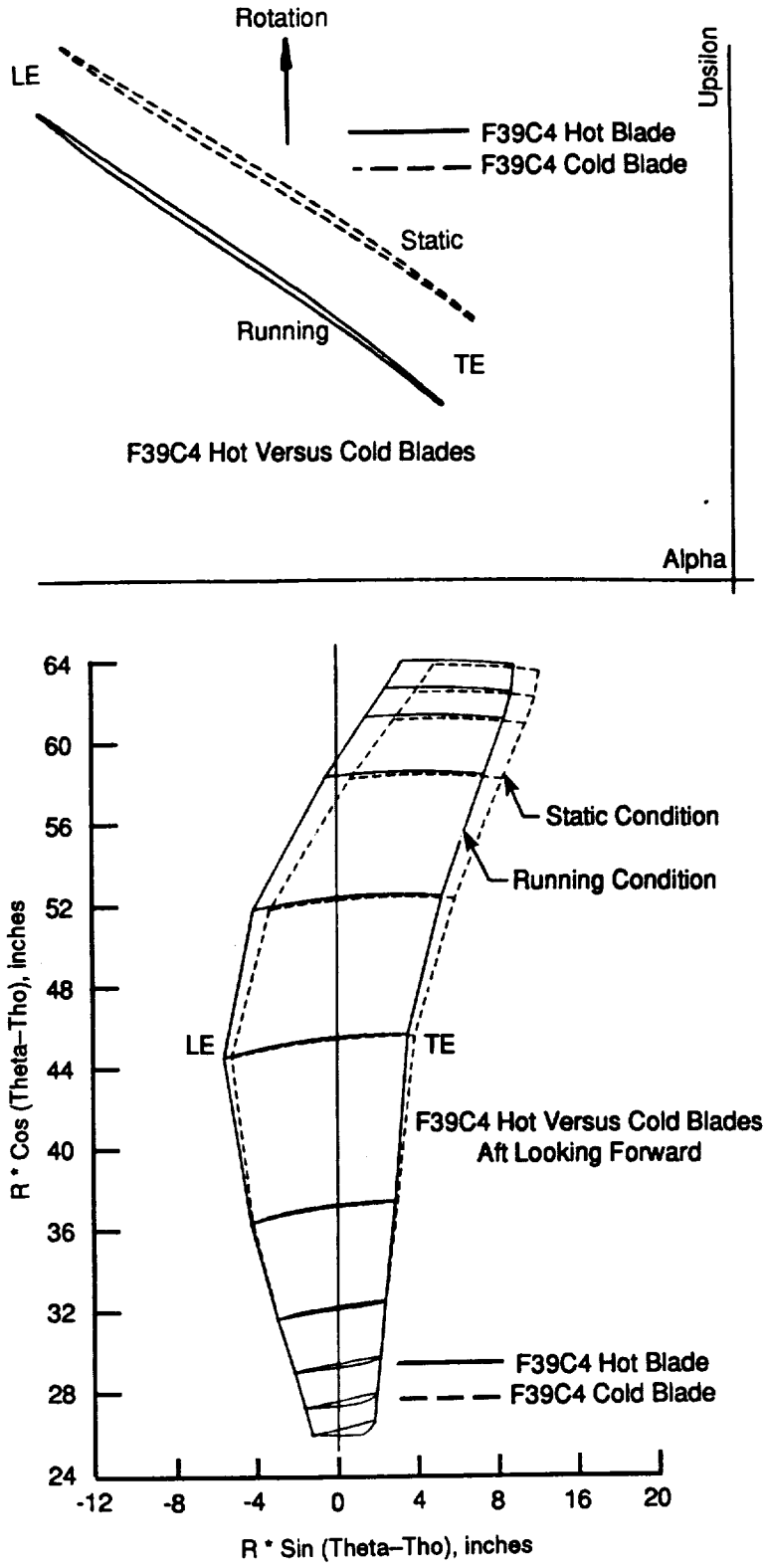

Figure 5. Deflection from Static to Design Point Running Condition.

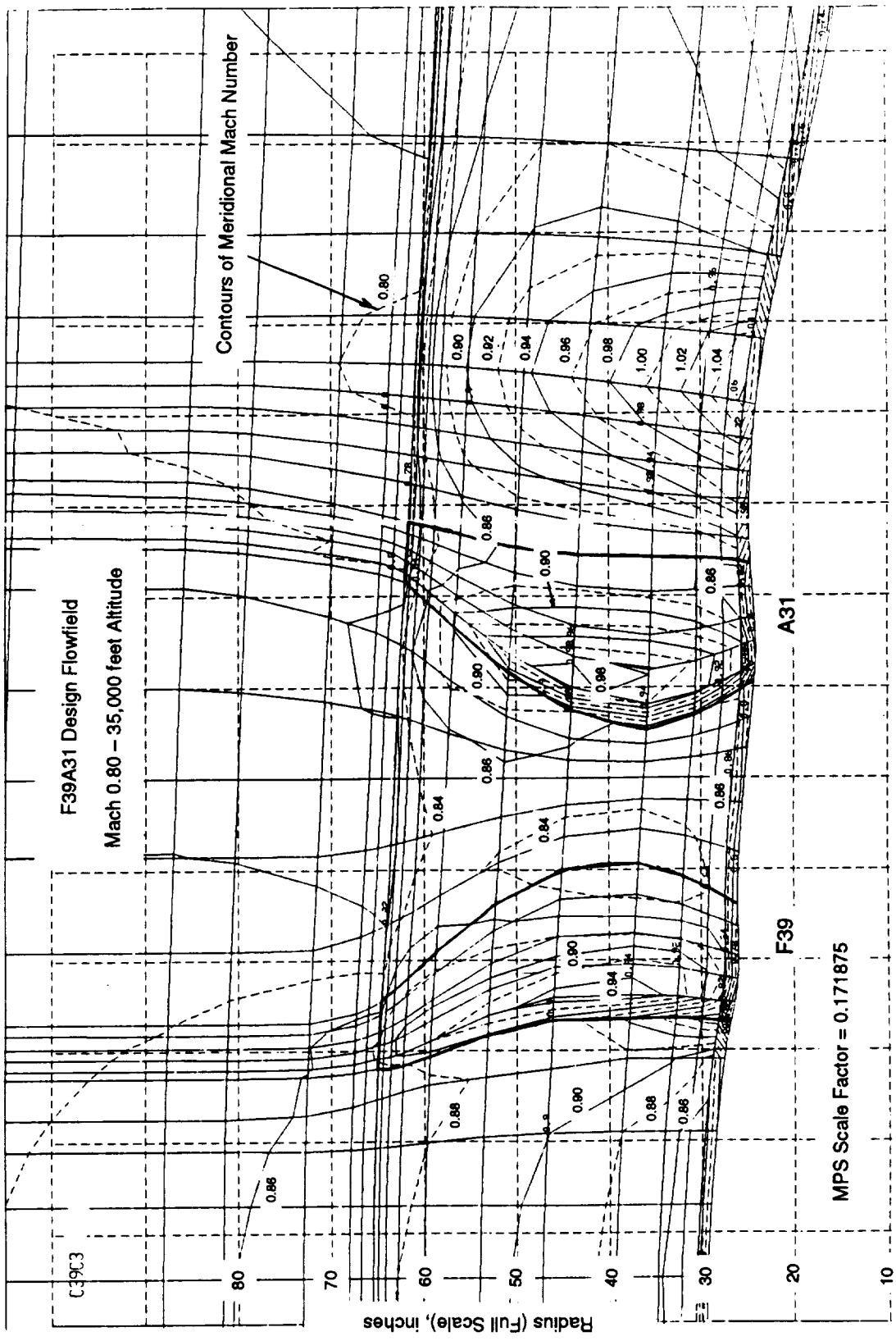

Figure 6. Contours of Meridional Mach Number for the F39A31 Configuration.

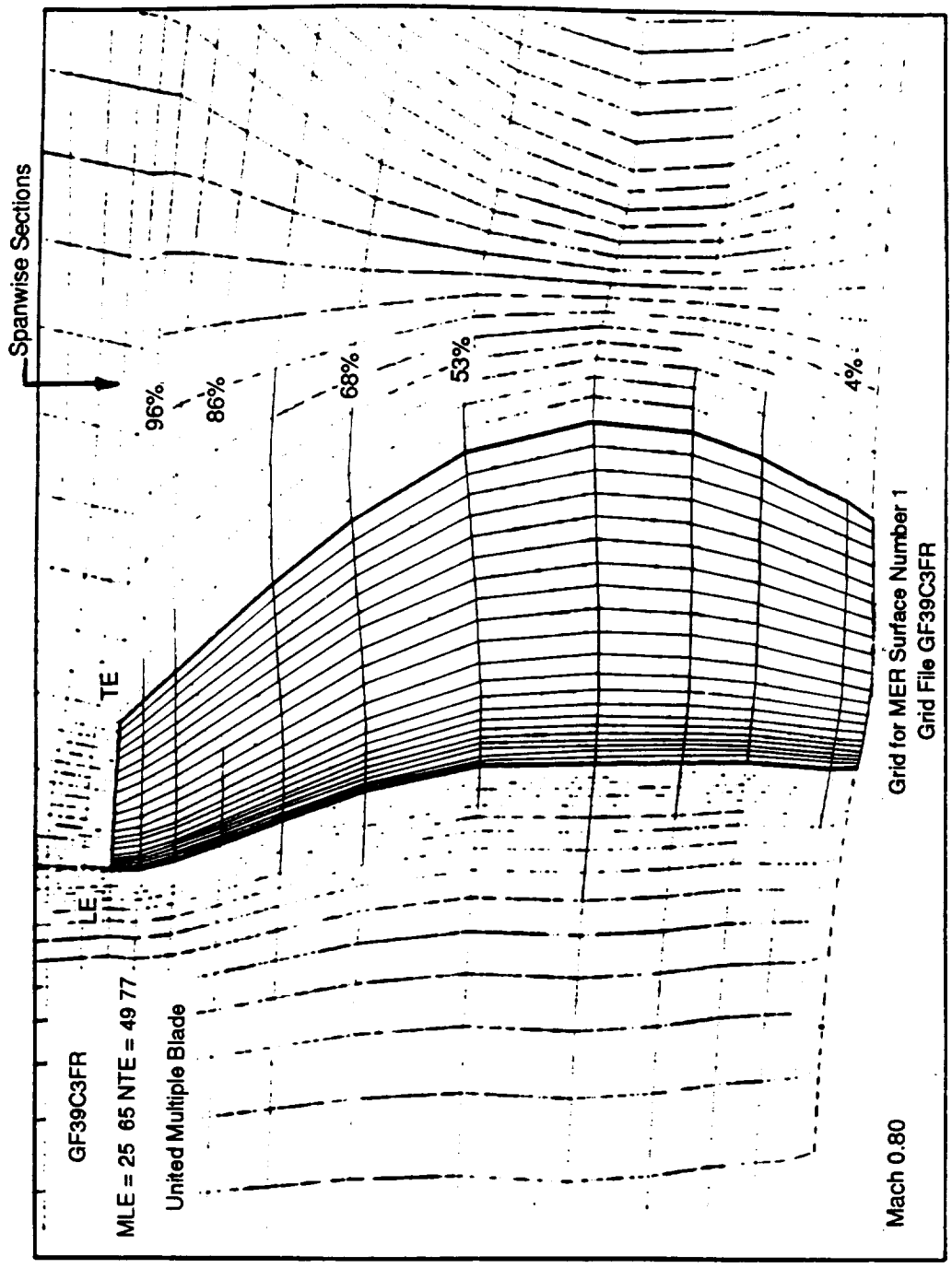

Figure 7. Meridional View of the F39 Euler Grid.

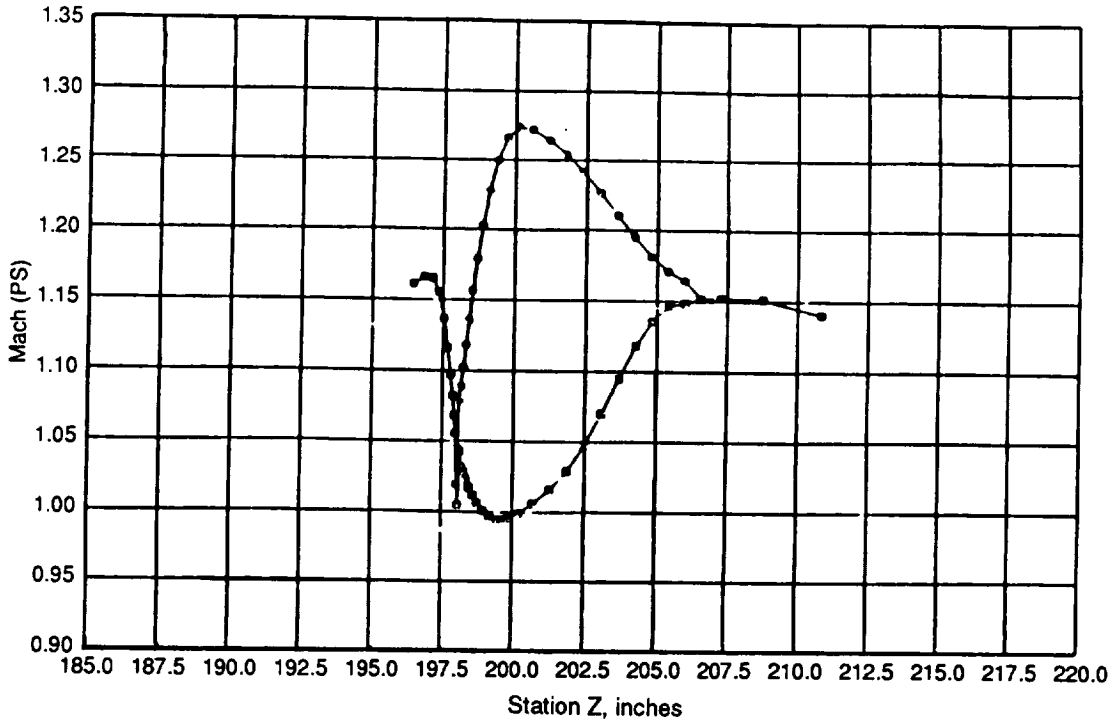

Figure 8. Velocity Distribution for the F39 Blade at 96% Span (Tip).

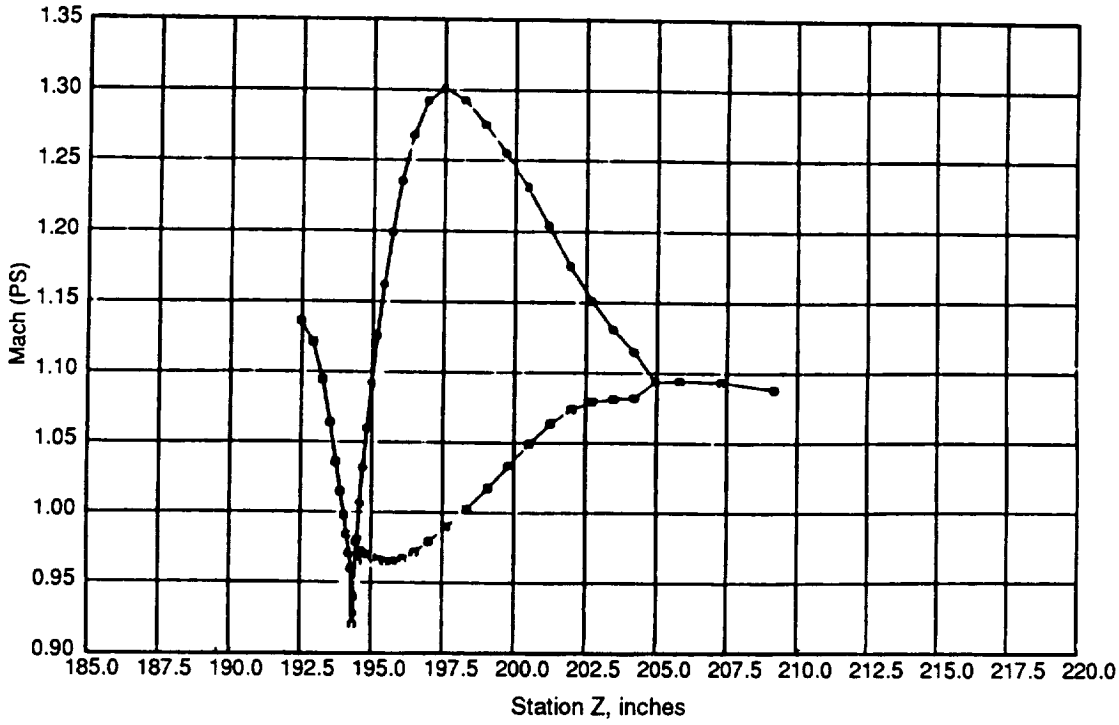

Figure 9. Velocity Distribution for the F39 Blade at 86% Span.

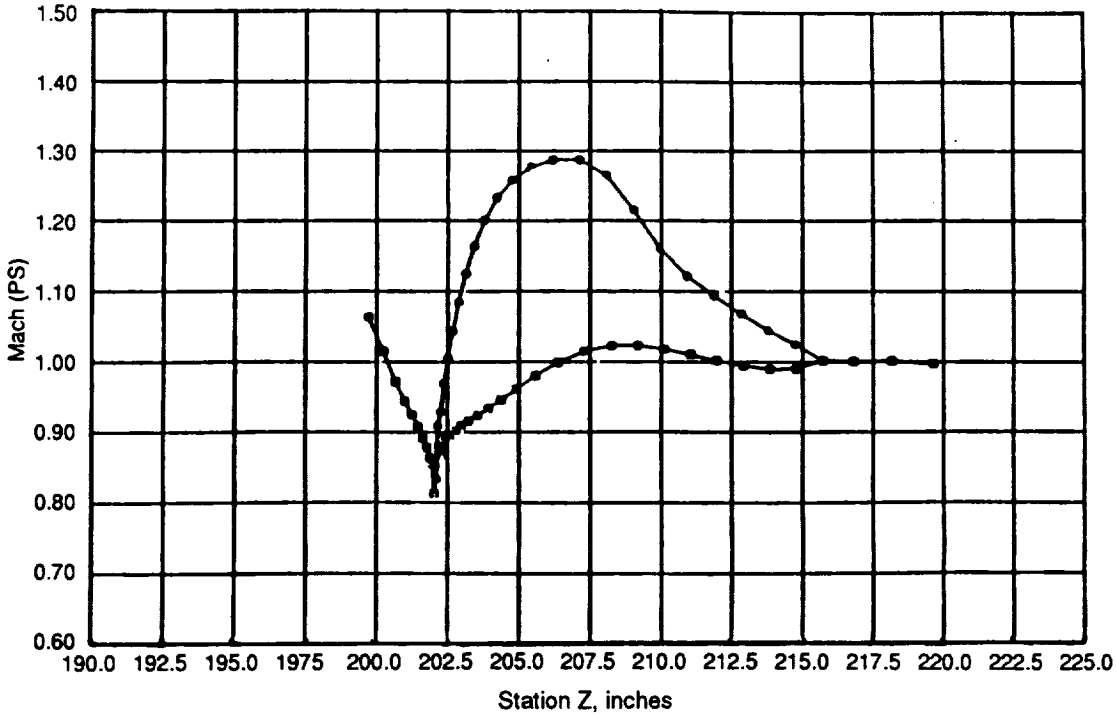

Figure 10. Velocity Distribution for the F39 Blade at 68% Span.

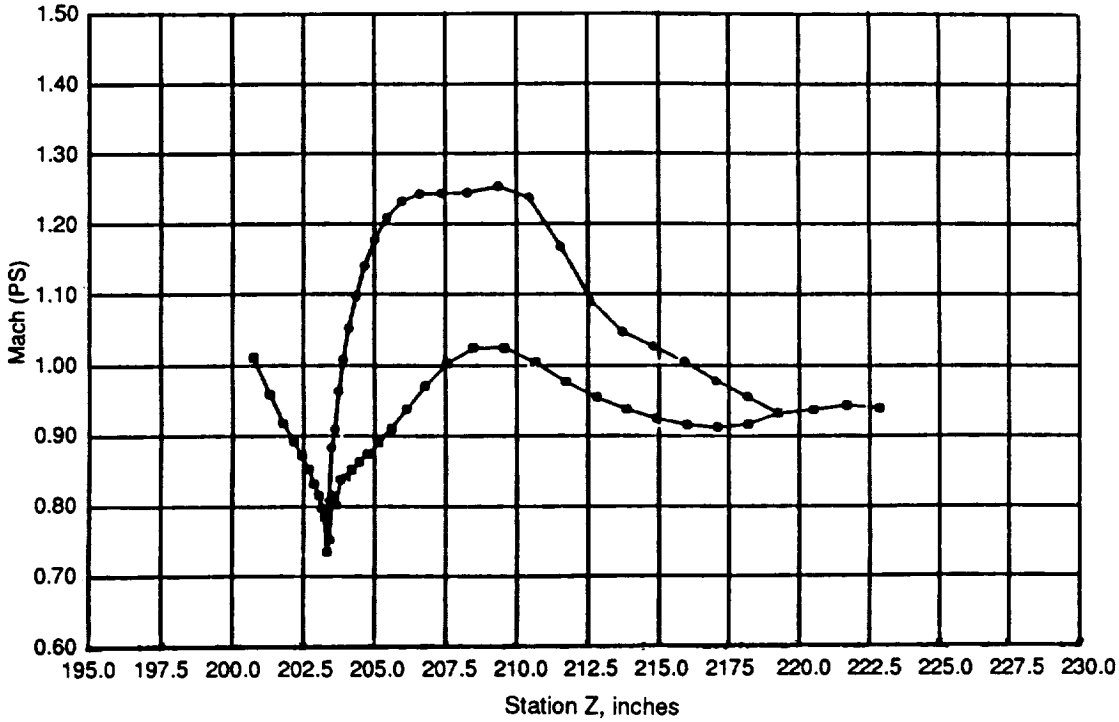

Figure 11. Velocity Distribution for the F39 Blade at 53% Span.

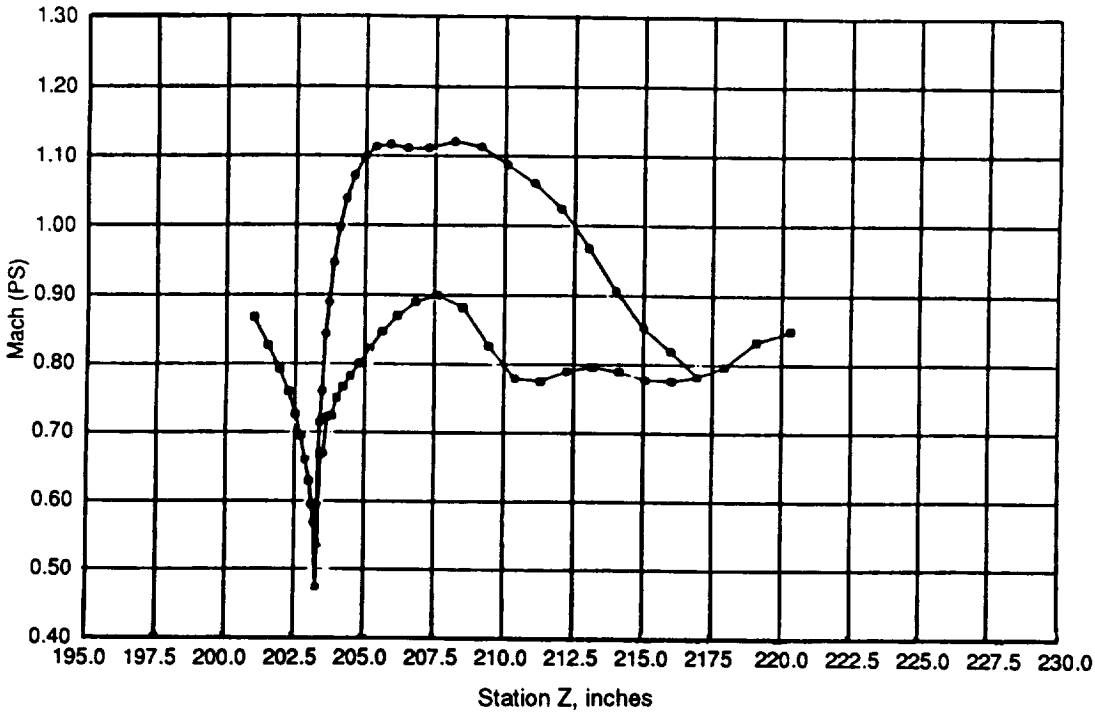

Figure 12. Velocity Distribution for the F39 Blade at 4% Span (Hub).

3.2 Aeromechanical Analysis

Section 4.1.2 contains a discussion of the aeromechanical stability issues for the forward-swept composite blades.

The forward-swept, unducted fan final blade design, F39C4, fabricated of IM7 material, was analyzed for flutter and divergence stability at design point (Mach = 0.80, 35,000 feet) in full scale. For comparison with the C4 design, all preliminary design iteration results are presented in ***Table 2***. The C4 design evolved as a restack of the C3 design. The General Aeroelastic Program (GAP) flutter analysis of the C4 design indicated that all modes were stable at design point, as shown in ***Figure 13***. The design point stability root locus plot of the forward-swept blade is shown in ***Figure 14***. The normal mode frequencies are indicated on the figure, as are the nodal diameters of each aeroelastic eigenvalue for the first mode family.

The GAP divergence assessment indicated that the blade is also divergence-free. The frequency drop of the first mode of the C4 blade was predicted to be 8%. This was somewhat less than the 11% drop predicted for the C3 blade, as indicated by the smaller mode shape slope of the C4 blade (in ***Table 2***).

The divergence characteristics of the forward-swept F39C4 blade were further studied using a finite element deflection analysis from the cold (as manufactured) geometry to the design point hot (intended shape) geometry. The effects of centrifugal forces and aerodynamic forces were evaluated both separately and in combination. The results of the study are summarized in ***Figure 15***. In the

Table 2. F39C4 Preliminary Design Mode Shape Slope Iterations.

Blade	Laminate	First Mode Frequency (full scale)	Slope
F39A4	AS4, 0° Ref	45.8 Hz	–0.157
F39B1	AS4, 0° Ref	46.0 Hz	–0.154
F39C3	AS4, 0° Ref	46.3 Hz	–0.170
F39C3	IM7, 0° Ref	47.1 Hz	–0.167
F39C3	IM7, –25° Ref	46.3 Hz	–0.136
F39C3	IM7, +25° Ref	45.8 Hz	–0.178
F39C3	IM7, –25° Ref, Tailored Layup	46.4 Hz	–0.118
F39C4	Restacked C3	46.4 Hz	–0.112

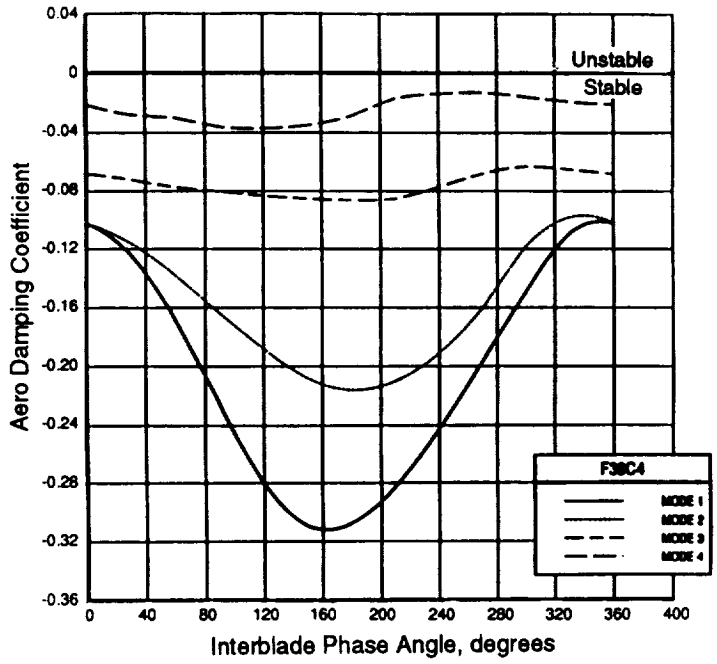

Figure 13. F39C4 Stability Analysis Results.

study, the aerodynamic load effects were included by applying the design point pressure loads along the blade model surface. Note that the analysis did not attempt to calculate intermediate aerodynamic loads as the blade deflected through intermediate geometries. The deflection analysis indicated that the effect of airloads alone would increase the incidence of the blade; that is, the blade would untwist or "open". The effects of centrifugal loads alone would decrease the incidence of the blade; that is, the blade would twist or "close". The net result of both centrifugal and aerodynamic loads would decrease the incidence or "close" the blade. The results of the design study indicated that the forward-swept F39C4 blade, consisting of IM7 material, should be divergence-free.

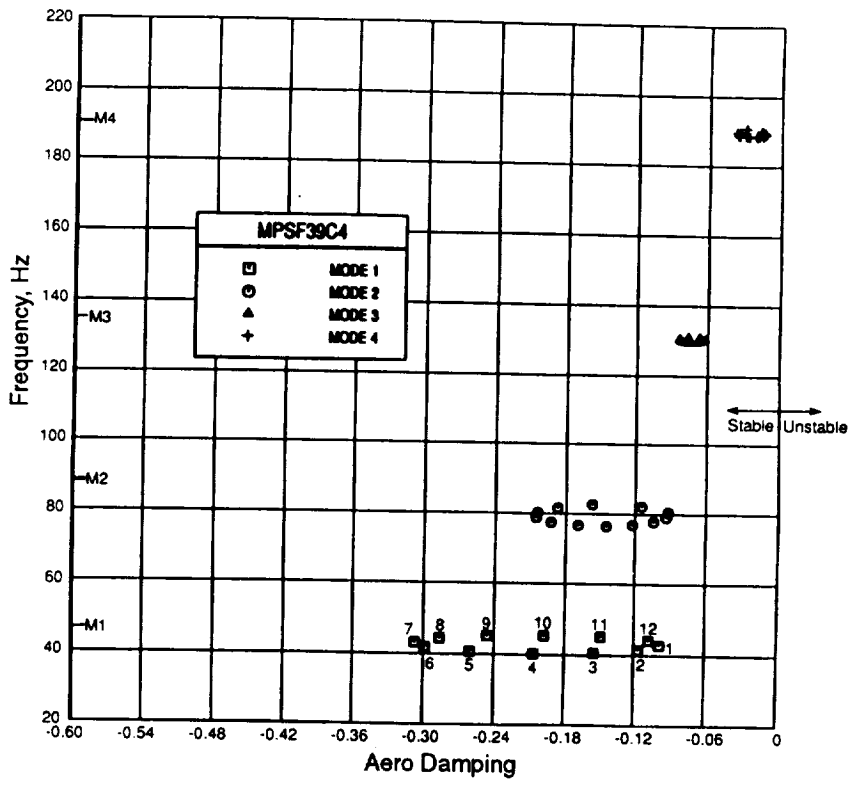

Figure 14. F39C4 Design Point Stability Root Locus Plot.

Blade Tip Leading Edge Deflection		
Condition	Untwist	Direction
without Air Load 100% Speed	–3.8°	Close
with Air Load 0% Speed	+2.0°	Open
with Air Load 100% Speed	–2.3°	Close
Design Intent	–2.6° to –2.7°	Close

- Result shows Divergent-free

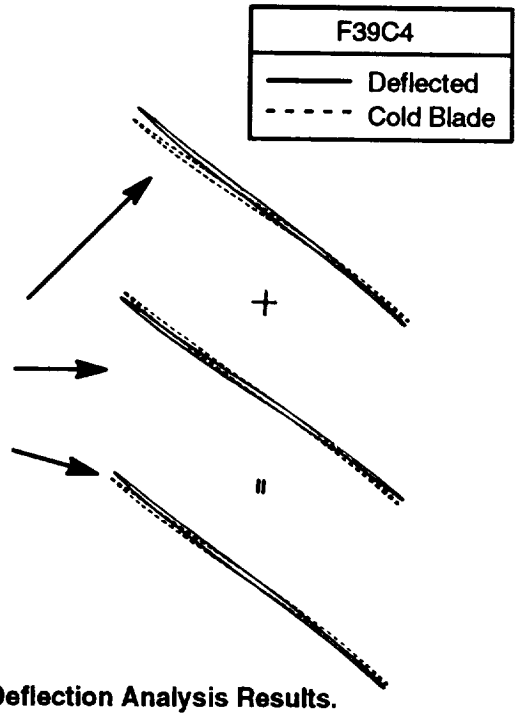

Figure 15. FEM Cold-to-Hot Blade Deflection Analysis Results.

3.3 Mechanical Design

After several aerodynamic, mechanical, and aeromechanical design iterations, the candidate blade shape at design point operating conditions, or hot shape, underwent final mechanical design analysis.

As was the case for previous scale-model unducted fan blades, the forward-swept F39 blade was constructed of a graphite composite shell surrounding a Ti 6-4 airfoil-shaped spar. The spar extended to approximately 50% of the blade height. The platform and trunnion sections that allowed the blade to be installed in the rotating hub assemblies were machined in one piece, integral with the spar. ***Figure 16*** is a schematic of the F39 blade. The size and shape of the spar is based on the F39 airfoil final design shape. The F39 trunnion was designed for use in the 12-blade forward rotor, 10-blade aft rotor (12 x 10) configuration which makes it the same size as the aft-swept F31 trunnion.

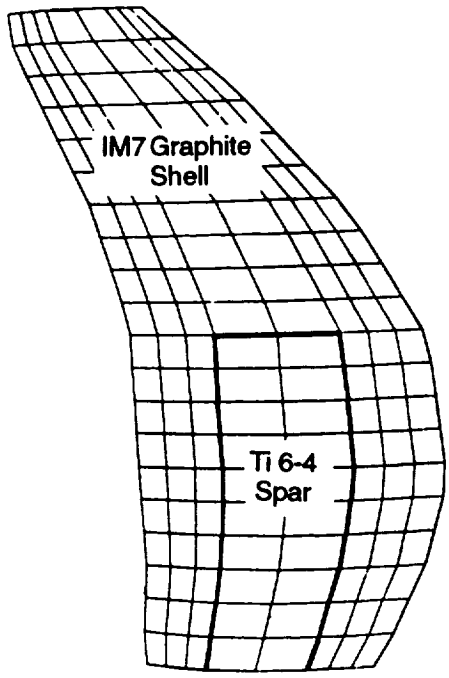

F39	F31
Forward-Swept	Aft-Swept
IM7 Graphite Material	80/20 Graphite/Glass Material
–25° Ref Angle	0° Ref Angle
[0/90/-45/90/0/-45]	[0/90/45/90/0/-45]

Figure 16. F39 Blade Schematic.

The final design shell material and ply lay-up combination were chosen to provide a stable blade at design point, with stresses lower than the capability of the material. The laminate selected for the F39 design was IM7 graphite material and was oriented -25° relative to the blade stacking axis. The IM7 graphite material properties are listed in ***Table 3***. The ply layup schedule was (0/90/-45/90/0/-45), where each ply was 0.0032 inch thick, followed by (0/45/0/-45/. . .), where each ply was 0.005 inch thick. The first 45° ply in the layup schedule was oriented opposite to that of the F31 design to provide more stability.

Table 3. Stable F39 Blade Ply Design Ultimate Strength Properties.

Material Property	Stable F39C4 (IM7 Graphite Material)
Longitudinal Ultimate Tensile Strength, ksi	210.7
Transverse Ultimate Tensile Strength, ksi	3.9
Longitudinal Ultimate Compressive Strength, ksi	111.3
Transverse Ultimate Compressive Strength, ksi	16.2
In-Plane Ultimate Shear Strength, ksi	12.2

To ensure safe operation over the full range of testing desired, stress and vibration characteristics for the forward-swept F39 blade were predicted using a finite element computer program that took the anisotropic nature of the composite material into account. A preprocessor, based on laminate plate theory, was used to convert individual ply properties into bulk element properties for use in the finite element analysis. A finite element model of the forward-swept F39 blade was analyzed using the GE TAMP-MASS program. The model represented the full-scale forward-swept F39 blade geometry. The elements consisted of eight-noded bricks that handled orthortropic material properties. As with previous composite blades, a 3 x 8 x 20-inch mesh was used: three elements through the thickness, eight elements across the chord, and 20 elements along the span. To establish fixed/free boundary conditions, the finite element model was fixed at the base of the spar. This resulted in a higher predicted frequency than actual since the hub and trunnion stiffnesses were not taken into account. However, experience has shown that the hub's rigidity had only a small effect on frequency. Trunnion stress analysis was performed using root reaction loads from the blade's finite element analysis to calculate tensile and bending stresses.

Using the finite element model established for the forward-swept F39 blade, a steady-state analysis was conducted at design loadings to obtain the calculated stresses and deflections presented in ***Figures 17*** and ***18***. A modal analysis was then run on the same model to determine blade frequencies and mode shapes. Since the forward-swept F39 blades would eventually run in the MPS test rig, the predicted blade frequencies were scaled to model size by a factor of 4.985

$$\left(= \frac{\text{full scale diameter}}{\text{model scale diameter}} \right)$$

The model scale blade frequencies and mode shapes are presented in ***Figure 19***. Blade flutter and divergence characteristics for the hot shape were next determined using a GE GAP code stability analysis. The results of this analysis were presented in Section 3.2. The hot shape steady-state, modal, and stability analyses results all indicated that blade stresses, frequencies, and overall stability were within acceptable limits for a forward-swept blade design with the ply layup and material selected.

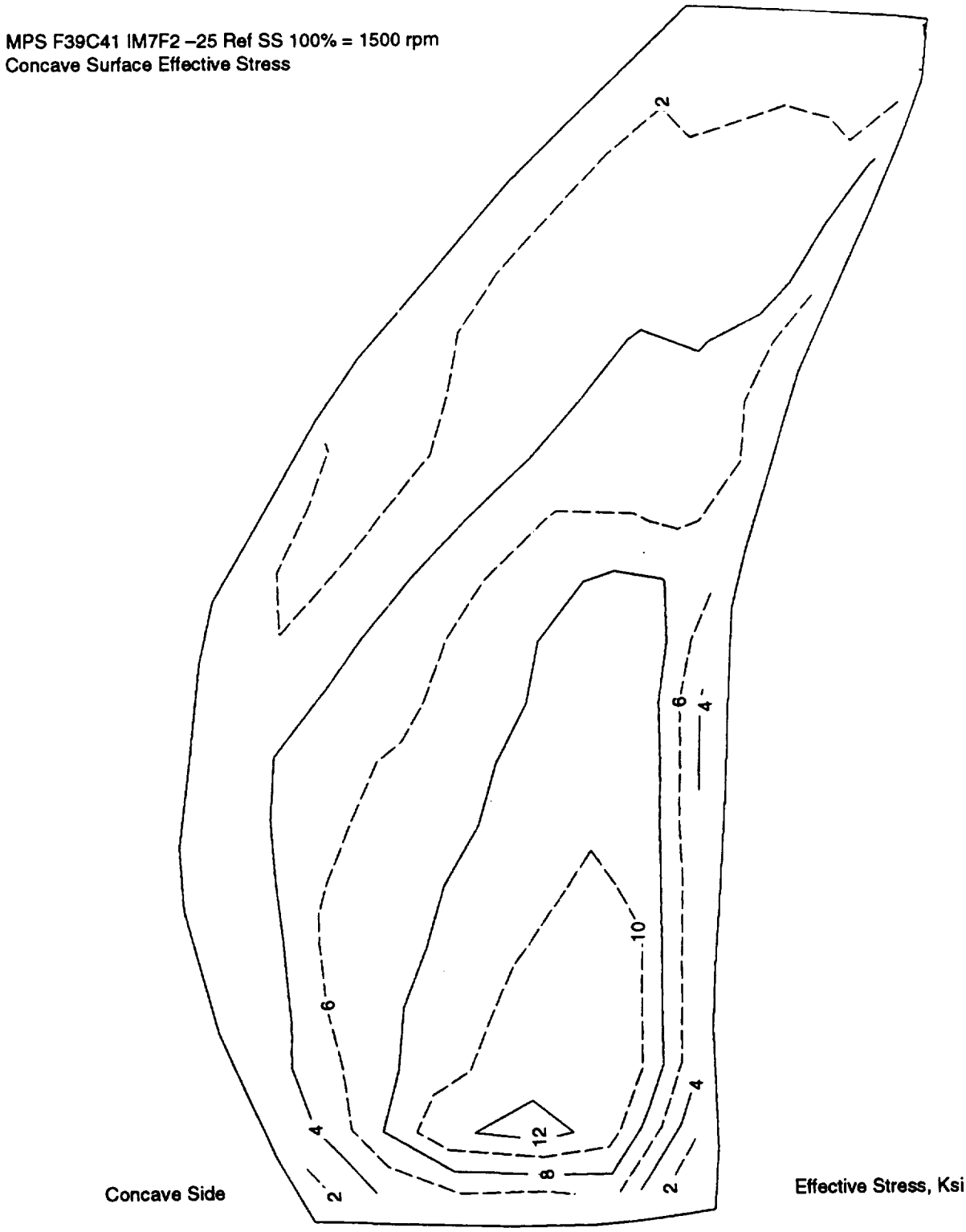

Figure 17. FEM Calculated Steady-State Stresses.

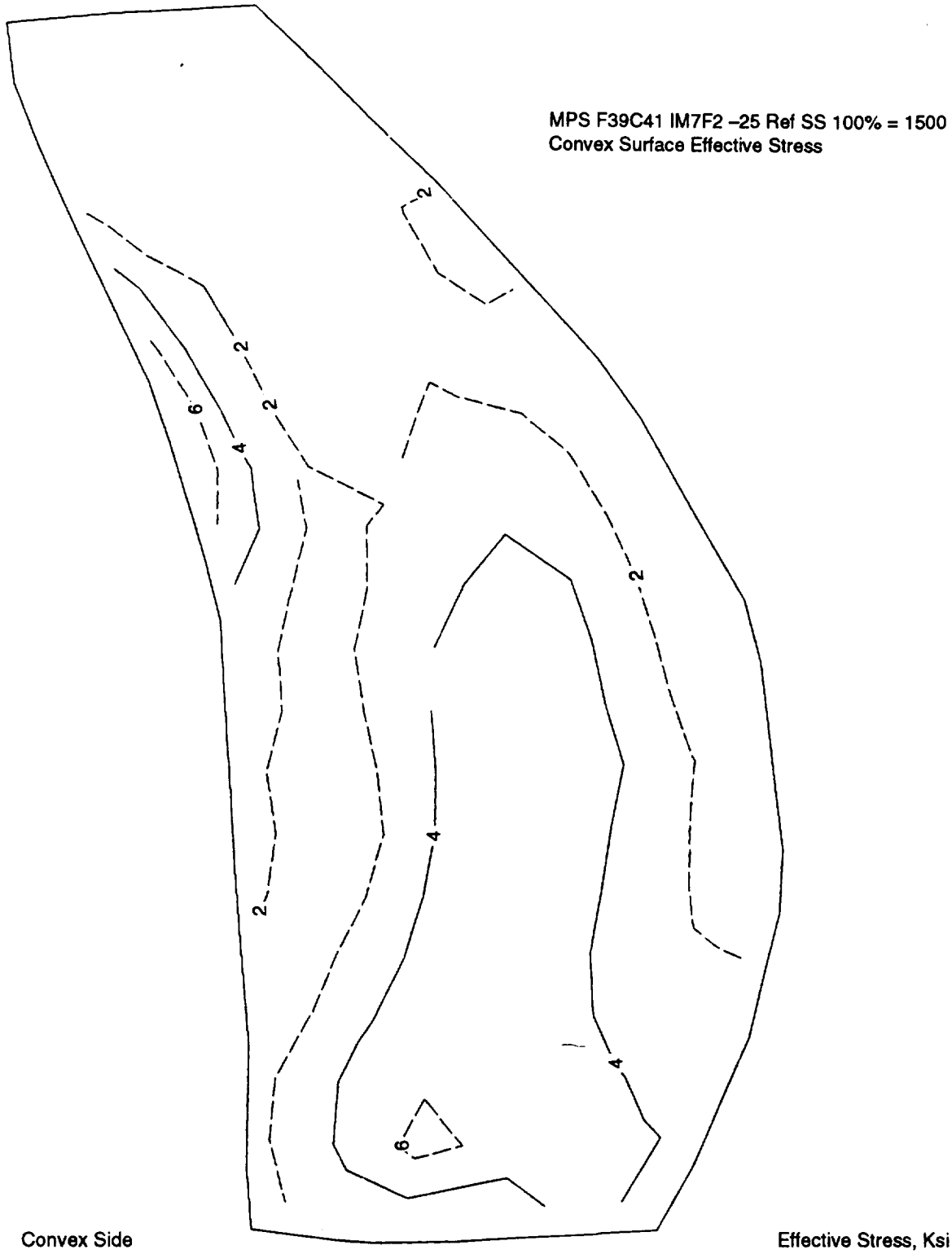

Figure 17. FEM Calculated Steady-State Stresses (concluded).

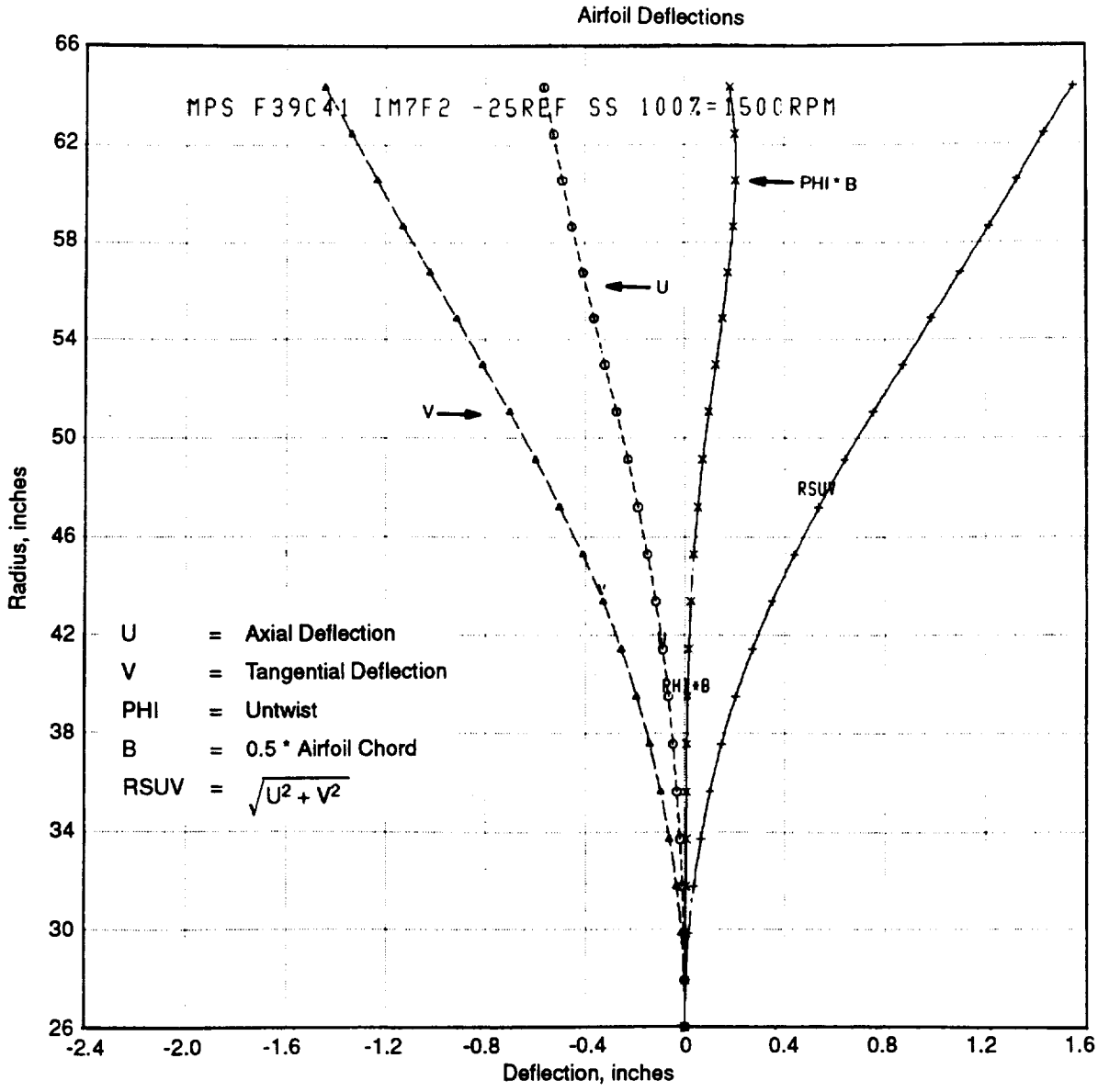

Figure 18. FEM Calculated Blade Deflections.

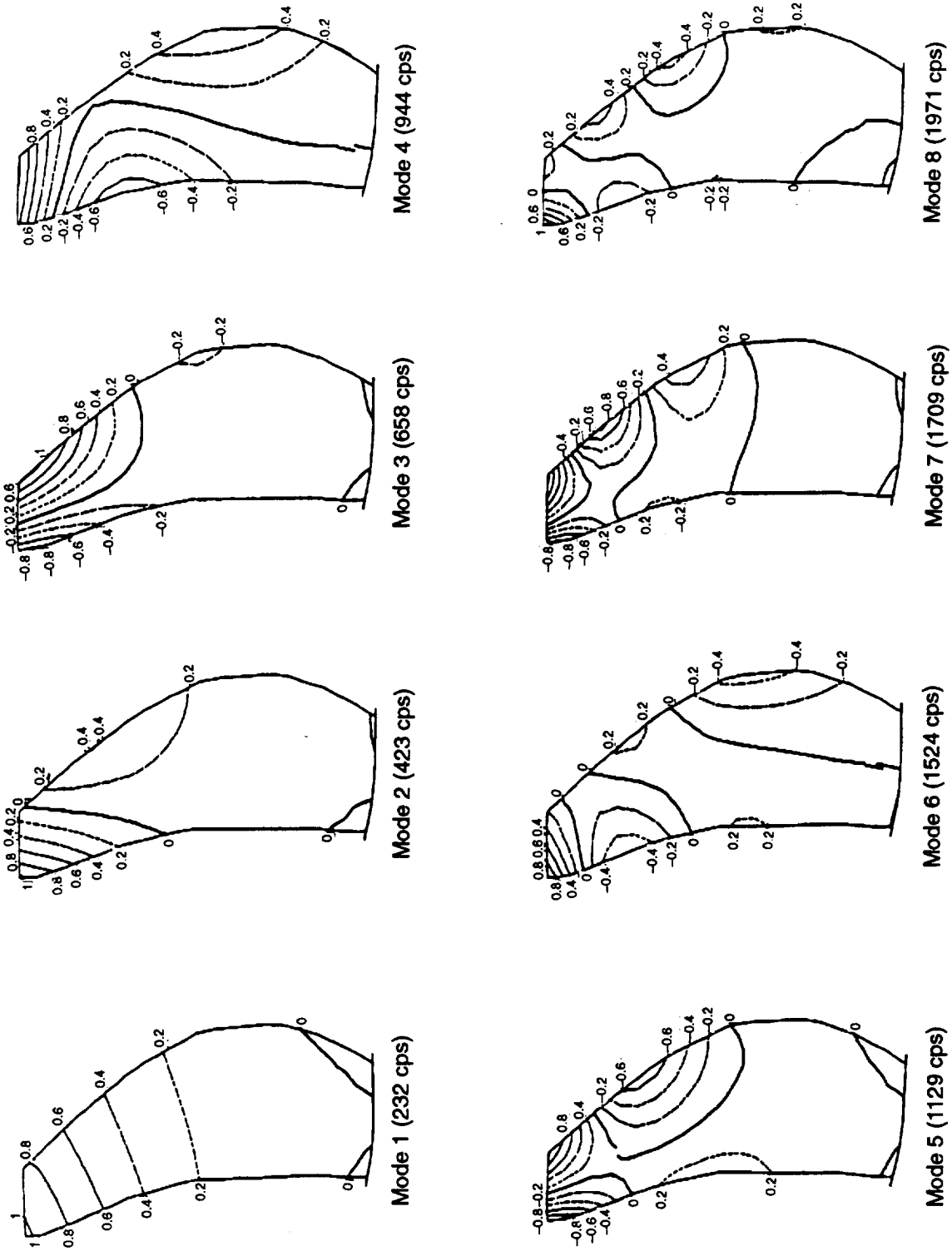

Figure 19. Final F39 Blade Calculated Frequencies (Model Scale) and Mode Shapes.

Once an acceptable hot shape blade design was established, the design process proceeded to the next step: defining a cold, or static, shape for the forward-swept F39 blade fabrication. For determining cold shapes of blades, an iterative procedure was used which recognized that deflections are usually large and non-linear. Using GE's TAMP-MASS computer program, the cold shape for the F39 blade was defined. The "hot-to-cold" conversion process in the TAMP-MASS computer program is automated and is summarized as follows:

1. Run hot shape model with applicable loading.
2. Subtract resultant deflections from original hot shape to obtain estimated cold shape.
3. Run estimated cold shape model with applicable loading.
4. Compare resultant hot shape to original hot shape.
5. Use difference between resultant hot shape and original hot shape to generate a new cold shape.
6. Repeat Steps 3 through 5 until a final cold shape deflects to the desired hot shape.

The accuracy of the TAMP-MASS deflection predictions depended a great deal on the gas loadings input from aerodynamic design.

3.4 Acoustic Analysis

The computer program used to predict the noise from counterrotating open rotors was developed at GE Aircraft Engines in the 1980's. It is described, in its essentials, in *References 3* and *4*. The most recent enhancement to the program, which was employed for the analysis discussed herein, allowed the radial location on the aft rotor of the streamline that passes through the tip of the forward rotor to vary as a function of total thrust, which allowed for the modeling of the streamtube contraction effect experienced under off-design conditions, such as takeoff. Outboard of this streamline, the aft rotor would experience the fluctuating velocities of the forward tip vortices alone; inboard, the velocity field would contain the effects of both tip vortex and wake from the individual forward rotor blades. The success of this computer program in predicting the noise from both model and full-scale UDF® engines has been demonstrated in both *References 3* and *4*. The input requirements are: description of the blade coordinates (chord distribution, thickness distribution, sweep and lean), the operating conditions (flight speed, rotor speed, atmospheric conditions of temperature and pressure, horsepower absorbed, loading distribution and spanwise distribution of forward rotor drag coefficient), and details of the location of the observer (sideline or arc prediction, distance or radius).

4.0 Blade Design Feasibility Studies

4.1 F39 and A39A Studies

4.1.1 Aerodynamic Design

An aft-swept, unducted fan rotor, A39A, was designed to run behind the forward-swept F39 rotor. The A39A blade was configured similar to the existing A31 blade using the design method described in Section 3.1. A quasi-3D throughflow analysis of the F39A39A configuration was performed. ***Figure 20*** shows the streamlines and meridional Mach number contours at the aero design point of Mach 0.8, 35,000 feet. The analysis indicated that when comparing the F39A39A configuration to the F39A31 configuration, very few differences in throughflow velocities were evident. The geometric constraints introduced by the aeromechanical requirements also confined the planform sweep, chord, and airfoil thicknesses to be similar to the A31 blade. These factors led to the conclusion that no significant performance improvement could be achieved with a new design of an aft-swept, aft rotor. Therefore, using the existing A31 rotor with the new forward-swept F39 rotor would be aerodynamically acceptable and most cost effective to the program.

4.1.2 Aeromechanical Analysis

There are two primary aeromechanical stability considerations for forward-swept composite blades: dynamic stability (flutter) and static stability (divergence). Previous experience with aft-swept, unducted fan blades has demonstrated that flutter is an important design consideration. With the incorporation of forward sweep, experience with wings indicates that divergence must also be considered.

Flutter is a condition where a coupled, aeromechanical vibratory mode of the blading is negatively damped. In flutter, vibratory motions of the blade extract energy from the airflow and increase in amplitude. Flutter can occur in different aerodynamic regimes, characterized by relative Mach number, reduced velocity, and incidence. For a blade operating at its design point (35,000 feet, Mach = 0.80), classical transonic flutter is the relevant consideration. For this condition, relative Mach numbers are high (transonic) and the blades are relatively lightly loaded with small incidence angles.

For a blade operating at low forward velocity at high loading (takeoff), stall flutter is the relevant consideration. Stall flutter is observed at conditions of high incidence and loading.

Divergence is a condition where the aeromechanical stiffness (structural stiffness plus aerodynamic stiffness) vanishes. The concept of aerodynamic stiffness arises from the consideration that the aerodynamic forces are deflection-dependent. Divergence has long been a consideration for wings. Conventional aft-swept wings have a favorable relationship between deflection and airloads: as the wing deflects, the incidence, and hence loading, is decreased, as shown in ***Figure 21***. Forward-swept wings deflect under airloads in a manner that increases incidence and hence, loading. A critical velocity, or dynamic pressure, can exist beyond which the structural restoring stiffness is overcome by the opposing aerodynamic stiffness. This is the divergence condition. At divergence,

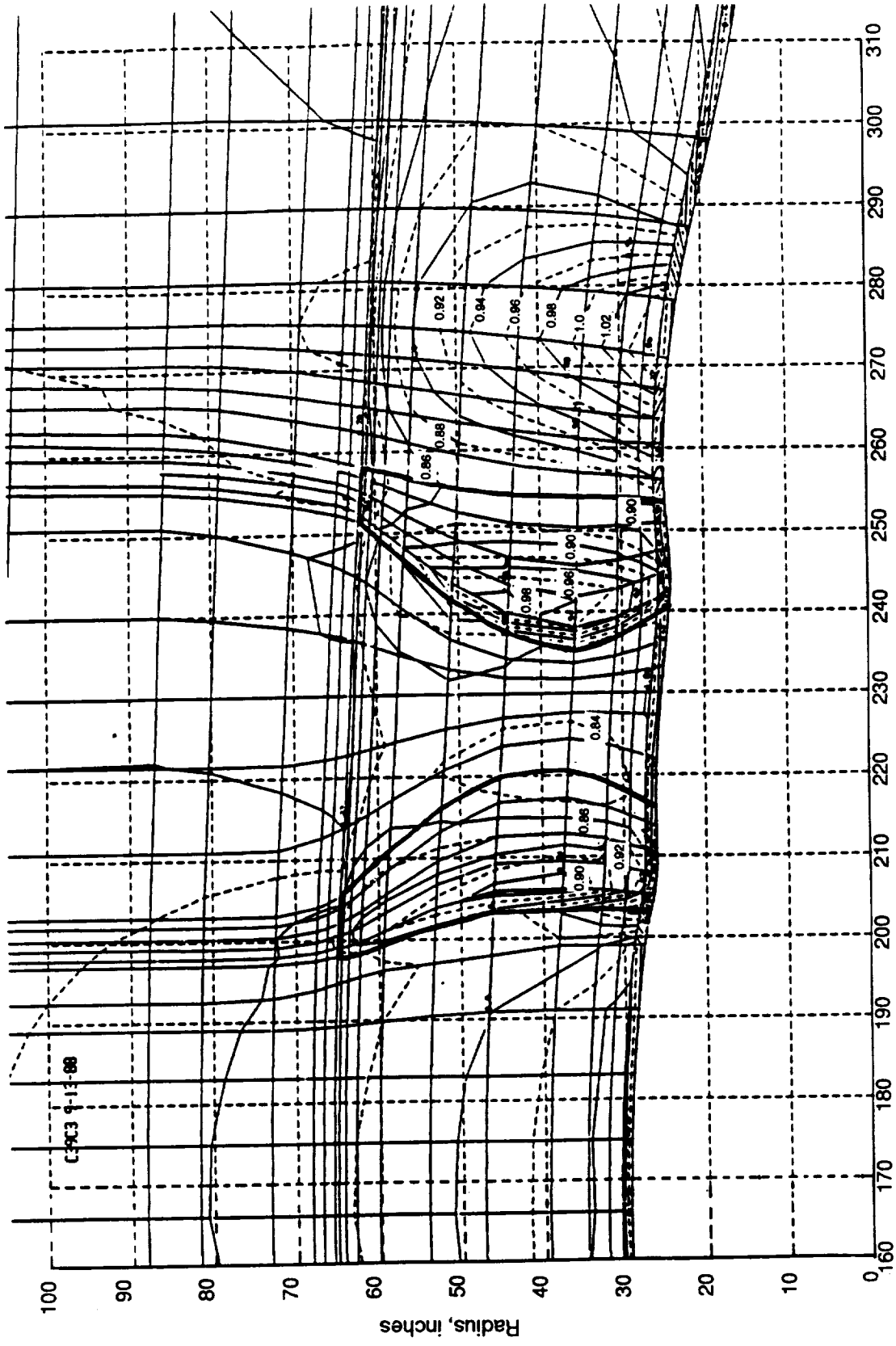

Figure 20. Contours of Meridional Mach Number from Quasi-3D Throughflow Analysis of F39A39A.

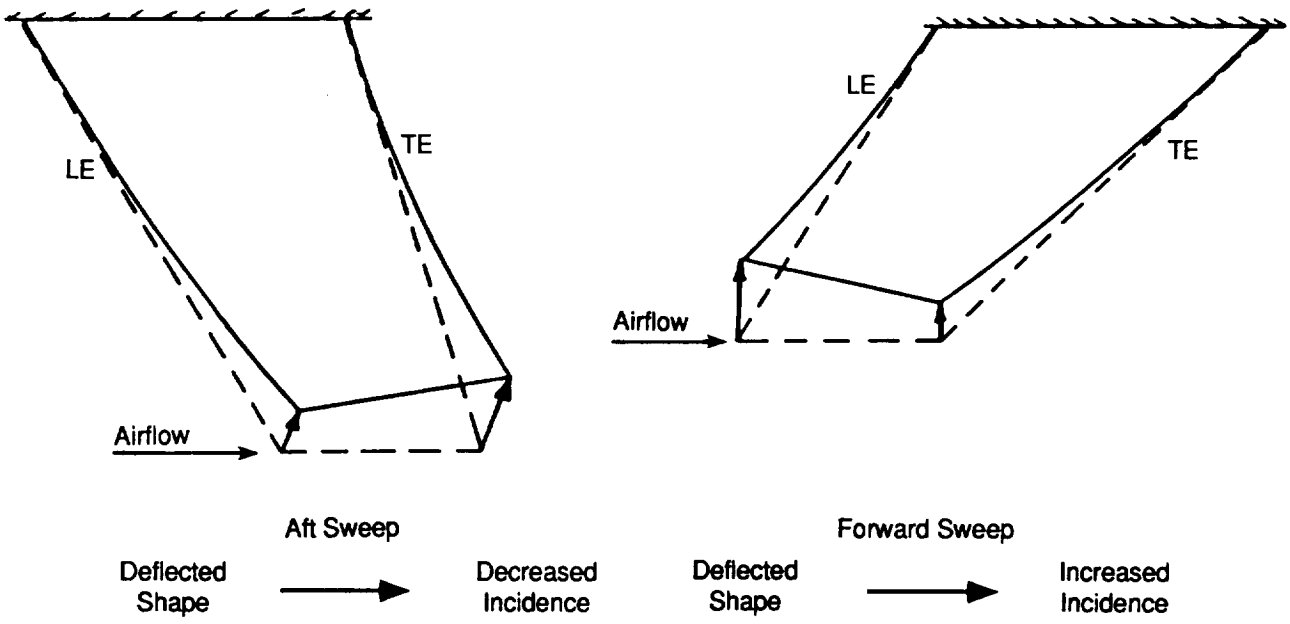

Figure 21. Isotropic Wings – Effect of Sweep Angle.

the deflection increases until either the wing fails or the deflection is limited by some non-linear phenomenon, such as stall. The directional stiffness of composite materials allows for tailoring these load-versus-deflection relationships, and can be used to compensate for forward sweep, as shown in ***Figure 22***. For rotating blades, the centrifugal loading also plays a role in the structural and aerodynamic force balance. In general, the centrifugal loading is a restoring force. In some cases, however, centrifugal effects can increase blade flexibility.

In the preliminary design phase, the mode shape slope, or twist-bend coupling, of the first-flex mode was kept as small as possible in order to minimize any flutter or divergence tendencies of the blade. The results of these preliminary design iterations are summarized in ***Table 2*** (on page 16). The initial baseline design was the F39A4, with AS4 material and the standard ply layup schedule at a 0° reference angle. Subsequent design iterations involved reducing the tip sweep and tailoring the laminate to minimize the mode shape slope and hence, minimize stability concerns. The result of the preliminary design effort was the definition of the F39C3 design.

The aeromechanical behavior of F39C3 was assessed with a dynamic stability analysis using the General Aeroelastic Program (GAP), a GEAE proprietary code. The GAP analysis consisted of a finite element structural dynamic normal mode analysis coupled to a kernel function cascade unsteady aerodynamic analysis. Both methods were linear, with the linearization about the blade design point condition, or hot shape. The preliminary F39C3 design was predicted to be dynamically stable (flutter-free) at the design point, as shown in ***Figure 23***. The divergence margin was determined, using the same dynamic stability analysis, by inspecting the predicted frequency decrease of the aeroelastic system modes compared to the frequency of the normal modes.

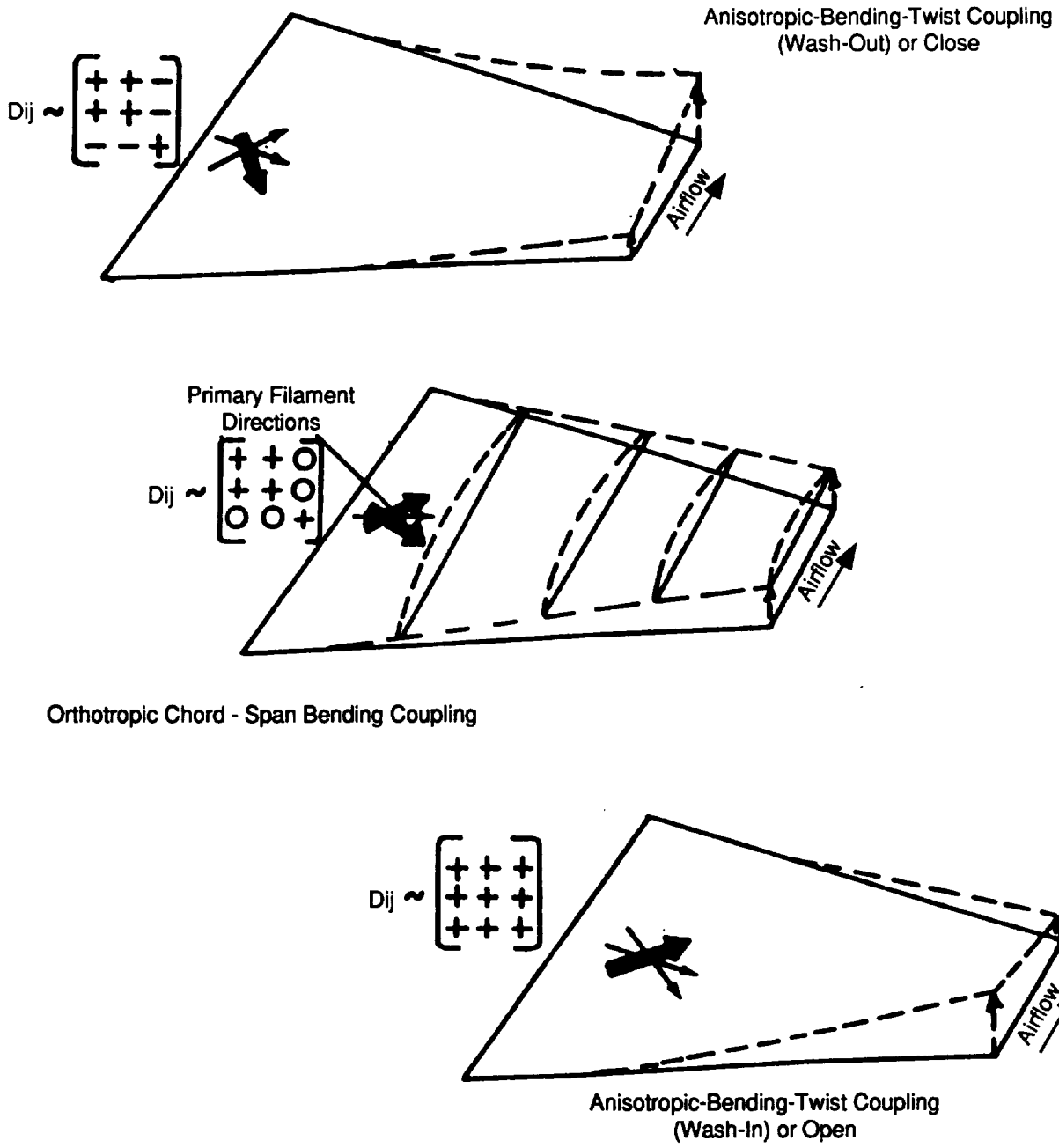

Figure 22. Fiber Alignment and the Effect on Composite Principle Stiffness Direction.

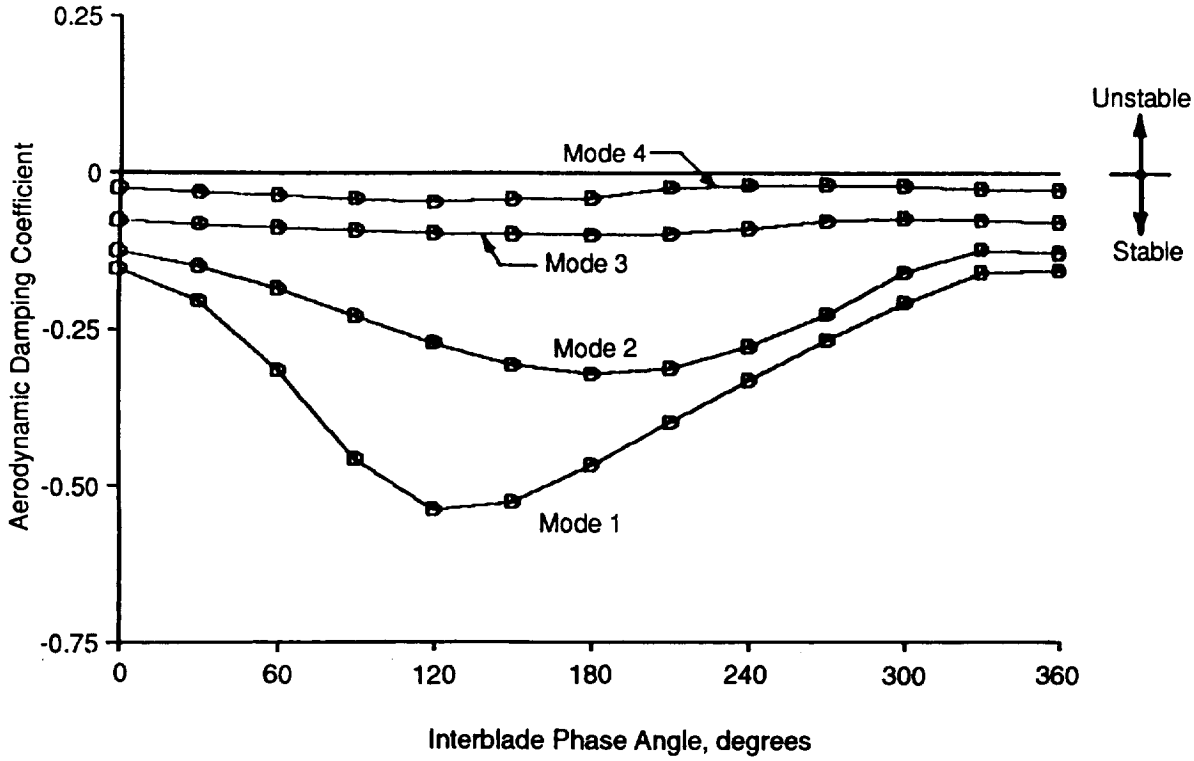

Figure 23. F39C3 Aeromechanical Stability.

Divergence can be thought of as analogous to buckling; that is, a static, zero-frequency instability. Since the first mode frequency reduction of the forward-swept F39C3 blade was predicted to be a modest 11%, the design was considered to be divergence-free.

4.1.3 Mechanical Design

To determine the mechanical integrity of a forward-swept blade design, stress and vibratory characteristics of the design were predicted using a finite element model of the full-scale hot blade shape. Both a forward-swept forward (F39) blade and a forward-swept aft (A39F) blade were evaluated. Based on previous experience with composite blade analysis and testing, the initial laminate selected for the F39 and A39F designs was AS4 graphite material and was oriented 0° relative to the blade stacking axis. The ply layup schedule was (0/90/-45/90/0/45), where each ply was 0.0032-inch thick, followed by a ply layup schedule of (0/-45/0/45/...), where each ply was 0.005-inch thick. To minimize stability concerns, a second laminate was evaluated. This laminate was IM7 graphite material and was oriented -25° relative to the blade stacking axis. The ply layup schedule was (0/90/-45/90/0/-45), where each ply was 0.0032-inch thick, followed by a ply layup schedule of (0/45/0/-45/...), where each ply was 0.005 inch thick. Shown in ***Figures 24*** through ***31*** are stress contour plots and mode shape plots, along with the predicted natural frequencies (model scale) for each case. The predicted natural frequencies were scaled to model size by a factor of 4.985

$$\left(= \frac{\text{full scale diameter}}{\text{model scale diameter}} \right)$$ for comparison to previous MPS designs.

Evaluation of both designs revealed that the forward-swept blade was to have stress and vibratory characteristics similar to previous aft-swept designs, and that the primary design driver would be stability.

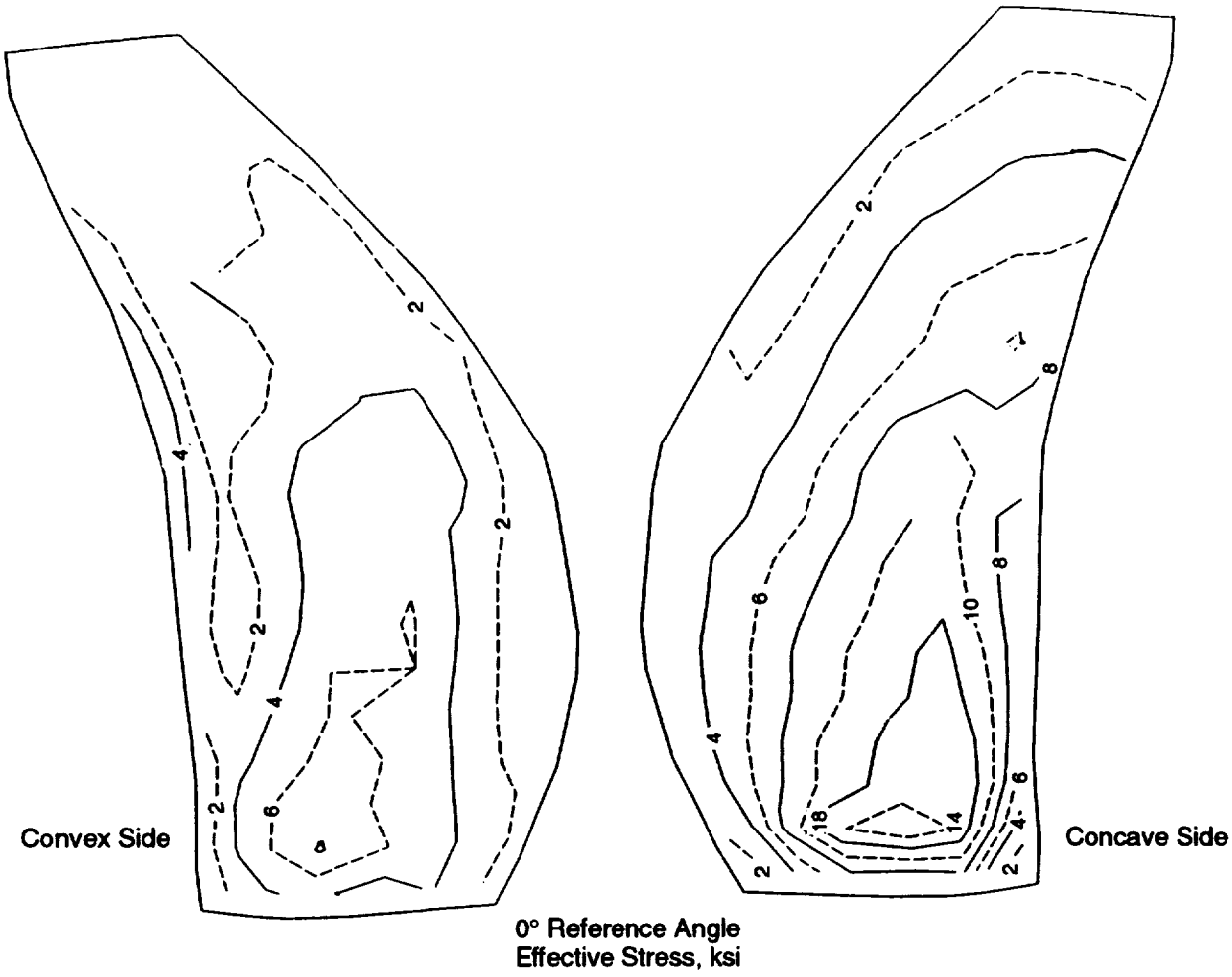

Figure 24. Preliminary F39, AS4 Material Blade Effective Stresses.

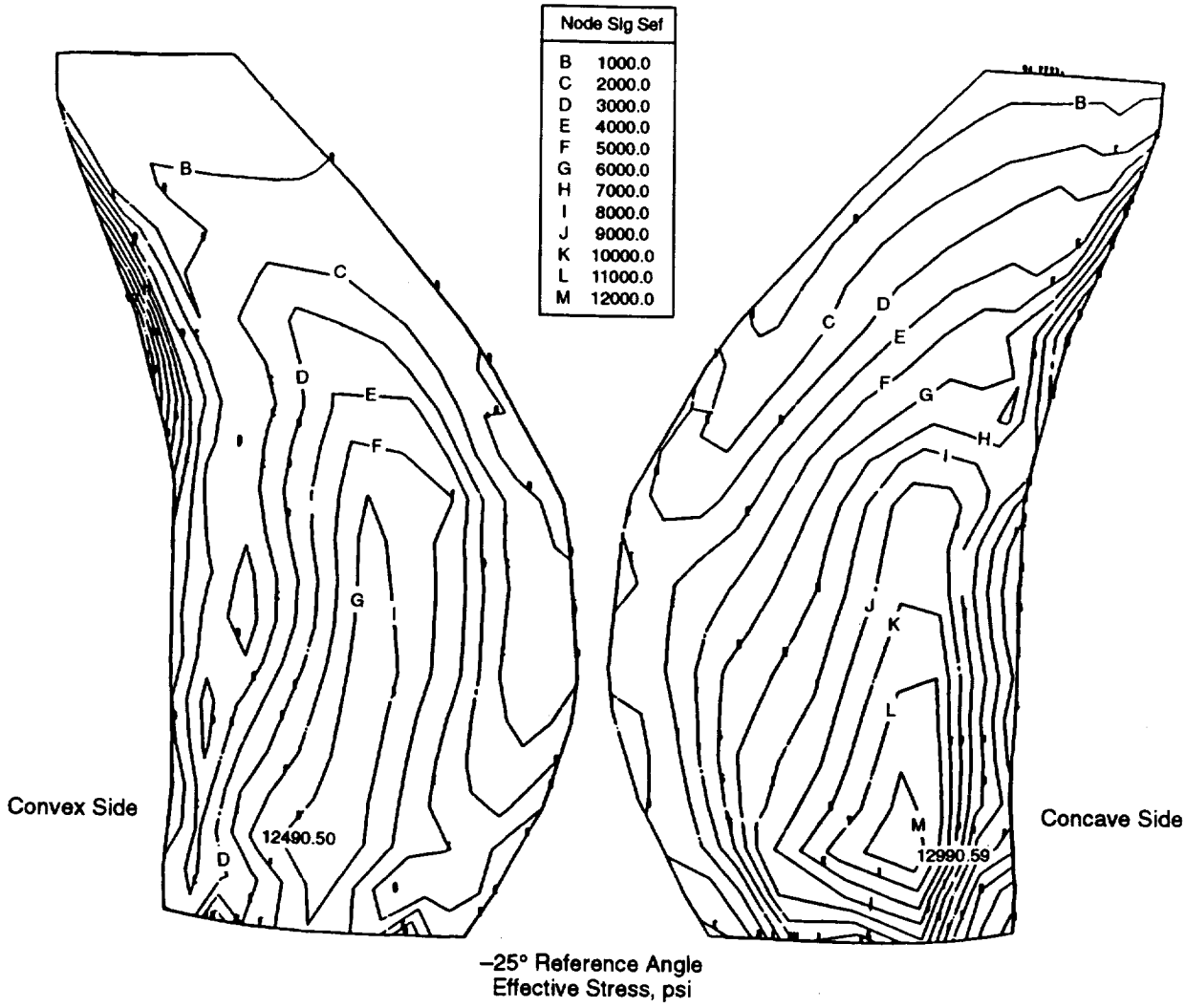

Figure 25. Preliminary F39, IM7 Material Blade Effective Stresses.

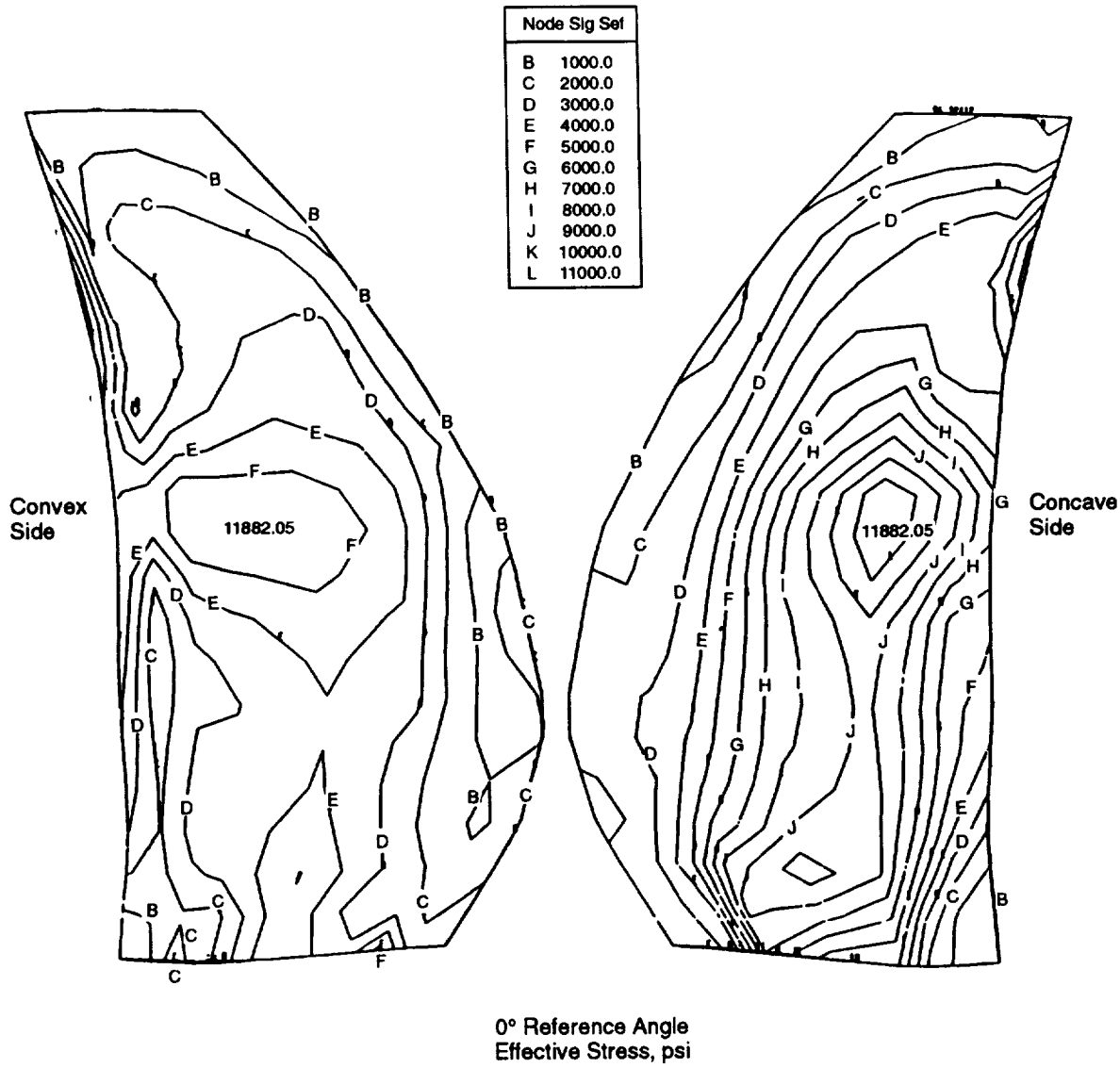

Figure 26. Preliminary A39F, AS4 Material Blade Effective Stresses.

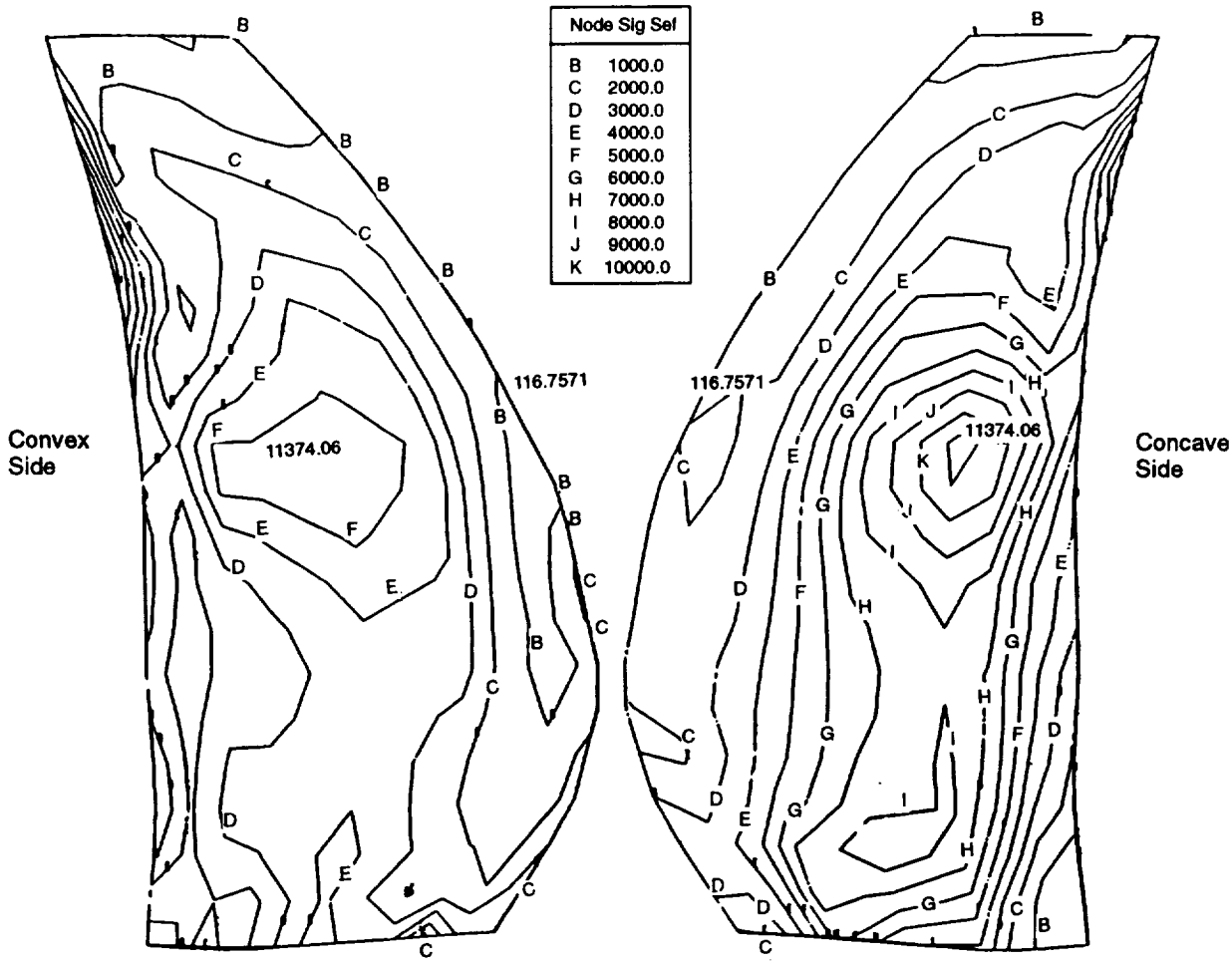

Figure 27. Preliminary A39F, IM7 Material Blade Effective Stresses.

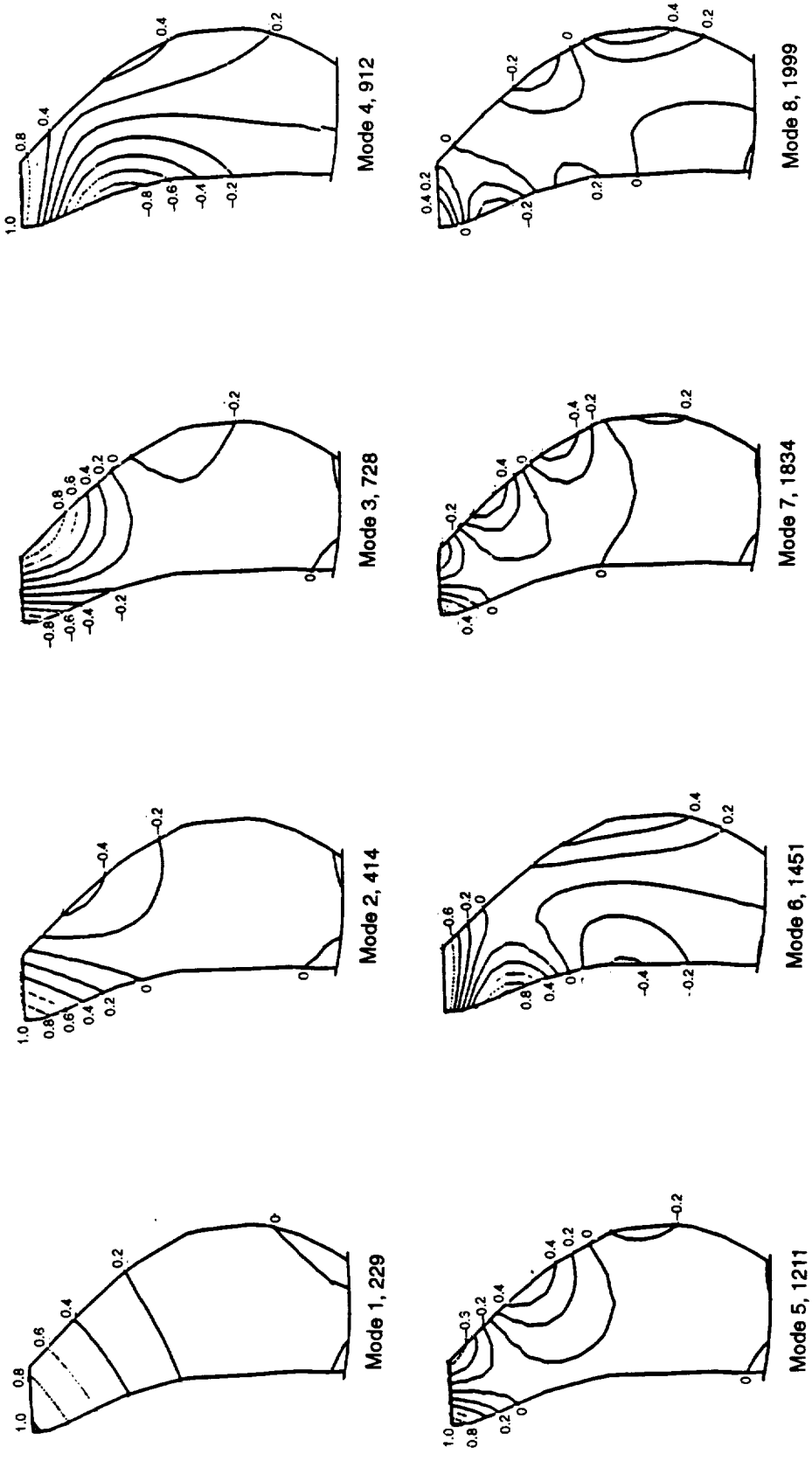

Figure 28. Preliminary F39, AS4 Material Blade Calculated Frequencies (Model Scale) and Mode Shapes.

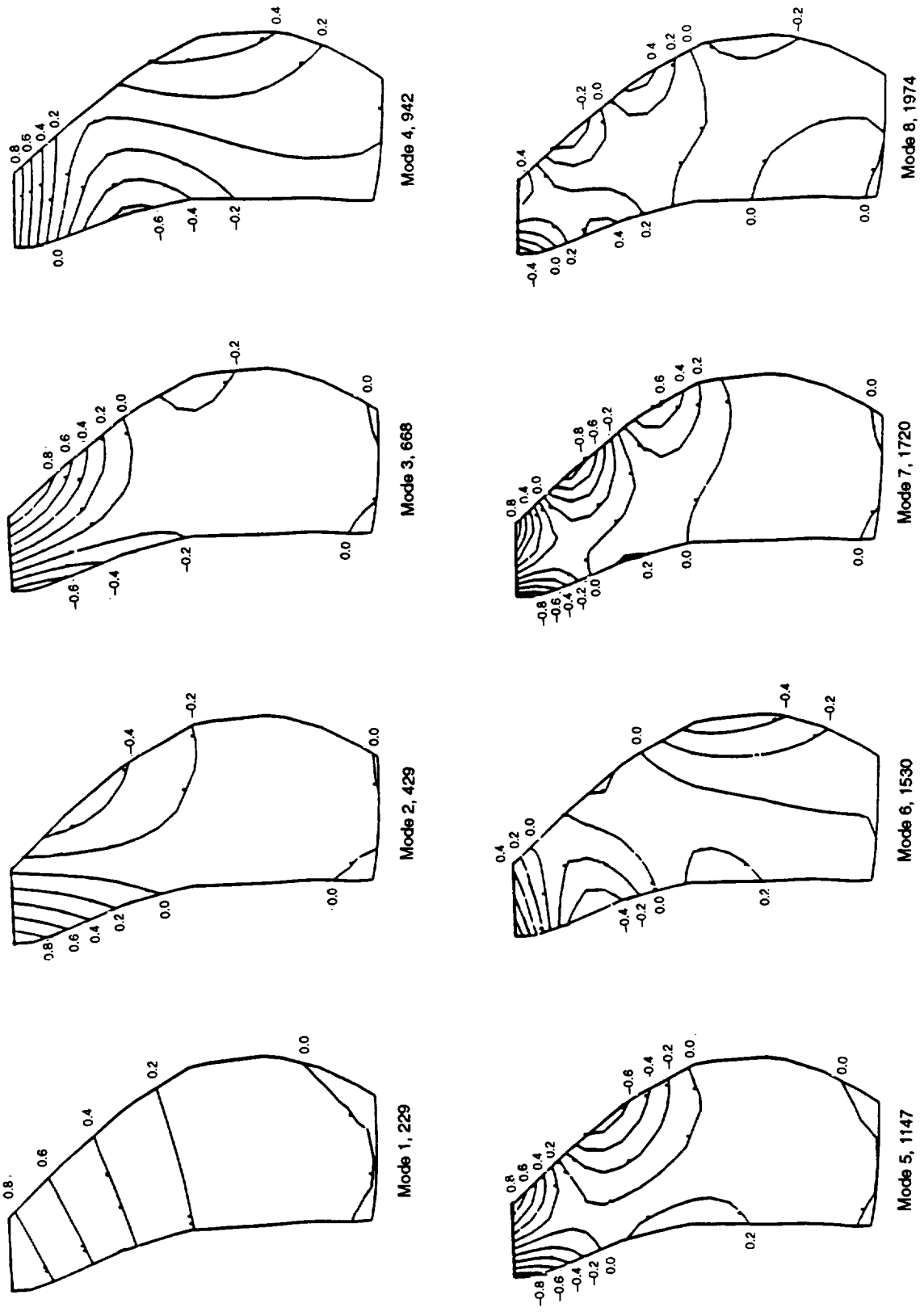

Figure 29. Preliminary F39, IM7 Material Blade Calculated Frequencies (Model Scale) and Mode Shapes.

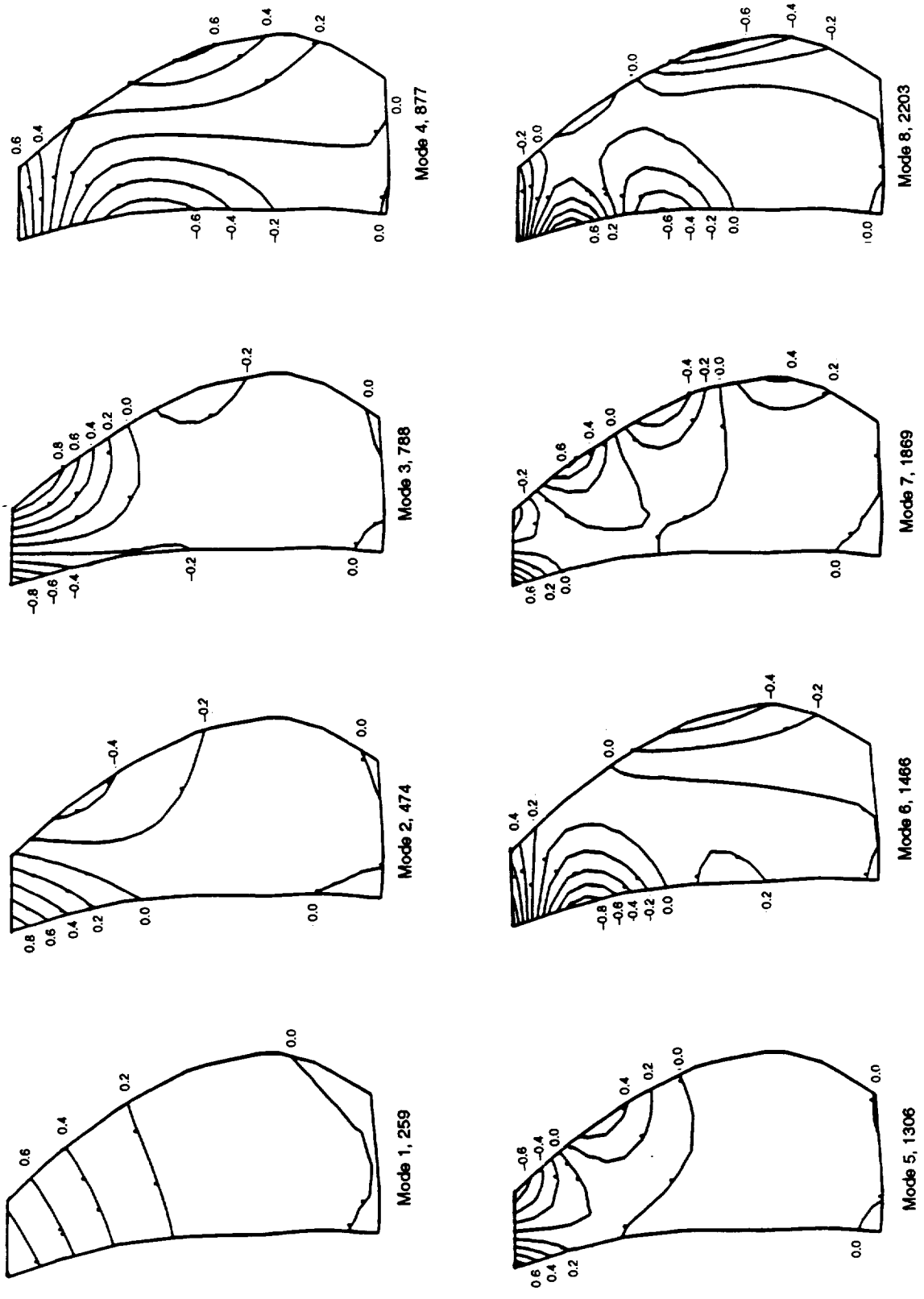

Figure 30. Preliminary A39F, AS4 Material Blade Calculated Frequencies (Model Scale) and Mode Shapes.

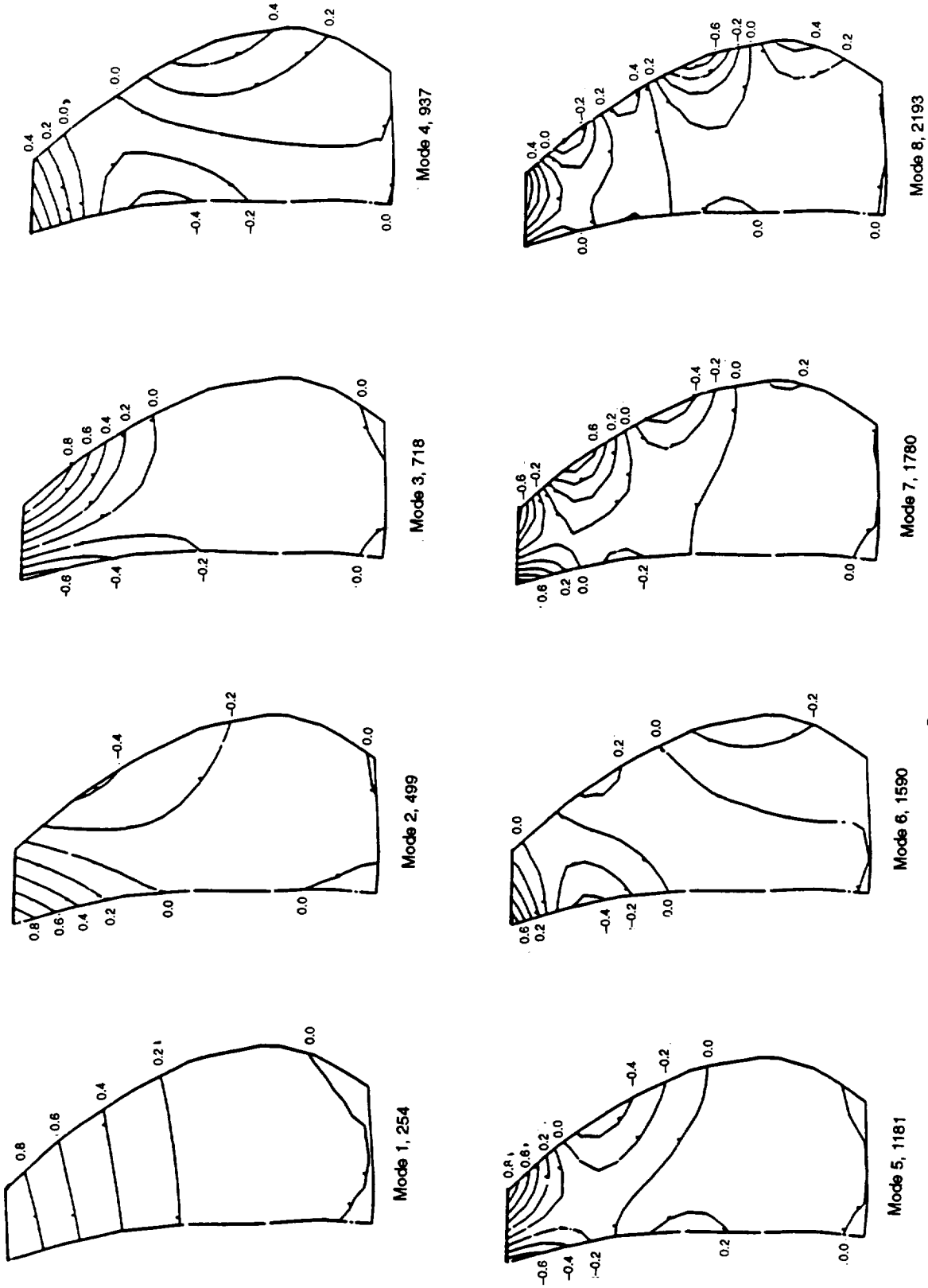

Figure 31. Preliminary A39F, IM7 Material Blade Calculated Frequencies (Model Scale) and Mode Shapes.

4.2 F39A31 Feasibility and A39F Design Studies

4.2.1 Aerodynamic Design

Aerodynamic design studies were performed to assess the feasibility and performance benefits of a forward-swept, aft rotor (A39F) designed to run behind the forward-swept, forward rotor (F39). The analytical studies included the throughflow calculation of the F39A39F configuration and the 3D Euler analysis of the blade-to-blade flow properties. The main purpose of the aero studies was to determine if the performance benefits warranted a recommendation to pursue the dual forward-swept rotors as opposed to only a forward rotor, forward-swept design. In the latter case, the existing aft-swept, aft rotor (A31) would be used in the proposed test program.

Aerodynamic analyses included a quasi-3D throughflow calculation of both configurations: F39A39F and F39A31. The A39F rotor was positioned on the existing UDF® nacelle hub flowpath to produce the most favorable throughflow velocities in the hub region. This resulted in the blade being located slightly forward relative to the A31 flowpath. The flowpath and meridional Mach number contours are shown in ***Figure 32*** for the Mach 0.8 design point calculation. The radial distributions of meridional Mach numbers at aft rotor internal blade stations as compared to the A31 values, are shown in ***Figure 33***.

In the forward portion of the A39F blade, the Mach numbers were generally lower at the inner region of the blade and higher near the tip. This primarily was due to the radial balance of flow influenced by the planform shape. The Mach numbers at the leading edge were slightly lower on average since the forward sweep of the blade at the tip allowed the blade to lie in a more open annulus area and created a different radial distribution of flow properties. In the trailing edge region, the A39F Mach numbers were slightly higher than the A31 values in the outer and inner regions of the blade, and were similar near the pitchline.

A three-dimensional Euler analysis with a coupled boundary layer calculation was run for the A39F blade using source terms to represent the presence of the F39 forward rotor. The calculation grid is shown in ***Figure 34***. Resulting surface Mach number distributions for three spanwise sections are shown in ***Figures 35*** through ***37***. A similar Euler calculation for the aft-swept A31 rotor was made. These resulting surface Mach number distributions are also shown in ***Figures 35*** through ***37*** for comparison. The forward-swept A39F rotor showed a distinct improvement in peak suction surface Mach numbers near the tip and had reduced diffusion rates from the peak location on the suction surface to the blade trailing edge. These findings were similar to those from the forward-swept forward rotor F39 analysis.

4.2.2 Acoustic Analysis

The concept of the Unducted Fan (UDF®) engine offers an attractive alternative to turbofan propulsion for certain future commercial applications because of its substantially higher propulsive efficiency potential. A major obstacle to the use of these engines, however, lies in the noise signature of the counterrotating fan. This may result in unacceptably high levels within the cabin of an aircraft under cruise conditions, and also in potential noise problems on the ground under typical takeoff and

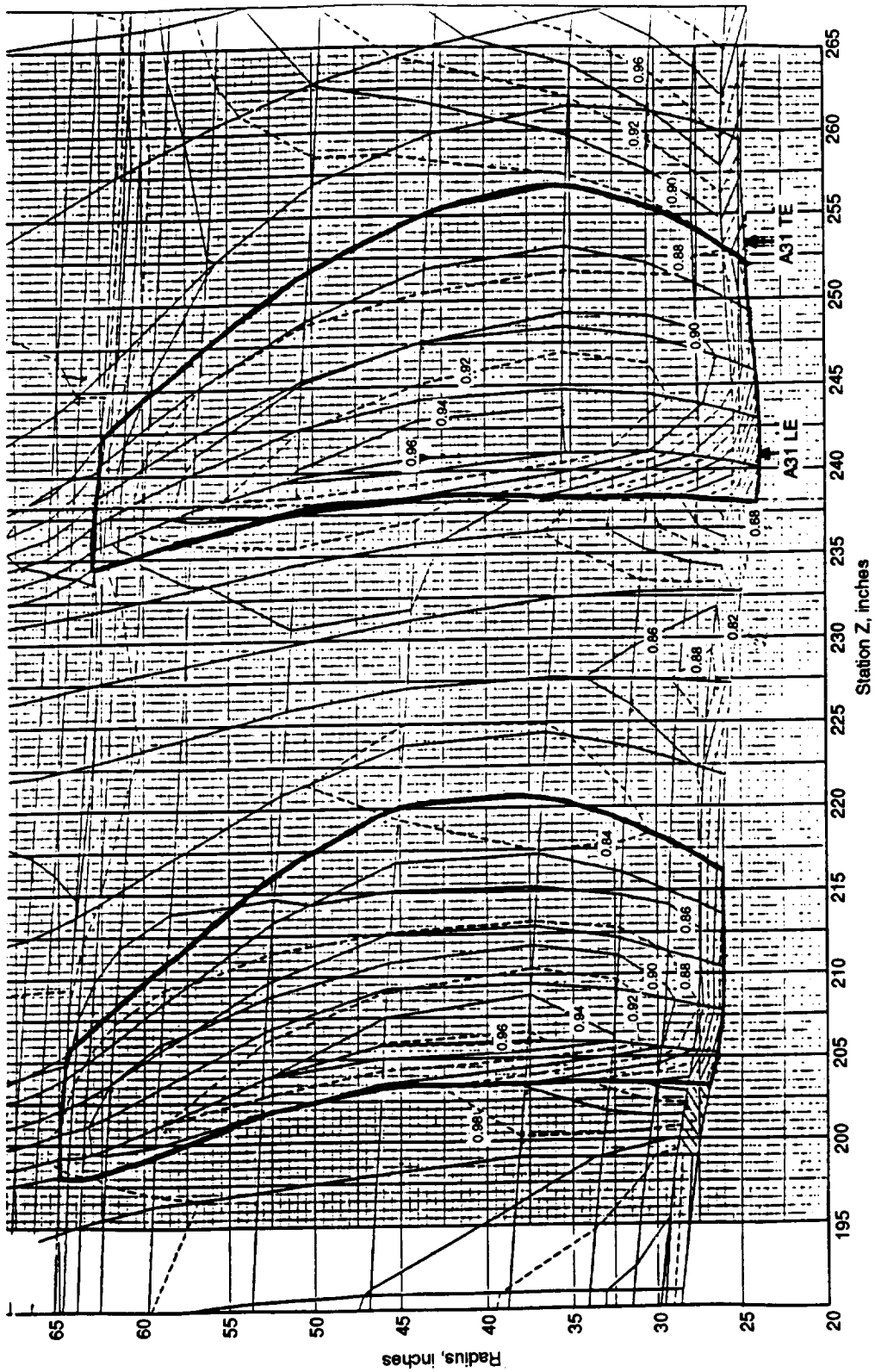

Figure 32. Contours of Meridional Mach Number for the F39A39F Configuration.

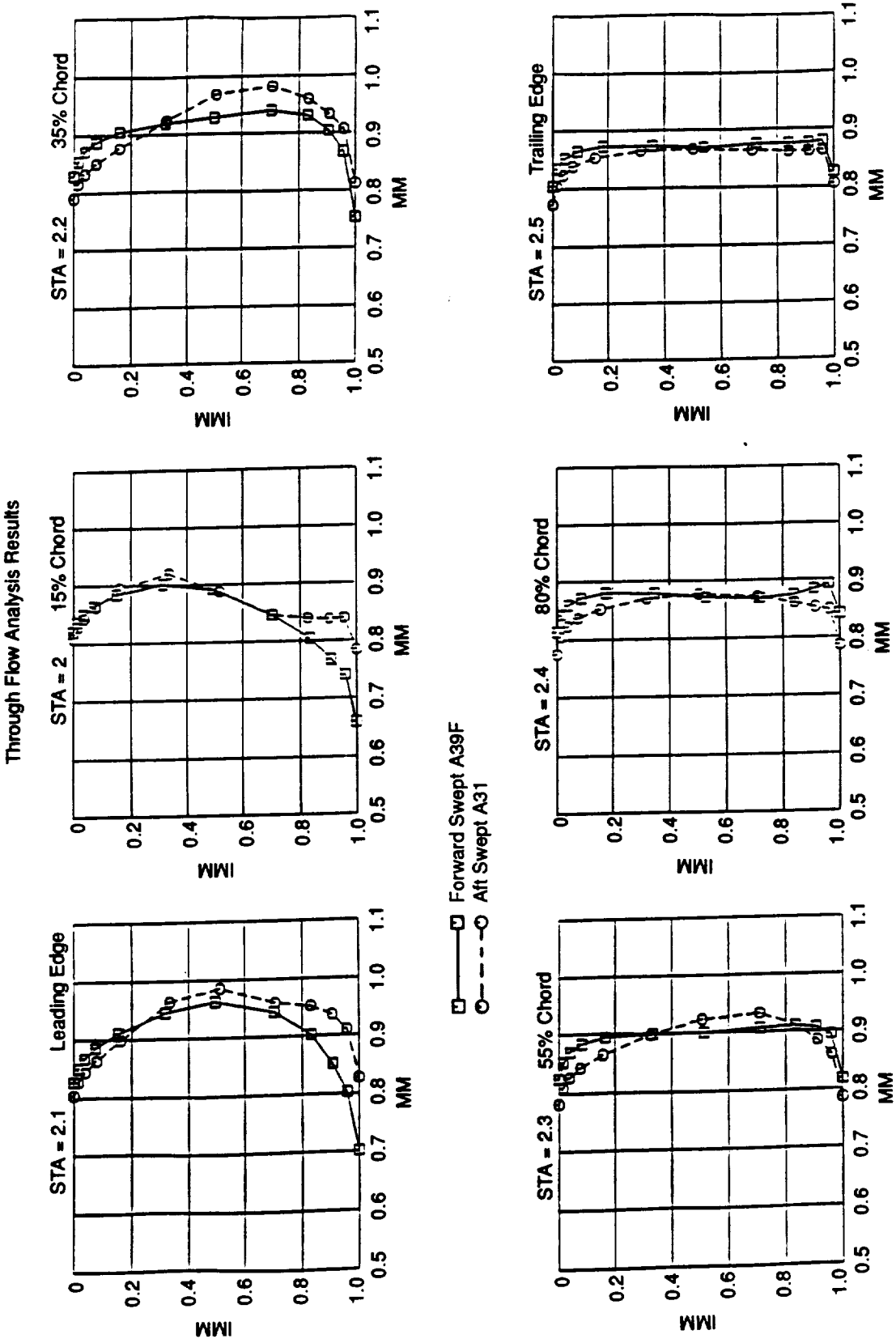

Figure 33. Comparison of A39F and A31 Radial Distributions of Meridional Mach Numbers.

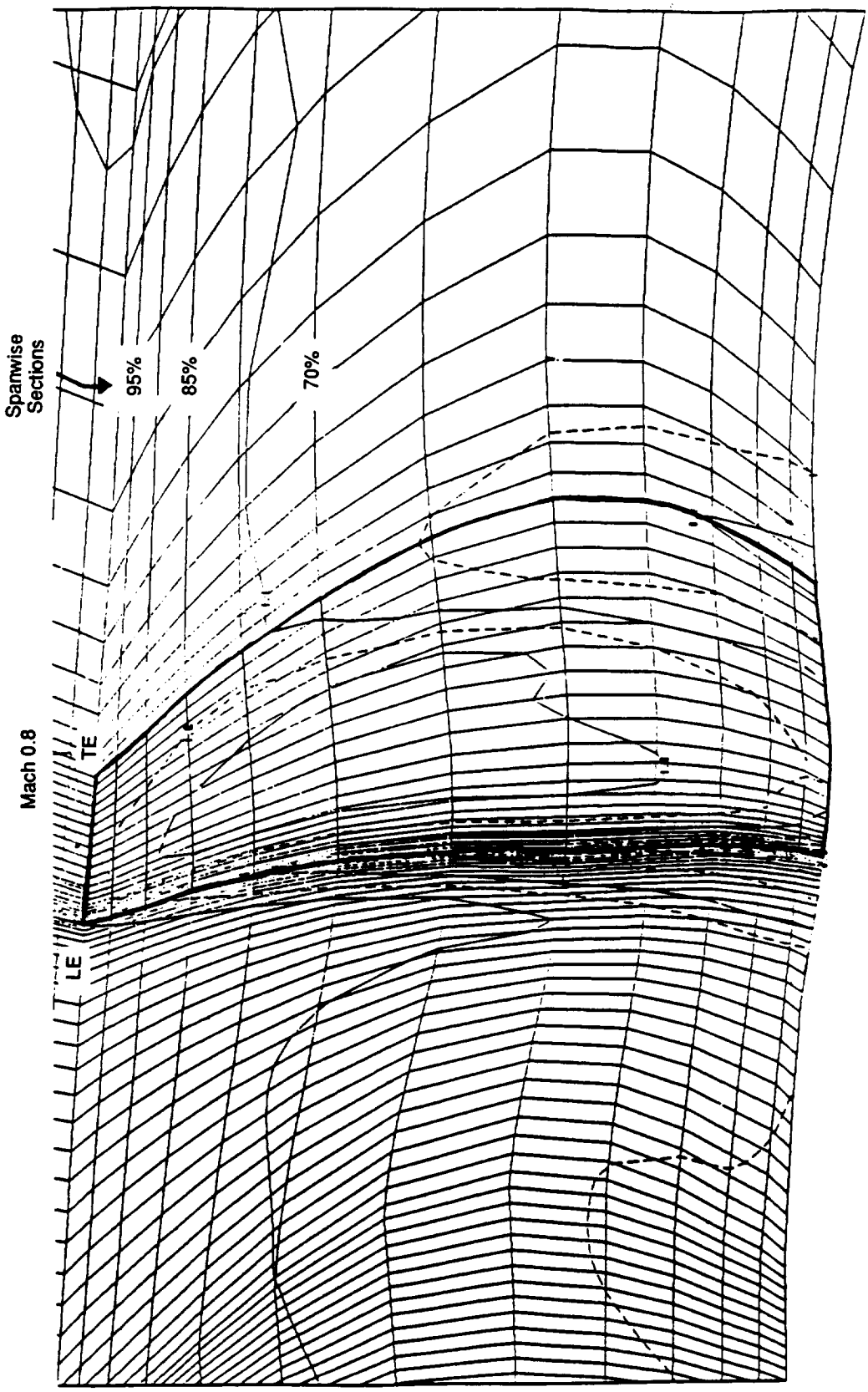

Figure 34. Meriodinal View of A39F Calculation Grid in Euler Analysis.

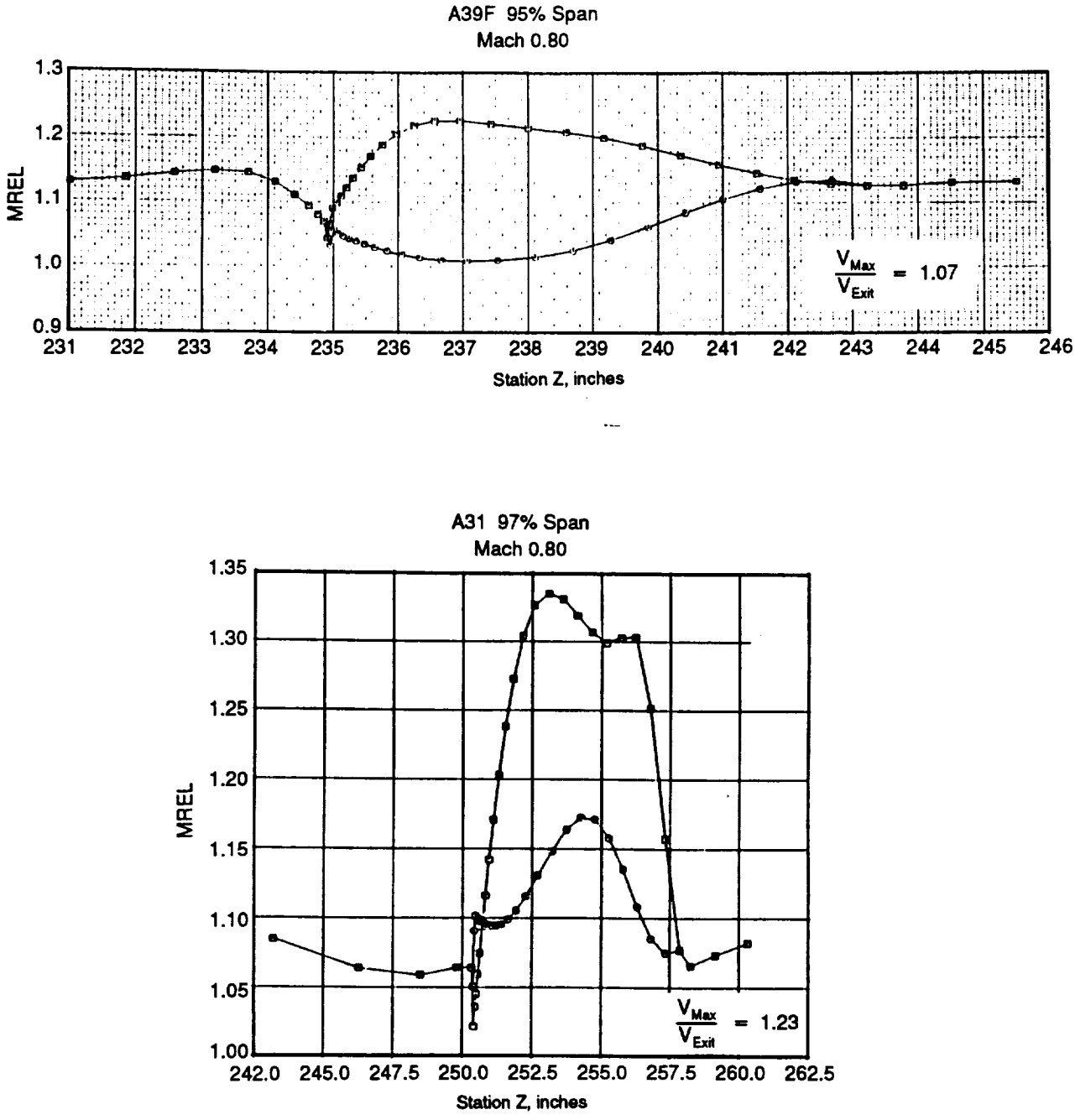

Figure 35. Comparison of A39F and A31 Surface Mach Number Distribution Near 95% Span.

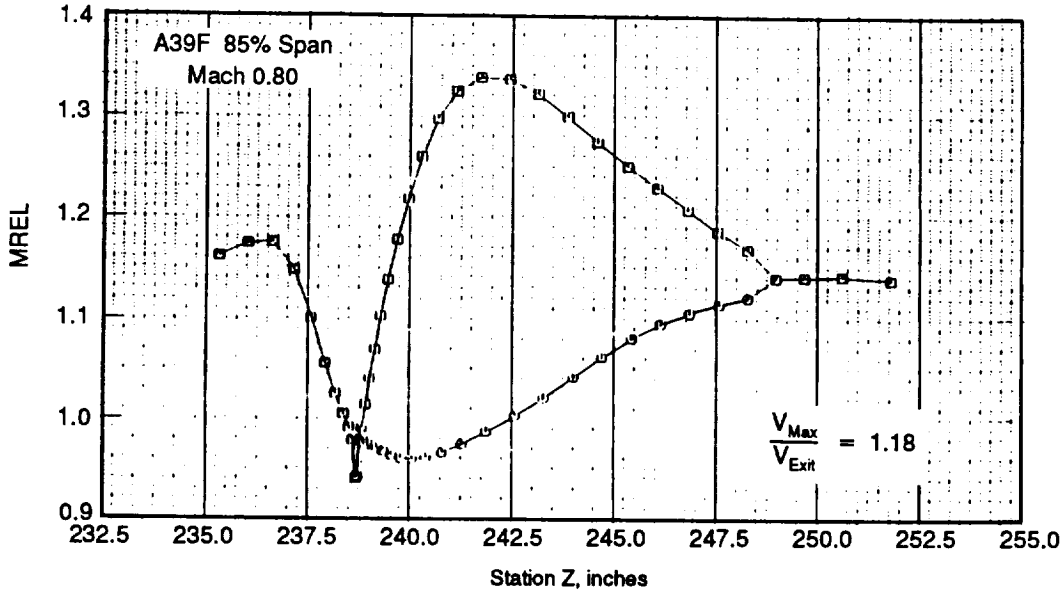

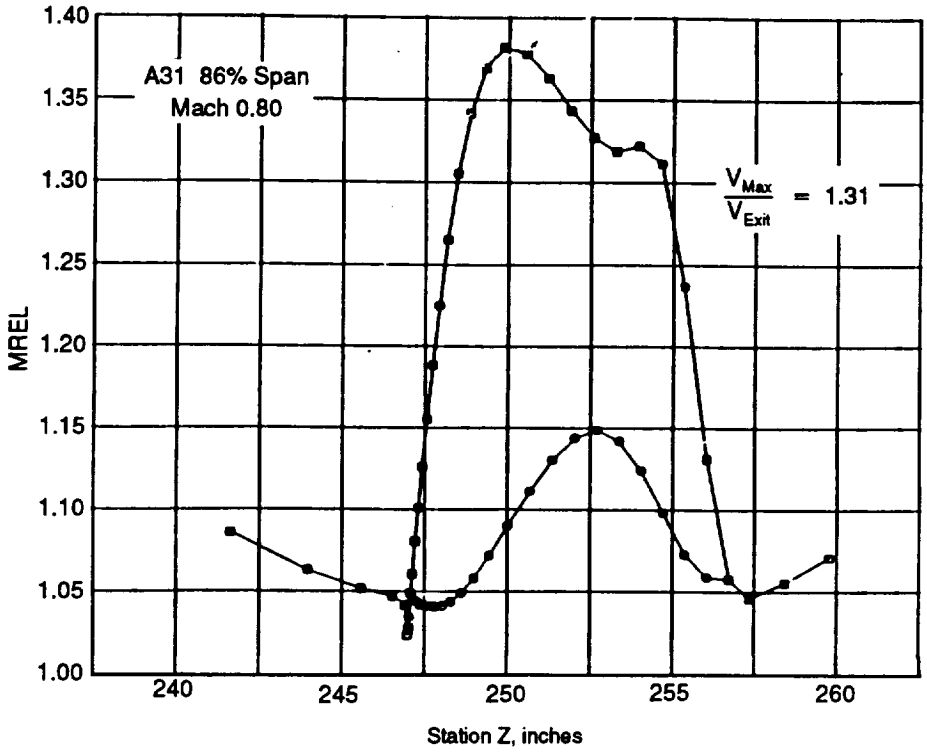

Figure 36. Comparison of A39F and A31 Surface Mach Number Distribution Near 85% Span.

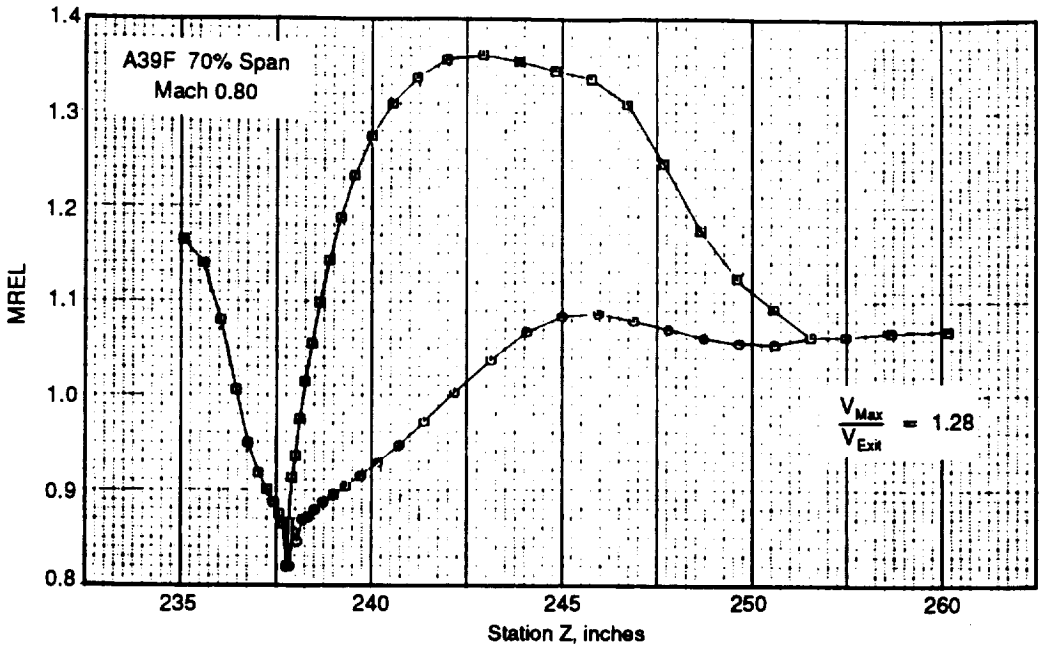

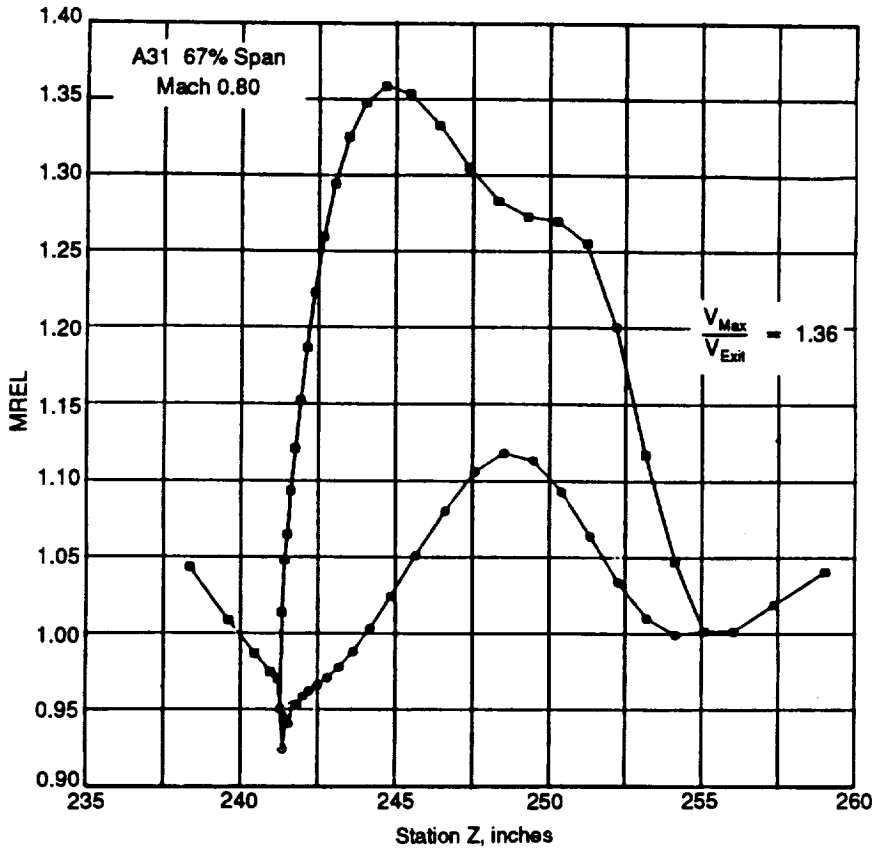

Figure 37. Comparison of A39F and A31 Surface Mach Number Distribution Near 70% Span.

approach conditions. The noise sources of concern differ between these two regimes. At high flight speed, as the relative Mach number on the blade tips becomes supersonic; the dominant noise sources are those of steady loading and thickness. The design of the blade planform becomes important in that phase cancellation between sources on the blade is achievable at high speeds. Noise generated by the interaction of the two blade rows has a minor role in the total noise picture under these conditions. At low flight speeds, such as those encountered in the takeoff and landing phases of a mission, the aerodynamic interactions between the blade rows become the main sources of the radiated noise. Wakes and vortices, shed from the forward blades, interact with the blading of the aft rotor to generate fluctuating lift forces on the rotating blades. These fluctuating loads are highly efficient noise generators at low flight speeds.

The acoustic benefit from the forward-swept forward rotor concept was anticipated to be twofold. First, by increasing the bladerow-to-bladerow distance in the vicinity of the rotor tips (where the most efficient acoustic sources are to be found), the wakes shed from the forward blades would have a further distance in which to decay prior to their encounter with the rear blading; hence, the magnitude of the fluctuating forces generated on the rear blades would be reduced and the corresponding sound levels would be lower. In addition, in a manner analogous to the behavior of a forward-swept wing, the leading edge vortex was expected to be directed inward rather than combining with the tip vortex, thus reducing the strength of the vortex that ultimately interacts with the tip region of the aft rotor blades. (On an aft-swept blade, the leading-edge vortex moves outward to combine with the tip vortex.)

The forward-swept F39 forward blade design is shown with the A31 aft blade design, and compared with the aft-swept F31 design under cruise conditions in ***Figure 38(a)*** and at takeoff in ***Figure 38(b)***. Noise predictions were made under the following conditions for the cruise configuration:

- Altitude: 35,000 feet
- Speed: Mach 0.8
- Performance: Design
- Sideline Distance: 7 feet (tip clearance/diameter ~ 0.16)
- Free Field Conditions (no fuselage reflection/refraction effects)

The required aerodynamic/performance input was obtained from the aerodynamic designers for both the F31A31 and F39A31 configurations. The results are shown in ***Figure 39*** for the predicted directivities of the forward rotor Blade Passing Frequency (BPF), 2BPF and 3BPF tones, the aft rotor BPF tone, and the first forward/aft rotor interaction tone. The predicted peak levels for the forward-swept F39 blade and F31 blade BPF tones were almost the same, with the F39 blade tones approximately 1 dB higher than the F31 blade tones. It could be seen that with increasing frequency, the forward-swept F39 blade levels were higher than those of the aft-swept F31 blade. These differences were thought to arise from the reduced sweep in the hub region of the F39 blade that provided less spanwise phase cancellation between the sources.

Under takeoff conditions, comparisons were made initially with the overall noise metrics used typically in community noise predictions. Comparisons between the F31A31 and F39A31 blade

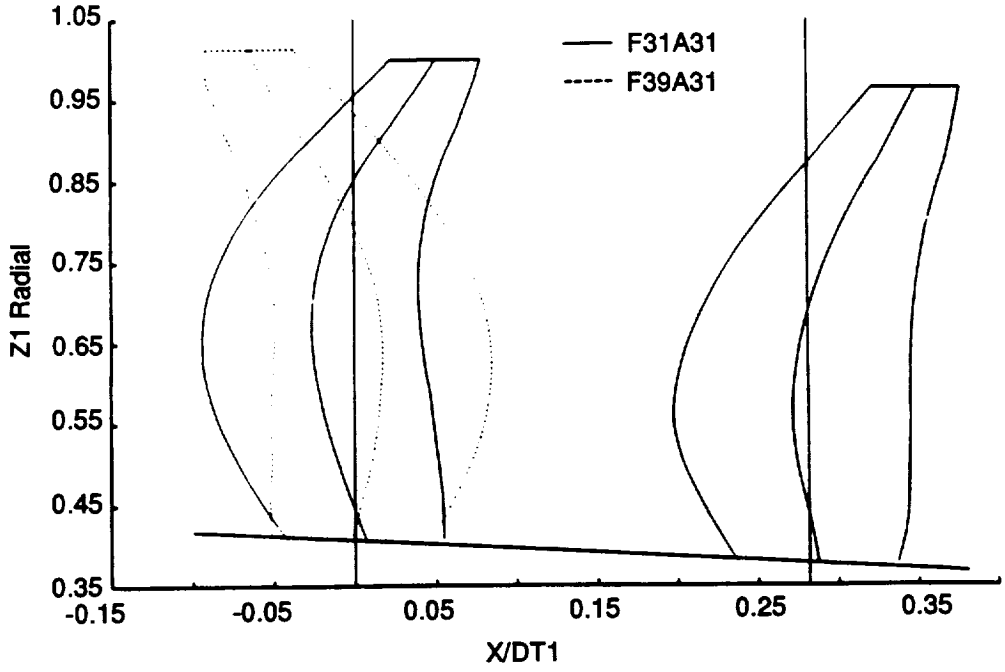

(a) Cruise Conditions

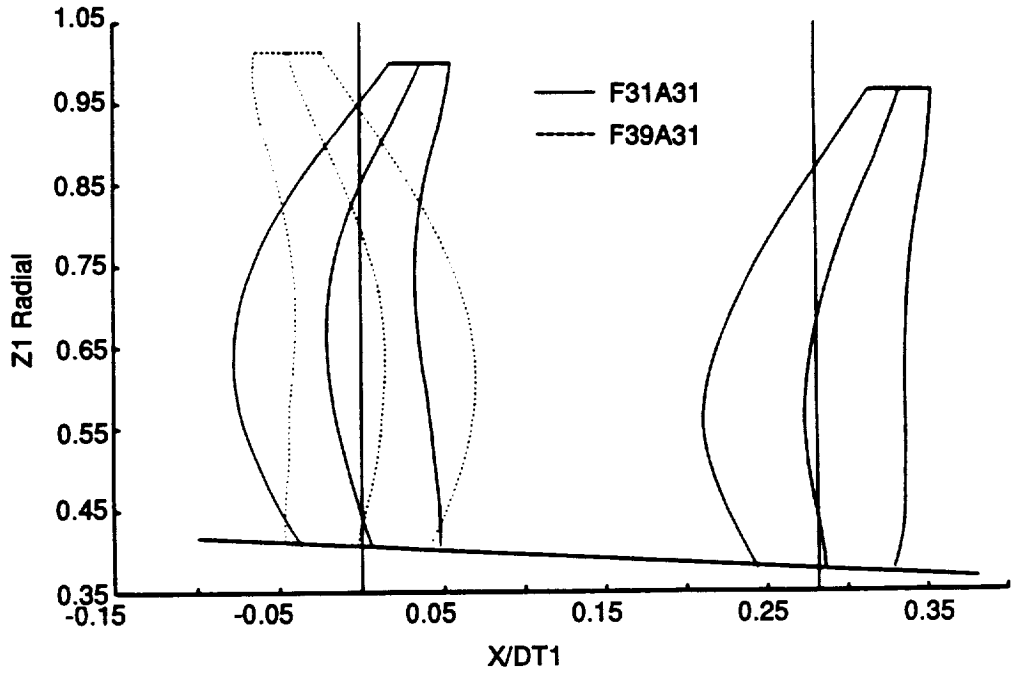

(b) Takeoff Conditions

Figure 38. Comparison of F31A31 and F39A31 Blade Designs.

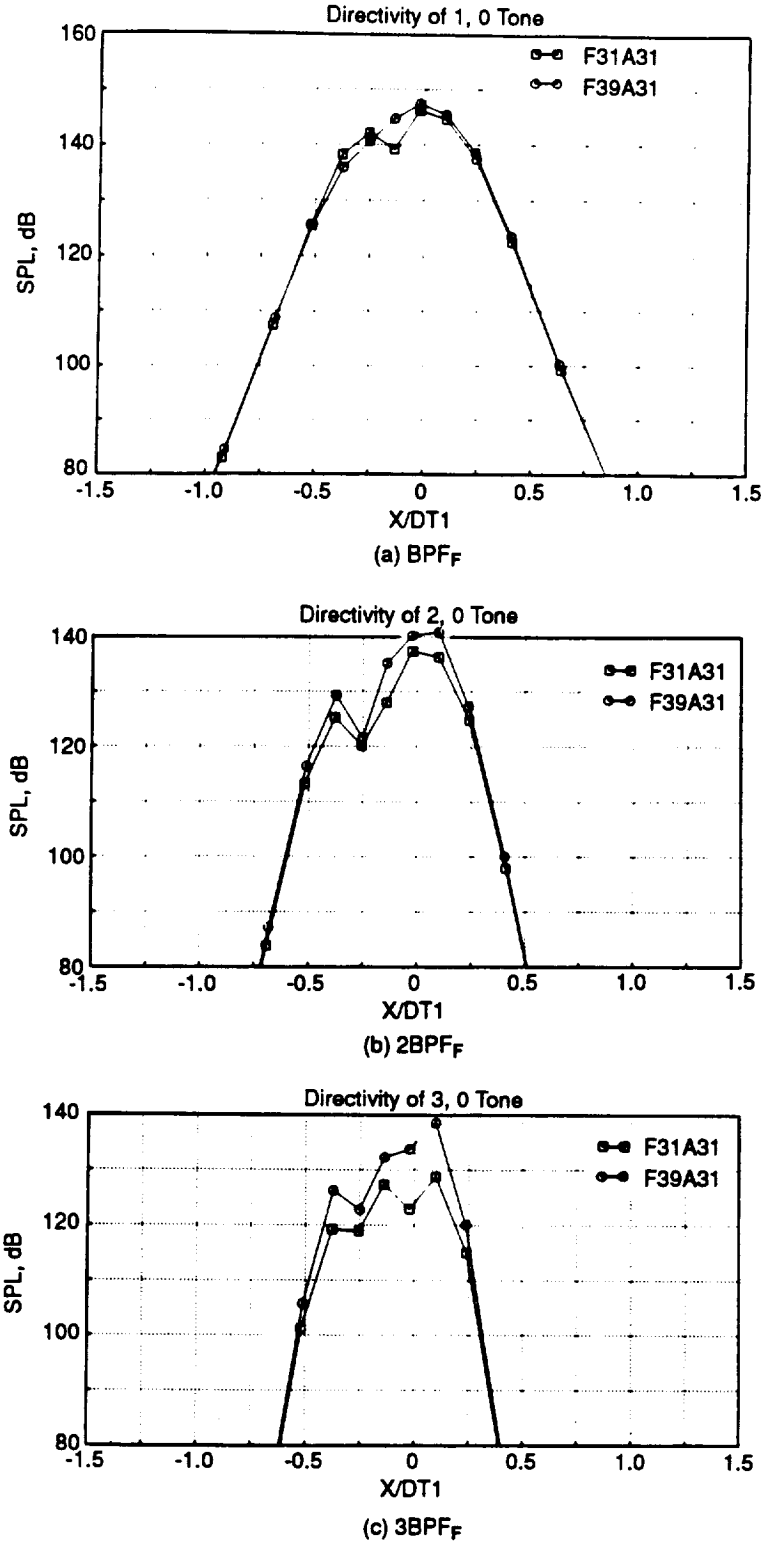

Figure 39. Comparison of F31A31 and F39A31 Uninstalled, Freefield Tone Directivities at Cruise.

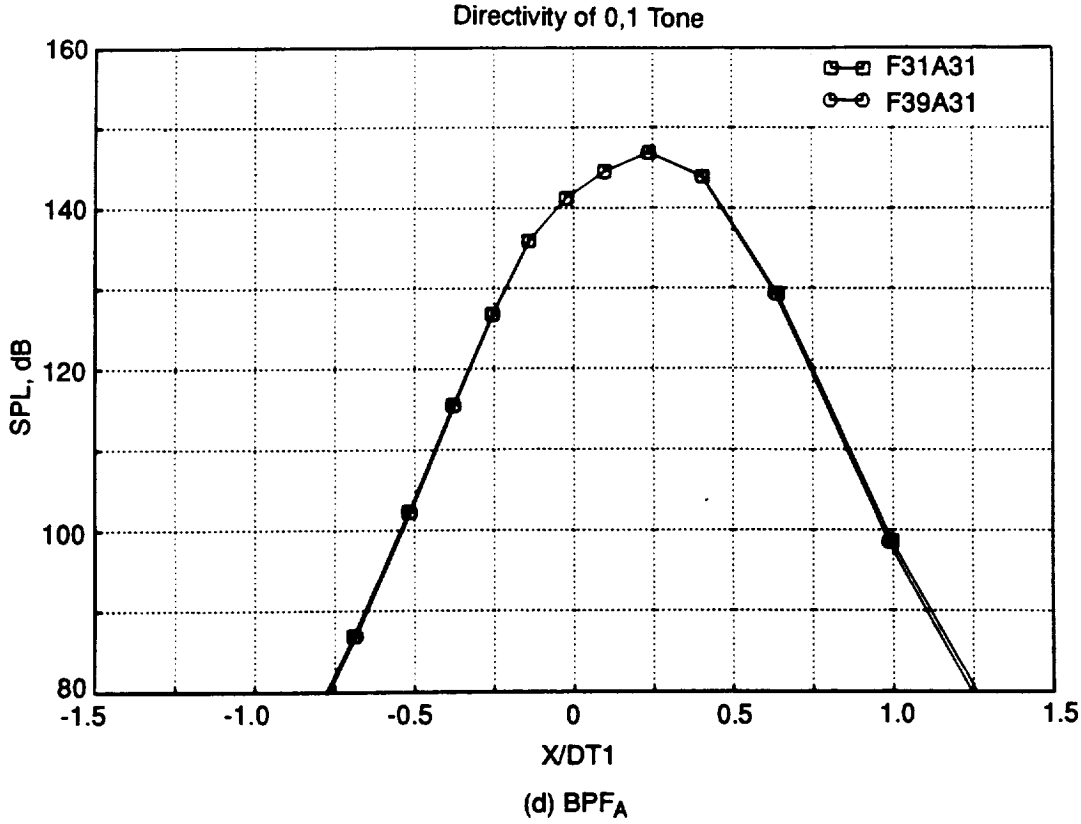

(d) BPF_A

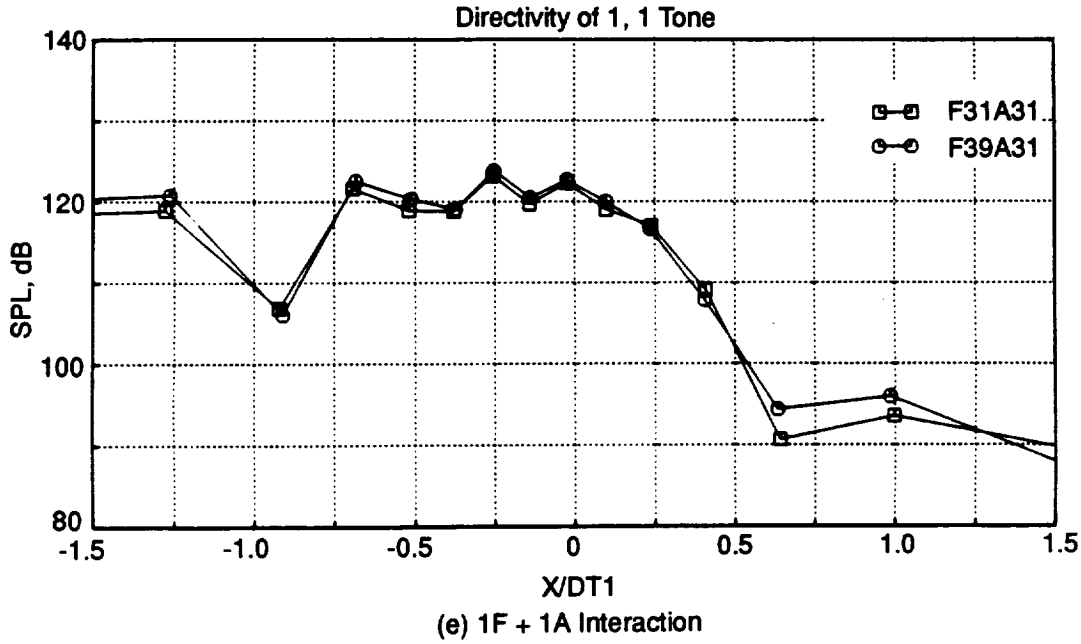

(e) 1F + 1A Interaction

Figure 39. Comparison of F31A31 and F39A31 Uninstalled, Freefield Tone Directivities at Cruise (concluded).

configurations are shown in ***Figure 40*** in terms of OASPL, dBA, PNL, and PNLT directivities. The predictions were made under the following conditions:

- Altitude: 800 feet — Tip Speed, ft/sec 760
- Sideline Distance: 1476 feet (Range: 1679 feet) — SHP/D2, HP/ft2 137
- Speed: Mach 0.25
- Performance: Off-design (Typical Takeoff Thrust)
- Single Engine; Uninstalled; Free-field Prediction

The results presented here showed that, except in the forward arc of the directivity pattern, at observer angles less than approximately 60°, there was no acoustic benefit gain predicted by using a forward-swept, forward blade under takeoff conditions.

The remainder of this section is devoted to the search for an explanation of this somewhat unexpected result.

At any angle in the directivity pattern, the noise spectrum of the counterrotating rotors consists of a series of pure tones superimposed on a broadboard background. The tones occur at the blade passing frequencies of the two rotors and their harmonics, and also at frequencies corresponding to the interactions between the rotors, 'm' x BPF_F + 'n' x BPF_A for example. In general, in the low-speed flight regime as encountered in the vicinity of an airport during takeoff and landing, the spectrum is dominated by these interaction tones; in particular, those generated by fluctuating loads on the aft rotor blades due to their encounter with the wakes and vortices shed from the forward rotor (*Reference 4*).

Figures 41 and ***42*** compare predicted tone SPL directivities at typical takeoff conditions for the F31A31 and F39A31, 12 x 10 blade configurations. In ***Figure 41***, the BPF tones of the aft-swept F31 and forward-swept F39 blades are compared. Under uninstalled takeoff conditions, this tone results from the steady aerodynamic loading on the blades, and it is noticeable that the levels are approximately 3 dB higher everywhere for the forward swept design. Examination of ***Figure 43*** shows that the spanwise loading distributions (defined as C_U/U

where

C_U = swirl velocity behind the rotor

U = local wheel speed)

used in the calculations are different in the region of the blade tip. In this region, where the sources are moving fastest and thus radiating most efficiently, the loading on the forward-swept F39 blade, while small, is predicted by the 3D Euler code used for the aerodynamic analysis at takeoff to be approximately twice that of the aft-swept F31 blade. This accounts for the difference in the predicted BPF SPL.

Figure 42 compares predicted levels of the rotor-rotor interaction tones that contribute to the "second" and "third" harmonics of the counterrotating fan noise:

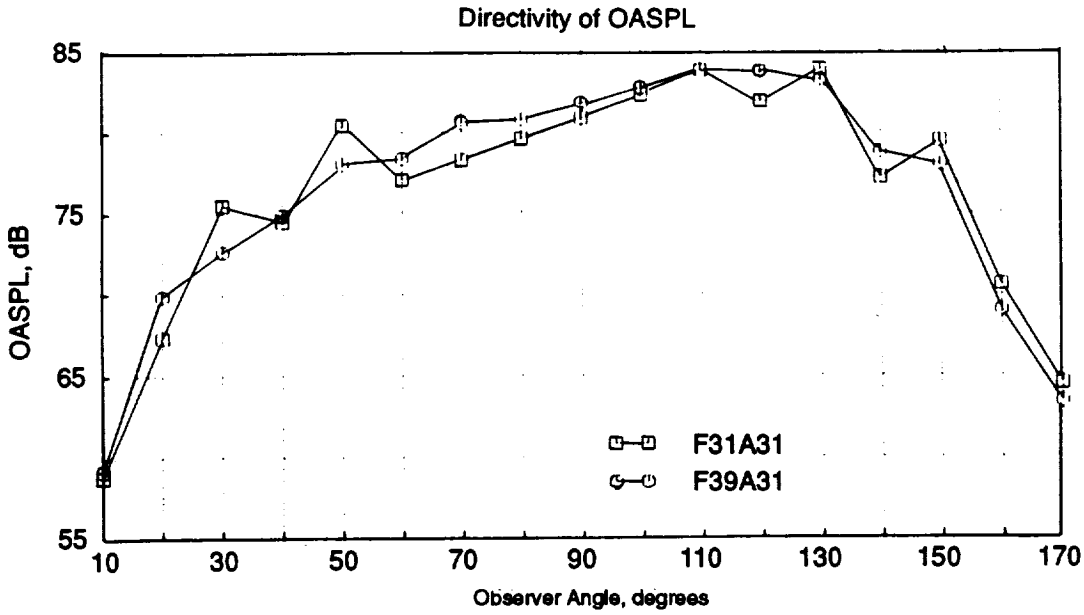

(a) OASPL

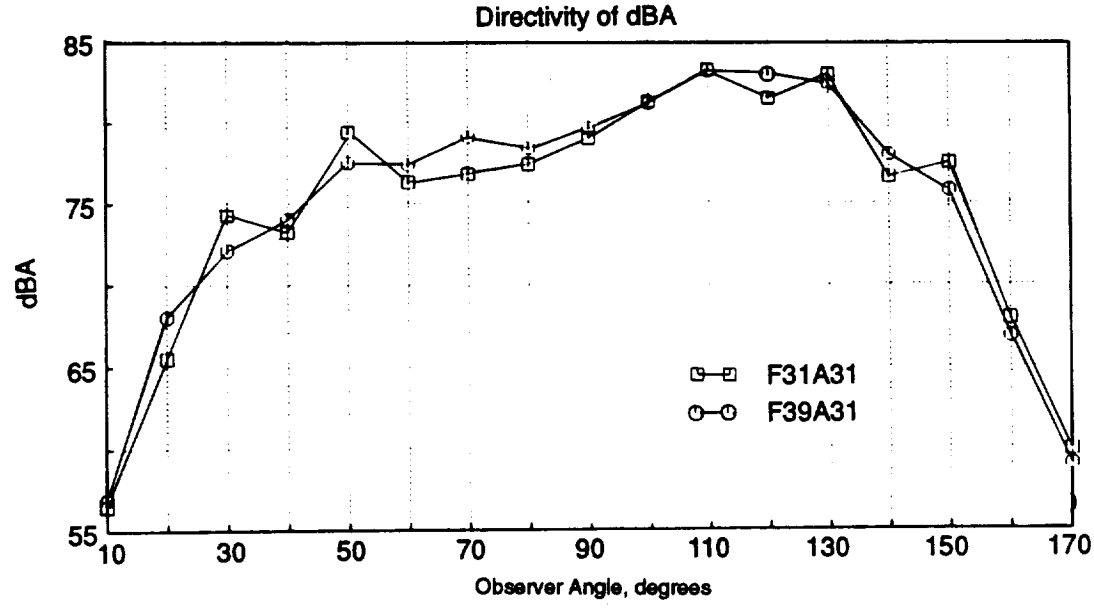

(b) dBA

Figure 40. Comparison of F31A31 and F39A31 Uninstalled, Freefield Directivities at Takeoff.

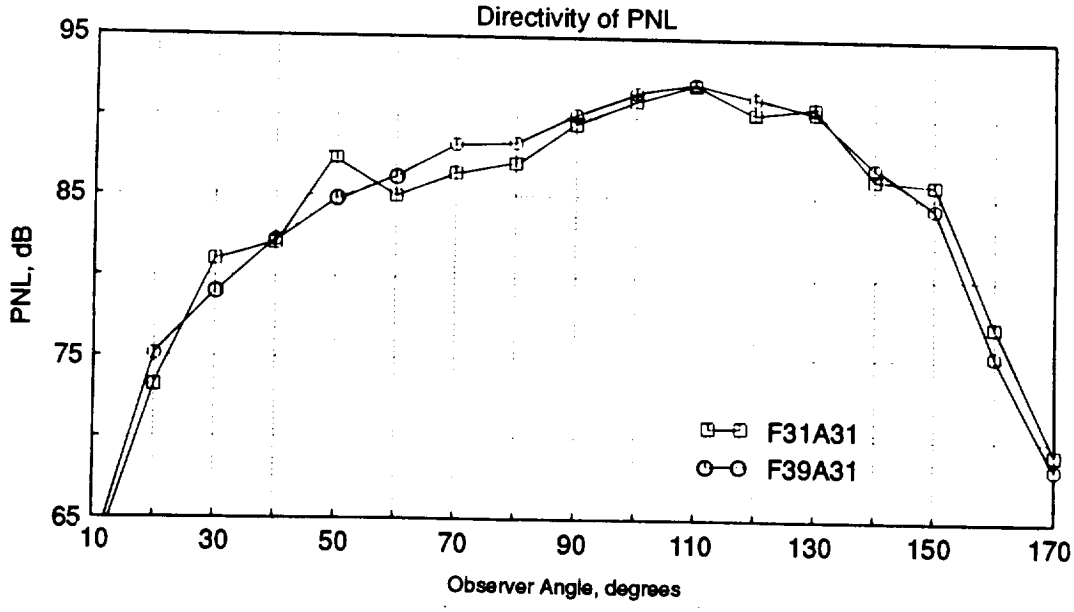

(c) PNL

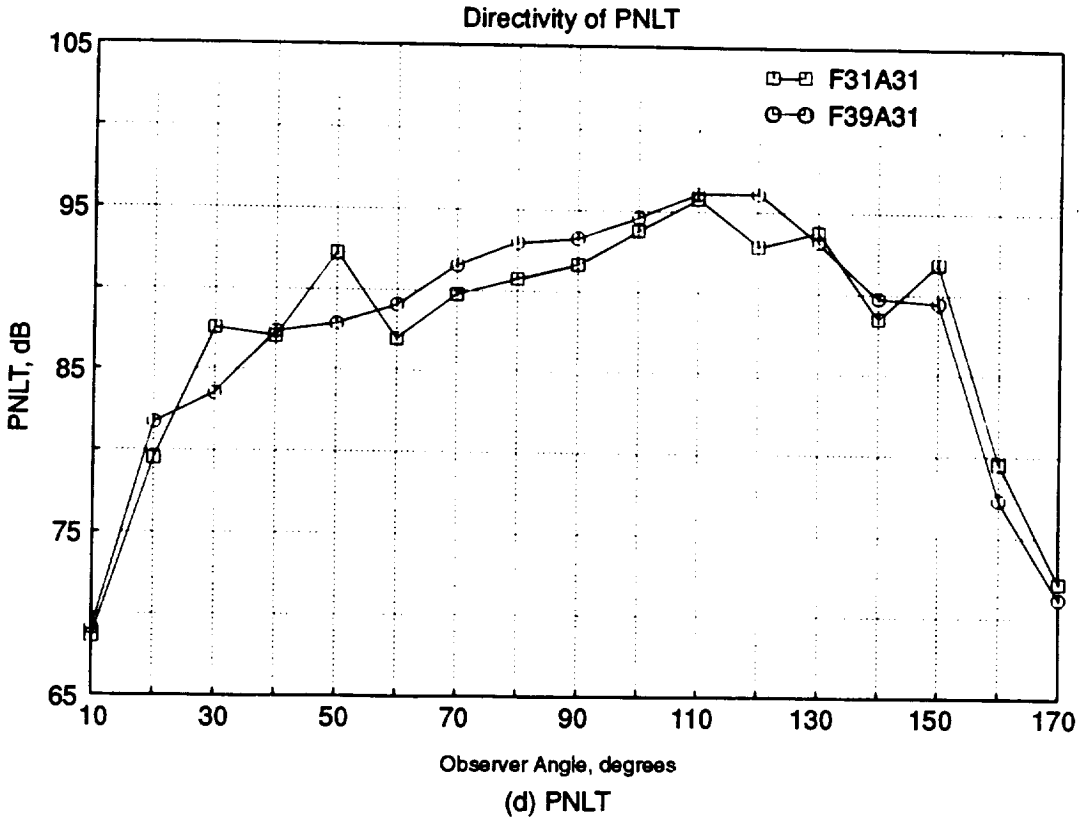

(d) PNLT

Figure 40. Comparison of F31A31 and F39A31 Uninstalled, Freefield Directivities at Takeoff (concluded).

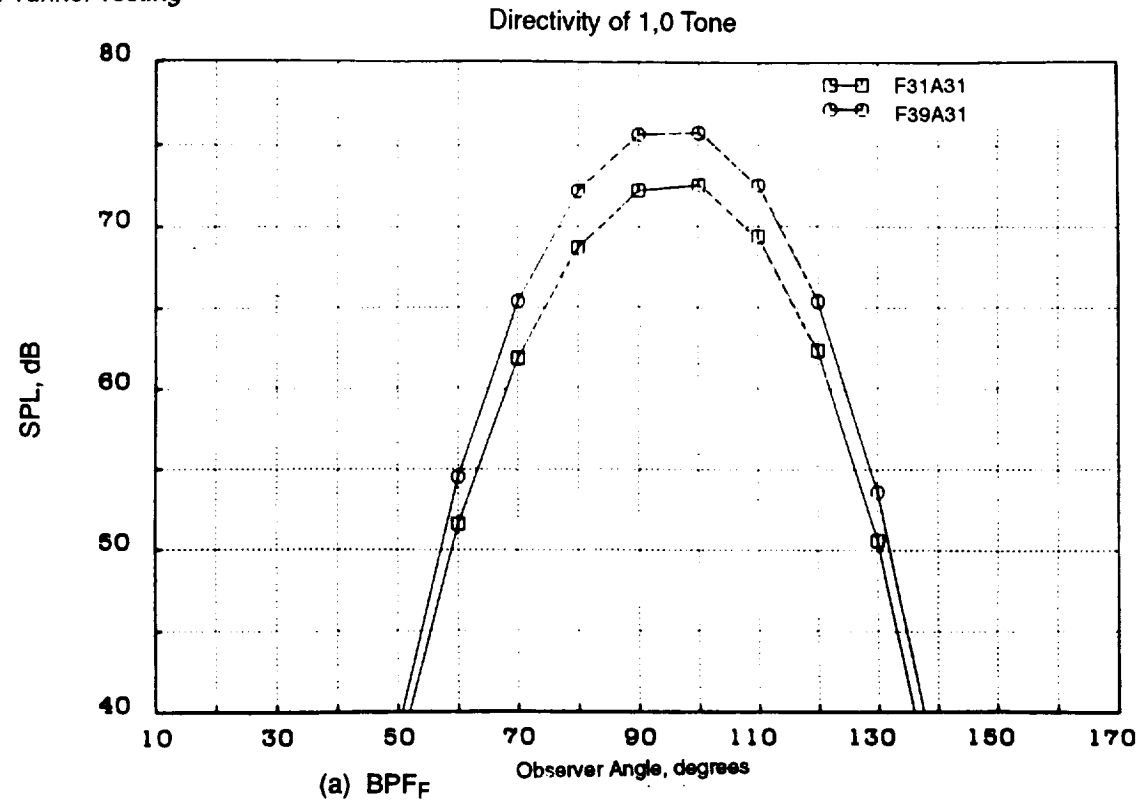

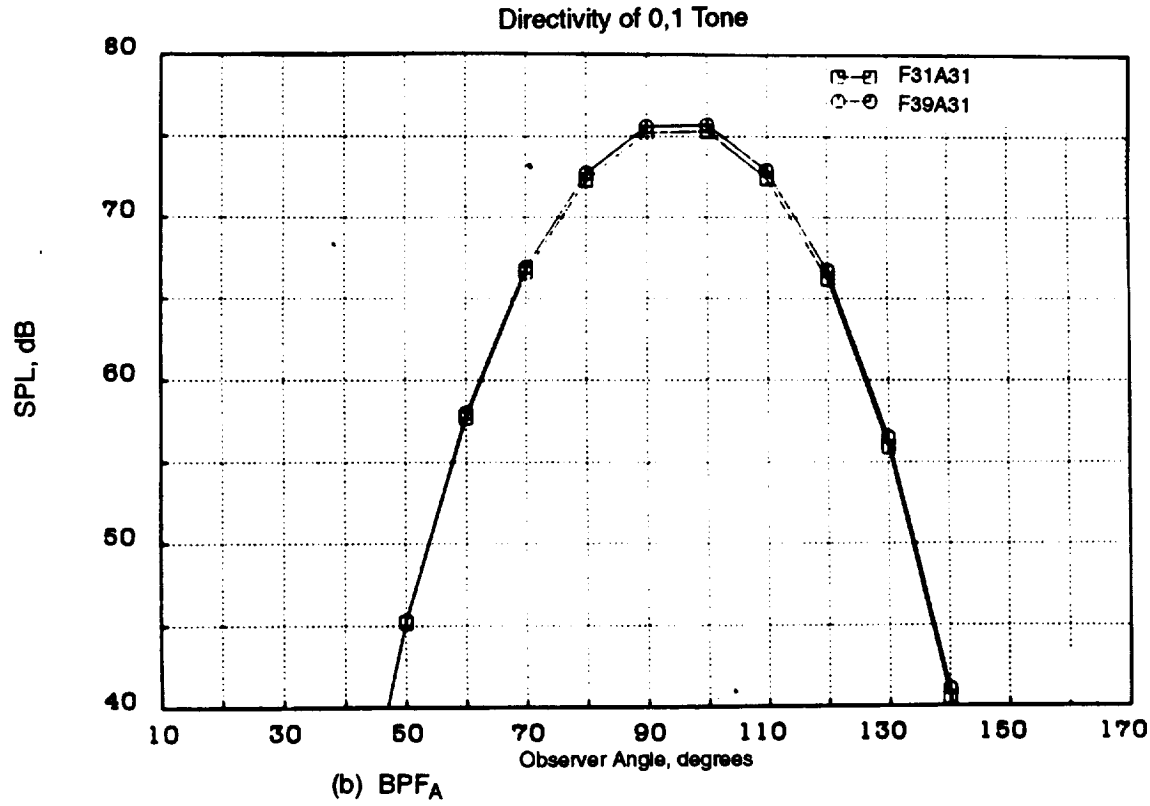

Figure 41. Comparison of F31A31 and F39A31 Uninstalled, Freefield Tone Directivities at Takeoff.

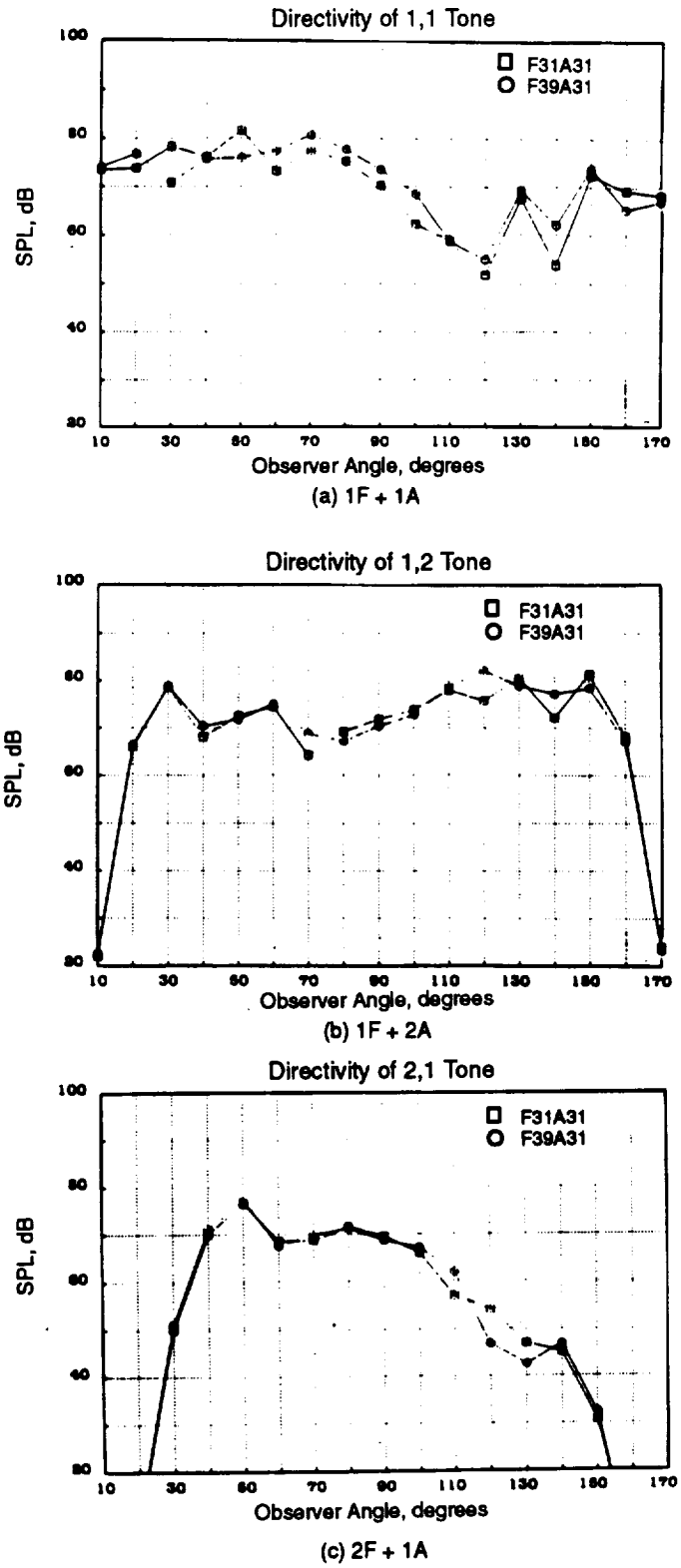

Figure 42. Comparison of F31A31 and F39A31 Uninstalled, Freefield, Interaction Tone Directivities at Takeoff.

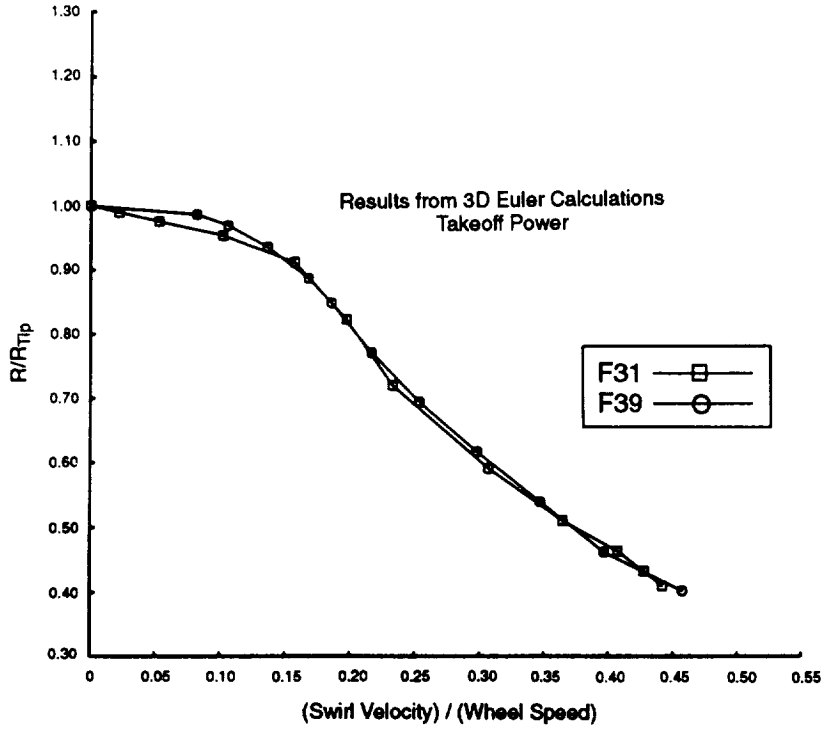

Figure 43. Comparison of Spanwise Loading Distributions Computed by 3D Euler Code for F31 and F39 at Takeoff.

the 1F + 1A, 1F + 2A, and 2F + 1A combinations, where 'F' and 'A' signify BPF_F and BPF_A, respectively. These plots are typical of all interaction tone comparisons made, as there is no obvious benefit predicted from the use of forward sweep.

Reference 5 describes the formation of a vortex, analogous to those created along the leading edge of a delta wing, along the outer portion of the leading edge of an aft-swept propfan blade that merges with the blade tip vortex. It was originally believed that sweeping the blade forward would inhibit the formation of this vortex and, should this vortex have formed, it would migrate toward the hub rather than toward the blade tip.

The vortex model employed in the computation of the fluctuating flowfield perceived by the aft rotor blade set is described in detail in *Reference 6*. It is semi-empirical in nature, with the empiricism arising from the use of certain constants whose values were selected based on data available at the time the model was formulated. It has been fine-tuned based on comparisons between acoustic data and prediction. As has been demonstrated in *References 3* and *4*, the agreement achieved between both scale-model and engine data and the prediction is impressive. One result of the approach taken, however, is that if a leading edge vortex (the type described in *Reference 5*) were indeed present, its effects would have already been taken into account in the fine-tuning of the model. The program will compute the flowfield by the rules provided that describe the vortex from an aft-swept blade, regardless of whether or not the geometry under consideration is, in fact, swept forward.

Figure 44 illustrates this graphically. Here the upwash component (that component of the velocity that is normal to the mean relative velocity) at the quarter-chord of the aft blade is plotted as a function of radius. The upwash velocity, Wn, is defined as the normal velocity relative to the forward rotor divided by the forward rotor wheel speed. The points plotted are phase-locked to the forward rotor in that all points occur at the same angular distance between wakes shed from adjacent blades. The minor perceived differences result because the loading in the tip region is not identical (***Figure 43***) and because the vortex trajectory is slightly different since the tip of the forward-swept F39 blade is (a) further forward and (b) at a slightly higher radius. It has been demonstrated (***Figure 45***) that the majority of the noise generation can be attributed to the effect of the tip vortex. This similarity in the upwash experienced by the aft rotor blades explains the similarities in the predicted noise signature.

4.2.2.1 Tip Vortex Trajectory and Strength Effects

Since the tip vortex model, as calibrated, could show no effects of forward sweep that were in agreement with those anticipated, an additional study was initiated to investigate the predicted effects of changes in the trajectory and strength of the vortex on the predicted noise. Trajectory and strength were selected as being those components most likely to be modified by the use of forward sweep.

Figure 46(a) shows a schematic of the trajectory of the vortex core. At any axial location, z_{vtx}, downstream of the trailing edge of the forward rotor tip, the radial distance, b_r, inward from that tip is given by the linear rational function:

$$\frac{b_r}{R_{tip}} = \frac{(TVTI) \times z_{vtx} / R_{tip}}{16\, z_{vtx} / R_{tip} + 1.0}$$

where TVTI, the Tip Vortex Trajectory Index, has been obtained from experimental data. Increasing the value of this parameter brings the vortex core closer to the hub region. Likewise, ***Figure 46(b)*** shows the effect on the predicted vortex flowfield of altering the Circulation Index parameter. The vortex circulation is defined as:

$$\Gamma_{vtx} = (CI)\ \{2\pi\ (V_\theta)_{max}\ a\}$$

where a, the core radius, is calculated as described in *Reference 6*. As implemented in the program, changes in the circulation index, CI, only affect the magnitude of $(V_\theta)_{max}$, as shown schematically in the figure. The values of CI and TVTI that have been found to give the best acoustic results for conventional blade designs are 1.5 and 2.0, respectively. Results of varying these parameters for the F39A31 combination examined previously are shown in ***Figure 47***, where it can be seen that in terms of OASPL, combinations of:

- TVTI = 0.5, CI = 1.5
- TVTI = 0.5, CI = 0.5
- TVTI = 2.0, CI = 0.5

all give very similar results to that shown in ***Figure 45*** for the wake alone.

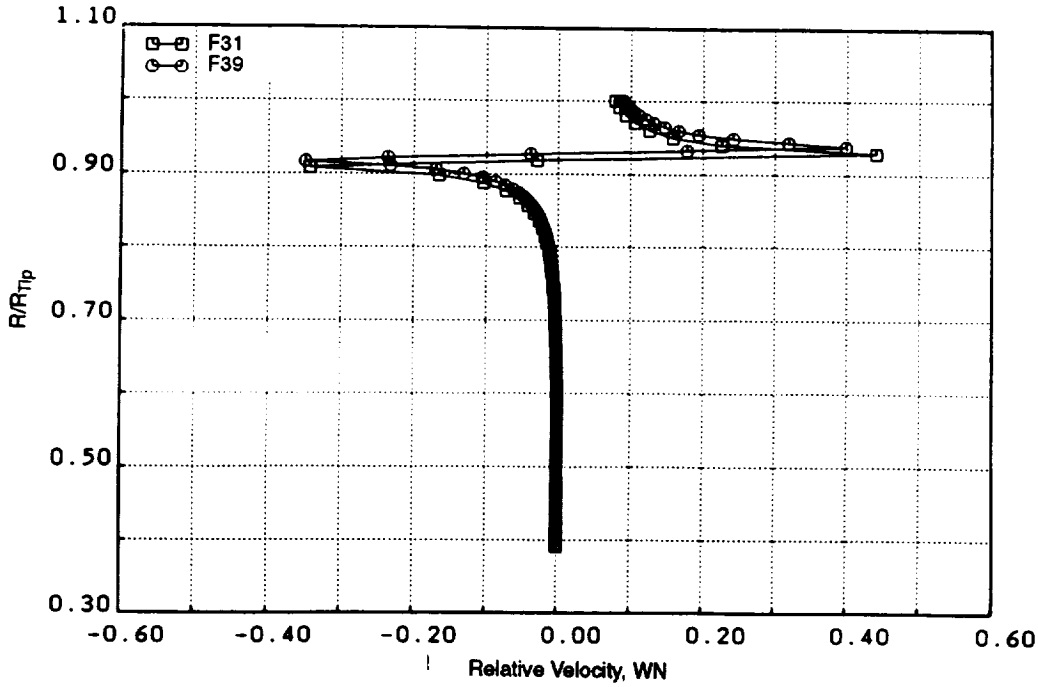

Figure 44. Spanwise Distribution of Upwash Velocity (WN) Generated by Tip Vortex at Aft Rotor Quarter-Chord

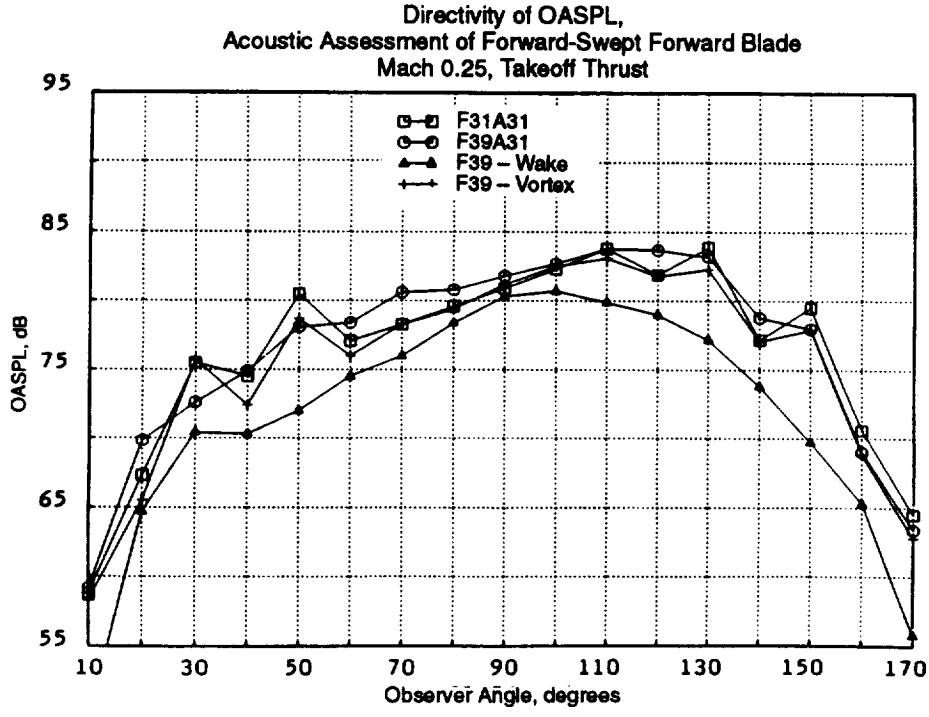

Figure 45. Predicted Contributions of Wake and Vortex to the OASPL of F39A31.

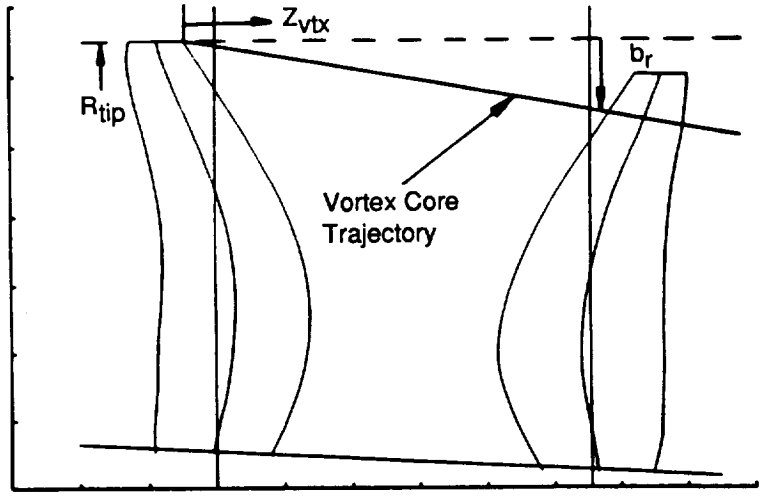

Tip Vortex Trajectory Index Adjusts Path of Vortex Core:

$$\frac{b_r}{R_{tip}} = \frac{(TVTI) \times (Z_{vtx})/R_{tip}}{16\,(Z_{vtx})/R_{tip} + 1.0}$$

(a) Trajectory

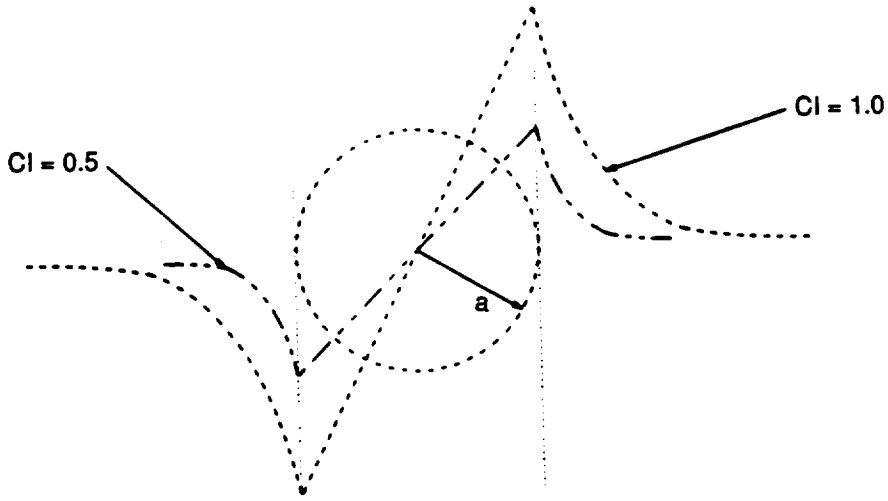

Cl Acts on Circulation as Follows: $(\Gamma)_{vtx} = Cl\,\{2\pi(V_\theta)_{max}a\}$

In the Program, Changing Cl Changes $(V_\theta)_{max}$

(b) Circulation

Figure 46. Tip Vortex Model.

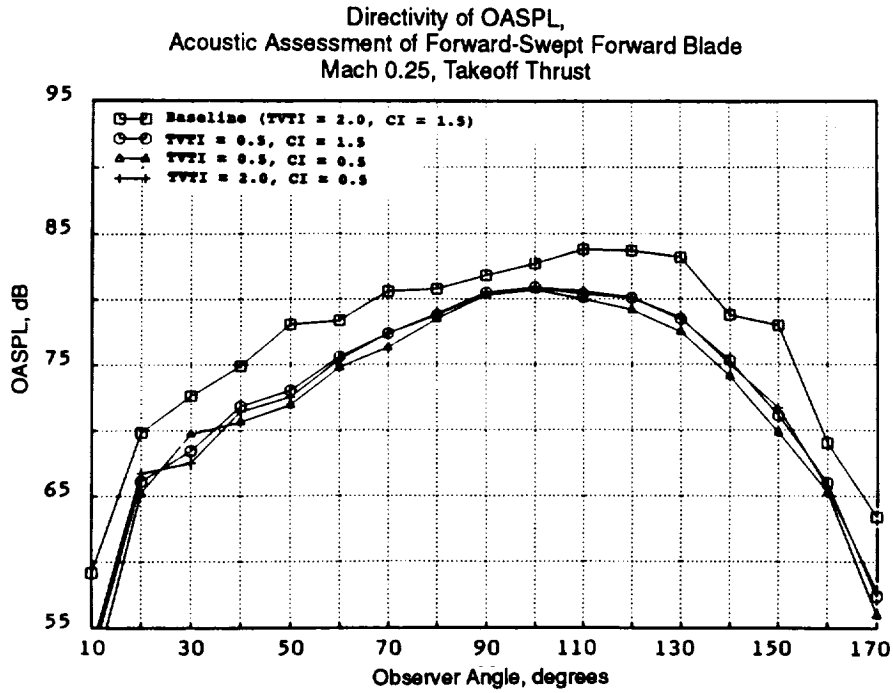

Figure 47. Effects of Changes in Tip Vortex Parameters on OASPL Directivity.

Some insight into these results may be obtained from examining ***Figure 48***. The fluctuating flowfield perceived by the aft rotor, as computed by the wake/vortex model in the code, has been Fourier transformed into its harmonic components as a function of radius. Plotted in this figure is the radial variation of the first wake/vortex harmonic that contributes to the OASPL plots of ***Figures 45*** and ***47***. ***Figure 48(a)*** shows the similarity between the F31A31 and F39A31 combinations described above. This figure also demonstrates the predicted influence of the tip vortex in the outer portion of the blade, and the area in which the influence of the wake is found. ***Figure 48(b)*** examines the effect on the predicted wake/vortex harmonic of the changes in TVTI and CI discussed above. The reduction in TVTI from 2.0 to 0.5 appears to have moved the vortex core just outboard of the aft rotor tip, thus reducing the strength of the fluctuations seen by the blade, while the reduction in CI from 1.5 to 0.5 produces a uniform reduction in gust harmonic amplitude over that portion of the span where vortex effects dominate.

4.2.2.2 Core Radius Effects

The data/theory comparisons of *References 3* and *4* clearly show the agreement obtained between data and prediction for both model and full-scale UDF® engine noise. This agreement has been obtained at both cruise and takeoff conditions using values of TVTI and CI of 2.0 and 1.5 as discussed above, with the core radius value, a, predicted by the tip vortex model of *Reference 6*.

Measurements taken between the rotors of the F4A4 blade combination under cruise conditions (*Reference 7*) indicated that for this design, under these conditions, the measured radius of the vortex

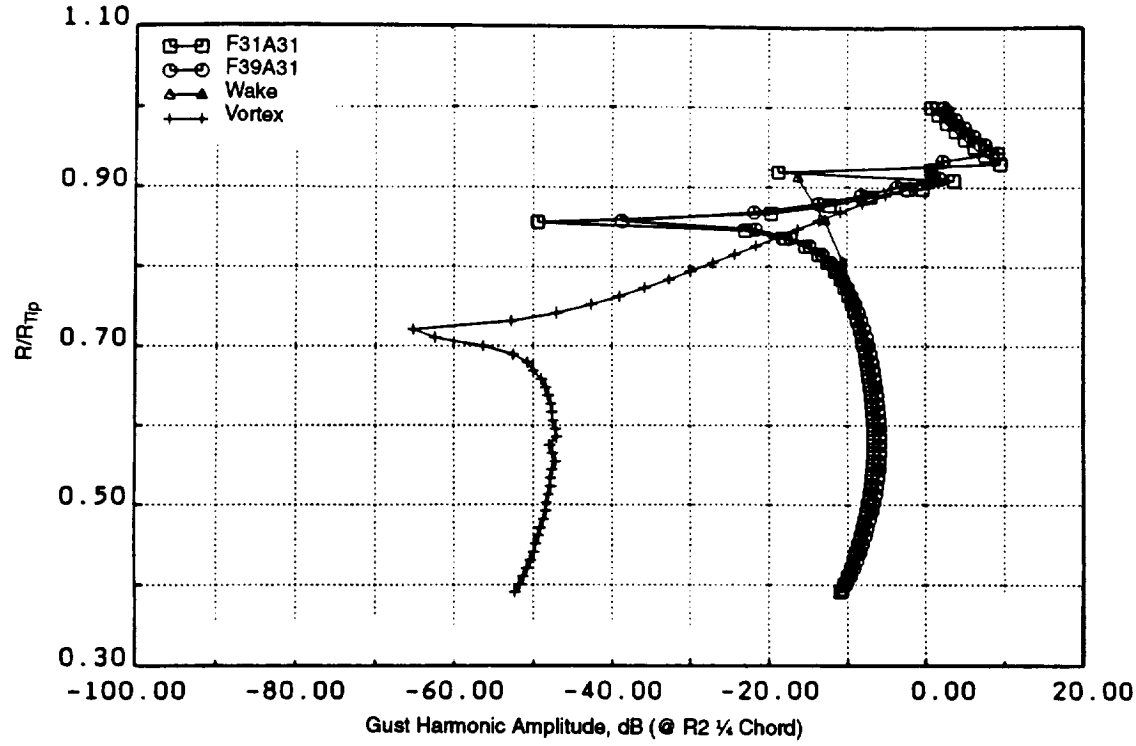

(a) "Standard" Vortex Parameters

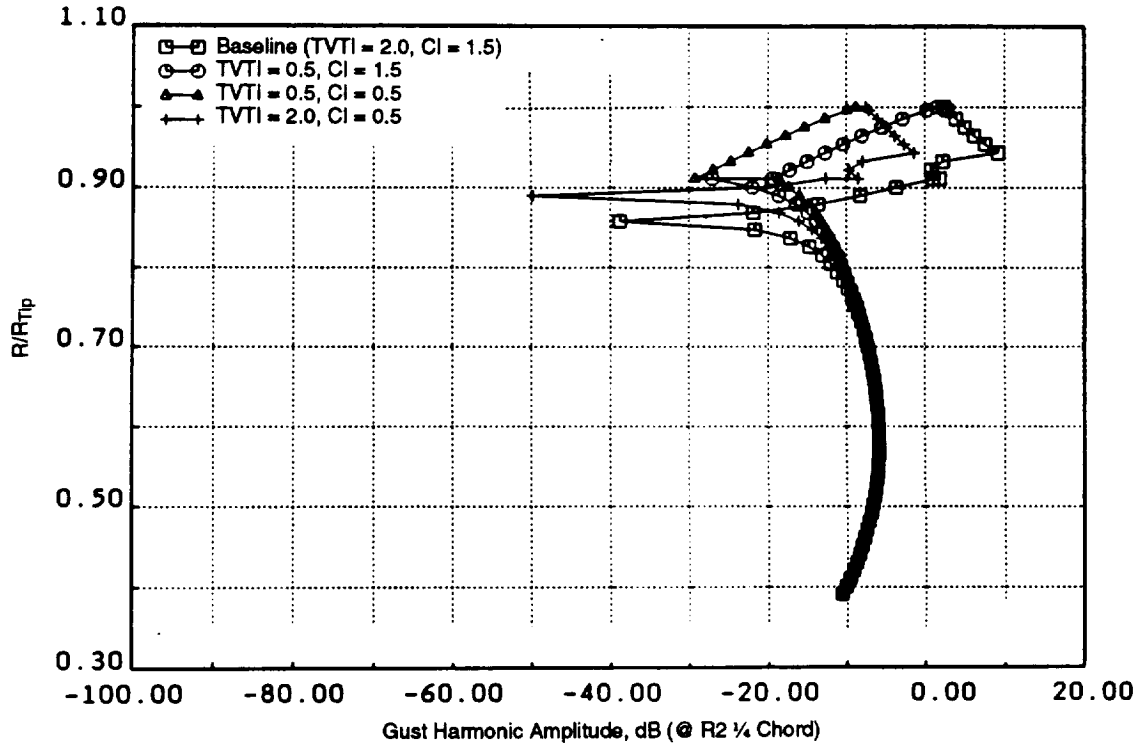

(b) Effect of Variation in Trajectory and Circulation

Figure 48. Spanwise Distribution of Wake/Vortex Flowfield Harmonic No. 1.

core was five times greater than that predicted by the model of *Reference 6*. The measured $(V_\theta)_{max}$ was, however, in general agreement with the model.

These measurements represent a painstaking mapping of the flowfield between the rotors. It is unfortunate that this effort was employed for the F4A4 blades, whose major feature was the reduced sweep resulting from their radial trailing edge, and under cruise conditions that were beyond the limits of the correlations used in the determination of the vortex core radius. (Since the major noise sources of concern at cruise were those resulting from steady loading and thickness, this limitation was not felt to be a serious problem in the development of the model of *Reference 6*.) Therefore, while questioning the relevance of these measurements to the more highly swept blades operating under takeoff conditions, a study was conducted to investigate the predicted effects of changes in core radius. For this study, the value of TVTI remained constant at 2.0.

Figure 49 shows schematically the effect on the vortex flowfield of the change requested. The baseline case is shown as CI = 1.5, Rad = 1x. An intermediate case, in which the vortex strength is maintained by reducing $(V_\theta)_{max}$ is also seen (CI = 0.3, Rad = 5x), as is the final scheme of CI = 1.2, Rad = 5x. Results of these changes on the model flowfield and noise are shown in ***Figure 50(a)*** and ***50(b)***, respectively. It can be seen that the "intermediate" case of ***Figure 49***, in which the vortex strength was maintained, results in a slight reduction in predicted OASPL over all angles. Likewise, the increase in core radius, when combined with the original $(V_\theta)_{max}$, leads to an increase in predicted OASPL of 5+ dB over the entire directivity pattern. As has been previously demonstrated

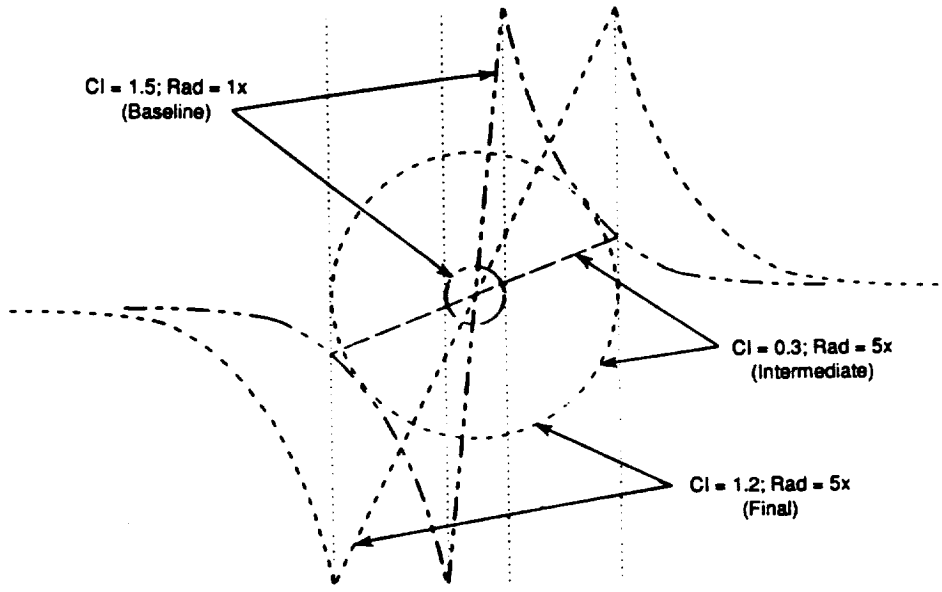

CI Acts on Circulation as Follows: $(\Gamma)_{vtx} = CI\ \{2\pi(V_\theta)_{max}{}^a\}$

In the Program, Changing CI Changes $(V_\theta)_{max}$

Figure 49. Effects of Changes in Vortex Core Radius and Circulation on the Flowfield Model.

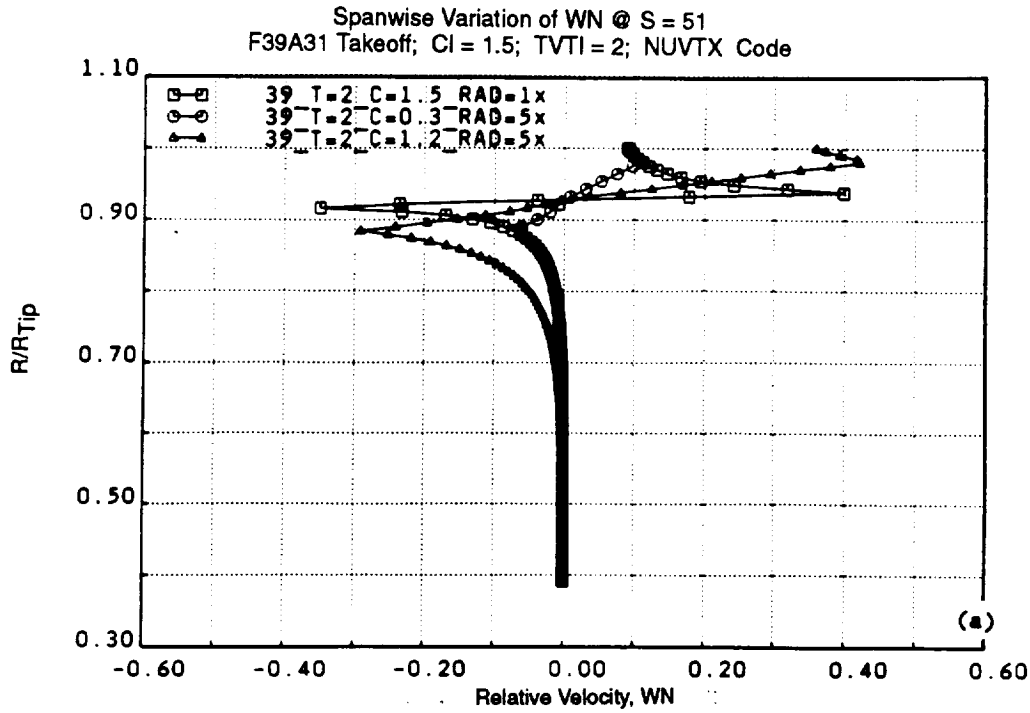

(a) Spanwise Distribution of Upwash Velocity (WN) Generated by Tip Vortex at Aft Rotor 1/4-Chord

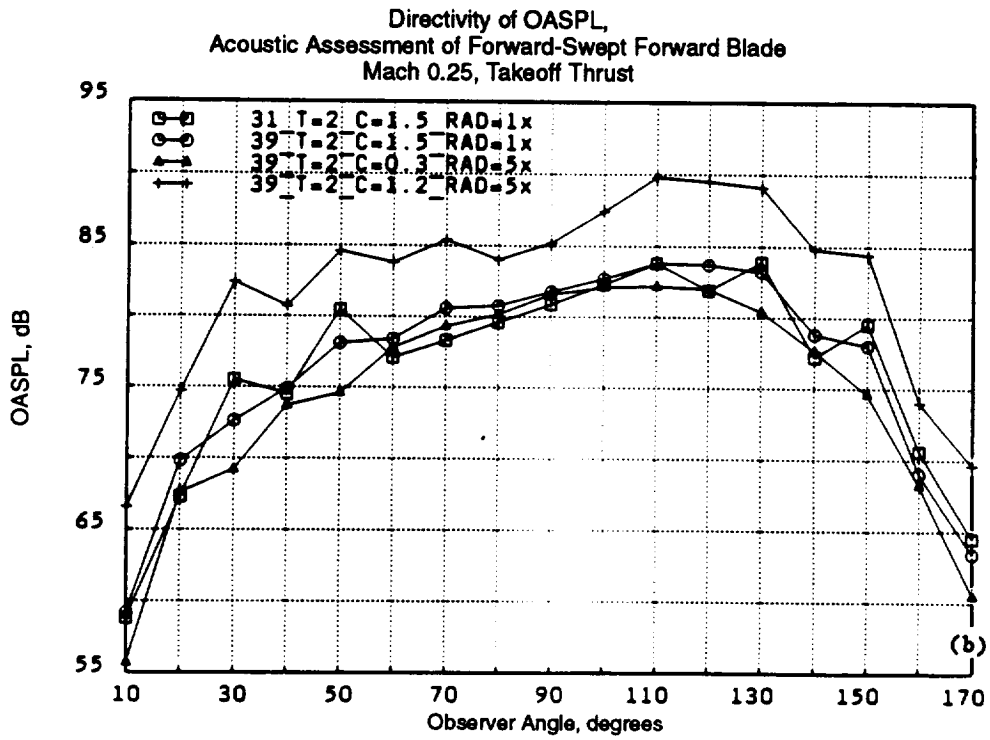

(b) Predicted OASPL Directivity

Figure 50. Effects of Change in Vortex Core Radius and Circulation.

in *Section 4.2.2.1*, changes in tip vortex trajectory will also affect the predicted noise, and no attempt has been made to relate the trajectory measured under design conditions to that existing at takeoff. This exercise demonstrates the extreme caution that must be exercised when applying measured data to a semi-empirical model. The same information gathered under takeoff conditions would have been of great value in the continuing evolution of the constants used in the model.

5.0 Forward-Swept F39 Blade Fabrication

5.1 Engineering Materials Technology Laboratories

5.1.1 Blade Fabrication Facility

Development of the spar/shell construction for composite blades was initially sponsored under NASA Contract NAS3-20402. Under this contract, full-scale fan blades, comprised of superhybrid composite shells surrounding metal spars, were successfully designed, manufactured, and tested at GE. The fabrication process was further refined and perfected under NASA Contract NAS3-24080 (*Reference 8*), where 2-foot diameter propulsion simulator composite blades, similar to this contract's blades, were produced.

The Engineering Materials Technology Laboratories (EMTL), located in GEAE's Evendale plant, are where the blade fabrication for these NASA-sponsored programs takes place. Originally, a small plastics shop, the EMTL fabrication facility has grown to its current 10,000 square foot size. This fully equipped workshop has produced a diversity of composite engine hardware, such as fan casings with integral stator vanes, honeycomb structures, integrally bladed rotors, ducts, acoustic duct liners, inlet cones, struts, flaps, vanes, and fan blades (both scale-model and full-scale). A complete listing of the primary equipment used in the EMTL facility is presented in ***Table 4***.

5.1.2 Blade Fabrication Technology

In order to produce high-quality composite blades, several factors must be considered prior to actual fabrication. This section addresses some of the main issues, which deal primarily with proper materials selection for both the blades and the adhesives.

5.1.2.1 Material Selection

The composite materials selected for the blade fabrication must meet the requirements of high strength, high stiffness, high fatigue resistance, and low weight in order to fulfill the blade design requirements of:

- Stiffness tailored to provide blade frequencies appropriate for operating speed conditions and to eliminate blade instabilities.
- Radial and flexural fatigue strength sufficient to provide adequate resistance to centrifugal and vibratory loadings.
- Lightweight material to minimize blade centrifugal stress and loading in the hub.
- Compression and shear strength adequate to meet stresses developed in the composite attachment.

5.1.2.2 Fiber Reinforcement

There are many different fiber types used in the preimpregnated, unidirectional tape materials that make up composite blades. ***Table 5*** presents several common fiber types along with their basic

Table 4. Equipment Capability in EMTL Composites Lab.

Presses	Capacity	
	Platen Size	Tonnage
Press 51	2 x 2	100
Press 52	1 x 1	20
Press 53	1.5 x 1.5	100
Press 54	1.5 x 1	50
Press 55	1.5 x 1.5	25
Press 58	3 x 3	300
B&T	4 x 4	300
Pasadena (Caps)	2 x 2	100
Pasadena (Caps)	2 x 2	100
Wilson (Caps)	4 x 4	500
Wilson (Caps)	4 x 4	500

Autoclaves
Redpoint Size: 3 x 4, 200 psi Biggs-United Size: 3.5 x 10, 200 psi Baron Blakeslee Size: 10 x 20, 300 psi

Ovens		
Oven No.	Size	Temperature Range
Oven 3	6 x 6	600
Oven 4	3 x 3	600
Oven 5	3 x 3	600
Oven 6	6 x 4	600
Oven 8	2 x 2	800
Oven 9	2 x 2	800
Oven 10	5 x 5	800
Oven 11	2 x 2	600
Oven 12	5 x 5	800
Oven 1A	12 x 12	800
Oven 2A	6 x 6	800
Oven 3A	6 x 6	800

Other Equipment
Eight 6 x 6 Freezers Steel Rule Die Press 15 x 20 Fabrication Room Two Down Draft Tables Two Grit Blasters Two Vacuum Pumps 8 x 8 Paint Spray Booth Two Bandsaws Drill Press/Mill

Table 5. Common Fiber Types and their Associated Properties.

Fiber Data					
Fiber Type	Strength (ksi)	Modulus (Msi)	Break %	Count K	Dia mic
G-40-700	722	43.5	1.66	12	4.9
G-40–800	800	43.5	1.84	12	4.6
IM-7	800	42.0	1.86	12	5
IM-X	860	46.2	1.91	–	5
T-40	820	42.0	1.8	12	5
T-650	700	42.0	1.7	12	5
Apollo-28	750	38.0	1.97	12	5
Apollo-43	650	43	1.5	12	5
AS4	520	34	1.5	12	8

properties. Of these, AS4 was the first material to be used in the fabrication of model propulsion simulator blades. Other fiber types with high strain, high stress, and high shear strength carbon fibers have since come into use as a function of the type of testing being conducted.

5.1.2.3 Epoxy Matrix Materials

The organic matrix material used in combination with the fiber reinforcement for past scale-model fan blades has been the PR288 system produced by the 3M Company. This particular system has become standard for this type of blade fabrication because this system has been the only one to meet the 0.0026-inch molded ply thickness requirement cost-effectively. The PR288 system has been used at GE since the mid-1970's for the fabrication of all types of composite and spar/shell-type composite blades and vanes, and has been fully characterized.

Table 6 summarizes the typical composite properties of the PR288 hybrid fiber system for several different environmental conditions. Although this hybrid fiber system exhibits improved impact properties over the pure AS4 material, the complexity involved with producing the 0.0026-inch hybrid tape makes AS4 the typically preferred material for blade fabrication.

5.1.2.4 Preimpregnated Tape

The preimpregnated unidirectional tape materials have been most commonly produced for GE by the 3M Company in accordance with GE specifications. The carbon fibers are engineered to produce a desired molded ply thickness material with a desired final molded fiber volume fraction, depending on the particular application. Incoming quality control (QC) physical and mechanical property data are then generated by the vendor and GE to ensure conformance with established specifications.

Table 6. PR288/AS4 – Glass Environmental Property Data.

Environment	Flexural Strength, psi			Flexural Modulus x 10^6, psi			Short Beam Shear Strength, psi			
	-65° F	+75° F	+250° F	-65° F	+75° F	+250° F	-65° F	+75° F	+250° F	+350° F
Initials							14,740	12,920	9,350	6,570
	97,200	161,500	134,520	10.8	11.2	9.7	15,380	14,980	9,650	5,990
	123,310	134,340	142,470	11.3	10.9	10.1	12,950	14,000	10,000	6,850
	120,670	154,270	144,800	10.8	11.3	10.4	14,710	14,160	10,110	6,930
	135,010	159,390	123,380	11.2	11.5	9.4	15,500	13,480	9,310	6,920
	119,048	152,380	136,290	11.0	11.2	9.9	14,660	13,910	9,680	6,650
Weather – 3 Months							15,690	13,200	8,930	5,600
	156,310	174,370	161,370	12.3	11.7	12.6	18,160	14,090	8,320	5,340
	148,380	155,170	149,380	11.1	11.8	11.3	15,820	12,750	8,230	5,930
	136,120	167,700	165,500	11.3	11.7	13.0	17,140	13,760	8,360	6,130
	157,510	166,540	130,120	11.1	11.2	10.4	15,850	13,460	8,390	5,620
	149,580	165,950	151,590	11.5	11.6	11.8	16,530	13,450	8,450	5,720
Weather – 6 Months							17,340	16,050	7,950	5,370
	144,860	179,730	139,730	10.9	11.2	10.0	18,300	14,330	6,990	5,350
	130,970	175,170	140,810	10.7	11.3	10.5	16,750	13,340	8,590	5,080
	144,120	173,290	139,460	11.2	11.2	10.7	16,190	14,260	8,700	5,070
	158,900	164,470	160,420	11.7	10.7	12.3	17,860	14,760	8,430	5,500
	144,710	173,170	145,110	11.1	11.1	10.9	17,290	14,550	8,130	5,270
Humidity – 180°F/97% RH/ Saturation			[2]			[2]	16,070	11,430	4,380	8,120
	176,340	180,150	150,620	11.1	12.1	10.9	15,160	11,820	4,830	8,610
	178,870	180,810	156,650	11.3	11.3	11.4	14,690	11,940	4,220	7,990
	189,460	184,100	141,820	11.2	11.7	11.1	14,830	9,960	4,380	8,230
	200,850	169,420	149,880	12.5	11.2	10.6	14,940	12,270	4,750	8,410
	186,380	178,620	149,740	11.5	11.6	11.0	15,140	11,480	4,510	8,270
Thermal Cycles – 250N/ -65° to +250°F							17,550	14,740	9,050	5,810
	178,030	159,660	160,780	12.6	11.0	10.8	15,630	13,410	9,000	6,060
	137,710	172,800	170,700	10.8	11.1	12.0	19,070	15,120	9,550	5,710
	149,680	169,050	131,090	11.4	11.1	9.7	17,400	16,170	9,530	5,780
	156,480	161,920	134,830	11.3	11.2	9.9	14,480	15,660	9,490	5,850
	155,480	165,860	149,350	11.5	11.1	10.6	16,830	15,020	9,320	5,840
Thermal Cycles – 500N/ -65° to +250°F								14,180	8,790	5,720
		153,950	153,060		10.6	11.4		13,290	9,490	5,990
	No	178,620	128,830	No	11.4	9.4	No	13,960	9,000	5,880
	Test	166,270	159,750	Test	11.9	11.3	Test	14,420	9,070	5,850
		175,540	146,600		11.6	10.2		12,750	9,660	5,480
		168,600	147,060		11.4	10.6		13,720	9,200	5,780

5.1.2.5 Adhesive Materials

The concept of a metallic spar/composite shell blade design necessitates selecting an adhesive that can provide a structural tie between the two different materials. The adhesive must also possess good ductility characteristics capable of withstanding thermal mismatches between the shell and the spar. Previous GE studies have shown that a combined use of titanium surface treatment, adhesive resin film, and resin primer provides improved adhesion properties compared with interposing and cocuring a special adhesive film between the shell and spar interface.

Table 7 presents some of the typical properties associated with different pretreatments of the titanium surface. The grit-blast, Pasa Jell, PR288 primer combination has the best strength retention capability in the 250° and 350° range and is, therefore, the preferred adhesion technique.

Table 7. Titanium Surface Treatment Evaluation.

Surface Treatment	Short Beam Shear Strength			Lap Shear Strength	
	RT	250°F	350°F	RT	350°F
Grit Blast No Primer	11,350	8,630	6,900	2,490	2,070
Grit Blast, PR288 Primer	13,220	10,210	7,950	3,060	2,630
Grit Blast Pasa Jell 107 PR288 Primer	12,950	10,320	9,870	2,710	2,840
Metex Etch, Pasa Jell 107 PR288 Primer	10,370	8,370	8,130	2,750	2,570
In all cases, the adhesive used was two plies of PR288/Type AS4-Glass Prepreg					

5.1.2.6 Blade Manufacturing Considerations

GE's Engineering Materials Technology Laboratories have overseen the successful fabrication of numerous polymeric composite fan blades and vanes in support of NASA, Air Force, and internal programs. Over the course of this fabrication process, considerable composite fabrication and processing technologies have been developed and are still able to meet today's more demanding fabrication requirements. EMTL's primary efforts have traditionally been in the area of titanium spar/composite shell blade fabrication using a compression molding technique. ***Figure 51*** depicts a typical spar/shell composite blade. However, alternative design studies continue in the production of all-composite airfoils. The elimination of the titanium spar leads to considerable reductions in fabrication costs.

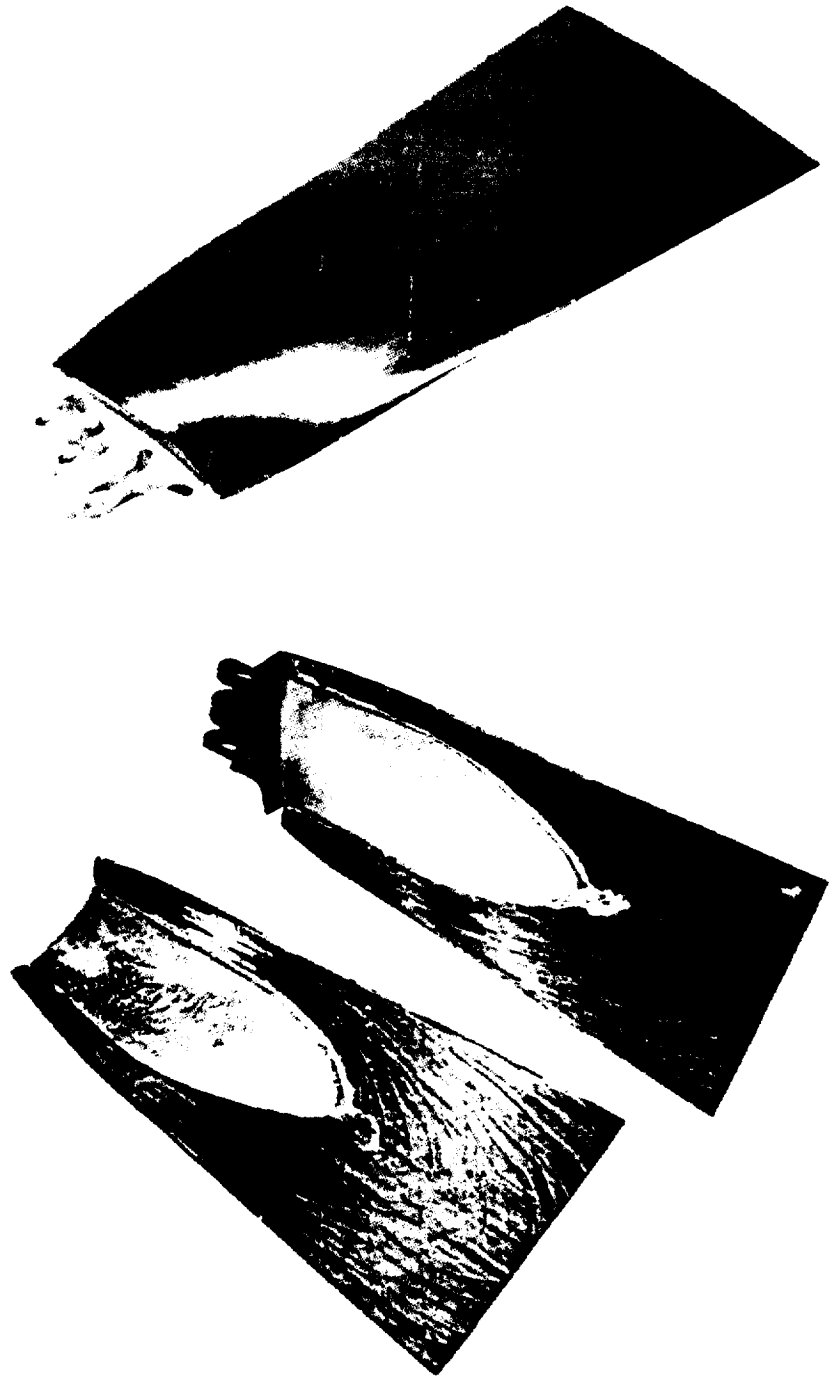

Figure 51. Typical Spar/Shell Composite Blade.

5.1.3 Blade Fabrication Process

Blade fabrication was achieved by using outside vendors to machine the titanium blade master-model and spars, and then by using existing GE facilities (EMTL) and personnel to apply the composite shells to the spars. An adequate quantity of blades was procured for required bench testing and the assurance of available blades for wind tunnel testing.

For each airfoil configuration, a metal master tool was machined to exact airfoil coordinates by an outside vendor. To ensure conformance with design drawings, the model was inspected at each airfoil section; a die was then cast from this master blade. Using the die, the composite shell was applied over the spar and was formed to the final blade shape through compression and subsequent curing. This method of fabrication produced very little variance from blade to blade. All blades were weighed, ultrasonically scanned, and inspected both visually and dimensionally.

5.1.3.1 General Compression Molding Process

The basic compression molding process developed by GE for scale-model composite airfoils is shown in ***Figure 52***. It consists of the following general activities:

- Ply Pattern Generation – The requisite number and geometry of laminate that would uniformly fill the mold and/or the volume between the metallic spar and the cavity are determined by scribing the metallic master-model blade topographically.
- Ply Assembly – Fixtures are manufactured for assembling the blade laminate in the correct sequence and relative location.
- Spar Preparation – Fully numerically controlled (NC) machined spars are chemically and mechanically etched and primed to prepare the surface for bonding to the composite airfoil during the cocuring process.
- Molding – Using a metallic, fully machined and approved master-model blade, epoxy mold tools are fabricated. The critical molding process is accurately controlled to ensure good consolidation of the composite, void-free laminates, and molding uniformity. Precise die-closure programs have been developed to produce blades of consistent quality.
- Finishing Operations – The minor finishing operations to the molded airfoils include deflashing and finishing of leading and trailing edges.

Although there were three independent blade sets fabricated under this contract, the molding process for all three sets was identical to that just described.

5.1.3.2 Quality Assurance

Manufacturing and quality control specifications, plans, and procedures were implemented to ensure the use of the highest quality materials, and to control the blade fabrication processes. The plans covered every aspect of the blade manufacturing process from the time the raw materials were procured until the part was delivered to test.

Process control records were maintained in individual files and included such information as routing cards, molding cycle charts, temperature recording charts, dimensional inspections, material

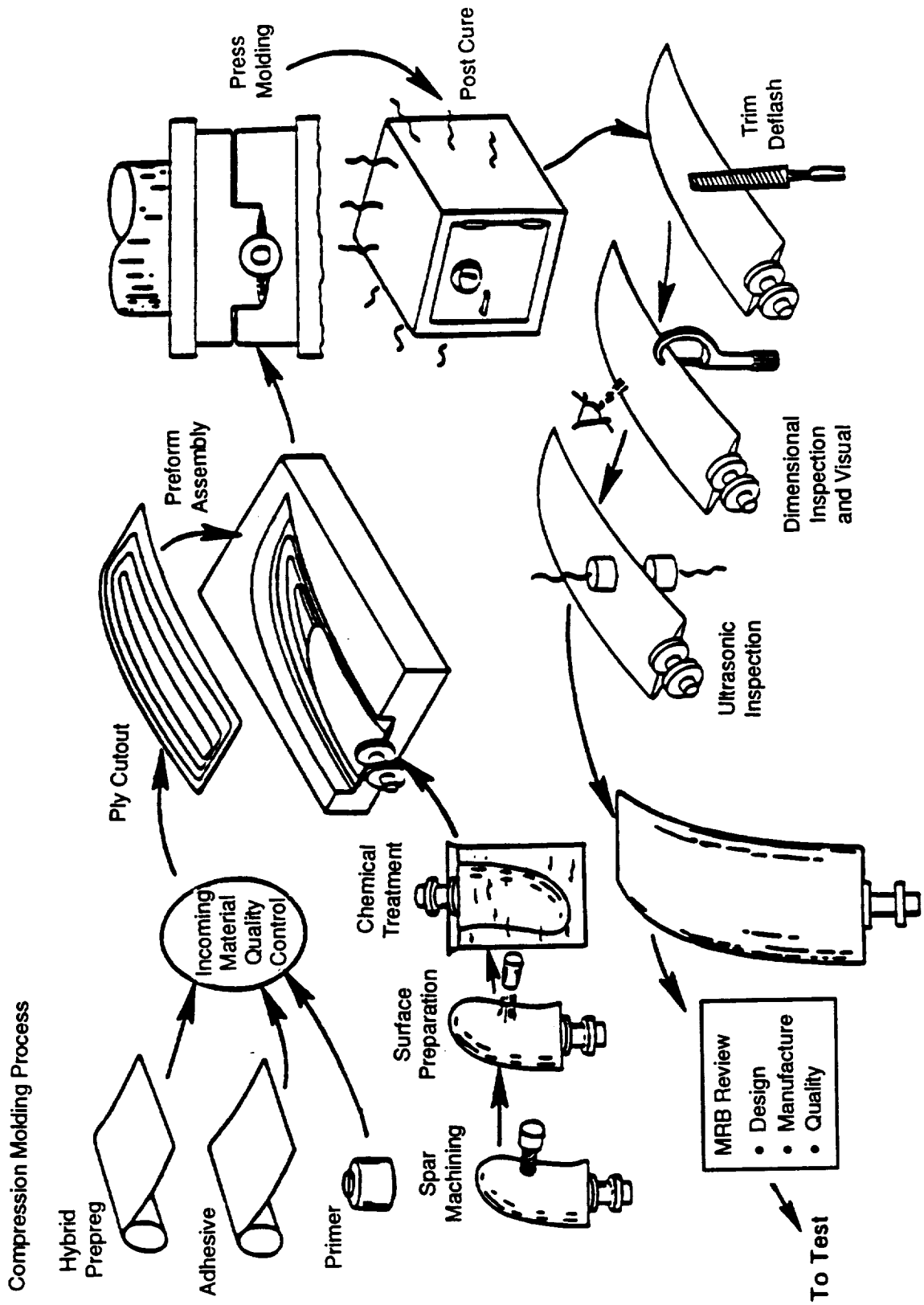

Figure 52. Basic MPS Blade Manufacturing Process.

properties, and chemical analyses. The blades were nondestructively inspected by ultrasonic through-transmission with a C-Scan printout record that also constituted part of the individual blade documentation.

Before any blade was released to test, a Material Review Board Committee (consisting of a cognizant design engineer, a manufacturing engineer, and a quality representative) visually reviewed the blade, together with the dimensional-inspection records, process records, and C-Scans to ensure acceptable quality levels.

5.1.3.3 F39 Blade Fabrication

The fabrication process for the forward-swept F39 blade set, developed under this NASA contract, followed the same procedure as was just described. Certain aspects of the fabrication process unique to the stable blade are discussed below.

The first set of forward-swept F39 blades was designed to be stable and to provide optimum performance at cruise conditions. The blade material selected was IM7 graphite. The ply design ultimate strength properties for this material are listed in ***Table 8***. In all, 16 blades were fabricated.

Table 8. IM7 Graphite Ply Design Ultimate Strength Properties.

Material Property	Stable F39C4 (IM7 Graphite Material)
Longitudinal Ultimate Tensile Strength, ksi	210.7
Transverse Ultimate Tensile Strength, ksi	3.9
Longitudinal Ultimate Compressive Strength, ksi	111.3
Transverse Ultimate Compressive Strength, ksi	16.2
In-Plane Ultimate Shear Strength, ksi	12.2

After fabrication was complete, each blade underwent a visual and dimensional inspection to ensure both quality and dimensional consistency in the fabrication process from blade to blade. A typical visual/dimensional inspection sheet is presented in ***Figure 53***. In the visual inspection operation, all anomalies were identified by an indication of the exact location on the blade schematic, accompanied by a brief description. Minor nicks and scratches were repaired by filing or sanding. If the anomaly was too severe, the blade and spar were separated and a new blade was layed-up. This, however, was not necessary for this blade set. The blade was then dimensionally inspected by means of thickness measurements taken at three cross-sectional cuts, made at the blade's root, mid, and tip regions. At each section, maximum thickness, leading edge thickness, trailing edge thickness, and blade chord length were determined. Once all blades had been dimensionally checked, the results were averaged at each blade section, and were compared to both drawing and master-model dimensions for acceptability.

ADVANCED COMPOSITES TECHNOLOGY - PROCESS PLAN ROUTE SHEET

Plan I.D. No. ACT - 0199 Rev. No. 00

PART/ASSEMBLY NO.	PART/ASSEMBLY NAME	ENGINE PROGRAM	SERIAL NO.
	MPS BLADE, F39 (8)	MPS PROJECT	F39- 12

QUALITY LEVEL	PROCESS PLANNER	Q.C. ENGINEER	LOT NO.	LOT QUANTITY
	B Fuhrmann			

Operation 110 - Visual Inspection

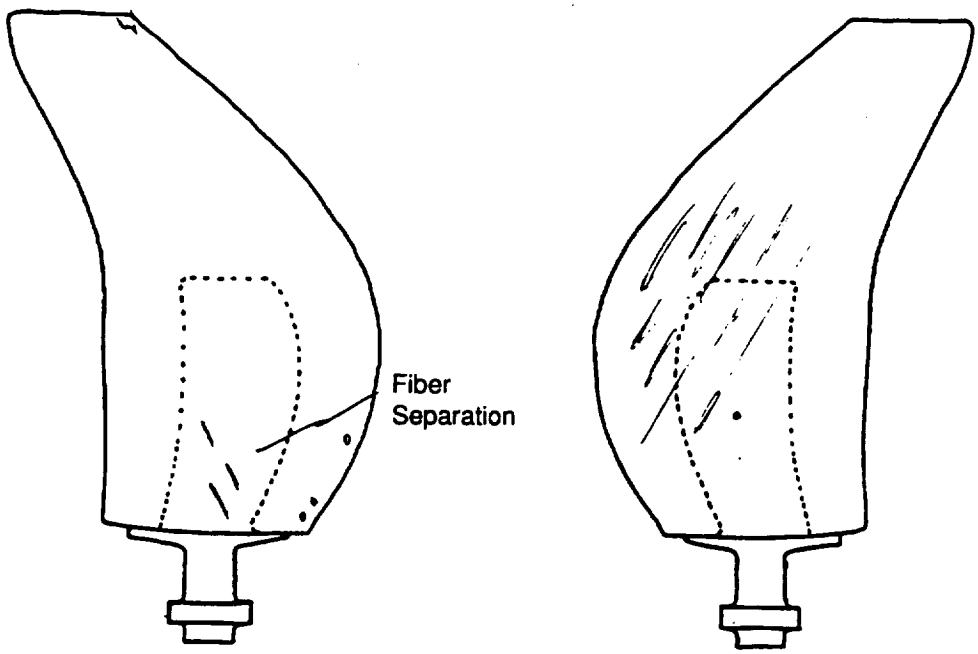

Operation 120 - Dimensional Inspection

Inspection Section	TM Maximum Thickness		Act.	Dev.	TL Leading Edge Thickness		Act.	Dev.	TU Trailing Edge Thickness		Act.	Dev.
EE	Drwg.	0.189	.185		Drwg.	0.054	.051		Drwg.	0.030	.026	
	Mstr.	0.189			Mstr.	0.058			Mstr.	0.031		
HH	Drwg.	0.100	.097		Drwg.	0.026	.027		Drwg.	0.017	.017	
	Mstr.	0.103			Mstr.	0.030			Mstr.	0.019		
NN	Drwg.	0.052	.047		Drwg.	0.018	.020		Drwg.	0.015	.015	
	Mstr.	0.054			Mstr.	0.021			Mstr.	0.019		
									Tolerance		+ .003 - .000	

Inspection Section	CH Chord Length		Act.	Dev.
EE	Drwg.	3.371	3.346	
	Mstr.	3.379		
HH	Drwg.	3.773	3.771	
	Mstr.	3.776		
NN	Drwg.	2.649	2.654	
	Mstr.	2.661		
	Tolerance		+ .007 - .000	

Figure 53. Typical Visual/Dimensional Inspection Sheet.

The results of this comparison for the stable-by-design build of the forward-swept F39 blade set are shown in ***Table 9***. The true blade dimensions are slightly less than the drawing and master-model dimensions. There is little-to-no variation from blade to blade, however, indicating excellent consistency in the fabrication process.

5.2 Mechanical Design

The mechanical design analysis methods necessary to establish the forward-swept F39 blade design concept are presented in Section 4.3. Only those aspects of mechanical design applicable to this specific blade set are presented in this section.

5.2.1 Blade Instrumentation and Bench Testing

Prior to operation on the test rig, all forward-swept F39 blades underwent a bench test procedure. Testing details and subsequent results related to this blade set are presented in this section.

One blade from the forward-swept F39 stable blade configuration was heavily instrumented with strain gages in order to determine the blade strain distribution for relevant excitation modes. The number and their locations for this blade set are illustrated in ***Figure 54***. The results of the strain distribution bench test are provided in *Appendix 1*.

The stable blade design was also frequency-checked to determine all natural frequencies and mode shapes that might be encountered during testing. Bench test frequencies and their comparison to scaled analytical frequencies are tabulated in ***Tables 10*** and ***11***. Mode shapes from bench testing are compiled in *Appendix 2*. The bench frequencies in *Appendix 2* are lowered by approximately 5% due to the application of reflective tape to the blade in order to highlight the nodal patterns for the different vibratory modes.

At cruise conditions, the radial load for the forward-swept blade designs was estimated to be 1,800 pounds, which was comparable to the radial load of the successfully tested F31 blade design. Because of the expected loading similarity, a pull test was not conducted on any of the forward-swept F39 blade designs.

5.2.2 Blade Instrumentation for Operational Testing

As previously mentioned, the forward-swept F39 stable blade configuration was bench-tested to determine both strain distribution and vibration characteristics. Strain gages were applied to a total of six blades for monitoring during wind tunnel testing. Four blades had three dynamic gages applied, and two blades had two static gages applied. Gage locations were based on analytical steady-state and vibratory stress data and from previous test experience. Since the analysis for the forward-swept design predicted low chordwise vibratory stress levels, and since tip gages oriented for chordwise bending modes from previous scale-model testing had seen very little response, all dynamic gages were positioned radially to record as many vibratory modes as possible within the simulator operating range. Gage locations for the forward-swept blades used for wind tunnel testing are identified in ***Figures 55*** and ***56***.

Table 9. Stable F39 Blade Dimensional Inspection Data Results.

Blade Number	Section EE				Section HH				Section NN				
	TM	TL	TU	CH	TM	TL	TU	CH	TM	TL	TU	CH	
1	0.183	0.048	0.025	3.366	0.096	0.03	0.017	3.773	0.046	0.018	0.014	2.638	
3	0.185	0.058	0.029	3.336	0.101	0.031	0.019	3.766	0.048	0.023	0.020	2.647	inst.
4	0.183	0.054	0.026	3.353	0.097	0.028	0.016	3.745	0.047	0.020	0.014	2.626	
6	0.187	0.057	0.026	3.367	0.097	0.030	0.017	3.769	0.048	0.019	0.015	2.646	
7	0.187	0.050	0.029	3.331	0.098	0.029	0.018	3.769	0.045	0.020	0.013	2.643	
8	0.191	0.057	0.028	3.339	0.105	0.028	0.017	3.753	0.051	0.022	0.016	2.629	
9	0.186	0.047	0.028	3.371	0.099	0.027	0.018	3.770	0.045	0.018	0.017	2.641	
10	0.187	0.053	0.026	3.363	0.099	0.028	0.017	3.749	0.048	0.019	0.016	2.666	
11	0.188	0.053	0.030	3.344	0.103	0.028	0.020	3.762	0.049	0.023	0.017	2.642	
12	0.186	0.053	0.026	3.360	0.100	0.026	0.017	3.774	0.046	0.020	0.014	2.647	inst.
13	0.189	0.052	0.027	3.334	0.100	0.028	0.016	3.761	0.049	0.021	0.015	2.650	
14	0.184	0.051	0.028	3.333	0.098	0.026	0.018	3.744	0.045	0.019	0.015	2.656	inst.
15	0.189	0.053	0.029	3.368	0.099	0.033	0.018	3.787	0.048	0.022	0.018	2.644	
16	0.182	0.051	0.025	3.343	0.095	0.029	0.018	3.727	0.043	0.021	0.016	2.622	inst.
17	0.188	0.053	0.030	3.339	0.098	0.028	0.020	3.735	0.049	0.022	0.018	2.630	
18	0.187	0.054	0.025	3.379	0.096	0.027	0.015	3.779	0.047	0.018	0.015	2.652	
Min.	0.182	0.047	0.025	3.331	0.095	0.026	0.015	3.727	0.043	0.018	0.013	2.622	
Max.	0.191	0.058	0.030	3.379	0.105	0.033	0.020	3.787	0.051	0.023	0.020	2.666	
Ave.	0.18660	0.05307	0.02747	3.35067	0.09900	0.02840	0.01760	3.75933	0.04720	0.02047	0.01593	2.64273	
Var.	0.00001	0.00001	0.00000	0.00024	0.00001	0.00000	0.00000	0.00026	0.00000	0.00000	0.00000	0.00013	
Std. Dev.	0.00230	0.00274	0.00167	0.01548	0.00250	0.00178	0.00136	0.01622	0.00201	0.00163	0.00177	0.01146	
Drawing	0.189	0.054	0.030	3.371	0.100	0.026	0.017	3.773	0.052	0.018	0.015	2.649	
Master	0.189	0.058	0.031	3.379	0.103	0.030	0.019	3.776	0.054	0.021	0.019	2.661	

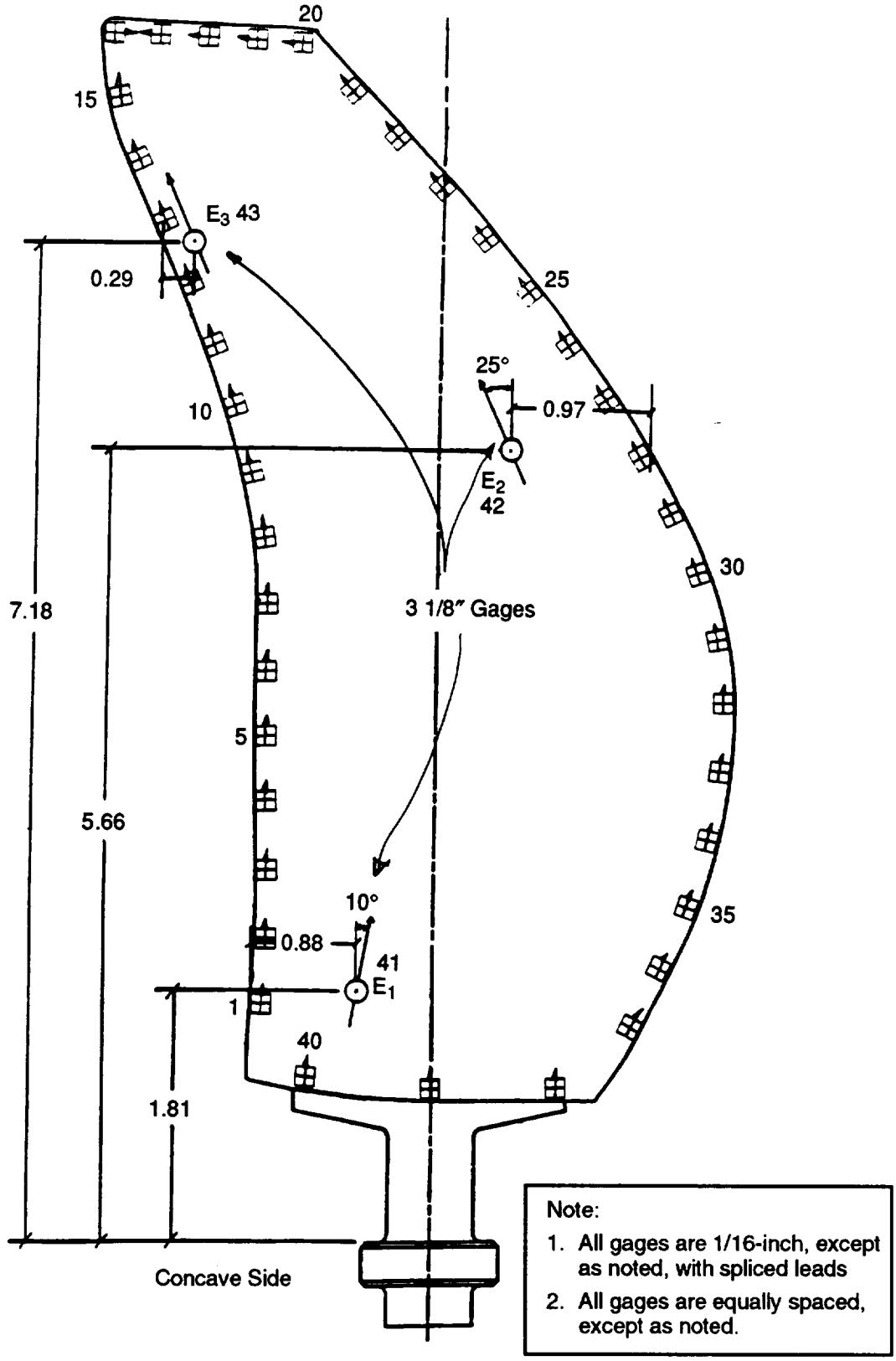

Figure 54. Stable F39 Blade Strain Distribution Instrumentation.

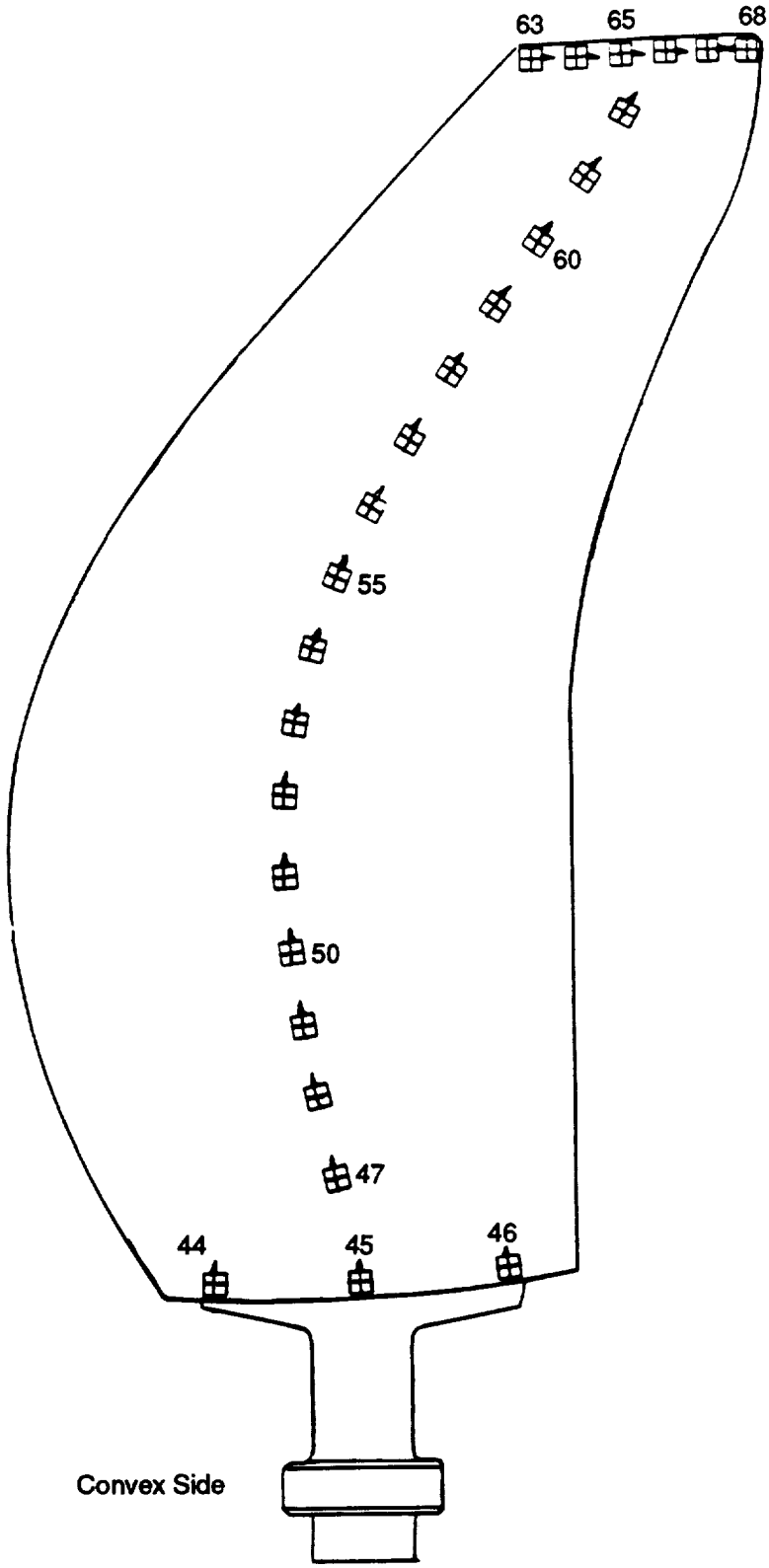

Figure 54. Stable F39 Blade Strain Distribution Instrumentation (concluded).

Table 10. Stable F39 Blade Bench Test Frequencies.

	Mode									
Serial No.	1 (1F)	2 (2F)	3 (1T)	4 (3F)	5 (3F')	6 (2T)	7	8	9	10
1	148	354	560	662	854	1008	1364	1534	1958	2234
3	148	354	560	652	854	1016	1368	1556	1970	2256
4	148	356	562	666	858	1016	1376	1540	1990	2184
6	145	352	547	669	848	989	1365	1507	1940	2191
7	148	356	560	650	856	1012	'382	1532	1972	2210
8	150	362	572	654	878	1050	1420	1574	2030	2308
9	146	354	556	660	852	1002	1370	1514	1948	2198
10	144	350	554	650	850	1004	1364	1524	1964	2204
11	148	354	560	646	856	1014	1378	1532	1974	1121
12	146	356	560	662	858	1012	1386	1530	1974	2224
13	146	356	560	658	858	1016	1380	1530	1962	2210
14	146	356	560	658	862	1024	1378	1552	1972	2232
15	144	352	554	662	850	998	1356	1514	1928	2196
16*	142	350	556	658	850	1008	1376	1512	1976	2182
17	148	354	560	660	862	1016	1376	1550	1970	2242
18	144	350	548	644	844	996	1354	1514	1928	2190
Avg	146	354	558	657	856	1011	1375	1532	1967	2218

Table 11. Comparison of Stable F39 Analytical (Model Scale) and Bench Test Frequencies.

Mode	Average Bench	Analytical 0% Speed (Model Scale)	Analytical 100% Speed (Model Scale)
1 (1F)	146	148	232
2 (2F)	354	384	423
3 (1T)	558	589	658
4 (3F)	856	839	944
5 (2T)	1011	1069	1129
6 (4F)	1375	1420	1524
7	1532	1648	1709
8	1967	1952	1971

Stress scope limits for gage monitoring were based on bench test strain distribution data. Material strengths for the blade layups were calculated using laminate plate theory with a first ply failure criterion. The endurance limit for vibratory stresses was assumed to be 30% of the steady-state limit.

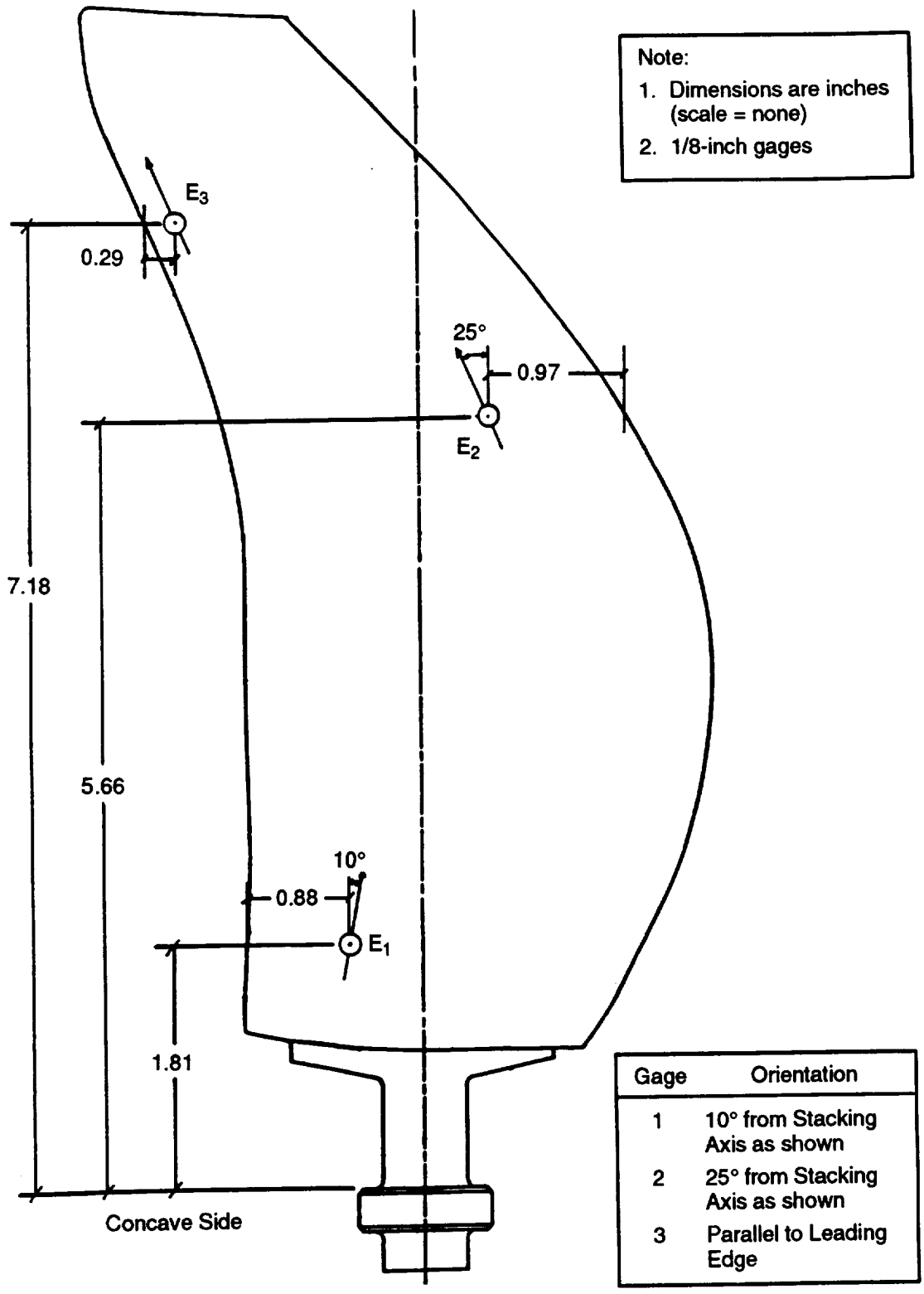

Figure 55. Stable F39 Blade Dynamic Gage Location.

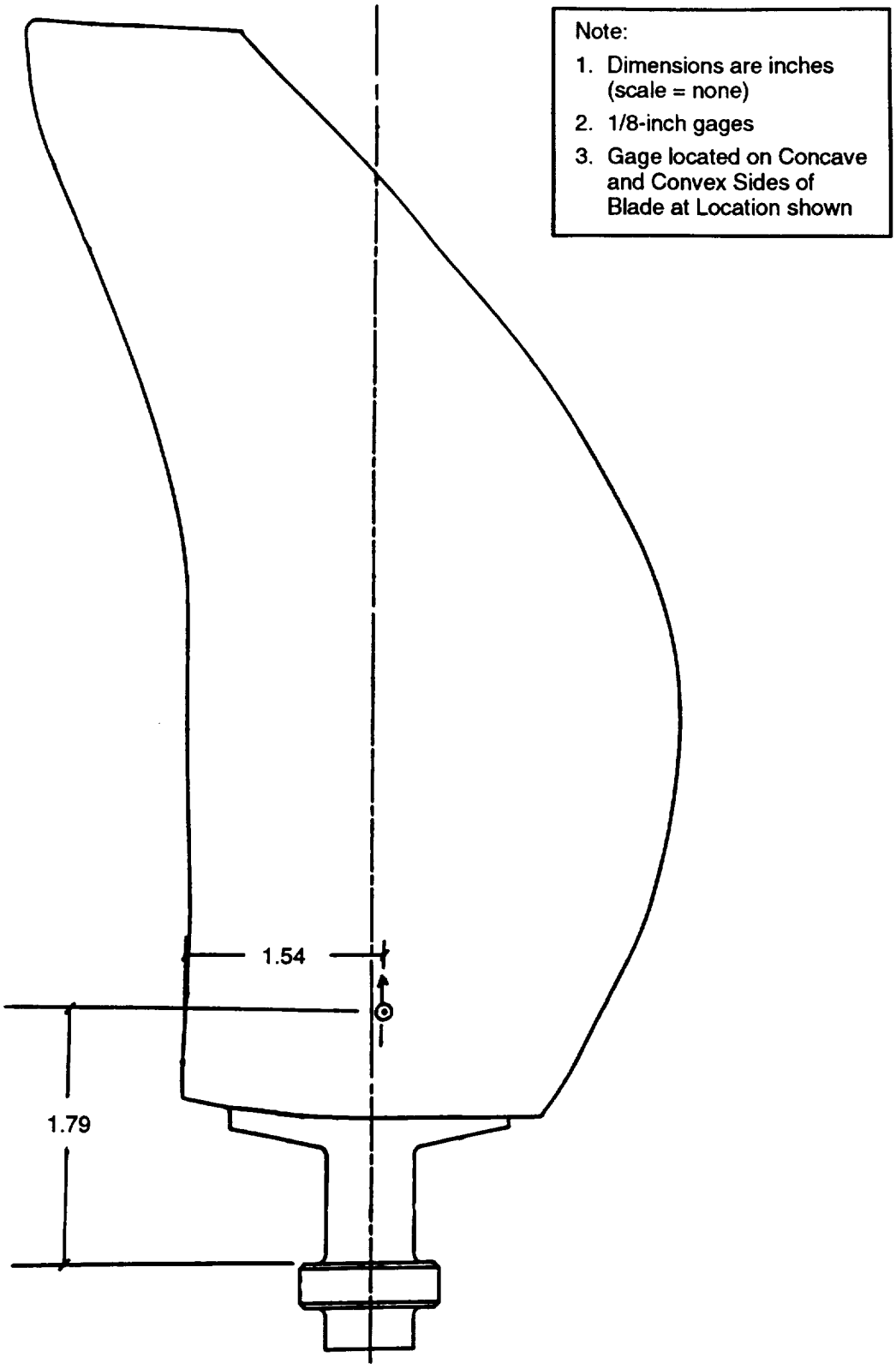

Figure 56. Stable F39 Blade Static Gage Location.

Goodman diagrams drawn from these two points had an assumed shaped based on previous test experience. Resulting scope limits for the forward-swept blade designs are tabulated in ***Table 12***.

Table 12. Stable F39 Blade Vibratory Scope Limits.

Stress Limit, ksi			
Mode	Gage 1 (Root)	Gage 2 (Mid)	Gage 3 (Tip)
1 (1F)	45	13	31
2 (2F	31	4	49
3 (1T)	35	25	10
4 (3F)	28	8	68
5 (2T)	16	0	66
6 (4F)	14	9	55
7	0	4	55
8	18	37	26

6.0 Forward-Swept F39 Divergent Blade Design and Fabrication

6.1 Aeromechanical Design and Analysis

To further investigate the aeromechanical issues associated with forward-swept, composite, unducted fan-type blading, an effort to design and fabricate a divergent blade set was undertaken. The goal was to design a blade set with a high probability of diverging, but with a sufficiently robust structure to safely endure multiple divergence events while mapping stability boundaries.

The primary design constraint was that the same tooling used in the fabrication of the stable blade set was to be used for the divergent blade set to minimize cost. Therefore, the divergent design was required to share the same cold geometric and aerodynamic airfoil shape as the stable design. AS4 material was selected for this blade design because its stiffness was lower than the stable blade's IM7 material and it had demonstrated ability to survive the large strains associated with violent instabilities.

To help define a laminate that satisfied the design requirements, a simple flat laminated plate wing divergence model was employed (*Reference 9*). The physical model is illustrated in ***Figure 57***, and the governing divergence equation is shown in ***Figure 58***. The governing nondimensional parameters of the model were: R, the ratio of torsion to bending stiffness; ψ, the normalized bending-torsion coupling; and γ, the elastic axis angle. The beam stiffness properties (EI, GJ, and K) were related to the laminate bending stiffness matrix Dij. A range of ply angle schedules was

Simplified Analysis – Forward-Swept Composite Wing

- Small Frequency Drop Indicated in First Attempt at Divergent Blade Design Motivated Simple Composite Tailoring Design Effort
- Simple Classical Laminated Plate Model Swept Forward in Airflow (Ref Weisshaar, J. Aircraft, Vol. 17, No. 6, 1980)

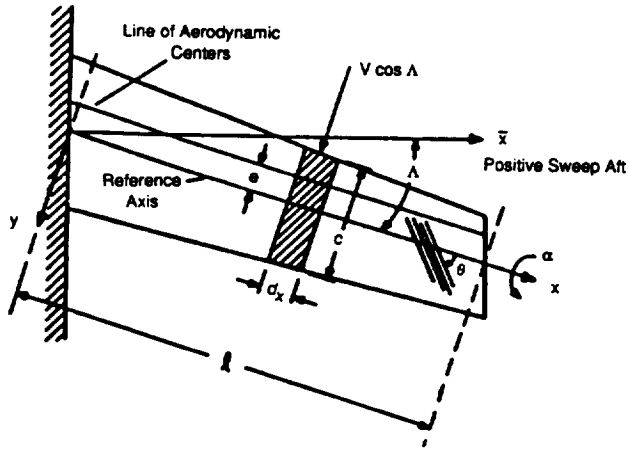

Figure 57. Physical Divergence Model of a Simple, Flat, Laminated Plate Wing.

Simplified Analysis – Forward-Swept Composite Wing

- Governing Divergence Equation (No Taper, No Twist):

$$\alpha_e''' + \frac{b(1-k\tan\Lambda)}{1-kg}\alpha_e' - \frac{a(g-\tan\Lambda)}{1-kg}\alpha_e = 0$$

- Where: $\alpha_e = \alpha - \frac{\partial h}{\partial y}\tan\Lambda \qquad k = \frac{K}{EI} \qquad g = \frac{K}{GJ}$

$$b = \frac{qcel^2\frac{\partial C_l}{\partial\alpha}\cos^2\Lambda}{GJ} \qquad a = \frac{qcl^3\frac{\partial C_l}{\partial\alpha}\cos^2\Lambda}{EI}$$

- Divergence Condition:

$$q_{div} = \frac{1}{2}\rho V_{div}^2 = \frac{2.47(1-kg)}{cl^3\frac{\partial C_l}{\partial\alpha}\cos^2\Lambda}\,\frac{EI}{\frac{1-k\tan\Lambda}{(l/e)(GJ/EI)} - 0.39(\tan\Lambda - g)}$$

Figure 58. Governing Divergence Equation for the Divergence Model.

considered and the resultant divergence speeds were determined. The results of the study are shown in ***Table 13***. The results were for a flat plate comprised of 20 plies of 0.0025-inch thick AS4 material with representative F39 geometry (sweep, span, chord, etc.). The ply layup schedule of the stable blade design, with IM7 material, is shown as Baseline IM7. The effect of the material change from the original IM7 material to the AS4 material (listed as Baseline in the table) was to decrease the divergence speed by 6%. Layups No. 3 and 4 were considered to be good candidates for a divergent blade design because of their high degree of twist-bend coupling, as indicated by the ψ and γ parameters. A set of unidirectional laminates were also studied: Nos. 5, 6, and 7. These laminates served to calibrate the range of coupling and divergence speeds that the model predicted for the extremes in laminate design. Laminates No. 8 and 9 were also considered; however, the ply layup schedules were judged to be inadequate to withstand the large strains of an instability.

With the candidate designs identified using the simple model (Layups No. 3 or 4), a finite element deflection analysis was performed to determine the best design for the divergent blade. The analysis was identical to that described in *Section 3.3*, with both design point air loads and centrifugal loads applied to the model. All of the models shared the same cold, or as-manufactured, geometry. The results of the study are shown in ***Table 14***. Layup No. 4 showed the smallest incidence decrease and, hence, was most likely to show divergence behavior. Therefore, Layup No. 4 was chosen as the ply layup schedule for the divergent blade set. The deflection of the stable blade set (IM7 material) along

Table 13. Simple Divergence Model Study Results.

Layup	Ply Schedule	R	Ψ	ϒ (°)	V_{div} [m/s]
Baseline	[0/90/–45/90/0/–45 |0/–45/0/45]s	0.72	0.17	–4.1	67.4
Baseline – IM7	[0/90/–45/90/0/–45 |0/45/0/–45]s	0.72	0.17	–4.1.	71.6
1	[0/90/–45/90/0/45 |0/–45/0/45]s	0.73	0.11	–2.7	65.5
2	[0/90/45/90/0/45 |0/–45/0/45]s	0.71	0.19	–4.6.	54.2
3	[0/90/45/90/0/45 |0/45/0/45]s	0.69	0.23	–5.4	52.6
4	[0/90/45/0/45/0 |45/0/45/0]s	0.64	0.23	–5.2	55.7
5	[010]s	0.16	0	0	63.4
6	[9010]s	1.87	0	0	26.9
7	[4510]s	2.81	0.48	–22.1	26.4
8	[0/90/30/0/30/0 |45/0/45/0]s	0.54	0.33	–6.8	53.4
9	[0/90/30/0/30/0 |30/0/30/0]s	0.52	0.34	–7.0	52.8

$$R = \frac{GJ}{EI} \quad \Psi = \sqrt{\frac{K^2}{EI\,GJ}} \quad \Upsilon = \arctan\left(\frac{-\Psi\sqrt{R}}{2}\right) = \text{elastic axis angle}$$

$$\frac{EI}{c} = D_{11} - \frac{D^2_{12}}{D_{22}} \qquad \frac{GJ}{c} = 4\left[D_{33} - \frac{D^2_{23}}{D_{22}}\right] \qquad \frac{K}{c} = 2\left[D_{13} - \frac{D_{12}\,D_{23}}{D_{22}}\right]$$

Table 14. Divergent F39 Finite Element Deflection Analysis Results.

Layup	Laminate	Mode 1 Frequency (Full Scale)	Mode Shape Slope	Untwist at LE Tip
MPSF39C4 (Stable)	IM7 Graphite Fiber, –25° Ref [0/90/–45/90/0/–45|0/45/0/–45]	46.4 Hz	–0.112	–2.3°
No. 1	AS4 Graphite Fiber, +25° Ref [0/90/–45/90/0/45|0/–45/0/45]	44.5 Hz	–0.181	–1.0°
No. 3	AS4 Graphite Fiber, + 25° Ref [0/90/45/90/0/45 | 0/45/0/45]	40.9 Hz	–0.172	–0.9°
No. 4 (Div Cand)	AS4 Graphite Fiber, +25° Ref [0/90/45/0/45/0 | 45/0/45/0]	40.3 Hz	–0.204	–0.8°
No. 7	AS4 Graphite Fiber, +25° Ref [45/45/45/45/45/45 | 45/45/45/45]	37.4 Hz	–0.291	–9.5°
Positive Untwist means in the open direction, increasing incidence				

with the (45_{10}) Layup No. 7 were included in ***Table 14*** to indicate the range of untwist that the analysis predicted.

A GAP analysis of the AS4 material, forward-swept F39 divergent blade, was performed at design point. The results predicted that the blade was dynamically stable (flutter-free), as shown in

Figure 59a. The design point stability root locus plot of the divergent blade is shown in ***Figure 59b***. The normal mode frequencies are indicated on the figure, as are the nodal diameter of each aeroelastic eigenvalue for the first mode family. A summary of the predicted frequency drops for the first three modes of several blades is shown in ***Figure 60***. The AS4 material, divergent blade set (Layup No. 4) was predicted to have a 24% reduction in first-mode frequency, compared to an 8% drop predicted for the stable blade set. Note that the (45_{10}) AS4 material laminate design was predicted to show a 37% first-mode frequency drop, indicating the upper limit achievable with ply angle design. In ***Figure 60***, the first-mode was predicted to be the mode that was most likely to demonstrate divergent behavior, since it was the mode showing the most significant frequency drops.

6.2 Engineering Materials Technology Laboratories

All information regarding the blade fabrication facility and general composite blade technology used in the fabrication of the forward-swept F39 stable blade set applies to the fabrication of the divergent blade set. Sections 5.2.1 and 5.2.2 present this information in detail. As a result, only those aspects of blade fabrication related to the divergent-by-design blade set are addressed in this section.

6.2.1 F39 Divergent Blade Fabrication

This second set of forward-swept F39 blades was designed with an inherently higher divergence than the original F39 blade set. The blade material selected was AS4 material. The ply design ultimate strength properties for this material are listed in ***Table 15***. The number of blades fabricated was again 16. In all, 12 blades were used at any given time for testing.

Upon completion of the fabrication process, each blade again underwent a visual and dimensional inspection by qualified EMTL personnel to ensure both blade quality and dimensional integrity during fabrication. No major flaws or defects were detected during the visual inspection. Minor nicks and scratches on a few blades were smoothed out with fine-grit sand paper. The blades were again dimensionally inspected through thickness measurements at three cross-sectional locations. The results were averaged at each blade section and were compared to both drawing and master model dimensions for acceptability.

The results and subsequent comparison of the dimensional inspection values for the divergent build of the forward-swept F39 blades are shown in ***Table 16***. Again, the true blade model dimensions were slightly less than both the drawing and Master Model dimensions.

There was good dimensional consistency, however, from blade to blade.

6.3 Mechanical Design

The mechanical design analysis methods necessary to establish the forward-swept F39 blade design concept are described in *Section 4.3*. All questions regarding this general information are directed to that particular section. Only those aspects of mechanical design applicable to the divergent blade design are presented in this section.

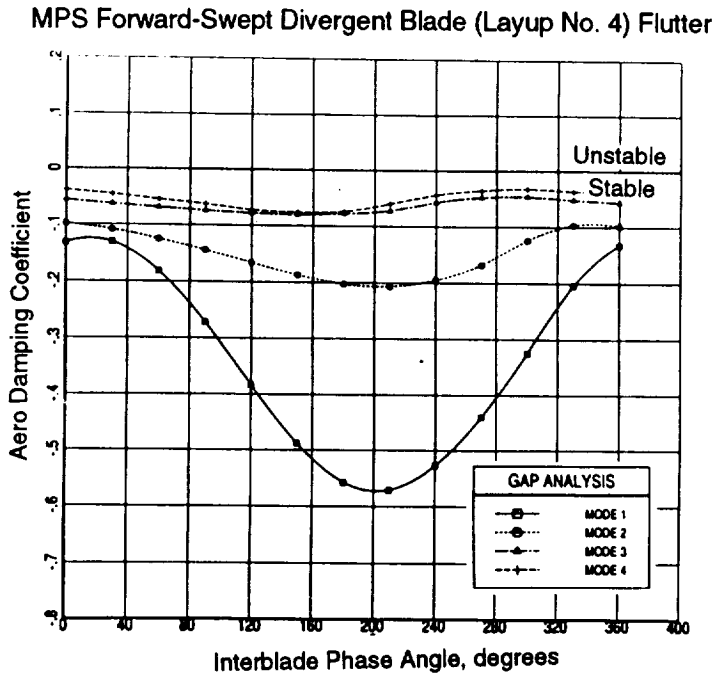

Figure 59a. Divergent F39 Blade Stability.

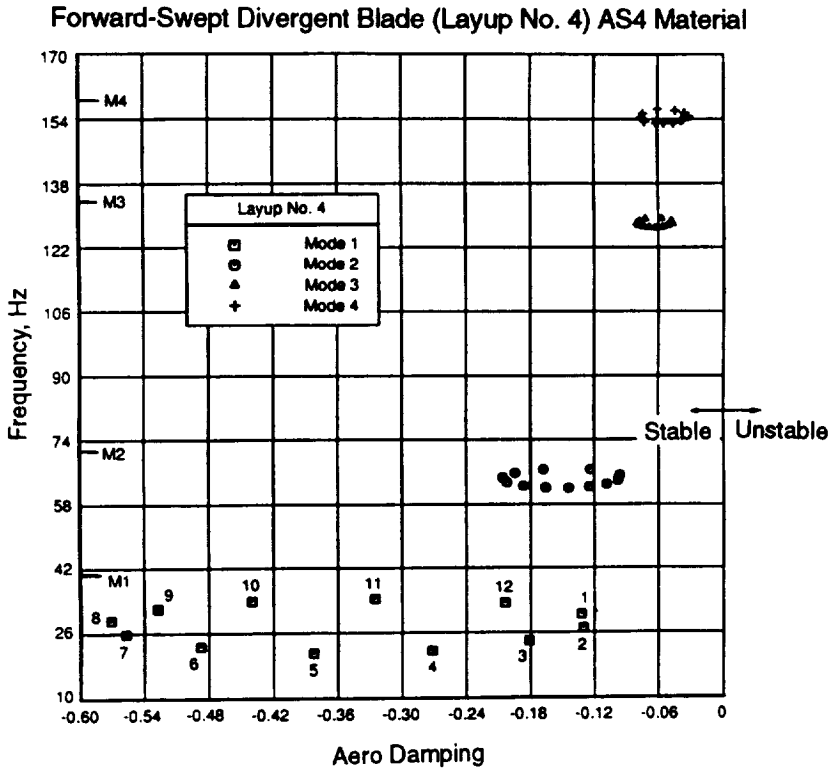

Figure 59b. Divergent Design Point Stability Root Locus Plot.

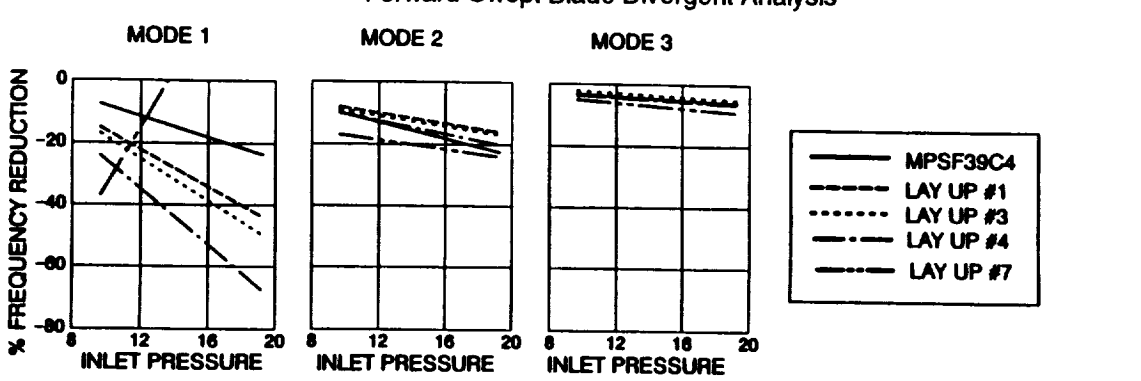

LAY UP	MODE 1 FREQUENCY REDUCTION @ DESIGN
MPSF39C4	8% (STABLE)
#1	15%
#3	17%
#4	24% (DIV. CAND.)
#7	37%

P_{inlet} = 9.65 psi
NASA 8 ft x 6 ft WIND TUNNEL CONDITIONS

Figure 60. Predicted Frequency Drops for the First Three Modes for Several Divergent Blade Candidates.

Table 15. Divergent F39 Blade Ply Design Ultimate Strength Properties.

Material Property	Unstable F39C4 (AS4 Graphite Material)
Longitudinal Ultimate Tensile Strength, ksi	129.5
Transverse Ultimate Tensile Strength, ksi	6.5
Longitudinal Ultimate Compressive Strength, ksi	124.2
Transverse Ultimate Compressive Strength, ksi	21.9
In-plane Ultimate Shear Strength, ksi	12.2

Once the ply layup schedule was selected, based on steady-state deflections and the frequency drop of the first mode shape slope, the candidate design was evaluated to ensure safe operation. To determine the mechanical integrity of the candidate design, stress and vibratory characteristics of the design were predicted using a finite element model of the full-scale cold blade shape. A steady-state analysis was conducted at design loadings to obtain predicted stresses and deflections. These are presented in ***Figures 61*** and ***62***, respectively. A modal analysis was run on the same model to determine blade frequencies and mode shapes. The predicted blade frequencies were scaled to model size by a factor of 4.985

$$\left(= \frac{\text{full scale diameter}}{\text{model scale diameter}} \right)$$ for comparison to previous MPS designs.

Table 16. Divergent F39 Blade Dimensional Inspection Data Results.

Blade Number	Section EE				Section HH				Section NN				
	TM	TL	TU	CH	TM	TL	TU	CH	TM	TL	TU	CH	
3	0.187	0.054	0.027	3.343	0.099	0.029	0.018	3.764	0.050	0.020	0.016	2.675	inst.
4	0.186	0.053	0.025	3.349	0.101	0.030	0.018	3.782	0.049	0.020	0.015	2.653	strain
5	0.186	0.053	0.027	3.343	0.099	0.029	0.017	3.766	0.049	0.020	0.015	2.656	inst.
6	0.186	0.051	0.026	3.336	0.098	0.029	0.017	3.756	0.047	0.021	0.016	2.637	
7	0.187	0.053	0.027	3.345	0.099	0.030	0.018	3.773	0.048	0.020	0.015	2.655	inst.
8	0.187	0.054	0.027	3.350	0.099	0.028	0.017	3.770	0.049	0.021	0.015	2.658	inst.
9	0.186	0.054	0.026	3.348	0.098	0.029	0.017	3.776	0.047	0.020	0.015	2.659	inst.
10	0.186	0.053	0.025	3.348	0.098	0.029	0.016	3.764	0.047	0.020	0.015	2.655	inst.
11	0.186	0.053	0.026	3.335	0.098	0.029	0.017	3.744	0.049	0.021	0.015	2.653	
12	0.185	0.052	0.027	3.345	0.098	0.028	0.017	3.754	0.048	0.020	0.015	2.638	
13	0.185	0.050	0.026	3.326	0.097	0.028	0.016	3.744	0.047	0.020	0.014	2.617	
14	0.187	0.053	0.027	3.339	0.100	0.031	0.017	3.742	0.049	0.021	0.015	2.640	
15	0.186	0.051	0.027	3.335	0.098	0.030	0.017	3.762	0.048	0.020	0.015	2.663	
16	0.186	0.054	0.027	3.342	0.099	0.031	0.017	3.762	0.048	0.021	0.015	2.654	
17	0.185	0.054	0.026	3.337	0.099	0.030	0.018	3.764	0.049	0.021	0.015	2.670	
20	0.187	0.051	0.026	3.347	0.097	0.028	0.017	3.771	0.049	0.021	0.016	2.622	
Min.	0.185	0.050	0.025	3.326	0.097	0.028	0.016	3.742	0.047	0.020	0.014	2.617	
Max.	0.187	0.054	0.027	3.350	0.101	0.031	0.018	3.782	0.050	0.021	0.016	2.675	
Ave.	0.18613	0.05269	0.02638	3.34175	0.09856	0.02925	0.01713	3.76213	0.04831	0.02044	0.01513	2.65031	
Var.	0.00000	0.00000	0.00000	0.00004	0.00000	0.00000	0.00000	0.00013	0.00000	0.00000	0.00000	0.00023	
Std. Dev.	0.00070	0.00126	0.00070	0.00639	0.00100	0.00097	0.00060	0.01129	0.00092	0.00050	0.00048	0.01530	
Drawing	0.189	0.054	0.030	3.371	0.100	0.026	0.017	3.773	0.052	0.018	0.015	2.649	
Master	0.189	0.058	0.031	3.379	0.103	0.030	0.019	3.776	0.054	0.021	0.019	2.661	

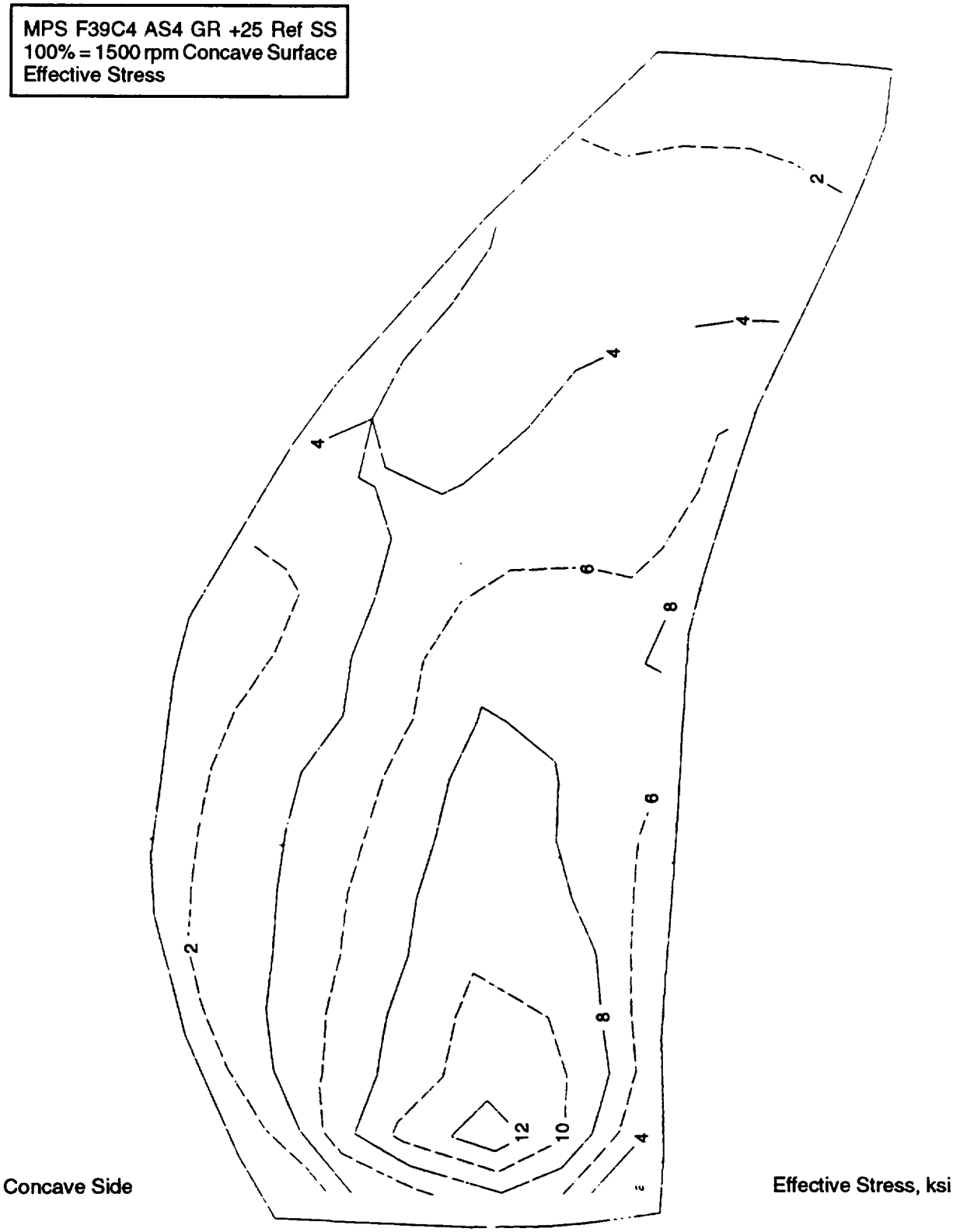

Figure 61. Divergent F39 Blade Predicted Stresses

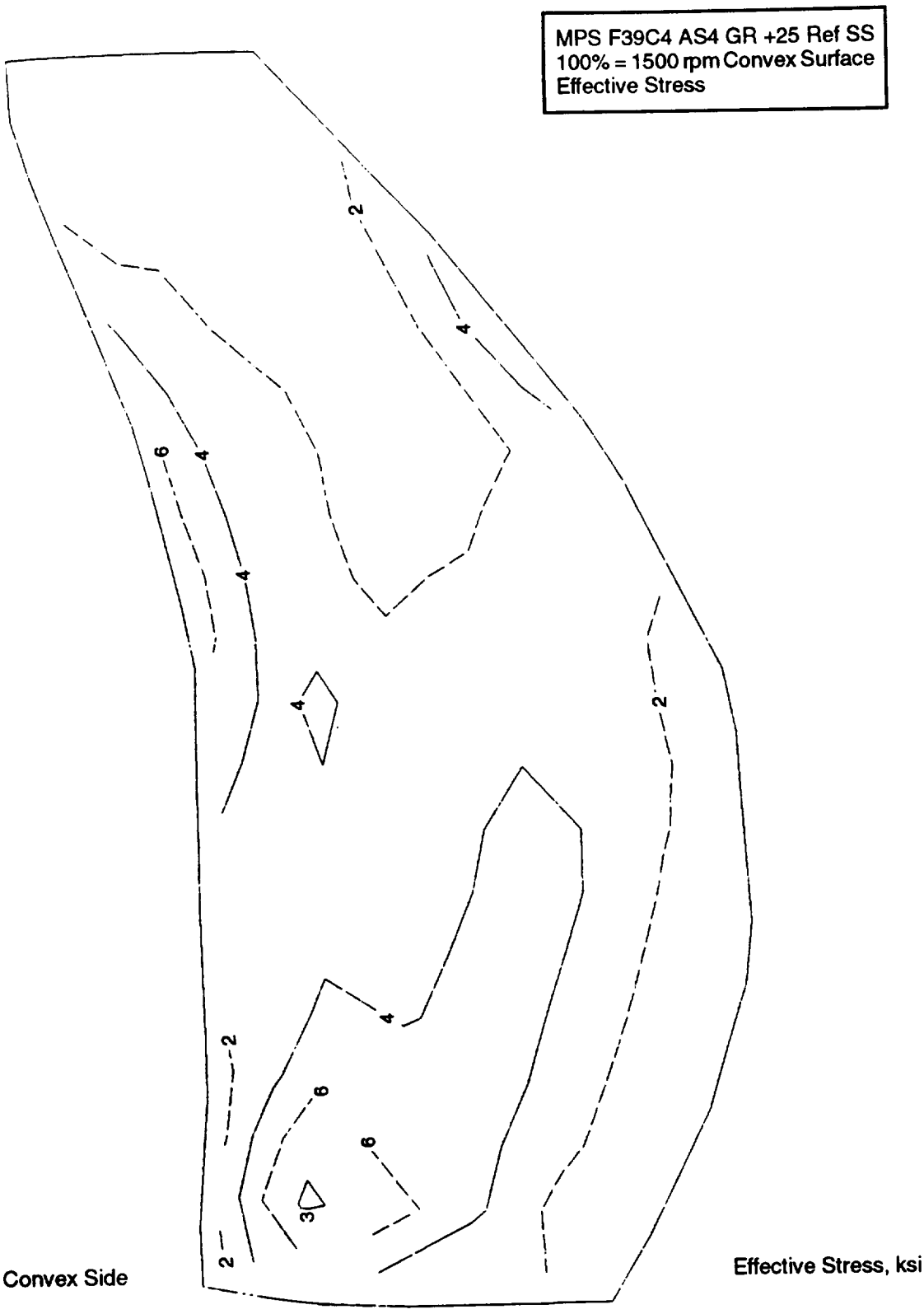

Figure 61. Divergent F39 Blade Predicted Stresses (concluded).

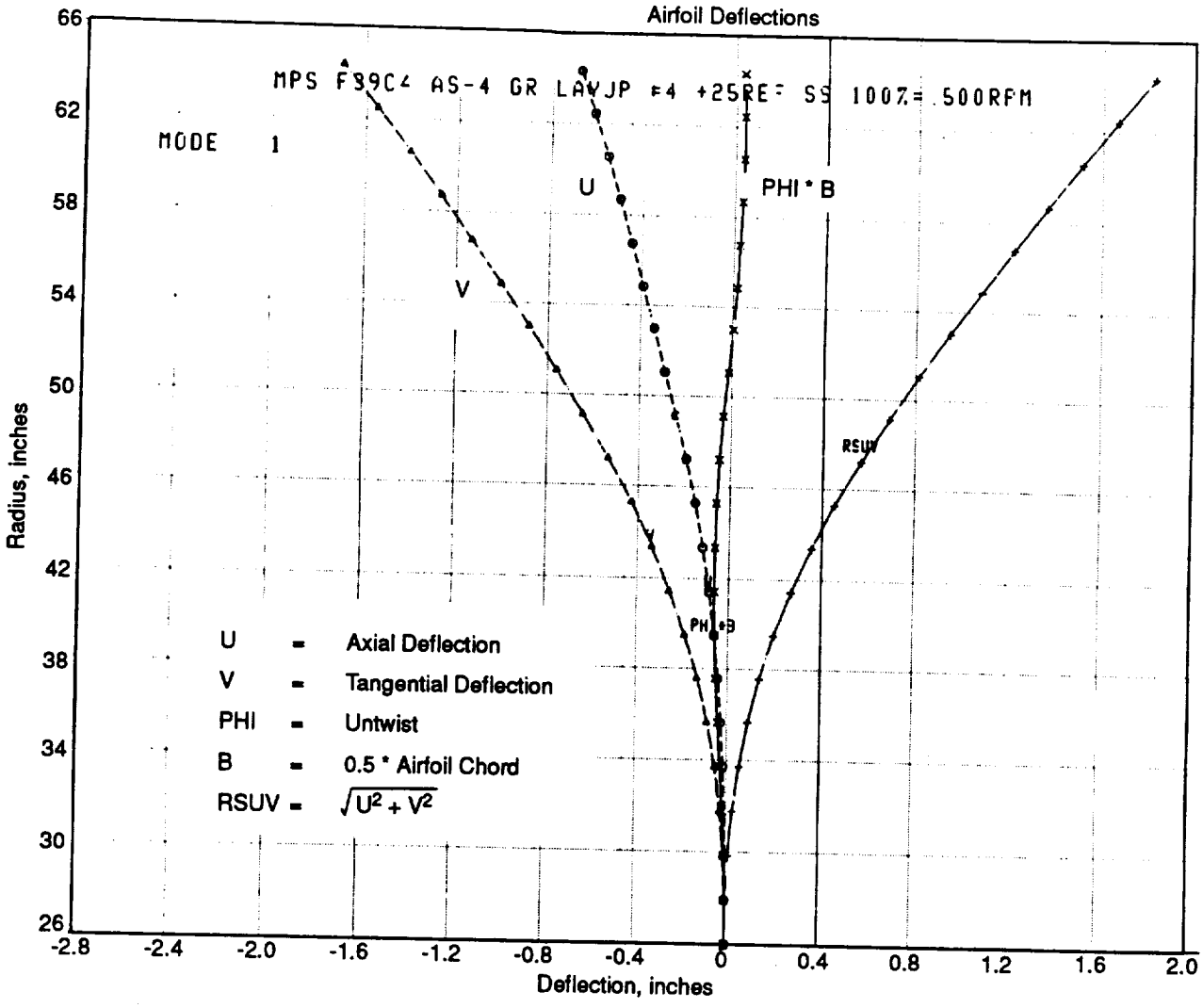

Figure 62. Divergent F39 Blade Predicted Deflections.

These are presented in ***Figure 63***. The stacking sequence for the candidate blade was (0/90/45/0/45/0), where each ply was 0.0032-inch thick, followed by (45/0/45/0/...), where each ply was 0.005-inch thick. The laminate was oriented +25° relative to the blade's stacking axis since initial analysis of the forward-swept design revealed that this reference angle had the highest level of twist-bend coupling of all angles investigated.

6.3.1 Blade Instrumentation and Bench Testing

Prior to operation on the test rig, all forward-swept F39 blades underwent a bench test procedure. Testing details and subsequent results related to the divergent blade set are presented in this section.

One blade from the forward-swept F39 divergent blade configuration was heavily instrumented with strain gages in order to determine the blade strain distribution for relevant excitation modes. The number of gages and their locations for this blade set are illustrated in ***Figure 64***. The results of the strain distribution bench test are provided in *Appendix 3*.

Prior to being instrumented for strain distribution, the divergent blade design was frequency checked to determine all natural frequencies and mode shapes that might be encountered during testing. Bench test frequencies and their comparison to analytical frequencies for this blade are tabulated in ***Table 17***. Mode shapes from bench testing are compiled in *Appendix 4*. The bench frequencies in *Appendix 4* are lowered by approximately 5% due to the application of reflective tape to the blade in order to highlight the nodal patterns for the different vibratory modes. The remainder of the divergent blade set was frequency-checked at NASA Lewis.

Table 17. Comparison of Divergent F39 Analytical (Model Scale) and Bench Test Frequencies.

Mode	Bench	Analytical 0% Speed (Model Scale)	Analytical 100% Speed (Model Scale)
1 (1F)	100	100	200
2 (2F)	258	270	352
3 (3F)	542	582	648
4 (1T)	638	652	786
5 (4F)	916	1003	1067
6 (2T)	1044	1126	1255
7	1498	1546	1598
8	1870	1700	1801

6.3.2 Blade Instrumentation for Operational Testing

As previously mentioned, the forward-swept F39 divergent blade configuration was bench-tested to determine both strain distribution and vibration characteristics. Strain gages were applied to a total of six blades for monitoring during wind tunnel testing. Four blades had three dynamic gages

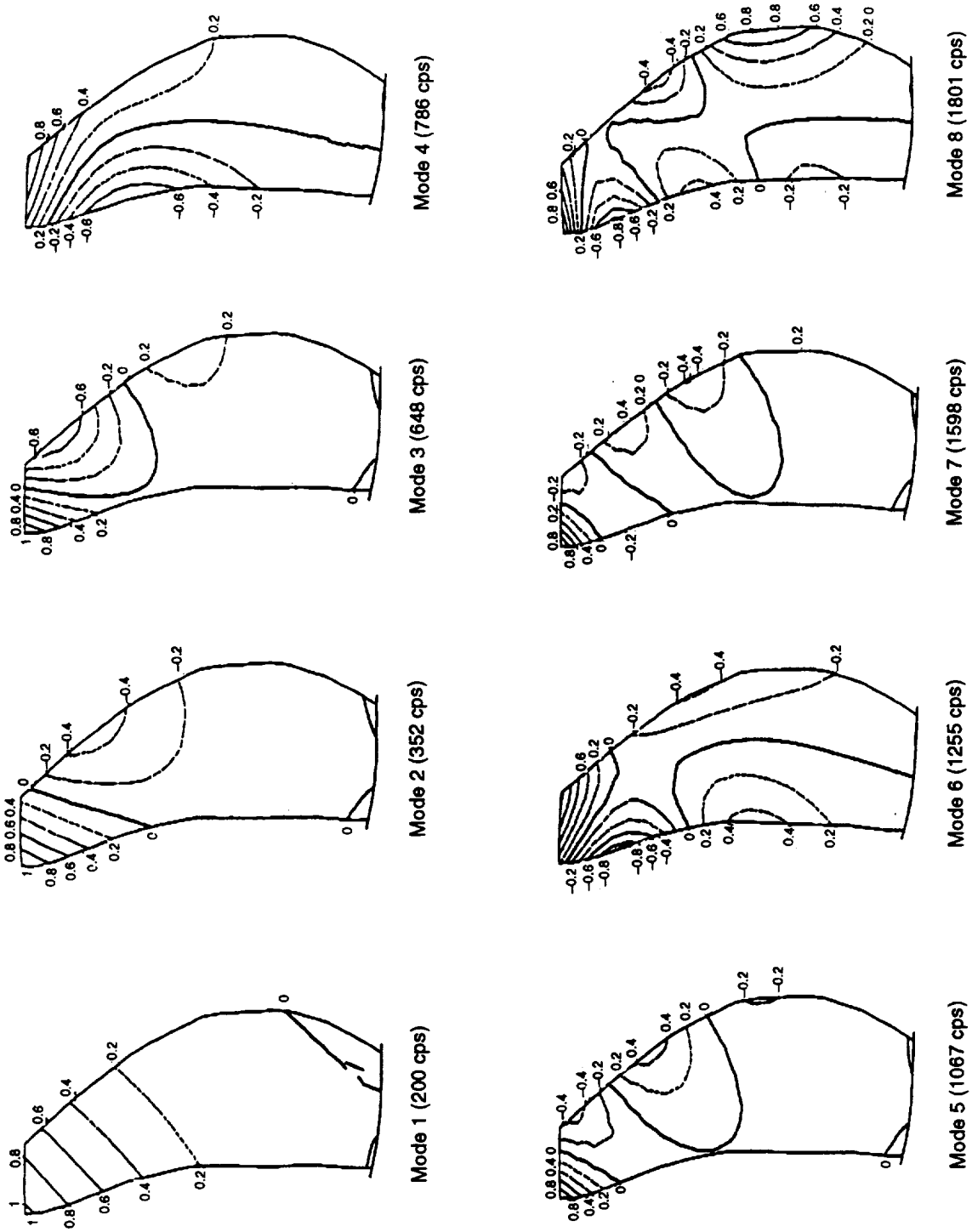

Figure 63. Divergent F39 Blade Calculated Frequencies (Model Scale) and Mode Shapes.

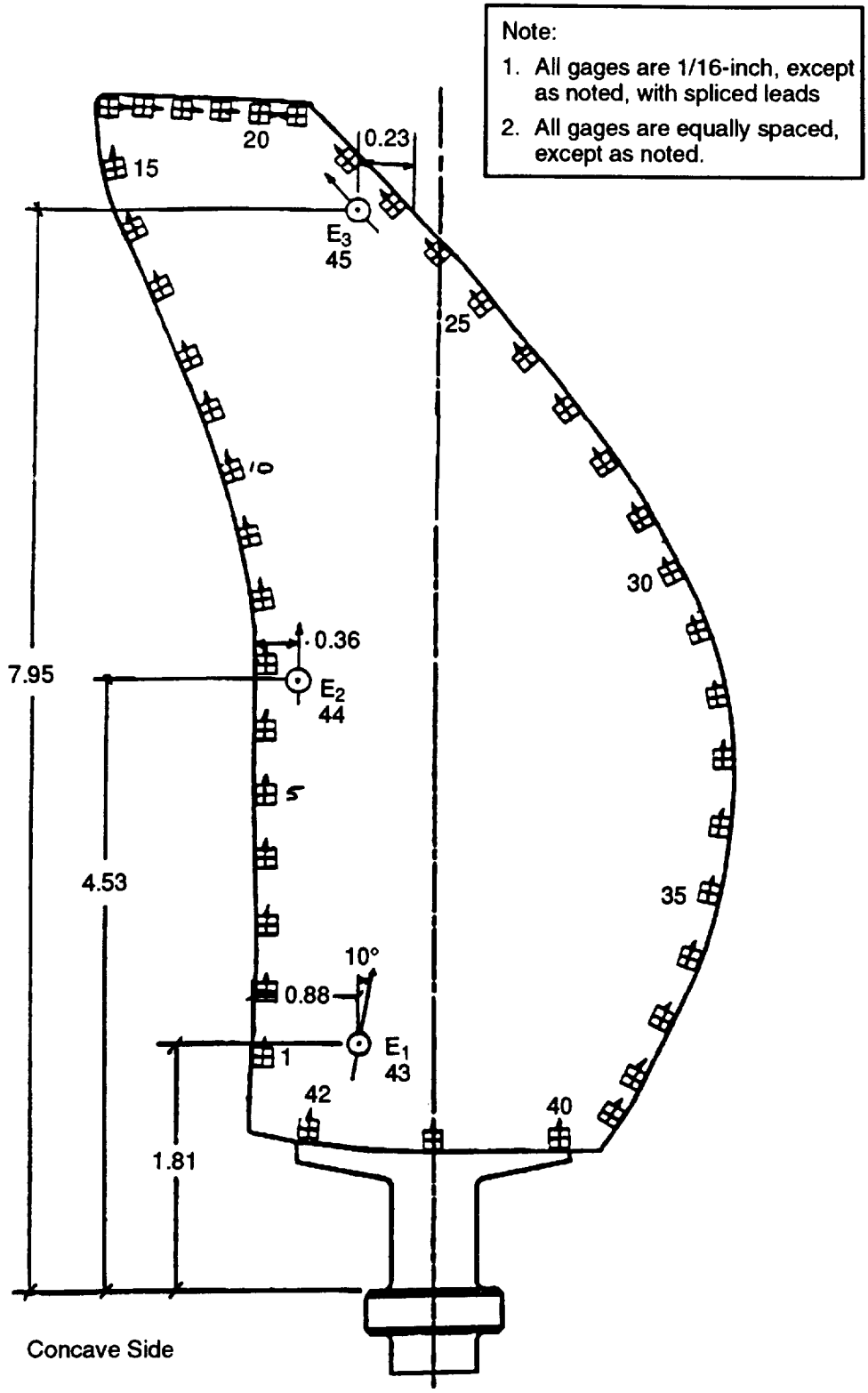

Figure 64. Divergent F39 Blade Strain Distribution Instrumentation.

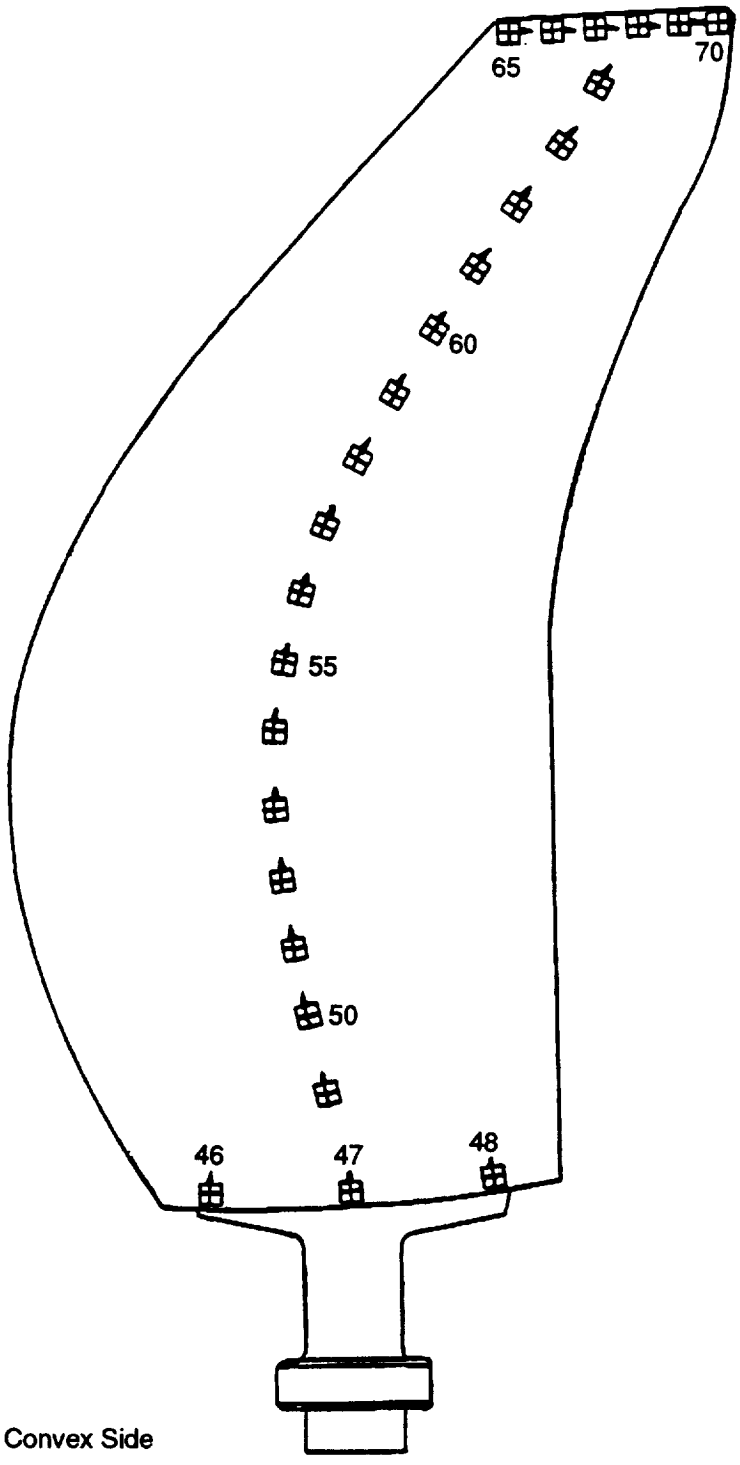

Figure 64. Divergent F39 Blade Strain Distribution Instrumentation (concluded).

applied, and two blades had two static gages applied. Gage locations were based on analytical steady-state and vibratory stress data and from previous test experience. Since the analysis for the forward-swept design predicted very low chordwise vibratory stress levels, and since tip gages oriented for chordwise bending modes from previous scale model testing had seen very little response, all dynamic gages were positioned radially to record as many vibratory modes as possible within the simulator operating range. The gage locations for the forward-swept blades used for wind tunnel testing are identified in ***Figures 65*** and ***66***.

Stress scope limits for gage monitoring were based on bench test strain distribution data. Material strengths for the blade layups were calculated using laminate plate theory with a first ply failure criterion. The endurance limit for vibratory stresses was assumed to be 30% of the steady-state limit. Goodman diagrams drawn from these two points had an assumed shape based on previous test experience. Resulting scope limits for the forward-swept blade designs are tabulated in ***Table 18***.

Table 18. Divergent F39 Blade Vibratory Scope Limits.

	Stress Limit, ksi		
Mode	Gage 1 (Root)	Gage 2 (Mid)	Gage 3 (Tip)
1 (1F)	9	1	24
2 (2F	15	0	37
3 (3F)	11	1	40
4 (1T)	6	27	31
5 (4F)	0	0	34
6 (2T)	4	0	22
7	5	31	11
8	0	0	9

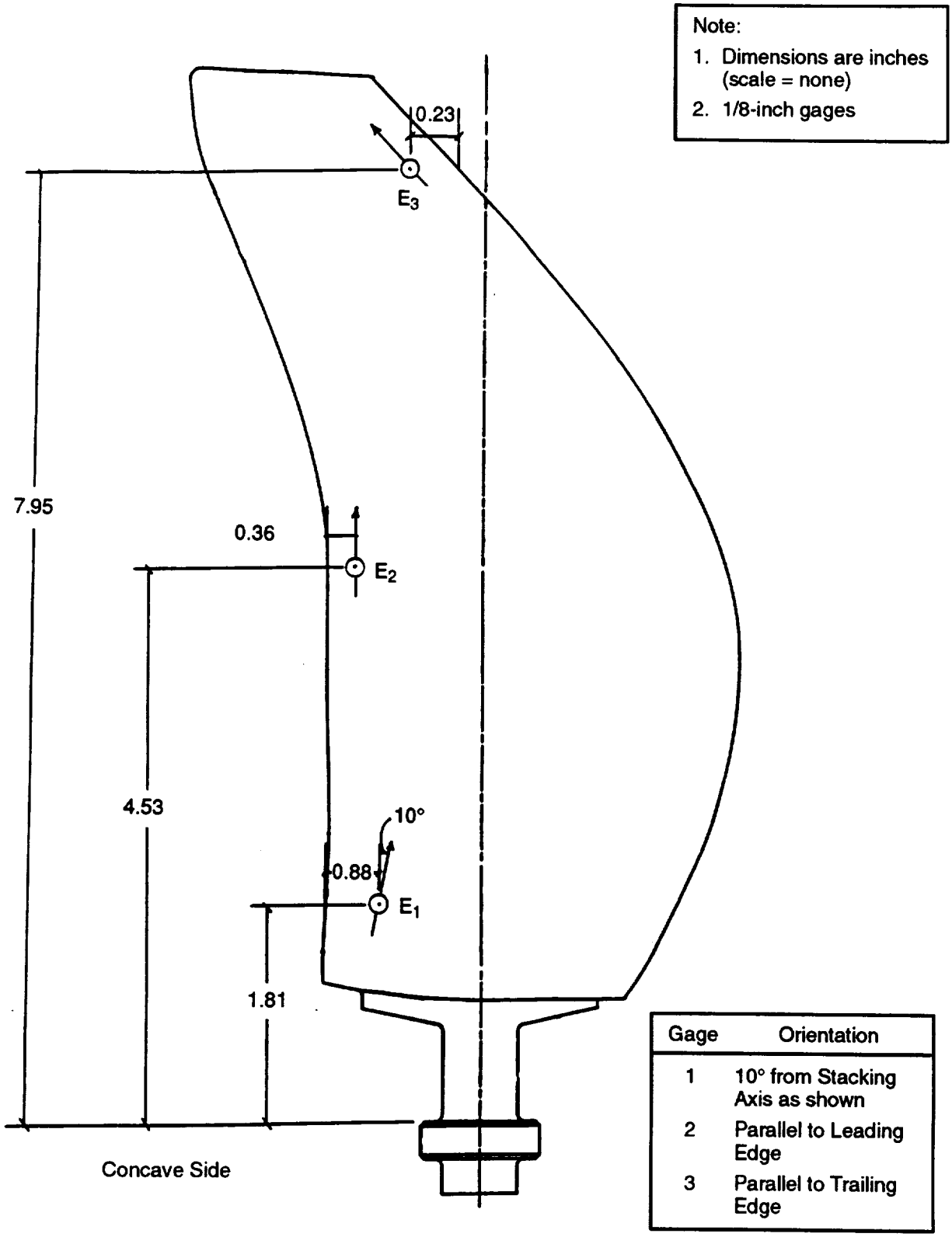

Figure 65. Divergent F39 Blade Dynamic Gage Locations.

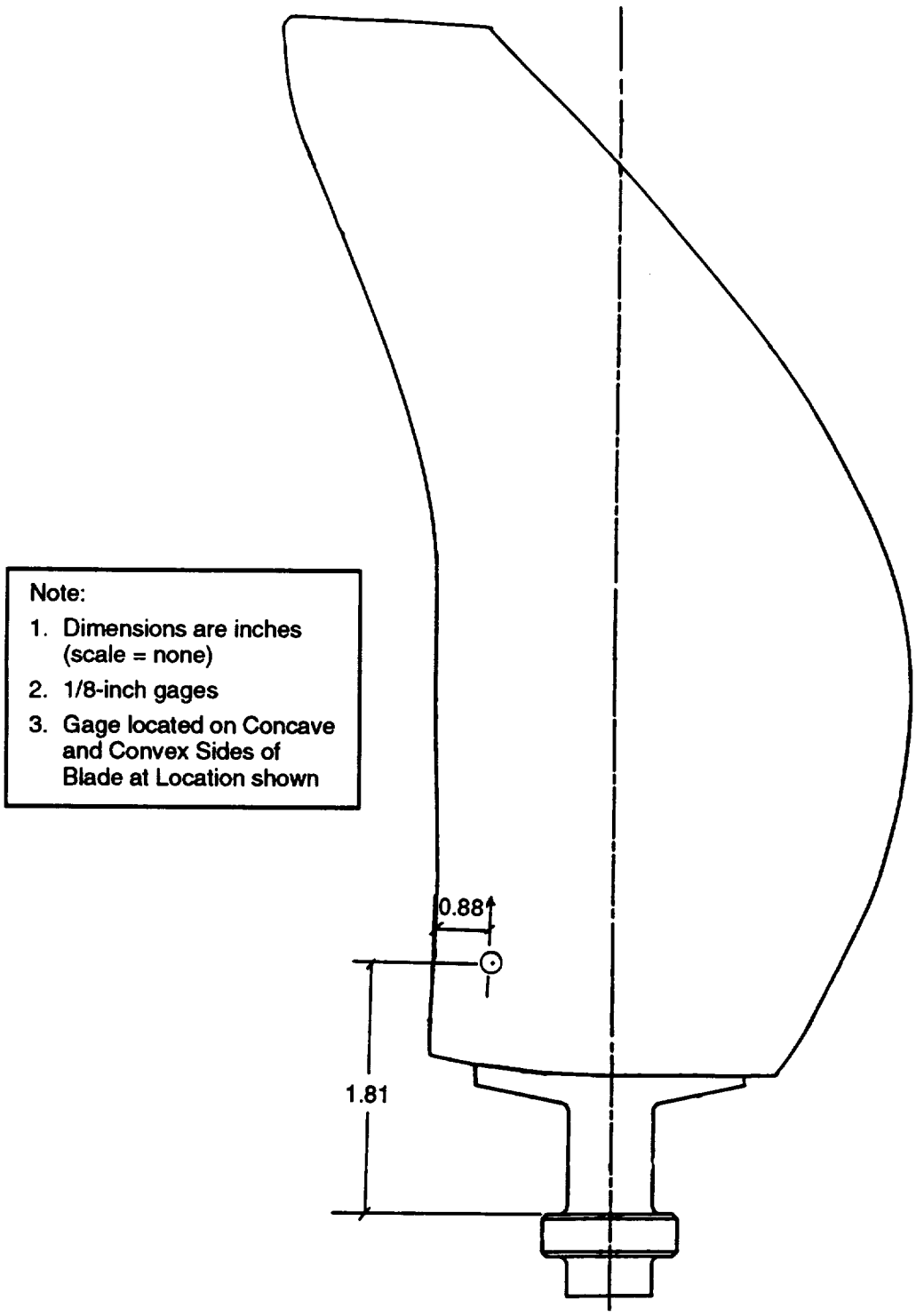

Figure 66. Divergent F39 Blade Static Gage Locations

7.0 Forward-Swept F39 Stiffened Blade Fabrication

7.1 Engineering Materials Technology Laboratories

All information regarding the blade fabrication facility and general composite blade technology used in the fabrication of the forward-swept F39 stable blade set also applies to the fabrication of the aeroelastically stiffened blade set. *Sections 5.2.1* and *5.2.2* present this information in detail. As a result, only those aspects of blade fabrication related to the aeroelastically stiffened blade set are addressed in this section.

7.1.1 F39 Stiffened Blade Fabrication

The third and final set of forward-swept F39 blades was designed with a geometry identical to the stable blade set, but with a different outer-ply material and layup to provide increased aeroelastic stiffness, especially in the first and second bending modes. Under this contract, NASA provided the blade spars from a previous blade set, the ply layup specifications, and the required material properties for the outermost six ply layers. The primary goal was to stiffen the blades to eliminate flutter, like that encountered with the first blade set produced.

The fiber material selected for the redesigned blade was T50 material. This provided the best balance of stiffness and strength. The ply design ultimate strength properties for this material are listed in ***Table 19***. Each ply was normally 0.005-inch thick, with the laminate oriented about the same -25° reference axis as was used in the original F39 blade design.

In all, 15 blades were produced. Twelve blades were required for testing at any given time. After being procured, each blade underwent a visual and dimensional inspection by qualified EMTL personnel for blade quality and dimensional integrity during fabrication.

Only one blade failed the visual inspection. A small portion of the leading edge was found to be missing. The defect could not be eliminated through filing and sanding without affecting the leading edge contour, and thus the overall blade geometry. As a result, the composite shell was separated from the spar and a new blade was produced that met inspection requirements. The inspection results and subsequent comparison of values for the stiffened build of the forward-swept F39 blades are shown in ***Table 20***.

Table 19. Stiffened F39 Blade Outer Ply Design Ultimate Strength Properties.

Material Property	Stiffened F39 (T50 Graphite Material)
Longitudinal Ultimate Tensile Strength, ksi	146.0
Transverse Ultimate Tensile Strength, ksi	15.0
Longitudinal Ultimate Compressive Strength, ksi	146.0
Transverse Ultimate Compressive Strength, ksi	21.0
In-Plane Ultimate Shear Strength, ksi	11.8

Table 20. Stiffened F39 Blade Dimensional Inspection Data Results.

Blade Number	Section EE				Section HH				Section NN				
	TM	TL	TU	CH	TM	TL	TU	CH	TM	TL	TU	CH	
4	0.185	0.049	0.028	3.333	0.098	0.027	0.017	3.774	0.048	0.022	0.015	2.653	inst.
5	0.185	0.051	0.026	3.320	0.096	0.029	0.016	3.762	0.046	0.020	0.014	2.678	
6	0.186	0.050	0.026	3.311	0.096	0.027	0.016	3.781	0.046	0.021	0.015	2.660	
7	0.184	0.052	0.025	3.335	0.098	0.027	0.016	3.772	0.046	0.021	0.015	2.685	
9	0.185	0.052	0.027	3.342	0.096	0.027	0.016	3.767	0.045	0.021	0.015	2.636	
10	0.185	0.050	0.025	3.325	0.097	0.028	0.016	3.770	0.046	0.019	0.015	2.658	
11	0.185	0.052	0.025	3.338	0.097	0.028	0.016	3.757	0.047	0.020	0.014	2.676	
12	0.185	0.051	0.026	3.346	0.097	0.027	0.017	3.771	0.047	0.020	0.015	2.654	inst.
13	0.186	0.050	0.025	3.340	0.097	0.027	0.017	3.779	0.047	0.021	0.015	2.677	
14	0.186	0.052	0.026	3.320	0.096	0.027	0.016	3.780	0.046	0.021	0.015	2.640	inst.
15	0.186	0.056	0.026	3.315	0.096	0.031	0.016	3.751	0.046	0.020	0.015	2.644	
16	0.185	0.048	0.025	3.340	0.097	0.027	0.016	3.770	0.046	0.020	0.015	2.641	inst.
16	0.186	0.052	0.026	3.328	0.096	0.028	0.016	3.775	0.046	0.020	0.014	2.652	
17	0.185	0.053	0.026	3.340	0.096	0.030	0.016	3.775	0.046	0.021	0.015	2.688	
20	0.184	0.054	0.025	3.320	0.097	0.029	0.015	3.765	0.046	0.021	0.015	2.653	
Min.	0.184	0.048	0.025	3.311	0.096	0.027	0.015	3.751	0.045	0.019	0.014	2.636	
Max.	0.186	0.056	0.028	3.346	0.098	0.031	0.017	3.781	0.048	0.022	0.015	2.688	
Ave.	0.18520	0.05147	0.02580	3.33020	0.09667	0.02793	0.01613	3.76993	0.04627	0.02053	0.01480	2.65967	
Var.	0.00000	0.00000	0.00000	0.00011	0.00000	0.00000	0.00000	0.00007	0.00000	0.00000	0.00000	0.00027	
Std. Dev.	0.00065	0.00193	0.00083	0.01068	0.00070	0.00124	0.00050	0.00817	0.00068	0.00072	0.00040	0.01647	
Drawing	0.189	0.054	0.030	3.371	0.100	0.026	0.017	3.773	0.052	0.018	0.015	2.649	
Master	0.189	0.058	0.031	3.379	0.103	0.030	0.019	3.776	0.054	0.021	0.019	2.661	

The stiffened blade set was not strain distribution-checked or vibratory bench-tested prior to shipment. All blades were expedited to NASA upon completion of the fabrication, inspection, and instrumentation process. Immediate shipment was essential to allow more time for data acquisition prior to the wind tunnel being shut down for an extended period.

8.0 Conclusions

8.1 Aerodynamic Design

The analyses conducted show that:

- The 3D Euler analysis of the F39 forward-swept blade indicated reduced shock losses in the tip region relative to the F31 aft-swept blade. An overall aero performance improvement should result.
- No significant aero performance improvement could be achieved with the design of a new aft-swept, A39A aft rotor to replace the existing A31 blade. The 3D analysis showed only very small differences in velocity distributions.
- The forward-swept A39F rotor shows a distinct improvement in airfoil surface velocity distributions relative to the A31 aft-swept blade. These results are similar to those indicated by the F39 forward–swept forward rotor analyses.

8.2 Aeromechanical Design

The analyses conducted show that:

- The F39 forward-swept composite unducted fan blades were designed and analyzed to meet the aeromechanical flutter and divergence requirements. Both the initial IM7 material fan and the 'divergent' AS4 material fan were predicted to be free of classical transonic flutter at the design point. Finite element deflection analysis of both designs indicated that the blades would 'close' or decrease in incidence at speed. This indicated favorable stall flutter characteristics since stall flutter is associated with increased incidence or loading. The decreased incidence prediction also indicated favorable divergence characteristics. In order to quantify the divergence margin of the designs, the frequency decrease of the aeroelastic modes (including the aerodynamic effects) relative to the structural dynamic modes was assessed. The frequency drop of the IM7 design was modest; therefore, it was predicted to be divergence-free.
- To further investigate the divergence issues for forward-swept fans, a 'divergent' version of the F39 fan was designed. This design employed a modified layup and the less stiff AS4 material. The divergent design was intended to provide divergence data for verification of analytical tools and to provide insight into divergence issues for forward-swept blades. A divergence tailored layup was designed using a simplified laminated plate analytical model. The divergent design was predicted to be free of classical unstalled flutter and to exhibit the smallest twist (closing) at the design point. The frequency drop of the AS4 design at the design point was predicted to be 24%, considered significant and likely to exhibit divergence behavior.
- While testing these blades was not included in this contract and did not involve GEAE participation, both the IM7 and 'divergent' AS4 designs exhibited apparent stall flutter when tested at takeoff conditions. Both designs were chord-cropped at the tip in order to achieve target test conditions, with limited success. Low speed acoustic and laser velocimeter data are presented in *References 10* and *11*. Wind tunnel maintenance schedules precluded design point testing in the transonic wind tunnel.

8.3 Mechanical Design

The analyses conducted show that:

- Using conventional analytical codes, the steady-state stress levels, steady-state deflections/ untwists, critical frequencies, and mode shapes for a forward-swept blade are similar to an aft-swept blade. Testing should be done to verify the analytical predictions.

8.4 Acoustic Analysis

The analyses conducted show that:

- Under cruise conditions the Blade Passing Frequency tone noise from the forward-swept F39 and aft-swept F31 blades is virtually identical. Higher harmonics of rotor-alone noise show some increase with forward sweep that has been ascribed to a reduction in sweep in the hub region of the blade, resulting in less phase cancellation effects.
- Under takeoff conditions, the noise generated is dominated by forward/aft rotor interaction effects; specifically those involving the wake/vortex flowfield of the forward rotor. The model used for these predictions was calibrated using aft-swept rotor data; forward-swept blades are outside the limits of current experience, consequently the results predicted for forward sweep are in close agreement with those obtained for aft sweep.
- Reevaluation of the semi-empirical constants used in predicting the wake/vortex flowfield should employ flowfield data and/or results from CFD simulations under appropriate conditions.

9.0 References

1. Smith, L.H., Jr., "Unducted Fan Aerodynamic Design," ASME Journal of Turbomachinery, Volume 109, 1987, pp. 313–324.

2. Theodorsen, T., Theory of Propellers, McGraw-Hill, New York, NY, 1948.

3. Whitfield, C.E., Mani, R., and Gliebe, P.R., "High Speed Turboprop Aeroacoustic Study (Counterrotation)," NASA CR-185241 and CR-185242, July 1990.

4. Whitfield, C.E. and Gliebe, P.R., "Predicted vs Scale Model and Flight Test UDF® Engine Noise," AIAA Paper 90-3936, October 1990.

5. Vaczy, C.M. and McCormick, D.C., "A Study of the Leading Edge Vortex and Tip Vortex on Prop-Fan Blades," ASME Paper 87-GT-234, May 1987.

6. Majjigi, R.K., Uenishi, K., and Gliebe, P.R., "An Investigation of Counterrotating Tip Vortex Interaction," NASA CR-185135, October 1989.

7. Podboy, G.G. and Krupar, M.J., "Laser Velocimeter Measurements of the Flowfield Generated by an Advanced Counterrotating Propeller," AIAA Paper 89-0434, January 1989 (also NASA TM-101437).

8. Hoff, G.E., "Experimental Performance and Acoustic Investigation of Modern, Counterrotating Blade Concepts," prepared under NASA Contract NAS3-24080, January 1990.

9. Weisshaar, T., "Divergence of Forward-Swept Composite Wings," J. Aircraft, Volume 17, No. 6, 1980

10. Woodward, R.P., Hall, D.G., Podboy, G.G., and Jeracki, R.J., "Takeoff/Approach Noise for a Model Counterrotation Propeller with a Forward-Swept Upstream Rotor," AIAA Paper 93-0596, January 1993 (also NASA TM-105979).

11. Podboy, G.G. and Krupar, M.J., "Laser Velocimeter Measurements of the Flowfield Generated by a Forward-Swept Propfan During Flutter," AIAA Paper 93-2919, July 1993 (also NASA TM-106195).

Appendix 1 – Stable F39 Blade Strain Distribution Bench Test Results

APPLIED MECHANICS LAB --STRAIN DIST-- 10-Jan-92 13:28:19
CONFIG: M.V02 DATA FILE: M.C01

MPS F39
SWEPT FAN BLADE
P/N 4013427-205

TIME: 13:26:28 DATE: 10-Jan-92 FREQUENCY: 138.00 HZ

PERCENT RELATIVE STRAIN

GAGE	PCT	ANGL	GAGE	PCT	ANGL	GAGE	PCT	ANGL	GAGE	PCT	ANGL
1	-18	90.0	18	-7	0.0	35	-30	90.0	52	100	90.0
2	-27	90.0	19	-7	0.0	36	-24	90.0	53	91	90.0
3	-22	90.0	20	-8	0.0	37	-17	90.0	54	83	90.0
4	-21	90.0	21	-12	90.0	38	-28	90.0	55	68	90.0
5	-13	90.0	22	-29	90.0	39	-37	90.0	56	70	90.0
6	-3	90.0	23	-42	90.0	40	-7	90.0	57	81	90.0
7	13	90.0	24	-48	90.0	41	-60	90.0	58	86	90.0
8	-11	90.0	25	-34	90.0	42	-19	90.0	59	79	90.0
9	-39	90.0	26	-17	90.0	43	-42	90.0	60	56	90.0
10	-59	90.0	27	-5	90.0	44	-3	90.0	61	37	90.0
11	-63	90.0	28	-8	90.0	45	52	90.0	62	15	90.0
12	-53	90.0	29	-17	90.0	46	16	90.0	63	-7	0.0
13	-42	90.0	30	-29	90.0	47	60	90.0	64	-11	0.0
14	-16	90.0	31	-33	90.0	48	60	90.0	65	-11	0.0
15	-7	90.0	32	-41	90.0	49	75	90.0	66	-6	0.0
16	-5	0.0	33	-37	90.0	50	84	90.0	67	-4	0.0
17	-8	0.0	34	-29	90.0	51	95	90.0	68	5	0.0

APPLIED MECHANICS LAB --STRAIN DIST-- 10-Jan-92 13:41:05
CONFIG: M.V02 DATA FILE: M.C02

MPS F39
SWEPT FAN BLADE
P/N 4013427-205

TIME: 13:39:55 DATE: 10-Jan-92 FREQUENCY: 341.00 HZ

PERCENT RELATIVE STRAIN

GAGE	PCT	ANGL	GAGE	PCT	ANGL	GAGE	PCT	ANGL	GAGE	PCT	ANGL
1	16	90.0	18	-15	0.0	35	35	90.0	52	-20	90.0
2	26	90.0	19	-12	0.0	36	35	90.0	53	-12	90.0
3	23	90.0	20	-12	0.0	37	28	90.0	54	-1	90.0
4	19	90.0	21	-19	90.0	38	33	90.0	55	25	90.0
5	21	90.0	22	-46	90.0	39	29	90.0	56	46	90.0
6	18	90.0	23	-64	90.0	40	2	90.0	57	74	90.0
7	23	90.0	24	-74	90.0	41	42	90.0	58	100	90.0
8	9	90.0	25	-55	90.0	42	-6	90.0	59	98	90.0
9	-18	90.0	26	-35	90.0	43	-54	90.0	60	80	90.0
10	-50	90.0	27	-13	90.0	44	0	90.0	61	58	90.0
11	-70	90.0	28	5	90.0	45	-42	90.0	62	27	90.0
12	-69	90.0	29	10	90.0	46	-5	90.0	63	-1	0.0
13	-59	90.0	30	15	90.0	47	-50	90.0	64	-10	0.0
14	-25	90.0	31	15	90.0	48	-42	90.0	65	-12	0.0
15	-9	90.0	32	19	90.0	49	-41	90.0	66	-5	0.0
16	-6	0.0	33	22	90.0	50	-35	90.0	67	-0	0.0
17	-11	0.0	34	26	90.0	51	-29	90.0	68	4	0.0

APPLIED MECHANICS LAB --STRAIN DIST-- 10-Jan-92 13:58:44
CONFIG: M.V02 DATA FILE: M.C03

MPS F39
SWEPT FAN BLADE
P/N 4013427-205

TIME: 13:58:02 DATE: 10-Jan-92 FREQUENCY: 545.00 HZ

PERCENT RELATIVE STRAIN

GAGE	PCT	ANGL	GAGE	PCT	ANGL	GAGE	PCT	ANGL	GAGE	PCT	ANGL
1	16	90.0	18	37	0.0	35	10	90.0	52	59	90.0
2	21	90.0	19	32	0.0	36	14	90.0	53	82	90.0
3	13	90.0	20	18	0.0	37	14	90.0	54	100	90.0
4	7	90.0	21	29	90.0	38	26	90.0	55	58	90.0
5	-4	90.0	22	62	90.0	39	33	90.0	56	36	90.0
6	-23	90.0	23	78	90.0	40	4	90.0	57	-1	90.0
7	-53	90.0	24	79	90.0	41	47	90.0	58	-59	90.0
8	-69	90.0	25	58	90.0	42	-34	90.0	59	-56	90.0
9	-65	90.0	26	27	90.0	43	14	90.0	60	-66	90.0
10	-32	90.0	27	-1	90.0	44	-7	90.0	61	-55	90.0
11	13	90.0	28	-40	90.0	45	-48	90.0	62	-32	90.0
12	26	90.0	29	-52	90.0	46	-11	90.0	63	-36	0.0
13	30	90.0	30	-53	90.0	47	-44	90.0	64	-14	0.0
14	11	90.0	31	-36	90.0	48	-30	90.0	65	-8	0.0
15	1	90.0	32	-24	90.0	49	-16	90.0	66	-9	0.0
16	18	0.0	33	-7	90.0	50	3	90.0	67	-11	0.0
17	25	0.0	34	3	90.0	51	30	90.0	68	-14	0.0

APPLIED MECHANICS LAB --STRAIN DIST-- 10-Jan-92 14:18:36
CONFIG: M.V02 DATA FILE: M.C04

MPS F39
SWEPT FAN BLADE
P/N 4013427-205

TIME: 14:17:55 DATE: 10-Jan-92 FREQUENCY: 655.00 HZ

PERCENT RELATIVE STRAIN

GAGE	PCT	ANGL	GAGE	PCT	ANGL	GAGE	PCT	ANGL	GAGE	PCT	ANGL
1	24	90.0	18	-4	0.0	35	5	90.0	52	7	90.0
2	39	90.0	19	-5	0.0	36	9	90.0	53	-6	90.0
3	34	90.0	20	-1	0.0	37	12	90.0	54	-25	90.0
4	23	90.0	21	-1	90.0	38	15	90.0	55	-30	90.0
5	35	90.0	22	9	90.0	39	16	90.0	56	-43	90.0
6	41	90.0	23	15	90.0	40	-1	90.0	57	-53	90.0
7	65	90.0	24	18	90.0	41	38	90.0	58	-53	90.0
8	65	90.0	25	10	90.0	42	11	90.0	59	-75	90.0
9	82	90.0	26	10	90.0	43	91	90.0	60	-62	90.0
10	82	90.0	27	11	90.0	44	-35	90.0	61	-51	90.0
11	94	90.0	28	16	90.0	45	-32	90.0	62	-23	90.0
12	100	90.0	29	13	90.0	46	22	90.0	63	31	0.0
13	91	90.0	30	8	90.0	47	-23	90.0	64	27	0.0
14	47	90.0	31	-0	90.0	48	-7	90.0	65	27	0.0
15	19	90.0	32	-2	90.0	49	6	90.0	66	18	0.0
16	-1	0.0	33	-2	90.0	50	15	90.0	67	9	0.0
17	-1	0.0	34	-0	90.0	51	17	90.0	68	2	0.0

APPLIED MECHANICS LAB --STRAIN DIST-- 10-Jan-92 14:22:25
CONFIG: M.V02 DATA FILE: M.C05

MPS F39
SWEPT FAN BLADE
P/N 4013427-205

TIME: 14:21:32 DATE: 10-Jan-92 FREQUENCY: 834.00 HZ

PERCENT RELATIVE STRAIN

GAGE	PCT	ANGL	GAGE	PCT	ANGL	GAGE	PCT	ANGL	GAGE	PCT	ANGL
1	11	90.0	18	7	0.0	35	51	90.0	52	27	90.0
2	19	90.0	19	3	0.0	36	56	90.0	53	25	90.0
3	17	90.0	20	6	0.0	37	47	90.0	54	20	90.0
4	11	90.0	21	12	90.0	38	47	90.0	55	10	90.0
5	14	90.0	22	34	90.0	39	25	90.0	56	-3	90.0
6	14	90.0	23	42	90.0	40	-0	90.0	57	-24	90.0
7	26	90.0	24	43	90.0	41	21	90.0	58	-43	90.0
8	25	90.0	25	29	90.0	42	-1	90.0	59	-72	90.0
9	41	90.0	26	19	90.0	43	88	90.0	60	-74	90.0
10	54	90.0	27	15	90.0	44	10	90.0	61	-67	90.0
11	82	90.0	28	8	90.0	45	-35	90.0	62	-33	90.0
12	100	90.0	29	-1	90.0	46	1	90.0	63	20	0.0
13	98	90.0	30	-1	90.0	47	-43	90.0	64	25	0.0
14	52	90.0	31	-1	90.0	48	-28	90.0	65	26	0.0
15	21	90.0	32	5	90.0	49	-13	90.0	66	16	0.0
16	3	0.0	33	17	90.0	50	3	90.0	67	5	0.0
17	8	0.0	34	30	90.0	51	20	90.0	68	1	0.0

APPLIED MECHANICS LAB --STRAIN DIST-- 10-Jan-92 14:27:30
CONFIG: M.V02 DATA FILE: M.C06

MPS F39
SWEPT FAN BLADE
P/N 4013427-205

TIME: 14:26:46 DATE: 10-Jan-92 FREQUENCY: 986.00 HZ

PERCENT RELATIVE STRAIN

GAGE	PCT	ANGL	GAGE	PCT	ANGL	GAGE	PCT	ANGL	GAGE	PCT	ANGL
1	-2	90.0	18	67	0.0	35	42	90.0	52	-66	90.0
2	6	90.0	19	55	0.0	36	35	90.0	53	-67	90.0
3	13	90.0	20	33	0.0	37	22	90.0	54	-44	90.0
4	17	90.0	21	46	90.0	38	9	90.0	55	18	90.0
5	39	90.0	22	69	90.0	39	-15	90.0	56	46	90.0
6	55	90.0	23	56	90.0	40	-4	90.0	57	53	90.0
7	76	90.0	24	24	90.0	41	-19	90.0	58	20	90.0
8	69	90.0	25	-10	90.0	42	-12	90.0	59	-17	90.0
9	59	90.0	26	-32	90.0	43	73	90.0	60	-52	90.0
10	50	90.0	27	-25	90.0	44	9	90.0	61	-69	90.0
11	80	90.0	28	1	90.0	45	19	90.0	62	-48	90.0
12	98	90.0	29	28	90.0	46	19	90.0	63	-59	0.0
13	100	90.0	30	54	90.0	47	6	90.0	64	-27	0.0
14	48	90.0	31	53	90.0	48	-4	90.0	65	-18	0.0
15	16	90.0	32	55	90.0	49	-15	90.0	66	-17	0.0
16	34	0.0	33	46	90.0	50	-31	90.0	67	-21	0.0
17	49	0.0	34	36	90.0	51	-51	90.0	68	-26	0.0

APPLIED MECHANICS LAB --STRAIN DIST-- 10-Jan-92 14:37:16
CONFIG: M.V02 DATA FILE: M.C07

MPS F39
SWEPT FAN BLADE
P/N 4013427-205

TIME: 14:36:32 DATE: 10-Jan-92 FREQUENCY: 1333.00 HZ

PERCENT RELATIVE STRAIN

GAGE	PCT	ANGL	GAGE	PCT	ANGL	GAGE	PCT	ANGL	GAGE	PCT	ANGL
1	-2	90.0	18	22	0.0	35	-22	90.0	52	1	90.0
2	-5	90.0	19	15	0.0	36	-23	90.0	53	-1	90.0
3	-5	90.0	20	9	0.0	37	-19	90.0	54	4	90.0
4	-4	90.0	21	14	90.0	38	-15	90.0	55	14	90.0
5	-7	90.0	22	29	90.0	39	-2	90.0	56	20	90.0
6	-5	90.0	23	22	90.0	40	-1	90.0	57	21	90.0
7	1	90.0	24	8	90.0	41	0	90.0	58	9	90.0
8	-1	90.0	25	-4	90.0	42	-5	90.0	59	-17	90.0
9	2	90.0	26	-9	90.0	43	73	90.0	60	-43	90.0
10	10	90.0	27	-7	90.0	44	-0	90.0	61	-59	90.0
11	44	90.0	28	-0	90.0	45	5	90.0	62	-38	90.0
12	80	90.0	29	-1	90.0	46	-3	90.0	63	0	0.0
13	100	90.0	30	-1	90.0	47	9	90.0	64	9	0.0
14	61	90.0	31	-1	90.0	48	4	90.0	65	13	0.0
15	25	90.0	32	-3	90.0	49	-1	90.0	66	7	0.0
16	12	0.0	33	-10	90.0	50	-0	90.0	67	1	0.0
17	21	0.0	34	-14	90.0	51	-2	90.0	68	-6	0.0

APPLIED MECHANICS LAB --STRAIN DIST-- 10-Jan-92 14:40:51
CONFIG: M.V02 DATA FILE: M.C08

MPS F39
SWEPT FAN BLADE
P/N 4013427-205

TIME: 14:40:09 DATE: 10-Jan-92 FREQUENCY: 1488.00 HZ

PERCENT RELATIVE STRAIN

GAGE	PCT	ANGL	GAGE	PCT	ANGL	GAGE	PCT	ANGL	GAGE	PCT	ANGL
1	-6	90.0	18	-89	0.0	35	61	90.0	52	-51	90.0
2	5	90.0	19	-73	0.0	36	34	90.0	53	-3	90.0
3	17	90.0	20	-44	0.0	37	12	90.0	54	62	90.0
4	30	90.0	21	-42	90.0	38	-15	90.0	55	72	90.0
5	50	90.0	22	-0	90.0	39	-34	90.0	56	42	90.0
6	43	90.0	23	60	90.0	40	-5	90.0	57	-15	90.0
7	8	90.0	24	100	90.0	41	-24	90.0	58	-74	90.0
8	-34	90.0	25	92	90.0	42	-49	90.0	59	-98	90.0
9	-68	90.0	26	56	90.0	43	-35	90.0	60	-71	90.0
10	-71	90.0	27	11	90.0	44	14	90.0	61	-35	90.0
11	-66	90.0	28	-37	90.0	45	44	90.0	62	-4	90.0
12	-59	90.0	29	-40	90.0	46	22	90.0	63	99	0.0
13	-50	90.0	30	3	90.0	47	17	90.0	64	74	0.0
14	-19	90.0	31	40	90.0	48	-13	90.0	65	69	0.0
15	4	90.0	32	78	90.0	49	-46	90.0	66	56	0.0
16	-45	0.0	33	88	90.0	50	-69	90.0	67	43	0.0
17	-63	0.0	34	70	90.0	51	-74	90.0	68	36	0.0

APPLIED MECHANICS LAB --STRAIN DIST-- 10-Jan-92 14:53:23
CONFIG: M.V02 DATA FILE: M.C09

MPS F39
SWEPT FAN BLADE
P/N 4013427-205

TIME: 14:52:39 DATE: 10-Jan-92 FREQUENCY: 1926.00 HZ

PERCENT RELATIVE STRAIN

GAGE	PCT	ANGL	GAGE	PCT	ANGL	GAGE	PCT	ANGL	GAGE	PCT	ANGL
1	0	90.0	18	54	0.0	35	33	90.0	52	9	90.0
2	4	90.0	19	38	0.0	36	23	90.0	53	21	90.0
3	7	90.0	20	22	0.0	37	13	90.0	54	13	90.0
4	9	90.0	21	20	90.0	38	2	90.0	55	-17	90.0
5	8	90.0	22	-4	90.0	39	-6	90.0	56	-21	90.0
6	-3	90.0	23	-42	90.0	40	0	90.0	57	-4	90.0
7	-25	90.0	24	-53	90.0	41	-1	90.0	58	27	90.0
8	-34	90.0	25	-33	90.0	42	20	90.0	59	35	90.0
9	-34	90.0	26	-0	90.0	43	54	90.0	60	17	90.0
10	-22	90.0	27	14	90.0	44	3	90.0	61	-14	90.0
11	7	90.0	28	10	90.0	45	8	90.0	62	-24	90.0
12	58	90.0	29	-8	90.0	46	7	90.0	63	-37	0.0
13	100	90.0	30	-24	90.0	47	0	90.0	64	-24	0.0
14	72	90.0	31	-19	90.0	48	-7	90.0	65	-21	0.0
15	30	90.0	32	-1	90.0	49	-12	90.0	66	-18	0.0
16	30	0.0	33	18	90.0	50	-10	90.0	67	-19	0.0
17	44	0.0	34	30	90.0	51	-1	90.0	68	-21	0.0

APPLIED MECHANICS LAB --STRAIN DIST-- 10-Jan-92 14:57:17
CONFIG: M.V02 DATA FILE: M.C10

MPS F39
SWEPT FAN BLADE
P/N 4013427-205

TIME: 14:56:33 DATE: 10-Jan-92 FREQUENCY: 2134.00 HZ

PERCENT RELATIVE STRAIN

GAGE	PCT	ANGL	GAGE	PCT	ANGL	GAGE	PCT	ANGL	GAGE	PCT	ANGL
1	-2	90.0	18	40	0.0	35	17	90.0	52	11	90.0
2	2	90.0	19	32	0.0	36	-5	90.0	53	36	90.0
3	8	90.0	20	27	0.0	37	-15	90.0	54	50	90.0
4	13	90.0	21	8	90.0	38	-21	90.0	55	12	90.0
5	17	90.0	22	-52	90.0	39	-12	90.0	56	-34	90.0
6	11	90.0	23	-74	90.0	40	-2	90.0	57	-59	90.0
7	16	90.0	24	-37	90.0	41	-1	90.0	58	-36	90.0
8	14	90.0	25	11	90.0	42	-5	90.0	59	7	90.0
9	42	90.0	26	45	90.0	43	-16	90.0	60	66	90.0
10	67	90.0	27	42	90.0	44	5	90.0	61	100	90.0
11	56	90.0	28	3	90.0	45	16	90.0	62	69	90.0
12	3	90.0	29	-31	90.0	46	1	90.0	63	-49	0.0
13	-67	90.0	30	-21	90.0	47	3	90.0	64	-64	0.0
14	-77	90.0	31	11	90.0	48	-15	90.0	65	-78	0.0
15	-42	90.0	32	45	90.0	49	-36	90.0	66	-62	0.0
16	11	0.0	33	60	90.0	50	-37	90.0	67	-37	0.0
17	20	0.0	34	39	90.0	51	-18	90.0	68	-16	0.0

APPLIED MECHANICS LAB --STRAIN DIST-- 13-Jan-92 08:11:08
CONFIG: M.V02 DATA FILE: M.C11

MPS F39
SWEPT FAN BLADE
P/N 4013427-205

TIME: 08:10:16 DATE: 13-Jan-92 FREQUENCY: 2522.00 HZ

PERCENT RELATIVE STRAIN

GAGE	PCT	ANGL	GAGE	PCT	ANGL	GAGE	PCT	ANGL	GAGE	PCT	ANGL
1	-1	90.0	18	92	0.0	35	-46	90.0	52	-35	90.0
2	-6	90.0	19	59	0.0	36	-27	90.0	53	-28	90.0
3	-9	90.0	20	36	0.0	37	-8	90.0	54	14	90.0
4	-10	90.0	21	14	90.0	38	1	90.0	55	23	90.0
5	0	90.0	22	-52	90.0	39	7	90.0	56	-8	90.0
6	17	90.0	23	-81	90.0	40	-2	90.0	57	-40	90.0
7	19	90.0	24	-20	90.0	41	-2	90.0	58	-21	90.0
8	0	90.0	25	52	90.0	42	-35	90.0	59	16	90.0
9	-31	90.0	26	81	90.0	43	28	90.0	60	46	90.0
10	-51	90.0	27	43	90.0	44	-4	90.0	61	28	90.0
11	-41	90.0	28	-25	90.0	45	-10	90.0	62	-2	90.0
12	20	90.0	29	-37	90.0	46	-2	90.0	63	-52	0.0
13	100	90.0	30	18	90.0	47	3	90.0	64	-54	0.0
14	96	90.0	31	59	90.0	48	18	90.0	65	-64	0.0
15	41	90.0	32	54	90.0	49	23	90.0	66	-53	0.0
16	52	0.0	33	5	90.0	50	9	90.0	67	-43	0.0
17	74	0.0	34	-36	90.0	51	-13	90.0	68	-37	0.0

APPLIED MECHANICS LAB --STRAIN DIST-- 13-Jan-92 09:23:03
CONFIG: M.V02 DATA FILE: M.C12

MPS F39
SWEPT FAN BLADE
P/N 4013427-205

TIME: 09:22:15 DATE: 13-Jan-92 FREQUENCY: 2867.00 HZ

PERCENT RELATIVE STRAIN

GAGE	PCT	ANGL	GAGE	PCT	ANGL	GAGE	PCT	ANGL	GAGE	PCT	ANGL
1	-1	90.0	18	-25	0.0	35	50	90.0	52	-4	90.0
2	-2	90.0	19	-14	0.0	36	6	90.0	53	-6	90.0
3	1	90.0	20	-13	0.0	37	-7	90.0	54	-13	90.0
4	1	90.0	21	-0	90.0	38	-15	90.0	55	-29	90.0
5	1	90.0	22	28	90.0	39	-1	90.0	56	-27	90.0
6	11	90.0	23	19	90.0	40	-1	90.0	57	-5	90.0
7	29	90.0	24	-10	90.0	41	1	90.0	58	14	90.0
8	30	90.0	25	-12	90.0	42	23	90.0	59	19	90.0
9	17	90.0	26	10	90.0	43	-13	90.0	60	-5	90.0
10	-9	90.0	27	43	90.0	44	-1	90.0	61	-36	90.0
11	-34	90.0	28	49	90.0	45	1	90.0	62	-38	90.0
12	-21	90.0	29	16	90.0	46	-8	90.0	63	7	0.0
13	19	90.0	30	21	90.0	47	5	90.0	64	25	0.0
14	43	90.0	31	32	90.0	48	1	90.0	65	41	0.0
15	27	90.0	32	74	90.0	49	-6	90.0	66	36	0.0
16	-4	0.0	33	100	90.0	50	-7	90.0	67	21	0.0
17	-11	0.0	34	81	90.0	51	-3	90.0	68	8	0.0

APPLIED MECHANICS LAB --STRAIN DIST-- 13-Jan-92 09:29:30
CONFIG: M.V02 DATA FILE: M.C13

MPS F39
SWEPT FAN BLADE
P/N 4013427-205

TIME: 09:28:36 DATE: 13-Jan-92 FREQUENCY: 2967.00 HZ

PERCENT RELATIVE STRAIN

GAGE	PCT	ANGL	GAGE	PCT	ANGL	GAGE	PCT	ANGL	GAGE	PCT	ANGL
1	1	90.0	18	60	0.0	35	30	90.0	52	-2	90.0
2	-1	90.0	19	35	0.0	36	23	90.0	53	-23	90.0
3	-1	90.0	20	29	0.0	37	10	90.0	54	-26	90.0
4	2	90.0	21	5	90.0	38	0	90.0	55	14	90.0
5	-7	90.0	22	-30	90.0	39	-0	90.0	56	16	90.0
6	-14	90.0	23	-3	90.0	40	-2	90.0	57	-12	90.0
7	-6	90.0	24	77	90.0	41	1	90.0	58	-38	90.0
8	6	90.0	25	100	90.0	42	-25	90.0	59	-28	90.0
9	19	90.0	26	57	90.0	43	25	90.0	60	12	90.0
10	22	90.0	27	6	90.0	44	2	90.0	61	47	90.0
11	37	90.0	28	-8	90.0	45	1	90.0	62	42	90.0
12	35	90.0	29	40	90.0	46	1	90.0	63	-14	0.0
13	14	90.0	30	68	90.0	47	1	90.0	64	-41	0.0
14	-7	90.0	31	22	90.0	48	-1	90.0	65	-67	0.0
15	-11	90.0	32	-24	90.0	49	-1	90.0	66	-61	0.0
16	22	0.0	33	-32	90.0	50	5	90.0	67	-41	0.0
17	39	0.0	34	14	90.0	51	6	90.0	68	-22	0.0

APPLIED MECHANICS LAB --STRAIN DIST-- 13-Jan-92 09:35:01
CONFIG: M.V02 DATA FILE: M.C14

MPS F39
SWEPT FAN BLADE
P/N 4013427-205

TIME: 09:34:14 DATE: 13-Jan-92 FREQUENCY: 3111.00 HZ

PERCENT RELATIVE STRAIN

GAGE	PCT	ANGL	GAGE	PCT	ANGL	GAGE	PCT	ANGL	GAGE	PCT	ANGL
1	4	90.0	18	44	0.0	35	-10	90.0	52	25	90.0
2	10	90.0	19	26	0.0	36	1	90.0	53	5	90.0
3	10	90.0	20	13	0.0	37	1	90.0	54	-13	90.0
4	6	90.0	21	6	90.0	38	2	90.0	55	-2	90.0
5	-1	90.0	22	-10	90.0	39	2	90.0	56	-7	90.0
6	-4	90.0	23	-2	90.0	40	-2	90.0	57	-20	90.0
7	0	90.0	24	29	90.0	41	11	90.0	58	-20	90.0
8	12	90.0	25	41	90.0	42	-16	90.0	59	3	90.0
9	9	90.0	26	12	90.0	43	-22	90.0	60	18	90.0
10	-23	90.0	27	-17	90.0	44	1	90.0	61	1	90.0
11	-64	90.0	28	-14	90.0	45	-1	90.0	62	-22	90.0
12	-36	90.0	29	17	90.0	46	1	90.0	63	-15	0.0
13	54	90.0	30	12	90.0	47	-12	90.0	64	-14	0.0
14	100	90.0	31	-14	90.0	48	-17	90.0	65	-16	0.0
15	56	90.0	32	-49	90.0	49	-13	90.0	66	-14	0.0
16	33	0.0	33	-48	90.0	50	-1	90.0	67	-17	0.0
17	44	0.0	34	-26	90.0	51	19	90.0	68	-19	0.0

APPLIED MECHANICS LAB --STRAIN DIST-- 13-Jan-92 09:51:16
CONFIG: M.V02 DATA FILE: M.C15

MPS F39
SWEPT FAN BLADE
P/N 4013427-205

TIME: 09:50:27 DATE: 13-Jan-92 FREQUENCY: 3270.00 HZ

PERCENT RELATIVE STRAIN

GAGE	PCT	ANGL	GAGE	PCT	ANGL	GAGE	PCT	ANGL	GAGE	PCT	ANGL
1	2	90.0	18	-84	0.0	35	-58	90.0	52	-10	90.0
2	3	90.0	19	-43	0.0	36	-17	90.0	53	-2	90.0
3	3	90.0	20	-17	0.0	37	1	90.0	54	16	90.0
4	4	90.0	21	17	90.0	38	8	90.0	55	-12	90.0
5	2	90.0	22	78	90.0	39	-1	90.0	56	-42	90.0
6	-6	90.0	23	47	90.0	40	1	90.0	57	-29	90.0
7	-23	90.0	24	-14	90.0	41	4	90.0	58	8	90.0
8	-29	90.0	25	15	90.0	42	-4	90.0	59	3	90.0
9	12	90.0	26	63	90.0	43	26	90.0	60	-30	90.0
10	35	90.0	27	100	90.0	44	-0	90.0	61	-41	90.0
11	81	90.0	28	45	90.0	45	1	90.0	62	-18	90.0
12	48	90.0	29	-24	90.0	46	4	90.0	63	24	0.0
13	-43	90.0	30	16	90.0	47	-5	90.0	64	47	0.0
14	-91	90.0	31	61	90.0	48	5	90.0	65	68	0.0
15	-45	90.0	32	58	90.0	49	5	90.0	66	62	0.0
16	-57	0.0	33	-10	90.0	50	-0	90.0	67	52	0.0
17	-77	0.0	34	-63	90.0	51	-9	90.0	68	42	0.0

APPLIED MECHANICS LAB --STRAIN DIST-- 13-Jan-92 09:55:59
CONFIG: M.V02 DATA FILE: M.C16

MPS F39
SWEPT FAN BLADE
P/N 4013427-205

TIME: 09:55:15 DATE: 13-Jan-92 FREQUENCY: 3489.00 HZ

PERCENT RELATIVE STRAIN

GAGE	PCT	ANGL	GAGE	PCT	ANGL	GAGE	PCT	ANGL	GAGE	PCT	ANGL
1	-2	90.0	18	98	0.0	35	4	90.0	52	2	90.0
2	-5	90.0	19	49	0.0	36	-18	90.0	53	21	90.0
3	-2	90.0	20	39	0.0	37	-14	90.0	54	-0	90.0
4	0	90.0	21	8	90.0	38	-7	90.0	55	-4	90.0
5	17	90.0	22	-1	90.0	39	0	90.0	56	13	90.0
6	21	90.0	23	54	90.0	40	1	90.0	57	7	90.0
7	-0	90.0	24	100	90.0	41	-12	90.0	58	-31	90.0
8	-18	90.0	25	27	90.0	42	20	90.0	59	-46	90.0
9	-20	90.0	26	-59	90.0	43	22	90.0	60	-11	90.0
10	-11	90.0	27	-59	90.0	44	1	90.0	61	30	90.0
11	12	90.0	28	31	90.0	45	-0	90.0	62	41	90.0
12	30	90.0	29	45	90.0	46	-1	90.0	63	4	0.0
13	40	90.0	30	-29	90.0	47	11	90.0	64	-39	0.0
14	22	90.0	31	-51	90.0	48	8	90.0	65	-88	0.0
15	2	90.0	32	13	90.0	49	-0	90.0	66	-87	0.0
16	38	0.0	33	78	90.0	50	-16	90.0	67	-63	0.0
17	69	0.0	34	54	90.0	51	-16	90.0	68	-34	0.0

APPLIED MECHANICS LAB --STRAIN DIST-- 13-Jan-92 10:00:32
CONFIG: M.V02 DATA FILE: M.C17

MPS F39
SWEPT FAN BLADE
P/N 4013427-205

TIME: 09:59:48 DATE: 13-Jan-92 FREQUENCY: 3782.00 HZ

PERCENT RELATIVE STRAIN

GAGE	PCT	ANGL	GAGE	PCT	ANGL	GAGE	PCT	ANGL	GAGE	PCT	ANGL
1	3	90.0	18	65	0.0	35	-73	90.0	52	7	90.0
2	7	90.0	19	16	0.0	36	-35	90.0	53	5	90.0
3	3	90.0	20	-6	0.0	37	-3	90.0	54	-21	90.0
4	2	90.0	21	-54	90.0	38	10	90.0	55	-53	90.0
5	-4	90.0	22	-71	90.0	39	3	90.0	56	-9	90.0
6	-16	90.0	23	43	90.0	40	-1	90.0	57	32	90.0
7	-17	90.0	24	75	90.0	41	12	90.0	58	15	90.0
8	-8	90.0	25	-18	90.0	42	54	90.0	59	-7	90.0
9	-2	90.0	26	-79	90.0	43	36	90.0	60	10	90.0
10	1	90.0	27	-2	90.0	44	-0	90.0	61	66	90.0
11	10	90.0	28	88	90.0	45	-4	90.0	62	76	90.0
12	32	90.0	29	21	90.0	46	1	90.0	63	15	0.0
13	10	90.0	30	-33	90.0	47	-11	90.0	64	-36	0.0
14	-21	90.0	31	13	90.0	48	-1	90.0	65	-82	0.0
15	-31	90.0	32	100	90.0	49	4	90.0	66	-86	0.0
16	44	0.0	33	76	90.0	50	9	90.0	67	-67	0.0
17	62	0.0	34	-29	90.0	51	10	90.0	68	-45	0.0

APPLIED MECHANICS LAB --STRAIN DIST-- 13-Jan-92 10:04:35
CONFIG: M.V02 DATA FILE: M.C18

MPS F39
SWEPT FAN BLADE
P/N 4013427-205

TIME: 10:03:30 DATE: 13-Jan-92 FREQUENCY: 3965.00 HZ

PERCENT RELATIVE STRAIN

GAGE	PCT	ANGL	GAGE	PCT	ANGL	GAGE	PCT	ANGL	GAGE	PCT	ANGL
1	-5	90.0	18	40	0.0	35	-14	90.0	52	-5	90.0
2	-5	90.0	19	17	0.0	36	-1	90.0	53	7	90.0
3	-3	90.0	20	5	0.0	37	2	90.0	54	15	90.0
4	1	90.0	21	-5	90.0	38	0	90.0	55	4	90.0
5	-5	90.0	22	-18	90.0	39	-1	90.0	56	2	90.0
6	-18	90.0	23	13	90.0	40	1	90.0	57	1	90.0
7	-19	90.0	24	23	90.0	41	-7	90.0	58	-10	90.0
8	2	90.0	25	-10	90.0	42	11	90.0	59	-6	90.0
9	36	90.0	26	-30	90.0	43	-76	90.0	60	17	90.0
10	37	90.0	27	-1	90.0	44	-1	90.0	61	21	90.0
11	-40	90.0	28	27	90.0	45	2	90.0	62	-7	90.0
12	-92	90.0	29	-2	90.0	46	-0	90.0	63	-8	0.0
13	-12	90.0	30	-20	90.0	47	7	90.0	64	-12	0.0
14	100	90.0	31	2	90.0	48	8	90.0	65	-18	0.0
15	71	90.0	32	30	90.0	49	4	90.0	66	-18	0.0
16	43	0.0	33	8	90.0	50	-3	90.0	67	-23	0.0
17	51	0.0	34	-16	90.0	51	-12	90.0	68	-25	0.0

APPLIED MECHANICS LAB --STRAIN DIST-- 13-Jan-92 10:10:33
CONFIG: M.V02 DATA FILE: M.C19

MPS F39
SWEPT FAN BLADE
P/N 4013427-205

TIME: 10:09:23 DATE: 13-Jan-92 FREQUENCY: 4345.00 HZ

PERCENT RELATIVE STRAIN

GAGE	PCT	ANGL	GAGE	PCT	ANGL	GAGE	PCT	ANGL	GAGE	PCT	ANGL
1	0	90.0	18	-64	0.0	35	-49	90.0	52	-1	90.0
2	1	90.0	19	-10	0.0	36	-37	90.0	53	-1	90.0
3	-1	90.0	20	9	0.0	37	-9	90.0	54	-17	90.0
4	-0	90.0	21	35	90.0	38	2	90.0	55	6	90.0
5	-7	90.0	22	-1	90.0	39	3	90.0	56	24	90.0
6	-6	90.0	23	-74	90.0	40	-1	90.0	57	-1	90.0
7	5	90.0	24	-5	90.0	41	6	90.0	58	-9	90.0
8	14	90.0	25	73	90.0	42	0	90.0	59	3	90.0
9	15	90.0	26	19	90.0	43	-3	90.0	60	0	90.0
10	10	90.0	27	-68	90.0	44	-5	90.0	61	-32	90.0
11	9	90.0	28	-17	90.0	45	-3	90.0	62	-47	90.0
12	0	90.0	29	65	90.0	46	-1	90.0	63	-32	0.0
13	-14	90.0	30	6	90.0	47	-2	90.0	64	11	0.0
14	-17	90.0	31	-43	90.0	48	3	90.0	65	58	0.0
15	-0	90.0	32	34	90.0	49	10	90.0	66	71	0.0
16	-48	0.0	33	100	90.0	50	4	90.0	67	63	0.0
17	-67	0.0	34	25	90.0	51	1	90.0	68	44	0.0

APPLIED MECHANICS LAB --STRAIN DIST-- 13-Jan-92 10:18:39
CONFIG: M.V02 DATA FILE: M.C20

MPS F39
SWEPT FAN BLADE
P/N 4013427-205

TIME: 10:16:58 DATE: 13-Jan-92 FREQUENCY: 4508.00 HZ

PERCENT RELATIVE STRAIN

GAGE	PCT	ANGL	GAGE	PCT	ANGL	GAGE	PCT	ANGL	GAGE	PCT	ANGL
1	-7	90.0	18	100	0.0	35	31	90.0	52	21	90.0
2	-4	90.0	19	28	0.0	36	-6	90.0	53	0	90.0
3	0	90.0	20	3	0.0	37	-8	90.0	54	-14	90.0
4	5	90.0	21	-9	90.0	38	-2	90.0	55	-10	90.0
5	2	90.0	22	49	90.0	39	-4	90.0	56	-14	90.0
6	-23	90.0	23	43	90.0	40	0	90.0	57	9	90.0
7	-34	90.0	24	-36	90.0	41	-10	90.0	58	39	90.0
8	-11	90.0	25	-29	90.0	42	-5	90.0	59	20	90.0
9	9	90.0	26	59	90.0	43	-20	90.0	60	-17	90.0
10	14	90.0	27	67	90.0	44	9	90.0	61	-26	90.0
11	-9	90.0	28	-28	90.0	45	6	90.0	62	8	90.0
12	-21	90.0	29	-13	90.0	46	2	90.0	63	49	0.0
13	7	90.0	30	63	90.0	47	5	90.0	64	-5	0.0
14	36	90.0	31	16	90.0	48	-0	90.0	65	-72	0.0
15	21	90.0	32	-47	90.0	49	-11	90.0	66	-84	0.0
16	41	0.0	33	18	90.0	50	-6	90.0	67	-66	0.0
17	86	0.0	34	62	90.0	51	10	90.0	68	-36	0.0

Appendix 2 – Stable F39 Blade Bench Test Vibratory Mode Shapes

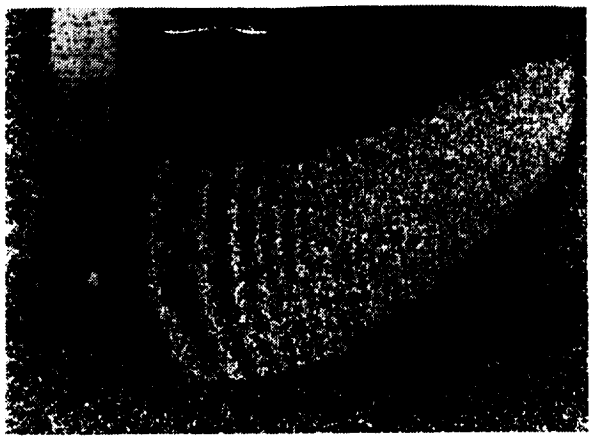

Frequency 00132 Hz

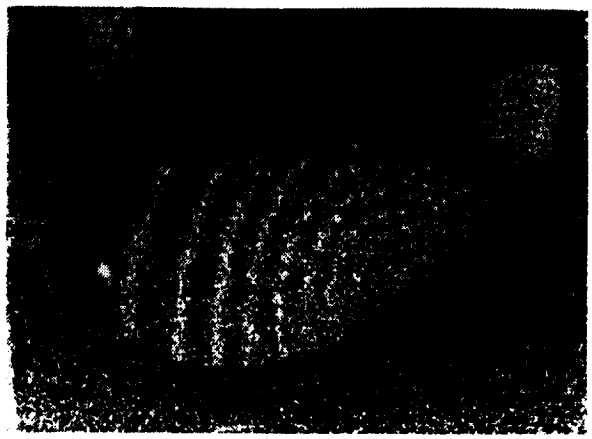

Frequency 00329 Hz

Frequency 00516 Hz

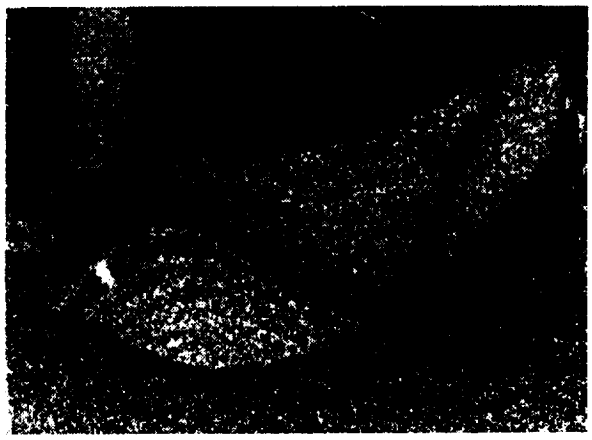

Frequency 00627 Hz

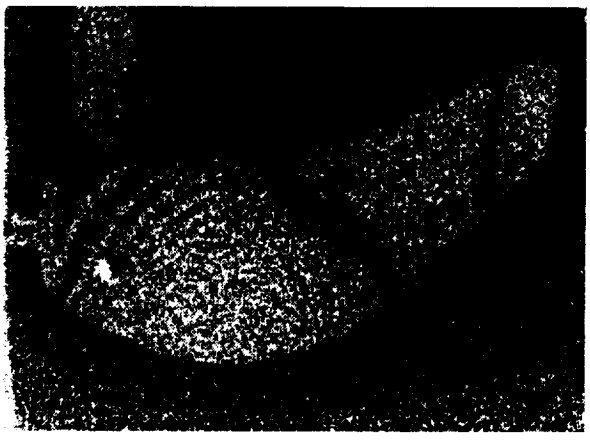

Frequency 00808 Hz

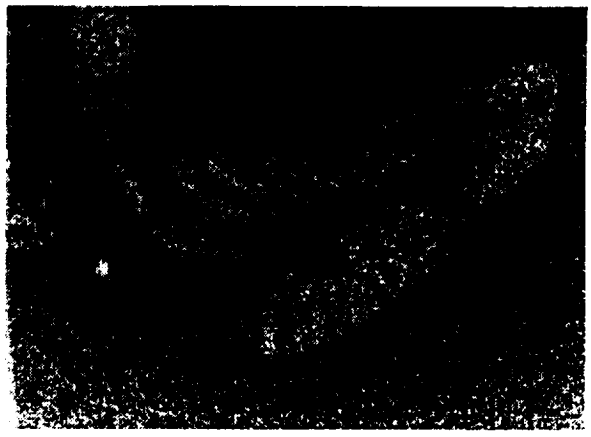

Frequency 00941 Hz

MPS Forward-Swept Fan Blade P/N 4013427-205

Frequency 01295 Hz

Frequency 01432 Hz

Frequency 01847 Hz

Frequency 02056 Hz

Frequency 02412 Hz

Frequency 02748 Hz

MPS Forward-Swept Fan Blade P/N 4013427-205

Frequency 02824 Hz

Frequency 03007 Hz

Frequency 03107 Hz

Frequency 03331 Hz

Frequency 03600 Hz

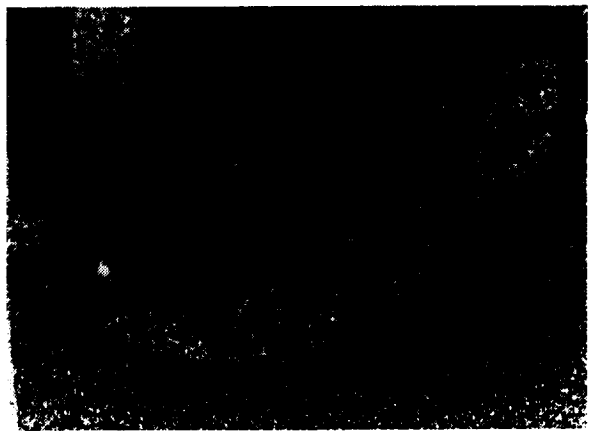

Frequency 03763 Hz

MPS Forward-Swept Fan Blade P/N 4013427-205

Frequency 03835 Hz

Frequency 04125 Hz

Frequency 04274 Hz

MPS Forward-Swept Fan Blade P/N 4013427-205

Appendix 3 – Divergent F39 Blade Strain Distribution Bench Test Results

APPLIED MECHANICS LAB --STRAIN DIST-- 08-May-92 08:19:33
CONFIG: P.V02 DATA FILE: P.C01

MPS F39
FORWARD SWEPT FAN BLADE
P/N 4013427-460

TIME: 08:17:21 DATE: 08-May-92 FREQUENCY: 97.00 HZ

PERCENT RELATIVE STRAIN

GAGE	PCT	ANGL	GAGE	PCT	ANGL	GAGE	PCT	ANGL	GAGE	PCT	ANGL
1	-1	90.0	19	-1	0.0	37	1	90.0	54	27	90.0
2	2	90.0	20	1	0.0	38	2	90.0	55	22	90.0
3	9	90.0	21	1	0.0	39	0	90.0	56	32	90.0
4	14	90.0	22	-6	90.0	40	-4	90.0	57	49	90.0
5	22	90.0	23	-24	90.0	41	-6	90.0	58	70	90.0
6	32	90.0	24	-45	90.0	42	-21	90.0	59	100	90.0
7	35	90.0	25	-52	90.0	43	-16	90.0	60	100	90.0
8	9	90.0	26	-53	90.0	44	-2	90.0	61	85	90.0
9	-32	90.0	27	-35	90.0	45	-42	90.0	62	52	90.0
10	-66	90.0	28	-0	90.0	46	2	90.0	63	36	90.0
11	-74	90.0	29	25	90.0	47	7	90.0	64	14	90.0
12	-52	90.0	30	11	90.0	48	15	90.0	65	-8	0.0
13	-38	90.0	31	24	90.0	49	9	90.0	66	-11	0.0
14	-14	90.0	32	-3	90.0	50	10	90.0	67	-10	0.0
15	-2	90.0	33	5	90.0	51	16	90.0	68	-4	0.0
16	-1	0.0	34	-1	90.0	52	20	90.0	69	0	0.0
17	0	0.0	35	1	90.0	53	25	90.0	70	0	0.0
18	-0	0.0	36	0	90.0						

APPLIED MECHANICS LAB --STRAIN DIST-- 08-May-92 08:47:32
CONFIG: P.V02 DATA FILE: P.C02

MPS F39
FORWARD SWEPT FAN BLADE
P/N 4013427-460

TIME: 08:46:17 DATE: 08-May-92 FREQUENCY: 253.00 HZ

PERCENT RELATIVE STRAIN

GAGE	PCT	ANGL	GAGE	PCT	ANGL	GAGE	PCT	ANGL	GAGE	PCT	ANGL
1	7	90.0	19	-4	0.0	37	1	90.0	54	-24	90.0
2	3	90.0	20	1	0.0	38	0	90.0	55	-16	90.0
3	1	90.0	21	4	0.0	39	-1	90.0	56	-11	90.0
4	1	90.0	22	-10	90.0	40	5	90.0	57	9	90.0
5	1	90.0	23	-39	90.0	41	11	90.0	58	39	90.0
6	2	90.0	24	-66	90.0	42	40	90.0	59	76	90.0
7	7	90.0	25	-65	90.0	43	25	90.0	60	97	90.0
8	0	90.0	26	-58	90.0	44	-1	90.0	61	100	90.0
9	-34	90.0	27	-34	90.0	45	-63	90.0	62	76	90.0
10	-72	90.0	28	-14	90.0	46	-3	90.0	63	61	90.0
11	-96	90.0	29	0	90.0	47	-16	90.0	64	26	90.0
12	-77	90.0	30	5	90.0	48	-20	90.0	65	-10	0.0
13	-66	90.0	31	1	90.0	49	-19	90.0	66	-15	0.0
14	-27	90.0	32	3	90.0	50	-20	90.0	67	-16	0.0
15	-7	90.0	33	1	90.0	51	-23	90.0	68	-8	0.0
16	1	0.0	34	3	90.0	52	-25	90.0	69	-1	0.0
17	-2	0.0	35	1	90.0	53	-26	90.0	70	1	0.0
18	-3	0.0	36	1	90.0						

APPLIED MECHANICS LAB --STRAIN DIST-- 08-May-92 09:03:57
CONFIG: P.V02 DATA FILE: P.C03

MPS F39
FORWARD SWEPT FAN BLADE
P/N 4013427-460

TIME: 09:03:13 DATE: 08-May-92 FREQUENCY: 530.00 HZ

PERCENT RELATIVE STRAIN

GAGE	PCT	ANGL	GAGE	PCT	ANGL	GAGE	PCT	ANGL	GAGE	PCT	ANGL
1	11	90.0	19	9	0.0	37	7	90.0	54	9	90.0
2	12	90.0	20	1	0.0	38	6	90.0	55	12	90.0
3	12	90.0	21	-8	0.0	39	3	90.0	56	24	90.0
4	13	90.0	22	10	90.0	40	3	90.0	57	29	90.0
5	17	90.0	23	48	90.0	41	9	90.0	58	22	90.0
6	22	90.0	24	66	90.0	42	43	90.0	59	2	90.0
7	23	90.0	25	45	90.0	43	19	90.0	60	-39	90.0
8	12	90.0	26	23	90.0	44	2	90.0	61	-76	90.0
9	20	90.0	27	3	90.0	45	68	90.0	62	-87	90.0
10	45	90.0	28	4	90.0	46	-2	90.0	63	-87	90.0
11	90	90.0	29	9	90.0	47	-17	90.0	64	-46	90.0
12	95	90.0	30	1	90.0	48	-6	90.0	65	6	0.0
13	100	90.0	31	20	90.0	49	-17	90.0	66	14	0.0
14	49	90.0	32	10	90.0	50	-14	90.0	67	22	0.0
15	15	90.0	33	12	90.0	51	-10	90.0	68	13	0.0
16	-1	0.0	34	6	90.0	52	-4	90.0	69	1	0.0
17	6	0.0	35	7	90.0	53	-1	90.0	70	-2	0.0
18	7	0.0	36	5	90.0						

APPLIED MECHANICS LAB --STRAIN DIST-- 08-May-92 09:08:07
CONFIG: P.V02 DATA FILE: P.C04

MPS F39
FORWARD SWEPT FAN BLADE
P/N 4013427-460

TIME: 09:07:18 DATE: 08-May-92 FREQUENCY: 684.00 HZ

PERCENT RELATIVE STRAIN

GAGE	PCT	ANGL	GAGE	PCT	ANGL	GAGE	PCT	ANGL	GAGE	PCT	ANGL
1	-5	90.0	19	7	0.0	37	5	90.0	54	-2	90.0
2	-3	90.0	20	-0	0.0	38	4	90.0	55	-1	90.0
3	-1	90.0	21	-8	0.0	39	-0	90.0	56	15	90.0
4	1	90.0	22	11	90.0	40	-1	90.0	57	33	90.0
5	-0	90.0	23	45	90.0	41	3	90.0	58	42	90.0
6	4	90.0	24	56	90.0	42	-29	90.0	59	35	90.0
7	11	90.0	25	30	90.0	43	-1	90.0	60	3	90.0
8	5	90.0	26	8	90.0	44	0	90.0	61	-43	90.0
9	7	90.0	27	-2	90.0	45	59	90.0	62	-66	90.0
10	25	90.0	28	6	90.0	46	0	90.0	63	-79	90.0
11	66	90.0	29	21	90.0	47	0	90.0	64	-41	90.0
12	87	90.0	30	12	90.0	48	-14	90.0	65	9	0.0
13	100	90.0	31	30	90.0	49	-3	90.0	66	19	0.0
14	52	90.0	32	12	90.0	50	-3	90.0	67	27	0.0
15	16	90.0	33	11	90.0	51	-4	90.0	68	16	0.0
16	-1	0.0	34	5	90.0	52	-6	90.0	69	3	0.0
17	5	0.0	35	4	90.0	53	-6	90.0	70	-1	0.0
18	6	0.0	36	3	90.0						

APPLIED MECHANICS LAB --STRAIN DIST-- 08-May-92 09:13:03
CONFIG: P.V02 DATA FILE: P.C05

MPS F39
FORWARD SWEPT FAN BLADE
P/N 4013427-460

TIME: 09:12:19 DATE: 08-May-92 FREQUENCY: 620.00 HZ

PERCENT RELATIVE STRAIN

GAGE	PCT	ANGL	GAGE	PCT	ANGL	GAGE	PCT	ANGL	GAGE	PCT	ANGL
1	16	90.0	19	-30	0.0	37	16	90.0	54	-31	90.0
2	25	90.0	20	-16	0.0	38	16	90.0	55	-44	90.0
3	29	90.0	21	-1	0.0	39	9	90.0	56	-44	90.0
4	26	90.0	22	5	90.0	40	-6	90.0	57	-17	90.0
5	33	90.0	23	-42	90.0	41	-3	90.0	58	0	90.0
6	43	90.0	24	-55	90.0	42	-20	90.0	59	5	90.0
7	69	90.0	25	-38	90.0	43	-10	90.0	60	15	90.0
8	73	90.0	26	-39	90.0	44	47	90.0	61	19	90.0
9	100	90.0	27	-29	90.0	45	-54	90.0	62	58	90.0
10	79	90.0	28	-30	90.0	46	2	90.0	63	52	90.0
11	44	90.0	29	15	90.0	47	3	90.0	64	52	90.0
12	30	90.0	30	35	90.0	48	36	90.0	65	47	0.0
13	8	90.0	31	50	90.0	49	-4	90.0	66	53	0.0
14	-2	90.0	32	28	90.0	50	-3	90.0	67	36	0.0
15	-1	90.0	33	25	90.0	51	-3	90.0	68	17	0.0
16	-2	0.0	34	12	90.0	52	-6	90.0	69	15	0.0
17	-21	0.0	35	12	90.0	53	-16	90.0	70	1	0.0
18	-29	0.0	36	9	90.0						

APPLIED MECHANICS LAB --STRAIN DIST-- 08-May-92 09:18:28
CONFIG: P.V02 DATA FILE: P.C06

MPS F39
FORWARD SWEPT FAN BLADE
P/N 4013427-460

TIME: 09:17:46 DATE: 08-May-92 FREQUENCY: 892.00 HZ

PERCENT RELATIVE STRAIN

GAGE	PCT	ANGL	GAGE	PCT	ANGL	GAGE	PCT	ANGL	GAGE	PCT	ANGL
1	-5	90.0	19	15	0.0	37	-9	90.0	54	-19	90.0
2	-5	90.0	20	4	0.0	38	-8	90.0	55	-17	90.0
3	-5	90.0	21	-9	0.0	39	-4	90.0	56	-16	90.0
4	-3	90.0	22	4	90.0	40	1	90.0	57	5	90.0
5	-0	90.0	23	35	90.0	41	-6	90.0	58	29	90.0
6	-1	90.0	24	30	90.0	42	-16	90.0	59	45	90.0
7	4	90.0	25	-1	90.0	43	-7	90.0	60	31	90.0
8	2	90.0	26	-23	90.0	44	-1	90.0	61	-6	90.0
9	-6	90.0	27	-23	90.0	45	37	90.0	62	-52	90.0
10	-4	90.0	28	-16	90.0	46	-1	90.0	63	-81	90.0
11	31	90.0	29	-1	90.0	47	9	90.0	64	-55	90.0
12	69	90.0	30	3	90.0	48	5	90.0	65	-3	0.0
13	100	90.0	31	-7	90.0	49	10	90.0	66	1	0.0
14	61	90.0	32	-4	90.0	50	6	90.0	67	17	0.0
15	21	90.0	33	-10	90.0	51	-0	90.0	68	14	0.0
16	1	0.0	34	-5	90.0	52	-3	90.0	69	0	0.0
17	11	0.0	35	-7	90.0	53	-12	90.0	70	-1	0.0
18	13	0.0	36	-7	90.0						

APPLIED MECHANICS LAB --STRAIN DIST-- 08-May-92 09:24:31
CONFIG: P.V02 DATA FILE: P.C07

MPS F39
FORWARD SWEPT FAN BLADE
P/N 4013427-460

TIME: 09:23:43 DATE: 08-May-92 FREQUENCY: 1345.00 HZ

PERCENT RELATIVE STRAIN

GAGE	PCT	ANGL	GAGE	PCT	ANGL	GAGE	PCT	ANGL	GAGE	PCT	ANGL
1	0	90.0	19	21	0.0	37	7	90.0	54	13	90.0
2	-2	90.0	20	7	0.0	38	6	90.0	55	5	90.0
3	0	90.0	21	-10	0.0	39	3	90.0	56	-14	90.0
4	-5	90.0	22	2	90.0	40	-1	90.0	57	-31	90.0
5	-10	90.0	23	9	90.0	41	3	90.0	58	-18	90.0
6	-16	90.0	24	-27	90.0	42	9	90.0	59	16	90.0
7	-20	90.0	25	-49	90.0	43	1	90.0	60	56	90.0
8	-13	90.0	26	-42	90.0	44	0	90.0	61	54	90.0
9	-25	90.0	27	-16	90.0	45	-16	90.0	62	2	90.0
10	-41	90.0	28	-3	90.0	46	1	90.0	63	-60	90.0
11	-31	90.0	29	-2	90.0	47	-6	90.0	64	-64	90.0
12	30	90.0	30	-3	90.0	48	-1	90.0	65	-17	0.0
13	100	90.0	31	-22	90.0	49	-4	90.0	66	-10	0.0
14	86	90.0	32	-12	90.0	50	1	90.0	67	14	0.0
15	35	90.0	33	-2	90.0	51	4	90.0	68	17	0.0
16	3	0.0	34	2	90.0	52	11	90.0	69	1	0.0
17	19	0.0	35	3	90.0	53	15	90.0	70	-0	0.0
18	22	0.0	36	4	90.0						

APPLIED MECHANICS LAB --STRAIN DIST-- 08-May-92 09:29:15
CONFIG: P.V02 DATA FILE: P.C08

MPS F39
FORWARD SWEPT FAN BLADE
P/N 4013427-460

TIME: 09:28:26 DATE: 08-May-92 FREQUENCY: 1016.00 HZ

PERCENT RELATIVE STRAIN

GAGE	PCT	ANGL	GAGE	PCT	ANGL	GAGE	PCT	ANGL	GAGE	PCT	ANGL
1	-31	90.0	19	-46	0.0	37	-53	90.0	54	32	90.0
2	-49	90.0	20	-30	0.0	38	-50	90.0	55	40	90.0
3	-50	90.0	21	-13	0.0	39	-27	90.0	56	28	90.0
4	-41	90.0	22	15	90.0	40	10	90.0	57	5	90.0
5	-41	90.0	23	21	90.0	41	-6	90.0	58	15	90.0
6	-44	90.0	24	13	90.0	42	-15	90.0	59	36	90.0
7	-38	90.0	25	-8	90.0	43	-8	90.0	60	31	90.0
8	-25	90.0	26	-26	90.0	44	-53	90.0	61	-8	90.0
9	-18	90.0	27	-14	90.0	45	19	90.0	62	-30	90.0
10	-10	90.0	28	17	90.0	46	-3	90.0	63	-48	90.0
11	24	90.0	29	-13	90.0	47	14	90.0	64	56	90.0
12	83	90.0	30	-33	90.0	48	-51	90.0	65	81	0.0
13	100	90.0	31	-99	90.0	49	33	90.0	66	96	0.0
14	52	90.0	32	-75	90.0	50	24	90.0	67	81	0.0
15	16	90.0	33	-77	90.0	51	15	90.0	68	47	0.0
16	-5	0.0	34	-41	90.0	52	17	90.0	69	34	0.0
17	-36	0.0	35	-46	90.0	53	22	90.0	70	4	0.0
18	-45	0.0	36	-36	90.0						

APPLIED MECHANICS LAB --STRAIN DIST-- 08-May-92 09:39:07
CONFIG: P.V02 DATA FILE: P.C09

MPS F39
FORWARD SWEPT FAN BLADE
P/N 4013427-460

TIME: 09:38:15 DATE: 08-May-92 FREQUENCY: 1464.00 HZ

PERCENT RELATIVE STRAIN

GAGE	PCT	ANGL	GAGE	PCT	ANGL	GAGE	PCT	ANGL	GAGE	PCT	ANGL
1	11	90.0	19	-72	0.0	37	29	90.0	54	-25	90.0
2	17	90.0	20	-44	0.0	38	26	90.0	55	-13	90.0
3	13	90.0	21	-17	0.0	39	14	90.0	56	-1	90.0
4	8	90.0	22	9	90.0	40	-10	90.0	57	8	90.0
5	3	90.0	23	11	90.0	41	-7	90.0	58	3	90.0
6	-0	90.0	24	71	90.0	42	-28	90.0	59	-2	90.0
7	-26	90.0	25	50	90.0	43	-8	90.0	60	-28	90.0
8	-41	90.0	26	36	90.0	44	-2	90.0	61	-58	90.0
9	-72	90.0	27	22	90.0	45	71	90.0	62	-29	90.0
10	-71	90.0	28	15	90.0	46	4	90.0	63	22	90.0
11	-41	90.0	29	-7	90.0	47	5	90.0	64	83	90.0
12	-1	90.0	30	-4	90.0	48	42	90.0	65	83	0.0
13	-22	90.0	31	27	90.0	49	-5	90.0	66	100	0.0
14	-33	90.0	32	38	90.0	50	-4	90.0	67	73	0.0
15	-22	90.0	33	42	90.0	51	-4	90.0	68	38	0.0
16	-12	0.0	34	23	90.0	52	-13	90.0	69	38	0.0
17	-58	0.0	35	25	90.0	53	-21	90.0	70	5	0.0
18	-70	0.0	36	20	90.0						

APPLIED MECHANICS LAB --STRAIN DIST-- 08-May-92 09:46:05
CONFIG: P.V02 DATA FILE: P.C10

MPS F39
FORWARD SWEPT FAN BLADE
P/N 4013427-460

TIME: 09:45:22 DATE: 08-May-92 FREQUENCY: 1818.00 HZ

PERCENT RELATIVE STRAIN

GAGE	PCT	ANGL	GAGE	PCT	ANGL	GAGE	PCT	ANGL	GAGE	PCT	ANGL
1	2	90.0	19	45	0.0	37	0	90.0	54	-1	90.0
2	4	90.0	20	22	0.0	38	0	90.0	55	11	90.0
3	7	90.0	21	0	0.0	39	0	90.0	56	30	90.0
4	9	90.0	22	-7	90.0	40	1	90.0	57	1	90.0
5	10	90.0	23	-33	90.0	41	-4	90.0	58	-35	90.0
6	7	90.0	24	-84	90.0	42	-9	90.0	59	-48	90.0
7	-1	90.0	25	-35	90.0	43	0	90.0	60	-4	90.0
8	-2	90.0	26	16	90.0	44	-0	90.0	61	55	90.0
9	-1	90.0	27	41	90.0	45	-82	90.0	62	59	90.0
10	-14	90.0	28	42	90.0	46	-1	90.0	63	-10	90.0
11	-42	90.0	29	4	90.0	47	6	90.0	64	-71	90.0
12	-8	90.0	30	-15	90.0	48	6	90.0	65	-41	0.0
13	73	90.0	31	31	90.0	49	1	90.0	66	-45	0.0
14	100	90.0	32	34	90.0	50	-2	90.0	67	-15	0.0
15	54	90.0	33	32	90.0	51	-10	90.0	68	5	0.0
16	10	0.0	34	15	90.0	52	-15	90.0	69	-8	0.0
17	42	0.0	35	8	90.0	53	-13	90.0	70	1	0.0
18	46	0.0	36	2	90.0						

APPLIED MECHANICS LAB --STRAIN DIST-- 08-May-92 09:59:22
CONFIG: P.V02 DATA FILE: P.C11

MPS F39
FORWARD SWEPT FAN BLADE
P/N 4013427-460

TIME: 09:58:39 DATE: 08-May-92 FREQUENCY: 1969.00 HZ

PERCENT RELATIVE STRAIN

GAGE	PCT	ANGL	GAGE	PCT	ANGL	GAGE	PCT	ANGL	GAGE	PCT	ANGL
1	2	90.0	19	35	0.0	37	18	90.0	54	-4	90.0
2	1	90.0	20	29	0.0	38	14	90.0	55	2	90.0
3	-0	90.0	21	28	0.0	39	6	90.0	56	0	90.0
4	-2	90.0	22	2	90.0	40	-5	90.0	57	5	90.0
5	-7	90.0	23	-14	90.0	41	-4	90.0	58	17	90.0
6	-14	90.0	24	-17	90.0	42	-17	90.0	59	17	90.0
7	-20	90.0	25	20	90.0	43	-2	90.0	60	-4	90.0
8	-13	90.0	26	7	90.0	44	-23	90.0	61	-14	90.0
9	12	90.0	27	-3	90.0	45	-30	90.0	62	12	90.0
10	61	90.0	28	5	90.0	46	2	90.0	63	36	90.0
11	100	90.0	29	1	90.0	47	3	90.0	64	6	90.0
12	41	90.0	30	-1	90.0	48	17	90.0	65	-19	0.0
13	-35	90.0	31	-12	90.0	49	0	90.0	66	-39	0.0
14	-52	90.0	32	-2	90.0	50	0	90.0	67	-59	0.0
15	-23	90.0	33	9	90.0	51	-0	90.0	68	-50	0.0
16	5	0.0	34	7	90.0	52	-3	90.0	69	-37	0.0
17	28	0.0	35	16	90.0	53	-6	90.0	70	-7	0.0
18	36	0.0	36	15	90.0						

APPLIED MECHANICS LAB --STRAIN DIST-- 08-May-92 10:02:54
CONFIG: P.V02 DATA FILE: P.C12

MPS F39
FORWARD SWEPT FAN BLADE
P/N 4013427-460

TIME: 10:02:10 DATE: 08-May-92 FREQUENCY: 2500.00 HZ

PERCENT RELATIVE STRAIN

GAGE	PCT	ANGL	GAGE	PCT	ANGL	GAGE	PCT	ANGL	GAGE	PCT	ANGL
1	1	90.0	19	3	0.0	37	23	90.0	54	1	90.0
2	0	90.0	20	-4	0.0	38	11	90.0	55	-1	90.0
3	1	90.0	21	-12	0.0	39	2	90.0	56	-6	90.0
4	1	90.0	22	-13	90.0	40	1	90.0	57	23	90.0
5	-3	90.0	23	-28	90.0	41	-1	90.0	58	26	90.0
6	-1	90.0	24	-22	90.0	42	-1	90.0	59	-11	90.0
7	11	90.0	25	22	90.0	43	1	90.0	60	-39	90.0
8	27	90.0	26	34	90.0	44	-6	90.0	61	-4	90.0
9	44	90.0	27	-6	90.0	45	-26	90.0	62	31	90.0
10	19	90.0	28	-46	90.0	46	-2	90.0	63	7	90.0
11	-68	90.0	29	-6	90.0	47	3	90.0	64	-36	90.0
12	-88	90.0	30	33	90.0	48	0	90.0	65	-20	0.0
13	6	90.0	31	-7	90.0	49	1	90.0	66	-16	0.0
14	100	90.0	32	-34	90.0	50	-3	90.0	67	15	0.0
15	67	90.0	33	-10	90.0	51	-5	90.0	68	39	0.0
16	-0	0.0	34	-0	90.0	52	-1	90.0	69	20	0.0
17	8	0.0	35	25	90.0	53	0	90.0	70	6	0.0
18	5	0.0	36	26	90.0						

APPLIED MECHANICS LAB --STRAIN DIST-- 08-May-92 10:15:00
CONFIG: P.V02 DATA FILE: P.C13

MPS F39
FORWARD SWEPT FAN BLADE
P/N 4013427-460

TIME: 10:14:11 DATE: 08-May-92 FREQUENCY: 2275.00 HZ

PERCENT RELATIVE STRAIN

GAGE	PCT	ANGL	GAGE	PCT	ANGL	GAGE	PCT	ANGL	GAGE	PCT	ANGL
1	-3	90.0	19	69	0.0	37	-6	90.0	54	-17	90.0
2	-6	90.0	20	39	0.0	38	-1	90.0	55	-24	90.0
3	-9	90.0	21	25	0.0	39	1	90.0	56	-5	90.0
4	-9	90.0	22	-5	90.0	40	1	90.0	57	42	90.0
5	-2	90.0	23	-60	90.0	41	5	90.0	58	26	90.0
6	3	90.0	24	-43	90.0	42	0	90.0	59	-30	90.0
7	4	90.0	25	73	90.0	43	-1	90.0	60	-67	90.0
8	-2	90.0	26	100	90.0	44	-1	90.0	61	-17	90.0
9	-2	90.0	27	47	90.0	45	-68	90.0	62	68	90.0
10	5	90.0	28	-13	90.0	46	-1	90.0	63	50	90.0
11	-17	90.0	29	-28	90.0	47	-7	90.0	64	-47	90.0
12	-19	90.0	30	10	90.0	48	-1	90.0	65	-34	0.0
13	39	90.0	31	-9	90.0	49	1	90.0	66	-60	0.0
14	99	90.0	32	-26	90.0	50	7	90.0	67	-46	0.0
15	66	90.0	33	-61	90.0	51	17	90.0	68	-19	0.0
16	17	0.0	34	-39	90.0	52	17	90.0	69	-31	0.0
17	71	0.0	35	-35	90.0	53	5	90.0	70	-4	0.0
18	77	0.0	36	-20	90.0						

APPLIED MECHANICS LAB --STRAIN DIST-- 08-May-92 10:18:48
CONFIG: P.V02 DATA FILE: P.C14

MPS F39
FORWARD SWEPT FAN BLADE
P/N 4013427-460

TIME: 10:18:01 DATE: 08-May-92 FREQUENCY: 2759.00 HZ

PERCENT RELATIVE STRAIN

GAGE	PCT	ANGL	GAGE	PCT	ANGL	GAGE	PCT	ANGL	GAGE	PCT	ANGL
1	-4	90.0	19	-31	0.0	37	18	90.0	54	-22	90.0
2	-4	90.0	20	-16	0.0	38	8	90.0	55	-23	90.0
3	-1	90.0	21	-12	0.0	39	0	90.0	56	0	90.0
4	0	90.0	22	1	90.0	40	-1	90.0	57	-2	90.0
5	6	90.0	23	14	90.0	41	-1	90.0	58	-28	90.0
6	14	90.0	24	-28	90.0	42	6	90.0	59	-27	90.0
7	22	90.0	25	-39	90.0	43	-2	90.0	60	8	90.0
8	18	90.0	26	14	90.0	44	4	90.0	61	24	90.0
9	16	90.0	27	64	90.0	45	-13	90.0	62	-11	90.0
10	5	90.0	28	81	90.0	46	1	90.0	63	-32	90.0
11	13	90.0	29	28	90.0	47	-1	90.0	64	6	90.0
12	23	90.0	30	11	90.0	48	-9	90.0	65	-1	0.0
13	-1	90.0	31	100	90.0	49	4	90.0	66	13	0.0
14	-48	90.0	32	75	90.0	50	5	90.0	67	19	0.0
15	-38	90.0	33	40	90.0	51	6	90.0	68	9	0.0
16	-9	0.0	34	5	90.0	52	3	90.0	69	16	0.0
17	-38	0.0	35	15	90.0	53	-6	90.0	70	0	0.0
18	-37	0.0	36	18	90.0						

APPLIED MECHANICS LAB --STRAIN DIST-- 08-May-92 10:26:05
CONFIG: P.V02 DATA FILE: P.C15

MPS F39
FORWARD SWEPT FAN BLADE
P/N 4013427-460

TIME: 10:25:18 DATE: 08-May-92 FREQUENCY: 2660.00 HZ

PERCENT RELATIVE STRAIN

GAGE	PCT	ANGL	GAGE	PCT	ANGL	GAGE	PCT	ANGL	GAGE	PCT	ANGL
1	1	90.0	19	51	0.0	37	10	90.0	54	3	90.0
2	2	90.0	20	35	0.0	38	-0	90.0	55	-8	90.0
3	3	90.0	21	33	0.0	39	-4	90.0	56	-32	90.0
4	3	90.0	22	7	90.0	40	4	90.0	57	-31	90.0
5	5	90.0	23	-13	90.0	41	1	90.0	58	1	90.0
6	14	90.0	24	41	90.0	42	17	90.0	59	15	90.0
7	17	90.0	25	61	90.0	43	-2	90.0	60	-7	90.0
8	8	90.0	26	8	90.0	44	19	90.0	61	-35	90.0
9	-20	90.0	27	-22	90.0	45	15	90.0	62	1	90.0
10	-19	90.0	28	-11	90.0	46	-2	90.0	63	43	90.0
11	38	90.0	29	38	90.0	47	1	90.0	64	12	90.0
12	59	90.0	30	44	90.0	48	-17	90.0	65	12	0.0
13	22	90.0	31	67	90.0	49	3	90.0	66	-17	0.0
14	-5	90.0	32	44	90.0	50	1	90.0	67	-53	0.0
15	2	90.0	33	100	90.0	51	-3	90.0	68	-57	0.0
16	13	0.0	34	46	90.0	52	-2	90.0	69	-49	0.0
17	58	0.0	35	52	90.0	53	5	90.0	70	-9	0.0
18	60	0.0	36	32	90.0						

APPLIED MECHANICS LAB --STRAIN DIST-- 08-May-92 10:31:44
CONFIG: P.V02 DATA FILE: P.C16

MPS F39
FORWARD SWEPT FAN BLADE
P/N 4013427-460

TIME: 10:30:58 DATE: 08-May-92 FREQUENCY: 2973.00 HZ

PERCENT RELATIVE STRAIN

GAGE	PCT	ANGL	GAGE	PCT	ANGL	GAGE	PCT	ANGL	GAGE	PCT	ANGL
1	-4	90.0	19	31	0.0	37	-14	90.0	54	-6	90.0
2	-4	90.0	20	11	0.0	38	-3	90.0	55	5	90.0
3	-2	90.0	21	6	0.0	39	-1	90.0	56	-4	90.0
4	0	90.0	22	-7	90.0	40	-3	90.0	57	-22	90.0
5	-1	90.0	23	-19	90.0	41	1	90.0	58	19	90.0
6	-4	90.0	24	50	90.0	42	-7	90.0	59	38	90.0
7	-9	90.0	25	51	90.0	43	-5	90.0	60	-11	90.0
8	-3	90.0	26	-32	90.0	44	-7	90.0	61	-43	90.0
9	28	90.0	27	-65	90.0	45	28	90.0	62	7	90.0
10	46	90.0	28	14	90.0	46	2	90.0	63	45	90.0
11	-8	90.0	29	79	90.0	47	1	90.0	64	-15	90.0
12	-82	90.0	30	2	90.0	48	-1	90.0	65	-5	0.0
13	-32	90.0	31	20	90.0	49	4	90.0	66	-24	0.0
14	100	90.0	32	62	90.0	50	7	90.0	67	-15	0.0
15	89	90.0	33	74	90.0	51	5	90.0	68	9	0.0
16	11	0.0	34	30	90.0	52	-2	90.0	69	-5	0.0
17	45	0.0	35	-4	90.0	53	-10	90.0	70	2	0.0
18	41	0.0	36	-18	90.0						

APPLIED MECHANICS LAB --STRAIN DIST-- 09-May-92 07:00:39
CONFIG: P.V02 DATA FILE: P.C17

MPS F39
FORWARD SWEPT FAN BLADE
P/N 4013427-460

TIME: 06:59:51 DATE: 09-May-92 FREQUENCY: 3243.00 HZ

PERCENT RELATIVE STRAIN

GAGE	PCT	ANGL	GAGE	PCT	ANGL	GAGE	PCT	ANGL	GAGE	PCT	ANGL
1	10	90.0	19	-40	0.0	37	-29	90.0	54	27	90.0
2	14	90.0	20	-14	0.0	38	-5	90.0	55	7	90.0
3	12	90.0	21	-12	0.0	39	-1	90.0	56	-35	90.0
4	12	90.0	22	-8	90.0	40	2	90.0	57	-30	90.0
5	-12	90.0	23	10	90.0	41	-1	90.0	58	-6	90.0
6	-20	90.0	24	-59	90.0	42	8	90.0	59	-34	90.0
7	-23	90.0	25	51	90.0	43	10	90.0	60	-47	90.0
8	24	90.0	26	100	90.0	44	-30	90.0	61	-9	90.0
9	47	90.0	27	40	90.0	45	-59	90.0	62	-2	90.0
10	43	90.0	28	-50	90.0	46	-2	90.0	63	-38	90.0
11	40	90.0	29	41	90.0	47	-1	90.0	64	-11	90.0
12	38	90.0	30	54	90.0	48	15	90.0	65	-41	0.0
13	20	90.0	31	-35	90.0	49	-11	90.0	66	-12	0.0
14	-41	90.0	32	-47	90.0	50	-7	90.0	67	22	0.0
15	-41	90.0	33	-26	90.0	51	-1	90.0	68	29	0.0
16	-14	0.0	34	-3	90.0	52	3	90.0	69	36	0.0
17	-60	0.0	35	-37	90.0	53	18	90.0	70	4	0.0
18	-55	0.0	36	-42	90.0						

APPLIED MECHANICS LAB --STRAIN DIST-- 09-May-92 07:05:35
CONFIG: P.V02 DATA FILE: P.C18

MPS F39
FORWARD SWEPT FAN BLADE
P/N 4013427-460

TIME: 07:04:50 DATE: 09-May-92 FREQUENCY: 3551.00 HZ

PERCENT RELATIVE STRAIN

GAGE	PCT	ANGL	GAGE	PCT	ANGL	GAGE	PCT	ANGL	GAGE	PCT	ANGL
1	-10	90.0	19	56	0.0	37	-7	90.0	54	2	90.0
2	-9	90.0	20	30	0.0	38	-13	90.0	55	1	90.0
3	-9	90.0	21	11	0.0	39	-5	90.0	56	27	90.0
4	-9	90.0	22	28	90.0	40	-5	90.0	57	37	90.0
5	-14	90.0	23	86	90.0	41	-1	90.0	58	-6	90.0
6	-30	90.0	24	92	90.0	42	-28	90.0	59	-17	90.0
7	-50	90.0	25	-48	90.0	43	-11	90.0	60	29	90.0
8	-48	90.0	26	9	90.0	44	-21	90.0	61	13	90.0
9	-44	90.0	27	100	90.0	45	97	90.0	62	-30	90.0
10	-37	90.0	28	79	90.0	46	3	90.0	63	10	90.0
11	-50	90.0	29	-44	90.0	47	0	90.0	64	42	90.0
12	-16	90.0	30	33	90.0	48	-2	90.0	65	79	0.0
13	24	90.0	31	87	90.0	49	6	90.0	66	31	0.0
14	17	90.0	32	-43	90.0	50	2	90.0	67	-32	0.0
15	20	90.0	33	12	90.0	51	-3	90.0	68	-61	0.0
16	19	0.0	34	43	90.0	52	-7	90.0	69	-62	0.0
17	78	0.0	35	87	90.0	53	-3	90.0	70	-12	0.0
18	73	0.0	36	46	90.0						

APPLIED MECHANICS LAB --STRAIN DIST-- 09-May-92 07:09:12
CONFIG: P.V02 DATA FILE: P.C19

MPS F39
FORWARD SWEPT FAN BLADE
P/N 4013427-460

TIME: 07:08:26 DATE: 09-May-92 FREQUENCY: 3662.00 HZ

PERCENT RELATIVE STRAIN

GAGE	PCT	ANGL	GAGE	PCT	ANGL	GAGE	PCT	ANGL	GAGE	PCT	ANGL
1	-5	90.0	19	-25	0.0	37	19	90.0	54	4	90.0
2	-6	90.0	20	-8	0.0	38	8	90.0	55	6	90.0
3	-8	90.0	21	-1	0.0	39	-1	90.0	56	13	90.0
4	-12	90.0	22	-2	90.0	40	-1	90.0	57	-5	90.0
5	-17	90.0	23	-27	90.0	41	1	90.0	58	16	90.0
6	-22	90.0	24	-10	90.0	42	-7	90.0	59	32	90.0
7	-29	90.0	25	100	90.0	43	2	90.0	60	-2	90.0
8	-38	90.0	26	37	90.0	44	-1	90.0	61	-6	90.0
9	-52	90.0	27	-32	90.0	45	-32	90.0	62	26	90.0
10	-24	90.0	28	37	90.0	46	1	90.0	63	-2	90.0
11	-2	90.0	29	61	90.0	47	-2	90.0	64	-23	90.0
12	-17	90.0	30	-27	90.0	48	-7	90.0	65	-47	0.0
13	-28	90.0	31	10	90.0	49	0	90.0	66	-16	0.0
14	-17	90.0	32	34	90.0	50	-2	90.0	67	23	0.0
15	-15	90.0	33	-3	90.0	51	-2	90.0	68	41	0.0
16	-14	0.0	34	-22	90.0	52	1	90.0	69	41	0.0
17	-49	0.0	35	-13	90.0	53	1	90.0	70	6	0.0
18	-42	0.0	36	8	90.0						

APPLIED MECHANICS LAB --STRAIN DIST-- 09-May-92 07:16:41
CONFIG: P.V02 DATA FILE: P.C20

MPS F39
FORWARD SWEPT FAN BLADE
P/N 4013427-460

TIME: 07:15:47 DATE: 09-May-92 FREQUENCY: 4034.00 HZ

PERCENT RELATIVE STRAIN

GAGE	PCT	ANGL	GAGE	PCT	ANGL	GAGE	PCT	ANGL	GAGE	PCT	ANGL
1	-2	90.0	19	35	0.0	37	15	90.0	54	1	90.0
2	-2	90.0	20	6	0.0	38	13	90.0	55	2	90.0
3	-4	90.0	21	-8	0.0	39	2	90.0	56	-13	90.0
4	-6	90.0	22	19	90.0	40	3	90.0	57	15	90.0
5	-5	90.0	23	76	90.0	41	-2	90.0	58	21	90.0
6	-2	90.0	24	-16	90.0	42	3	90.0	59	-11	90.0
7	-7	90.0	25	-75	90.0	43	-0	90.0	60	5	90.0
8	-19	90.0	26	100	90.0	44	1	90.0	61	27	90.0
9	-21	90.0	27	73	90.0	45	24	90.0	62	-23	90.0
10	-0	90.0	28	-78	90.0	46	-2	90.0	63	-3	90.0
11	-11	90.0	29	29	90.0	47	1	90.0	64	39	90.0
12	-24	90.0	30	73	90.0	48	-8	90.0	65	75	0.0
13	-23	90.0	31	-29	90.0	49	-0	90.0	66	39	0.0
14	34	90.0	32	6	90.0	50	-0	90.0	67	-18	0.0
15	50	90.0	33	33	90.0	51	1	90.0	68	-48	0.0
16	20	0.0	34	-3	90.0	52	-0	90.0	69	-54	0.0
17	79	0.0	35	-44	90.0	53	-0	90.0	70	-7	0.0
18	64	0.0	36	-20	90.0						

APPLIED MECHANICS LAB --STRAIN DIST-- 09-May-92 07:29:33
CONFIG: P.V02 DATA FILE: P.C21

MPS F39
FORWARD SWEPT FAN BLADE
P/N 4013427-460

TIME: 07:28:48 DATE: 09-May-92 FREQUENCY: 4180.00 HZ

PERCENT RELATIVE STRAIN

GAGE	PCT	ANGL	GAGE	PCT	ANGL	GAGE	PCT	ANGL	GAGE	PCT	ANGL
1	0	90.0	19	-1	0.0	37	-21	90.0	54	-3	90.0
2	1	90.0	20	17	0.0	38	-10	90.0	55	-20	90.0
3	-3	90.0	21	-1	0.0	39	1	90.0	56	-4	90.0
4	-8	90.0	22	11	90.0	40	-1	90.0	57	6	90.0
5	-11	90.0	23	-4	90.0	41	0	90.0	58	24	90.0
6	-8	90.0	24	-32	90.0	42	7	90.0	59	37	90.0
7	-1	90.0	25	60	90.0	43	6	90.0	60	-6	90.0
8	6	90.0	26	-38	90.0	44	-1	90.0	61	-12	90.0
9	8	90.0	27	-52	90.0	45	-46	90.0	62	2	90.0
10	-13	90.0	28	100	90.0	46	2	90.0	63	-41	90.0
11	-75	90.0	29	-6	90.0	47	-2	90.0	64	-11	90.0
12	1	90.0	30	-48	90.0	48	-3	90.0	65	-6	0.0
13	97	90.0	31	72	90.0	49	-5	90.0	66	-7	0.0
14	-30	90.0	32	18	90.0	50	-1	90.0	67	3	0.0
15	-80	90.0	33	-4	90.0	51	1	90.0	68	-3	0.0
16	-11	0.0	34	16	90.0	52	12	90.0	69	11	0.0
17	-40	0.0	35	39	90.0	53	14	90.0	70	-2	0.0
18	-23	0.0	36	5	90.0						

Appendix 4 – Divergent F39 Blade Bench Test Vibratory Mode Shapes

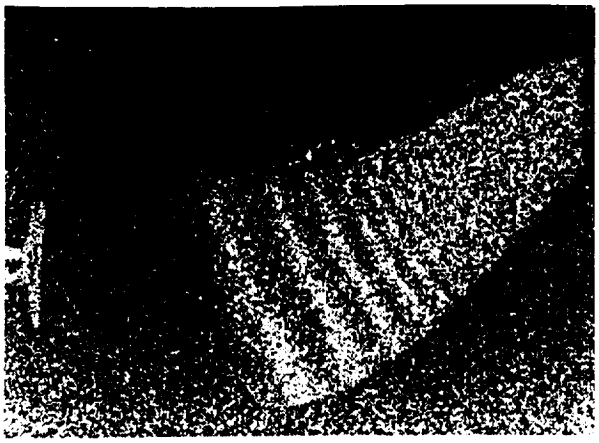

Frequency 00094 Hz

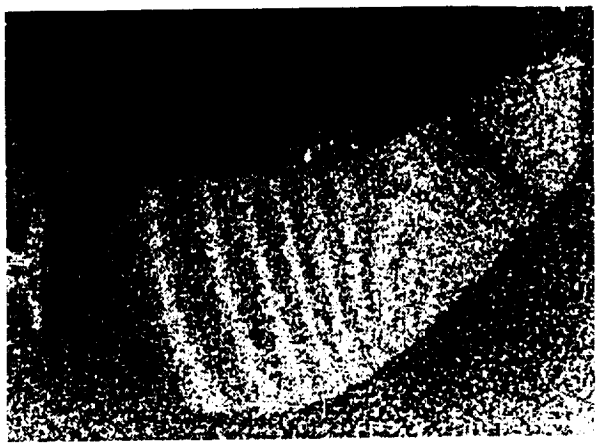

Frequency 00246 Hz

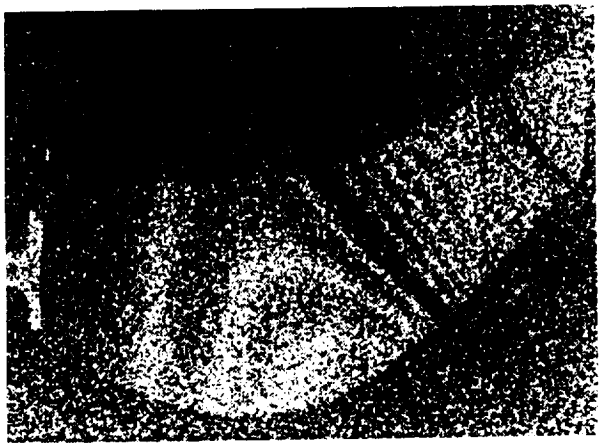

Frequency 00515 Hz

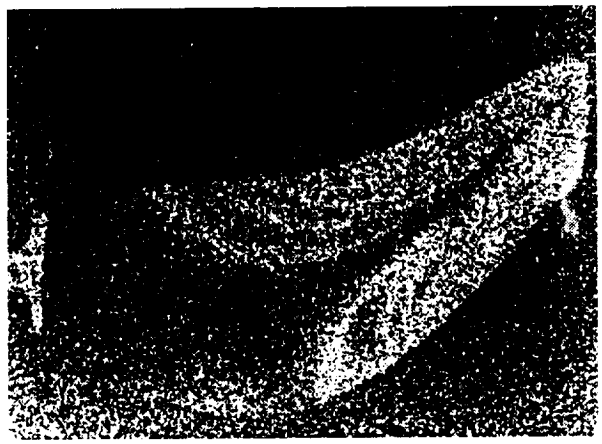

Frequency 00586 Hz

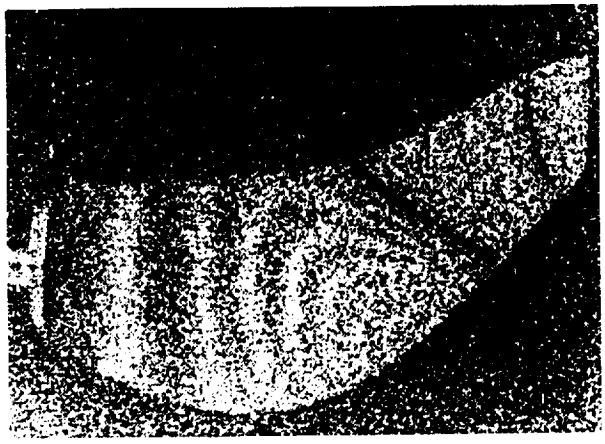

Frequency 00663 Hz

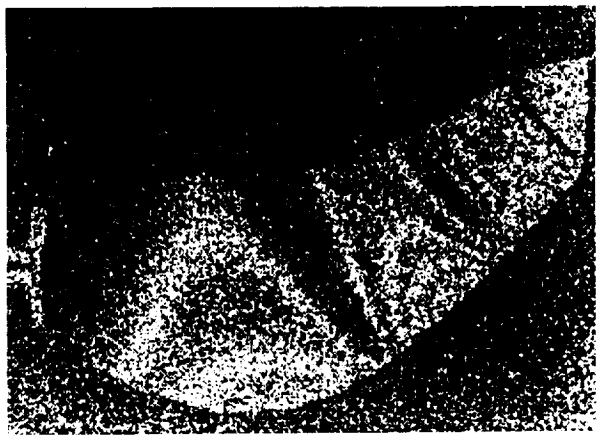

Frequency 00870 Hz

MPS Forward-Swept Fan Blade P/N 4013427-460

Frequency 00975 Hz

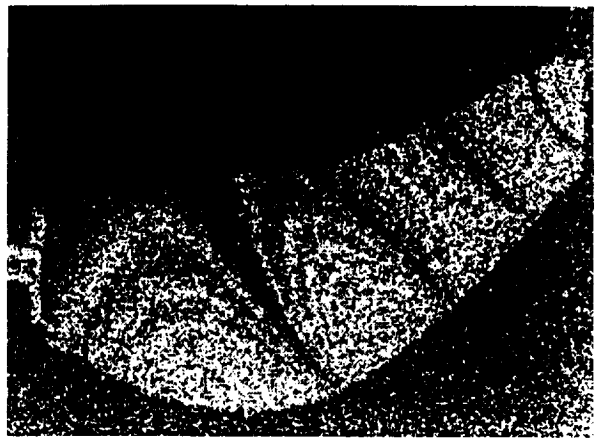

Frequency 01308 Hz

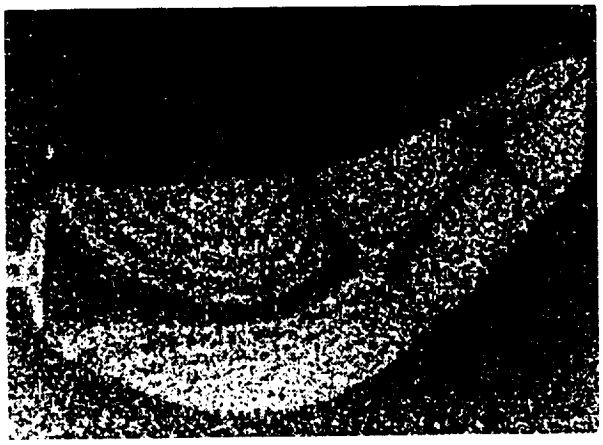

Frequency 01405 Hz

Frequency 01750 Hz

Frequency 01889 Hz

Frequency 02082 Hz

MPS Forward-Swept Fan Blade P/N 4013427-460

Frequency 02383 Hz

Frequency 02631 Hz

Frequency 02832 Hz

Frequency 03011 Hz

Frequency 03403 Hz

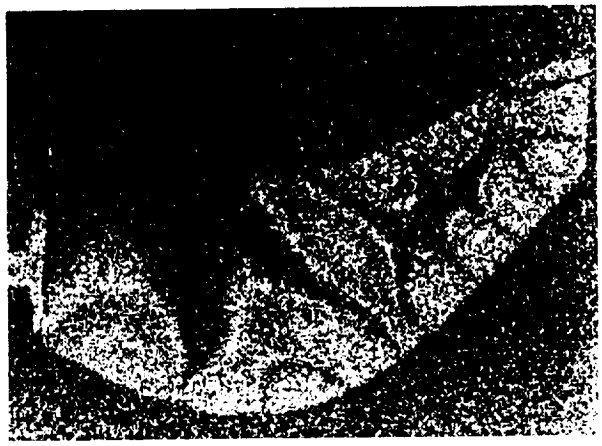

Frequency 03506 Hz

MPS Forward-Swept Fan Blade P/N 4013427-460

Frequency 03919 Hz

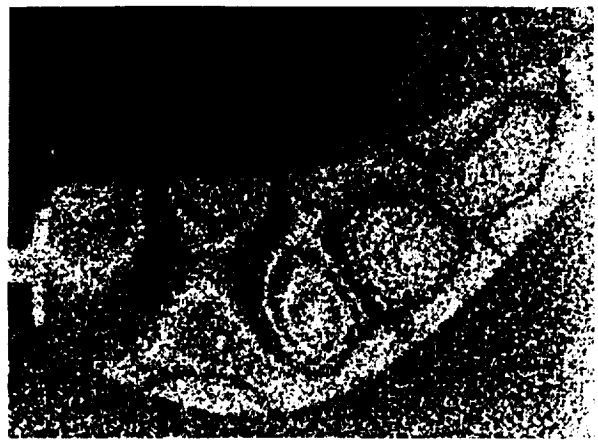

Frequency 04046 Hz

Frequency 04254 Hz

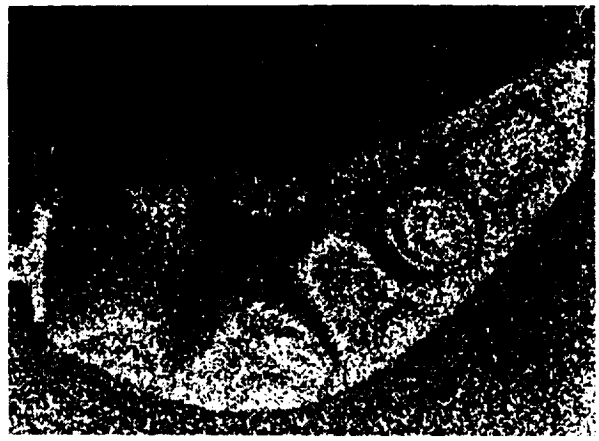

Frequency 04364 Hz

MPS Forward-Swept Fan Blade P/N 4013427-460